COMPATIBLE STRESS FIELD DESIGN OF STRUCTURAL CONCRETE

Principles and Validation

Walter Kaufmann et al.

Prof. Dr. Walter Kaufmann

Walter Kaufmann is the Chair of Structural Engineering (Concrete Structures and Bridge Design) at ETH Zurich. He is the Chairman of the Swiss Concrete Code Commission and is a Lead Principal Investigator at the Swiss National Centre of Competence in Research (NCCR) in Digital Fabrication. His research focuses on innovative structures, the load-bearing and deformation capacity of concrete structures, the assessment of the structural safety of existing structures, and digital fabrication methods.

He obtained his degrees from ETH Zurich in 1992 (dipl. Bau-Ing.) and 1998 (Dr. sc. techn.). Prior to joining ETH Zurich in 2014, he was active in the industry for more than 15 years, working mainly in Spain and Switzerland. During this time, he directed numerous structural engineering projects for buildings and bridges, participated successfully in many bridge design competitions, and was involved in a large number of expert appraisals.

COMPATIBLE STRESS FIELD DESIGN OF STRUCTURAL CONCRETE

PRINCIPLES AND VALIDATION

ETH Zurich, Institute of Structural Engineering
IDEA StatiCa s.r.o., Brno, Czech Republic

July 2020

Walter Kaufmann, Jaime Mata-Falcón, Marius Weber, Tena Galkovski, Duc Thong Tran, Jaromir Kabelac, Michael Konecny, Jaroslav Navratil, Michal Cihal, Petra Komarkova

Coverdesign: Arte 73 s.r.o., Brno, Czech Republic

ISBN 978-3-906916-95-8

Contents

1 Introduction

1.1 Current structural concrete practice

Today, powerful software is available for the design of concrete structures. Linear elastic finite element programs allow even complex structures to be analyzed in a relatively short period of time, and many of these programs include post-processing modules for automated dimensioning or the checking of reinforcement and concrete dimensions. State-of-the-art frame analysis programs feature modules providing automatic checks of ultimate load and serviceability criteria, including deformations and crack widths, based on sectional forces obtained from FE analysis. Such modules allow the user to efficiently dimension structures (or parts thereof) in cases where all static and geometric quantities vary only gradually and hence Bernoulli's hypothesis of plane sections remaining plane applies. While one might argue that linear elastic calculations do not reflect the real behavior of concrete structures, these calculations usually yield safe designs, as further outlined in Chapter 2.

However, the most critical parts of structures are typically regions where abrupt changes in geometry occur, or large concentrated loads are applied, such as corbels, deep beams, walls with openings, dapped beam-ends and frame corners. Since sectional design principles cannot be applied at these locations, which are known as *discontinuity regions*, semi-empirical design rules were used in the past for their dimensioning. Fortunately, these rules have been superseded mainly over the past decades by strut-and-tie models (Schlaich et al. 1987) and stress fields (Marti 1985) , which are featured in modern design codes and frequently used by designers today. These models, further outlined in Chapter 2, are mechanically consistent, powerful tools that yield direct insight into load-carrying behavior and give the engineer control over the design, allowing the dimensioning of reinforcement while taking practical considerations into account. Note that stress fields can generally be either continuous or discontinuous, and that strut-and-tie models are a special case in terms of *discontinuou*s stress fields (e.g., uniaxial stress inside a strut, with stress-free concrete immediately next to it, and biaxially stressed concrete in the nodes at its ends).

In spite of the evolution of computational tools over the past decades, stress fields and strut-and-tie models are essentially still being used as hand calculations. This makes their application tedious and time-consuming since iterations are required, and several load cases need to be considered when dealing with real-life structures. Furthermore, the checking of concrete dimensions is based on semi-empirical, somewhat arbitrary rules for the effective concrete compressive strength, undermining the mechanical consistency of the methods, and it is impossible to verify deformation capacity – particularly with regard to reinforcement ductility. In addition, these methods are not suitable for checking serviceability criteria (deformations, crack widths, etc.). Hence, due to the lack of efficiency and the need to recur to other models for serviceability checks in any case, designers tend to favor linear elastic finite element wall analyses over strut-and-tie

models and stress fields, despite the often impractical and inefficient reinforcement layouts obtained. The latter problem occurs because such linear elastic analyses completely neglect the non-symmetric strength of concrete and the non-isotropic behavior (even in the case of orthogonal, isotropic reinforcement) of reinforced concrete during the calculation of internal forces, and only account for these effects in the post-processing stage, i.e., when dimensioning the reinforcement and checking the dimensions of concrete, which is typically carried out using yield conditions based on plasticity theory.

While existing general non-linear FE programs overcome the aforementioned oversimplifications of linear elastic analysis and allow real structural behavior to be replicated providing correct mechanical models and material parameters are defined, these methods are not suitable for design purposes. The complexity of the implemented mechanical methods requires very high amounts of expertise and modeling time, while the results can be very sensitive to the choice of material parameters that were unknown during the design phase. Furthermore, the mechanical models implemented in non-linear FE analyses typically are not code-compliant, as their hypotheses differ very significantly from those of classical reinforced concrete design (e.g., concrete tensile stresses often contribute to the resistance of the members in NLFEA) and the partial safety factor format cannot be applied. In consequence, non-linear FE analysis is only useful for research and assessment purposes.

The tendency towards using either linear elastic wall calculations or general non-linear FE analysis, which is already strong today, is being fostered by the development of increasingly powerful and user-friendly programs for such analyses. As a result, it can be anticipated that the application of strut-and-tie models and stress fields will soon be limited to the realms of engineering education unless equally user-friendly computer programs that allow efficient analysis based on strut-and-tie models and stress fields become available soon. Hence, in order to exploit the potential of stress fields and strut-and-tie models in terms of economical design and practical reinforcement layouts in the future, it is essential to develop computer programs that overcome their drawbacks without impairing their advantages of transparency and the control they provide over the design produced.

1.2 Computer-aided truss models and stress fields

Several attempts to develop programs for computer-aided truss modeling have been made over the past decades. Many existing applications implementing strut-and-tie models for specific regions, such as corbels and pile caps, have had limited impact due to their restricted scope. Only a few tools, such as CAST (Tjhin and Kuchma 2002) and AStrutTie (2017), are more general and allow the design of arbitrary discontinuity regions. Although these applications are very interesting, they have not found widespread application in engineering practice to date, presumably because the user has to devise an initial strut-and-tie model and assign a “correct” effective concrete compressive strength to each individual truss member or node. In spite of being implemented in

a computer program, this process is typically still time-consuming, affects user-friendliness and efficiency, and is somewhat arbitrary.

These problems are avoided with the elastic-plastic stress field method (EPSF), developed by Fernández Ruiz and Muttoni (2007). The method achieves this by considering continuous stress fields rather than strut-and-tie models, and by determining the effective concrete compressive strength from transverse strains, as specified by modern design codes. This is similar as in compression field analyses accounting for compression softening (Vecchio and Collins 1986; Kaufmann and Marti 1998). Basically, this method constitutes a simplified version of nonlinear finite element analysis. Contrary to general nonlinear FE calculations, however, only standard material parameters known at the design stage are required as input. The EPSF method yields excellent failure load predictions (Muttoni et al. 2015), but its user-friendliness is limited since it was not developed as a commercial program. Moreover, since it neglects tension stiffening, the EPSF method cannot be directly used for serviceability checks, nor can it be employed for elements with insufficient deformation capacity.

1.3 The Compatible Stress Field Method

This book presents the principles and a validation of the Compatible Stress Field Method (also referred to in the book as the CSFM), a new method for the design and assessment of concrete structures particularly suitable for so-called *discontinuity regions*, for which it overcomes the aforementioned limitations of classical design tools and existing computer-aided models while keeping the advantages of stress fields and strut-and-tie models:

- Only material parameters that are perfectly known at the design stage are required as input, neglecting concrete tensile strength for equilibrium (ensuring code-compliance).
- A clear understanding of the force flow is provided.
- The user has full control over the design.

The CSFM, similarly as EPSF, consists of a simplified non-linear finite element-based continuous stress field analysis procedure that automatically computes the effective compressive strength of concrete. By considering equilibrium at stress-free cracks, simple uniaxial constitutive laws provided in concrete standards for concrete and reinforcement are implemented without the need for the additional material properties required to perform nonlinear FE analyses. This makes the CSFM suitable for engineering practice.

While the concrete tensile strength is neglected in terms of strength (just as in standard structural concrete design), the CSFM accounts for its influence on members stiffness (i.e., tension stiffening) in order to cover all design code prescriptions, including serviceability, load-deformation and deformation capacity aspects, which are not consistently addressed by previously formulated approaches.

The CSFM has been implemented in *IDEA StatiCa Detail*, a new user-friendly commercial software program developed jointly by ETH Zurich and the software company IDEA StatiCa as part of the DR-Design Eurostars-10571 project. Unless stated otherwise, all of the verifications included in Chapters 4, 5 and 6 were carried out with *IDEA StatiCa Detail 9.1*, which was released in October 2018.

1.4 Outline

Chapter 2 of this book provides an overview of the historical development and theoretical background of structural concrete design with strut-and-tie models and stress fields. This lays the groundwork for an in-depth presentation of the Compatible Stress Field Method in Chapter 3.

Chapters 4, 5 and 6 cover the verification of the CSFM and its implementation in *IDEA StatiCa Detail 9.1* software. Chapter 4 validates the proper numerical implementation of the mechanical models of the CSFM by means of the simple cases of pure tension, pure compression and pull-out loading. Chapter 5 compares the results of the CSFM with code calculations for several examples, and Chapter 1 finally verifies the method by comparing analyses carried out using the CSFM with experimental results covering a wide range of applications.

Finally, Chapter 7 summarizes and discusses the results obtained in the previous sections.

1.5 Acknowledgments

This work is part of the DR-Design Eurostars-10571 project and has received partial funding from the Eurostars-2 joint program with co-funding from the European Union Horizon 2020 research and innovation program. The authors would like to express their gratitude to all the people who contributed to this book, from researching to sharing their ideas and experiences to editing the content of the manuscript: Petr Sevcik, Libor Michalcik, Rostislav Krc, Filip Svoboda, Petr Foltyn, Filip Adler, Lukas Juricek, Lukas Bobek and Roger Turland.

2 Structural concrete design with strut-and-tie models and stress fields

2.1 Introduction

This chapter provides an overview of the historical development and theoretical background of structural concrete design with strut-and-tie models and stress fields in order to prepare the ground for the presentation of the Compatible Stress Field Method in the following chapter.

2.2 Historical background

Strut-and-tie models and stress fields are popular methods for the design, dimensioning and detailing of concrete structures. They are particularly suitable for what are known as *discontinuity regions,* where abrupt changes in geometry and/or concentrated loads render Bernoulli's hypothesis of plane sections remaining plane inappropriate, meaning that the design of such regions cannot be based on a sectional analysis. Strut-and-tie models and stress fields are lower bound limit analysis methods based on the theory of plasticity, as opposed to kinematic or upper bound methods based on the same theory, such as the yield line method (Johansen 1962).

The origins of limit analysis methods date back to the early days of reinforced concrete. For example, Ritter (1899) and Mörsch (1908-1920) sketched truss models and even stress fields to explain the load-bearing behavior of reinforced concrete (Fig. 2.1a-b); Ingerslev (1923) analyzed the failure mechanisms of slabs (Fig. 2.1c); Marcus (1932) designed slabs by sharing the load among orthogonal strips (Fig. 2.1d); and Rosenblueth (1955) visualized the equilibrium of membrane elements using Mohr's circles (Fig. 2.2a) in a manner very similar to that of current compression field approaches (Fig. 2.2b). However, these methods, particularly truss models and stress fields, did not become established as scientific methods and, consequently, were not widely used in the actual dimensioning of reinforced concrete structures. Instead, design codes were mainly based on the comparison of elastically determined stresses (e.g., principal tensile stresses in the webs of girders) to admissible values. When calculating elastic stresses, it was usually implicitly assumed that the loading history was exactly known, and those structural systems were free from residual stresses and restraints. This hardly ever applies in the case of real structures, as pointed out by Melan (1938): "*Da […] die Reihenfolge der Belastungen willkürlich zu sein pflegt, hat die Frage nach einem Spannungszustand bei einer bestimmten Belastung keinen Sinn {Since […] the sequence of loading is typically arbitrary, asking for the state of stress under a certain load does not make sense}*". Melan's observation is particularly true for concrete structures, where the initial stresses caused by the restraint of imposed deformations (such as shrinkage strains), construction stages and other factors, are indeed largely unknown. In spite of this, admissible stress design continued to be used until the second half of the 20th century. It was only

through the advent of the theory of plasticity that truss models and stress fields, and limit analysis methods in general, were given a solid theoretical basis, opening the way for their implementation in design codes.

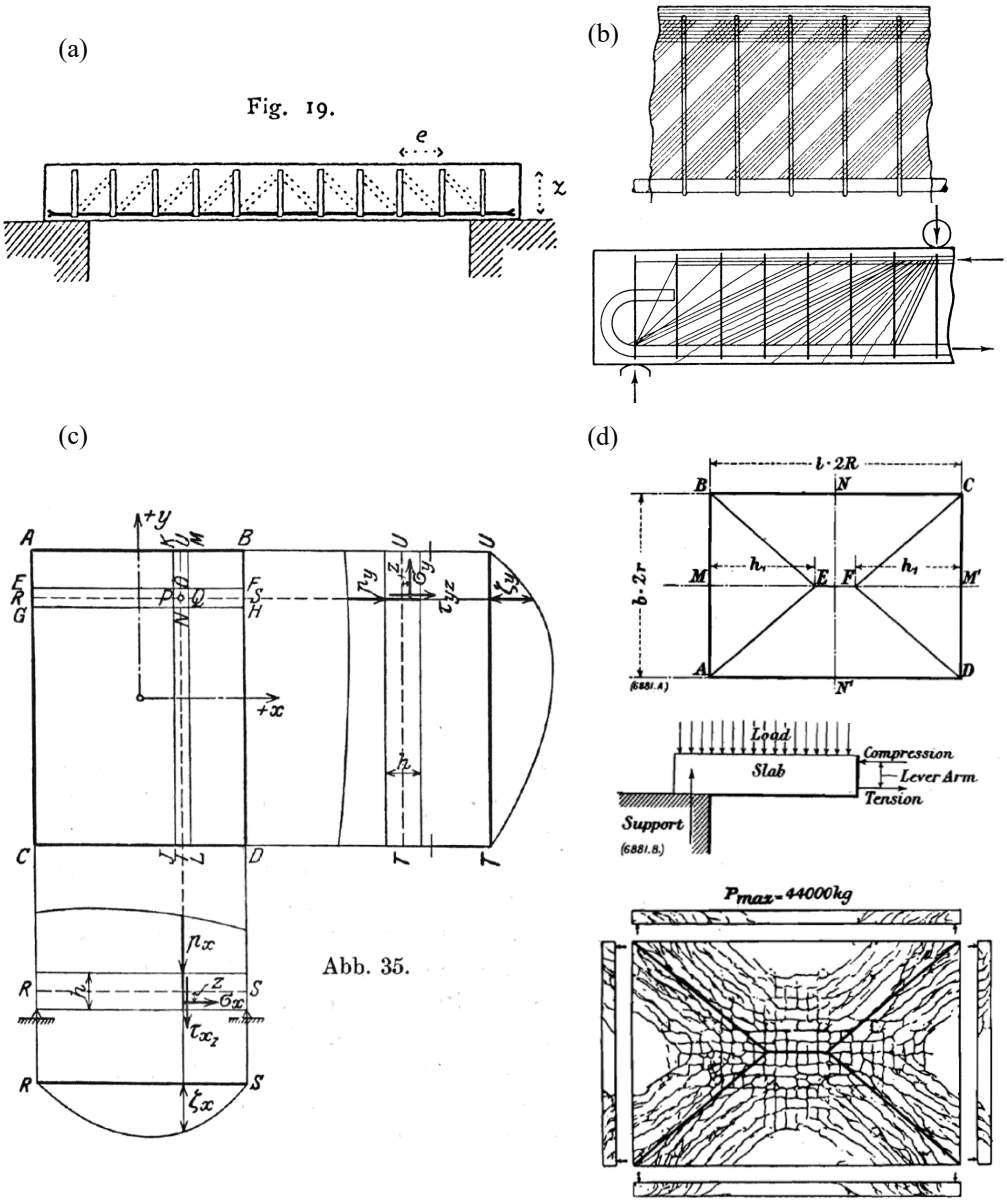

Abb. 35.

Fig. 2.1. Early design methods for concrete structures: (a) Ritter (1899), explanation of Hennebique's construction system with a truss; (b) Mörsch (1908) , truss model and stress field; (c) Marcus (1932), load sharing among orthogonal strips in a slab; (d) Ingerslev (1923), equilibrium at the rigid parts of a failure mechanism in a slab.

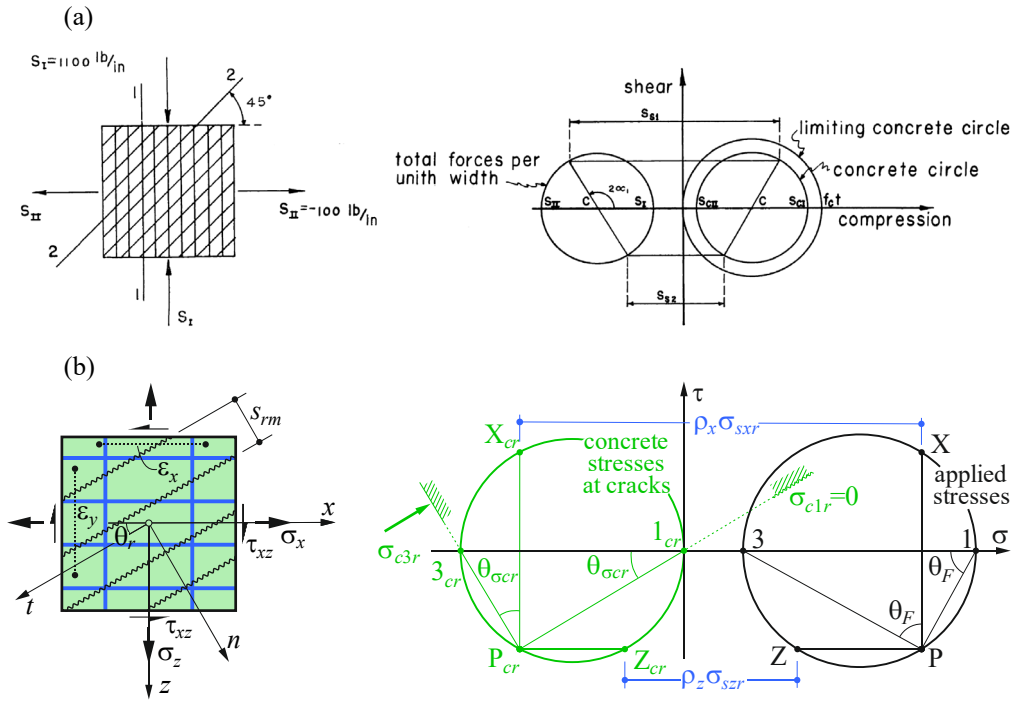

Fig. 2.2. Graphic design of membrane elements: (a) Rosenblueth (1955), equilibrium using Mohr's circles; (b) current compression field approaches.

2.3 Limit analysis methods

2.3.1 Theorems

Limit analysis methods solve the intrinsic problem of admissible stress design: If sufficient ductility is ensured, the ultimate load is independent of residual stresses and restraints. Assuming perfectly plastic behavior and postulating the principle of maximum dissipation energy (or, equivalently, applying the theory of plastic potential, i.e., convexity of the yield condition and orthogonality of the plastic strain increments to the yield surface), the following theorems can be derived (wording extracted from Marti (2013)):

The *lower bound theorem*: Every loading for which it is possible to specify a statically admissible stress state (i.e., a stress state satisfying equilibrium and static boundary conditions) that does not infringe the yield condition is not greater than the ultimate load.

The *upper bound theorem*: Every loading that results from equating the work of external forces for a kinematically admissible deformation state with the associated dissipation work is not less than the limit load.

The application of these theorems leads to the so-called static and kinematic methods of limit analysis, which define lower and upper bounds for the ultimate load, allowing it to be bracketed.

If the upper and lower bound coincide, the actual ultimate limit load is found. In this case it is neither necessary to verify the existence of a statically admissible stress state for the governing deformation state, nor to identify a kinematically admissible deformation state for the governing stress state; this is known as the *compatibility theorem*.

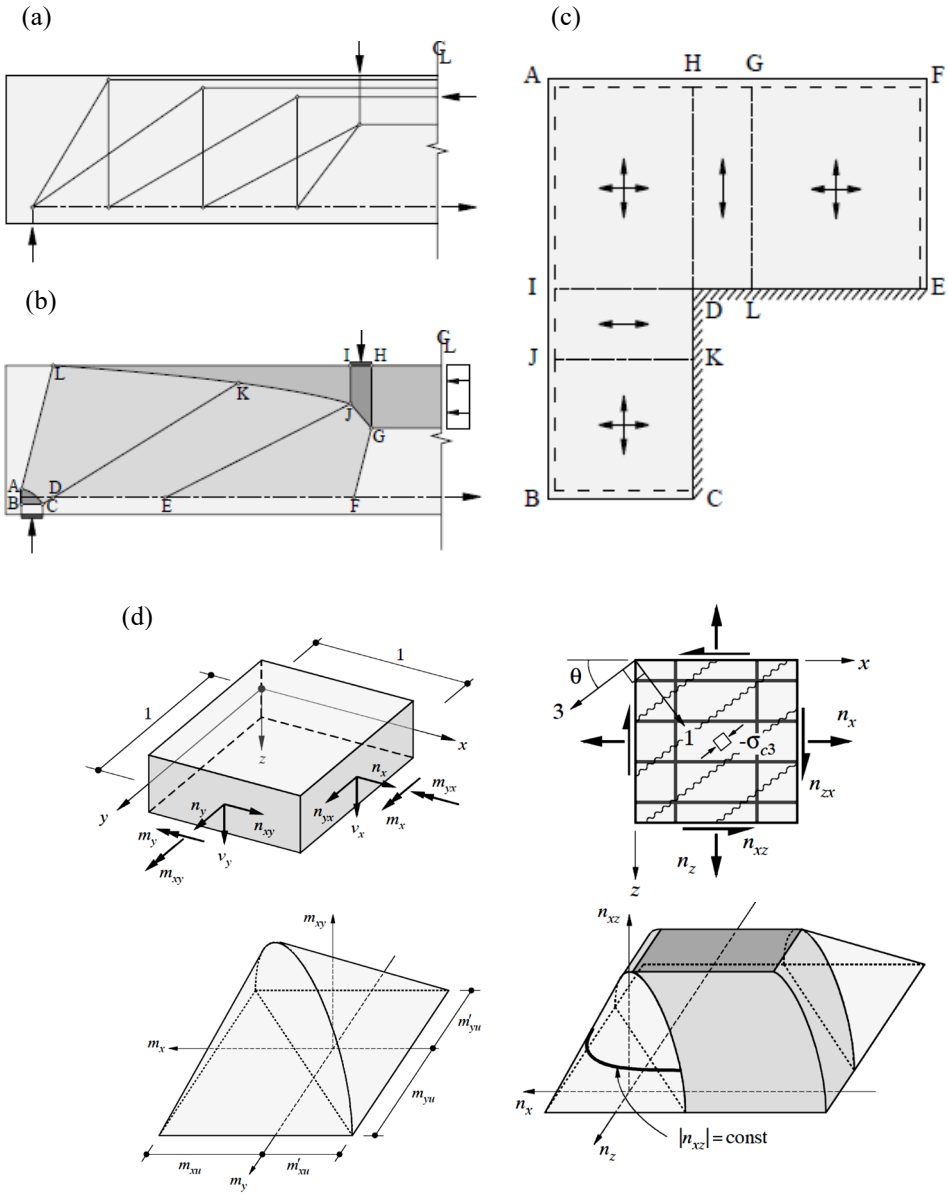

Fig. 2.3. Examples of modern lower bound solutions of limit analysis: (a) Truss model and (b) corresponding, statically equivalent stress field; (c) Hillerborg's strip method; (d) yield conditions for slab and membrane elements. Adapted from Marti et al. (1999).

2.3.2 Application to structural concrete

In the second half of the last century, pioneers like Nielsen (1984) and Thürlimann et al. (1983) dared to apply the theory of plasticity to reinforced concrete. They were, of course, fully aware of the limited ductility of concrete and even reinforcement. Therefore, they completely neglected the tensile strength of concrete and addressed further concerns regarding ductility by providing minimum reinforcement (to avoid its rupture at cracking) and using conservative limits for the effective concrete compressive strength, as well as upper limits for the reinforcement quantities and corresponding compression zone depths (to avoid brittle failures due to concrete crushing).

Furthermore, they performed large-scale tests on structural elements to validate the results of limit analysis design, which was key to overcoming the initially fierce opposition that the pioneers of limit analysis were facing from many colleagues that were still advocating the use of the theory of elasticity. Later on, extensive investigations into the deformation capacity of structural concrete were carried out in order to determine the limits of applicability of limit analysis methods (e.g., Vecchio and Collins (1986), Sigrist (1995), Alvarez (1998), Kaufmann (1998), Marti et al. (1998), Hoang and Nielsen (1998)). The results of these investigations are partly reflected in current design codes, e.g. through limits for moment redistribution in hyperstatic girders, bounds for the inclination of compression struts or compressive stress bands and, in particular, detailed rules for the determination of effective concrete compressive strength.

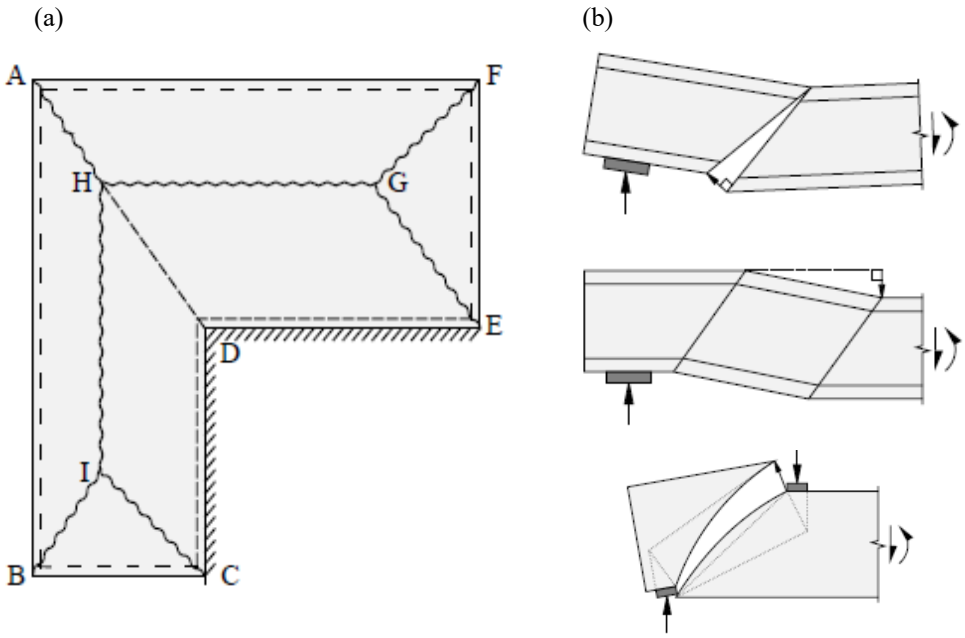

Fig. 2.4. Examples of modern upper bound limit solutions of limit analysis: (a)Yield line method; (b) failure mechanisms of beams and walls. Adapted from Marti et al. (1999).

Lower bound solutions (Fig. 2.3) provide a uniform basis for the safe design of concrete structures, and they often allow straightforward reinforcement design based on applied loads, including the consistent dimensioning and detailing of reinforcement with respect to the overall flow of forces. These aspects make them suitable for application in engineering practice, and consequently many provisions in modern design codes are based on lower bound limit analysis solutions. While upper bound approaches (Fig. 2.4) have not reached the same level of acceptance in engineering practice, they are powerful tools for the strength assessment of existing structures (Marti et al. 1999).

2.4 Strut-and-tie models and stress fields

Strut-and-tie models and stress fields are popular tools in engineering practice because they yield direct insight into load-carrying behavior and allow the dimensioning of reinforcement according to practical considerations. They share a mechanical basis through plasticity theory and are consistent with the lower bound theorem presented in the previous section. Hence, strut-and-tie models and stress fields typically result in conservative designs provided that sufficient deformation capacity is available. While they are commonly used for the design of discontinuity regions, they can essentially be applied for the dimensioning and detailing of any concrete region, and entire structures as well.

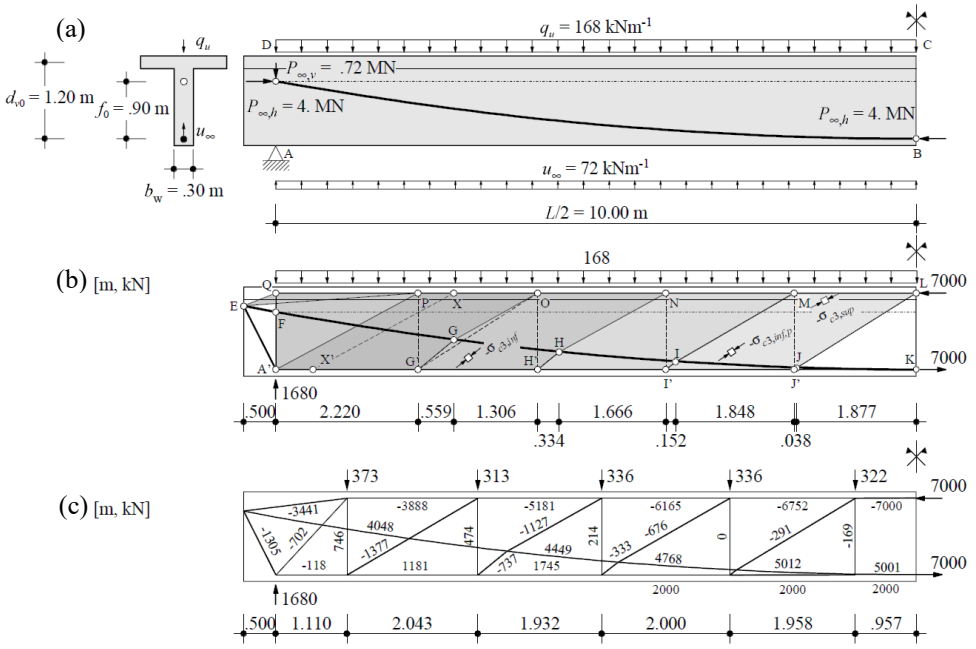

Fig. 2.5. Examples of lower bound solutions for a T-beam with a post-tensioning cable: (a) Geometry and loads; (b) stress fields; (c) corresponding, statically equivalent strut-and-tie model. Figure adapted from Marti and Stoffel (1999).

Fig. 2.3a, b and Fig. 2.5 show examples of statically equivalent stress fields and strut-and-tie models for beams with point loads and distributed loads, including a post-tensioning cable. In these examples, the dimensions are consistently linked to the concrete compressive strength for both the stress fields as well as the strut-and-tie models, which is a prerequisite to finding strict lower bound solutions. However, strictly linking the dimensions to the concrete strength may severely complicate calculations, as iterative procedures (or the solution of differential equations) are required to define the geometry. If concrete strut and node dimensions are only linked to the concrete compressive strength at selected, often obviously critical locations within the structure (as promoted, e.g., by Schlaich et al. (1987)), the design process is much simpler. While lacking the rigor of the strict solutions, this type of approach has certainly helped to popularize the equilibrium-based analysis of discontinuity regions, as well as to extend their applicability to any kind of concrete region. In fact, simplified strut-and-tie models and stress fields strictly based on concrete compressive strength are best used as complementary tools when detailing concrete regions. Designers can typically start with simple strut-and-tie models of a structure and refine them whenever necessary by replacing the truss members with struts, ties, nodes, fans and arches with finite dimensions that respect the concrete compressive strength and the reinforcement layout, leading to stress fields. A detailed description of the basic elements of strut-and-tie models and stress fields can be found elsewhere (Marti 1985).

Strut-and-tie models consider a rigid, ideally plastic behavior of the material, without any kinematic considerations. Hence, even when assigning approximate elastic stiffnesses to the struts and ties, serviceability criteria (deformations, crack widths, etc.) cannot be reliably verified by using these methods, and the verification of the ductility requirements can only be carried out based on empirical rules. Moreover, as these tools are typically applied as hand calculations, their use is tedious and time-consuming since iterations are required and several load cases need to be considered in real-life structures. All these drawbacks can be overcome when considering kinematic compatibility and assigning appropriate stiffness and ductility to the materials, as is performed in the computer-aided stress field analysis presented in this book.

2.5 Code provisions

Strut-and-tie models are currently included in most design codes as a consistent tool for concrete detailing in general that is particularly suitable for use where a non-linear strain distribution exists. A brief summary based mainly on the provisions of ACI 318-14, EN 1992-1-1 and *fib* Model Code 2010 is given below.

Ties

The amount of reinforcement required in ties is typically designed neglecting concrete tensile strength and considering the design yield strength of the reinforcement:

$$f_{yd} = \frac{f_{yk}}{\gamma_s} \tag{2.1}$$

where f_{yk} denotes the characteristic yield strength of the reinforcement and γ_s its safety coefficient.

For ties representing the resultant of a tensile field with finite dimensions, the required reinforcement should be distributed over the entire tensile field.

Struts

The dimensioning of struts is carried out considering the effective concrete compressive strength as follows:

$$f_{cd} = \frac{f_{ck,red}}{\gamma_c} = \frac{k_c \cdot f_{ck}}{\gamma_c} \tag{2.2}$$

where f_{ck} denotes the concrete cylinder characteristic strength, γ_c is the concrete safety coefficient and k_c is a reduction factor that accounts for different phenomena, such as the softening effect of cracked concrete, the increase in concrete brittleness with strength, and long term loading effects.

Table 2.1. Concrete compressive strength reduction factors for plastic analysis (k_c) specified by different design codes for various states of stress.

	Undisturbed uni-axial compression	Tension normal to the direction of compression	Tension oblique to the direction of compression
	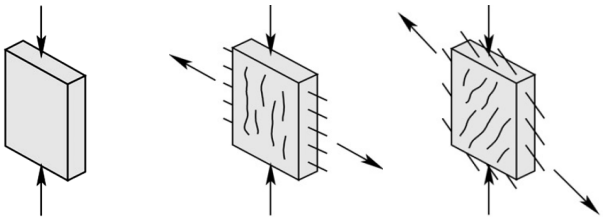		
EN 1992-1-1	1.00	$0.60 \cdot \nu'$	
(f_{ck}=30 MPa)		(0.53)	
(f_{ck}=50 MPa)		(0.48)	
fib MC 2010	$1.00 \cdot \eta_{fc}$	$0.75 \cdot \eta_{fc}$	$0.55 \cdot \eta_{fc}$
(f_{ck}=30 MPa)	(1.00)	(0.75)	(0.55)
(f_{ck}=50 MPa)	(0.84)	(0.63)	(0.46)
SIA 262:2013	$1.00 \cdot \eta_{fc}$	$0.80 \cdot \eta_{fc}$	$0.55 \cdot \eta_{fc}$
(f_{ck}=30 MPa)	(1.00)	(0.80)	(0.55)
(f_{ck}=50 MPa)	(0.84)	(0.67)	(0.46)
EHE-08	1.00	0.70	0.60

The reduction of compressive strength is typically specified by design codes for different stress states with small variations depending on the compressive strength, as indicated in Table 2.1. ACI 318-14 proposes a more complex classification to evaluate the softening level, which includes the presence or absence of a certain amount of transverse reinforcement. The application of these code provisions to real structures is challenging even for experienced designers, as some regions do not clearly fit the existing classifications. In this sense, it should be noted that some codes, e.g., EN 1992-1-1 , allow the use of alternative, more rigorous approaches. The Compatible Stress Filed Method (CSFM) presented in this book is such an approach, as explained in the next chapter.

Besides these provisions regarding the reduction factors for cracked concrete, design codes also allow the uniaxial concrete compressive strength to be increased when confinement conditions can result in a triaxial compressive state.

Nodal zones

Just as with struts, the verification of nodal zones is code dependent. Design code provisions only cover simple cases concerning nodal areas. As an example, Fig. 2.6 illustrates the verification models included in EN 1992-1-1.

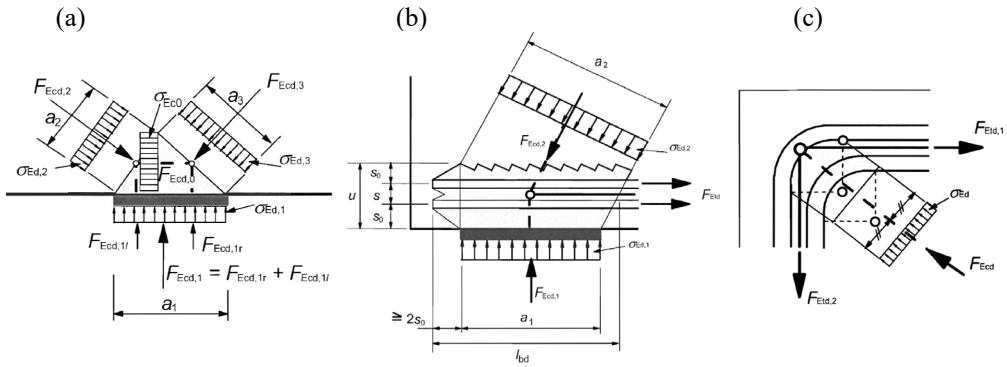

Fig. 2.6. Models for the verification of nodal zones according to EN 1992-1-1:
(a) Compression node without ties; (b)-(c) compression-tension nodes with reinforcement provided in one and two directions, respectively.

Further provisions

Apart from the discussed verifications of the basic elements composing the models, additional guidelines usually need to be respected when conceiving stress fields and strut-and-tie models. These guidelines are specified in order to implicitly guarantee proper serviceability behavior and sufficient deformation capacity, which essentially are prerequisites for the application of plastic design methods like stress fields and strut-and-tie models. Among the guidelines which are typically specified are the following:

- Minimum reinforcement and detailing rules.
- Minimum values for the angles between the struts and ties (e.g., according ACI 318-14 at least 25º is required).
- Reduced values for steel stresses compared to the design strength of the reinforcement used for strength verifications (e.g., in EHE-08 a maximum stress of 400 MPa is specified, while for conventional European reinforcement with f_{yk}=500 MPa the design yield strength is typically 435 MPa).
- In order to limit the amount of plastic redistribution required, stress fields should not differ excessively from the cracked-elastic or uncracked stress field.

While it is recommended that these guidelines be followed, it should be noted that they are somewhat arbitrary and based mainly on empirical observations. More importantly, they (i) do not always guarantee proper serviceability behavior (as in the case of, e.g., dapped-end beams, as reported by Mata-Falcón (2015)) and (ii) are not applicable to innovative materials with different properties from conventional concrete and reinforcement.

When kinematic compatibility is introduced to these models, and the stiffness and ductility of the materials are defined by means of mechanically consistent models, these issues are solved, as serviceability aspects and deformation capacity can be directly verified. Such a model is presented in the following chapter.

3 The Compatible Stress Field Method

3.1 Scope of the method

This chapter presents the principles of the Compatible Stress Field Method (also referred to hereinafter as the CSFM), a method for computer-aided stress field design that allows the automatic design and assessment of structural concrete members subjected to in-plane loading, i.e., beams, walls and, in particular, discontinuity regions.

The method consists of a compatible, FE-based stress field analysis. The classic stress field solutions discussed in Chapter 2 are complemented with kinematic considerations, i.e., the state of strain is evaluated throughout the structure. Hence, the effective compressive strength of concrete (see Section 2.5) can be automatically computed based on the state of transverse strain in a similar manner as in compression field analyses that account for compression softening (Vecchio and Collins 1986; Kaufmann and Marti 1998), or the EPSF method (Fernández Ruiz and Muttoni 2007). Moreover, the CSFM considers tension stiffening, providing realistic stiffnesses to the elements and covering all design code prescriptions (including serviceability and deformation capacity aspects), which are not consistently addressed by previous approaches. As will be described in Section 3.3, the CSFM uses exclusively common uniaxial constitutive laws provided by design standards for concrete and reinforcement. These are known at the design stage, which allows the partial safety factor method to be used. Hence, designers do not have to provide additional, often arbitrary material properties as are typically required for nonlinear FE-analyses, making the method perfectly suitable for engineering practice.

To foster the use of computer-aided stress fields by structural engineers, these methods need to be implemented in user-friendly software environments. To this end, the CSFM has been applied in *IDEA StatiCa Detail*, a new user-friendly software tool developed jointly by ETH Zurich and the software company IDEA StatiCa within the DR-Design Eurostars-10571 project. In the program, the geometry and loading of the region of interest can be defined by itself (standalone use) or imported from other programs (e.g., frame corners from a frame analysis). Subsequently, users can specify the reinforcement layout based on experience or by making use of linear elastic stress trajectories and a topology optimization algorithm, both of which are implemented in the program as support tools (see Section 3.4.2). In the next step, the program adjusts the amounts of reinforcement that the user wants to be dimensioned, following the procedure described in Section 3.4. The last step comprises the verification process (see Section 3.4.3), where the program performs ultimate limit state (ULS) and serviceability limit state (SLS) analyses for the different load combinations, carrying out all required checks, including deformations and crack widths.

The details of the implementation of the CSFM into *IDEA StatiCa Detail* software are given in Section 3.6, which also provides additional details regarding the constitutive relationships for anchorage length verifications that were preliminarily introduced in Section 3.3.

3.2 Main assumptions and limitations

The CSFM assumes fictitious, rotating, stress-free cracks that open without slip (see Fig. 3.1a) and considers the equilibrium at the cracks together with the average strains of the reinforcement. Hence, the model considers maximum concrete (σ_{c3r}) and reinforcement stresses (σ_{sr}) at the cracks while neglecting the concrete tensile strength ($\sigma_{c1r}=0$), except for its stiffening effect on the reinforcement. The consideration of tension stiffening allows the average reinforcement strains (ε_m), and hence the overall stiffness, to be realistically captured.

According to the assumptions of the model, the principal directions of stresses and strains coincide, and the behavior of the principal directions in the cracked state is decoupled except for the compression softening effect (see Section 2.5). This justifies the use of the simple uniaxial laws presented in the following sections.

In spite of their simplicity, similar assumptions have been demonstrated to yield accurate predictions for reinforced members subjected to in-plane loading (Kaufmann 1998; Kaufmann and Marti 1998) if the provided reinforcement avoids brittle failures at cracking. Furthermore, neglecting any contribution of the tensile strength of concrete to the ultimate load is consistent with the principles of modern design codes.

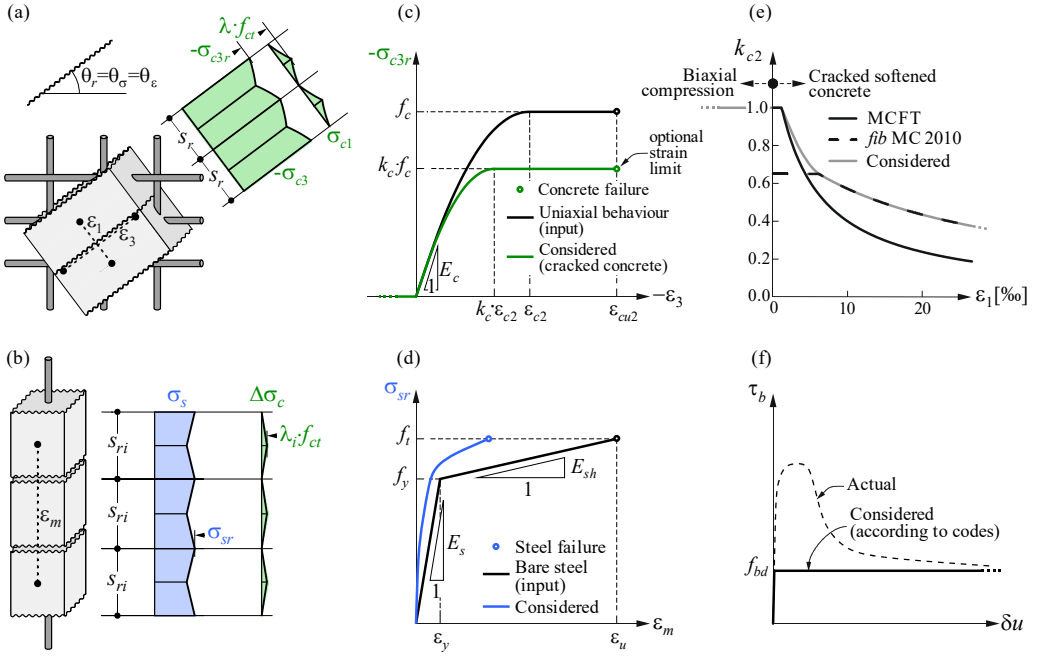

Fig. 3.1 Basic assumptions of the CSFM: (a) Principal stresses in concrete; (b) stresses in the reinforcement direction; (c) stress-strain diagram of concrete in terms of maximum stresses with consideration of compression softening (for $\varepsilon_1>0$ and $\varepsilon_3<0$); (d) stress-strain diagram of reinforcement in terms of stresses at cracks and average strains; (e) compression softening law; (f) bond shear stress-slip relationship for anchorage length verifications.

However, the method is not suited for slender elements without transverse reinforcement, since relevant mechanisms for such elements as aggregate interlock, residual tensile stresses at the crack tip and dowel action – all of them relying directly or indirectly on the tensile strength of the concrete – are disregarded. While some design standards allow the design of such elements based on semi-empirical provisions, the CSFM is not intended for this type of potentially brittle structure.

3.3 Constitutive models

3.3.1 Concrete

The concrete model implemented in the CSFM is based on the uniaxial compression constitutive laws prescribed by design codes for the design of cross-sections, which only depend on the concrete compressive strength. The parabola-rectangle diagram specified EN 1992-1-1 (Fig. 3.1c) is used by default in the CSFM, but designers can also choose a more simplified elastic-ideally plastic relationship. As previously mentioned, the tensile strength is neglected, as it is in classic reinforced concrete design.

The effective compressive strength is automatically evaluated for cracked concrete based on the principal tensile strain (ε_1) by means of the k_{c2} reduction factor, as shown in Fig. 3.1c-e. The implemented reduction relationship (Fig. 3.1e) is a generalization of the *fib* Model Code 2010 proposal for shear verifications, which contains a limiting value of 0.65 for the maximum ratio of effective concrete strength to concrete compressive strength, which is not applicable to other loading cases. This compression softening law is consistent with the main assumptions (see section 3.2) since it is also derived in terms of maximum stresses at the cracks. As outlined in Kaufmann et al. (2018), the reduction of the concrete compressive strength derived in terms of average stresses (i.e., accounting for the contribution of concrete tensile stresses to the strength), as is found in, e.g., the Modified Compression Field Theory (MCFT) by Vecchio and Collins (1986) (Fig. 3.1e), may be excessive when applied to models such as the CSFM, which consider maximum stresses at cracks (i.e., without any contribution from concrete in tension).

Using default settings, the current implementation of the CSFM in *IDEA StatiCa Detail* does not consider an explicit failure criterion in terms of strains for concrete in compression (i.e., it considers a quasi-infinitely plastic branch after the peak stress is reached, which has a very large strain limit to merely ensure numerical stability, as described in Section 3.6.7). This simplification does not allow the deformation capacity of structures failing in compression to be verified. However, their ultimate capacity is properly predicted when, in addition to the factor of cracked concrete (k_{c2} defined in Fig. 3.1e), the increase in the brittleness of concrete as its strength rises is considered by means of the η_{fc} reduction factor defined in *fib* Model Code 2010 as follows:

$$f_{cd} = \frac{f_{ck,red}}{\gamma_c} = \frac{k_c \cdot f_{ck}}{\gamma_c} = \frac{\eta_{fc} \cdot k_{c2} \cdot f_{ck}}{\gamma_c} \qquad \left(\eta_{fc} = \left(\frac{30}{f_{ck}} \right)^{\frac{1}{3}} \leq 1 \right) \tag{3.1}$$

where k_c is the global reduction factor of the compressive strength, k_{c2} is the reduction factor due to the presence of transverse cracking and f_{ck} is the concrete cylinder characteristic strength (in MPa for the definition of η_{fc}). Note that the use of this approach is consistent with classical strut-and-tie models, where the effective compressive strength of the concrete is limited according to Eq. (3.1) without any consideration of deformations, i.e., allowing arbitrary, potentially very large strains in the struts and ties.

Alternatively, an explicit concrete compression check, defined by the ultimate strain limit allowed by design codes (ε_{cu2}), can be set. In this case, the CSFM directly verifies the deformation capacity for structures failing in compression, and the use of a η_{fc} coefficient is not required. To prevent the strains from exhibiting local mesh size dependency, the strain limit should be imposed on an average strain calculated over a characteristic crushing band length. The characteristic crushing band length has to be set by the user, but a small value lying between the depth of the compression zone and the thickness of the section is recommended. In *IDEA StatiCa Detail 9.1* only advanced users can use this alternative approach, which involves manually defining the characteristic crushing band length in which the program should average the strains. The verifications presented in Chapters 4 and 5 were carried out considering an infinite plastic branch of concrete in compression, while in all the verifications of Chapter 6 a strain limit $\varepsilon_{cu2} = 3.5‰$ was imposed over a crushing length equal to the thickness of the region.

It should be noted that the concrete model used in serviceability analysis differs from that presented above (used for ultimate limit state), which enables it to consider the effect of long-term actions. The particularities of the model for serviceability verifications will be given in Section 3.5.3.

3.3.2 Reinforcement

By default, the idealized bilinear stress-strain diagram for the bare reinforcing bars typically defined by design codes (Fig. 3.1d) is considered. The definition of this diagram only requires basic properties of the reinforcement to be known during the design phase (strength and ductility class). Whenever known, the actual stress-strain relationship of the reinforcement (hot-rolled, cold-worked, quenched and self-tempered, …) can be considered. While an elastic-ideally plastic formulation (as used in the EPSF method) could also be used, this would not allow the deformation capacity to be verified due to the lack of explicit failure criteria.

Tension stiffening is accounted for by modifying the input stress-strain relationship of the bare reinforcing bar in order to capture the average stiffness of the bars embedded in the concrete (ε_m). The implementation of tension stiffening will be discussed in Section 3.3.4.

3.3.3 Verification of anchorage length

Bond-slip between reinforcement and concrete is introduced in the finite element model for ultimate limit state load cases by considering the simplified rigid-perfectly plastic constitutive relationship presented in Fig. 3.1f, with f_{bd} being the design value of the ultimate bond stress specified by the design code for the specific bond conditions. The details of the constitutive relationship that ensures the numerical stability of this model will be presented in Section 3.6.5. This is a

simplified model with the sole purpose of verifying bond prescriptions according to design codes (i.e., anchorage of reinforcement). The reduction of the anchorage length when using hooks, loops, and similar bar shapes can be considered by defining a certain capacity at the end of the reinforcement, as will be described in Section 3.6.5. It should be noted that a different bond shear stress-slip model is considered for tension stiffening (Section 3.3.4) and crack width calculations (Section 3.5). In such cases, the model considers average bond shear stresses instead of characteristic values in order to capture the average behavior of the elements.

3.3.4 Tension stiffening

The implementation of tension stiffening distinguishes between cases of stabilized and non-stabilized crack patterns. In both cases, the concrete is considered fully cracked before loading by default, but the initial uncracked stiffness can be taken into account for research purposes.

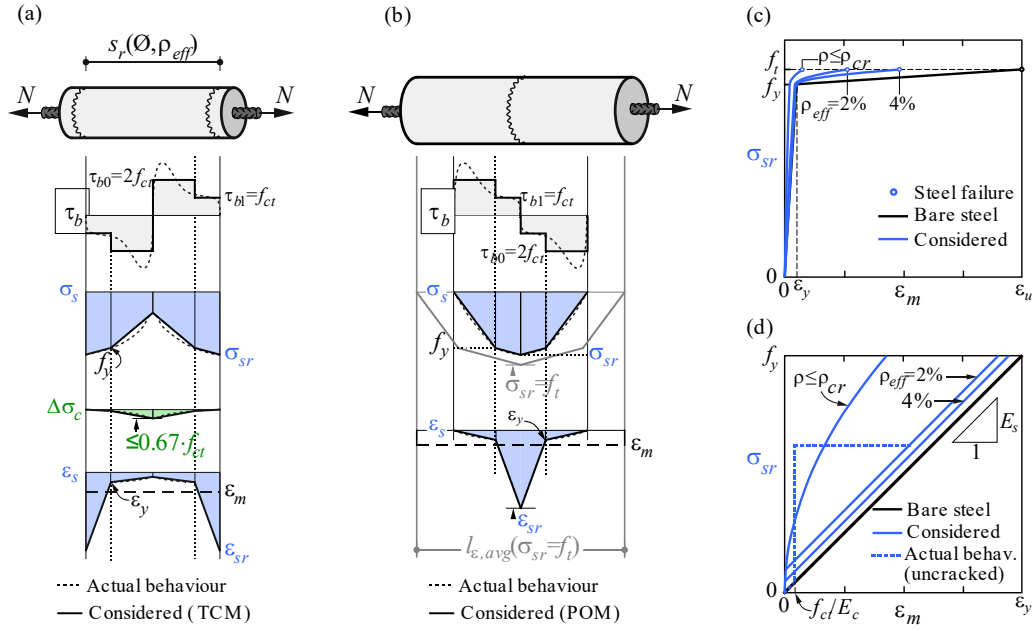

Fig. 3.2 Tension stiffening model: (a) Tension chord element for stabilized cracking with the distribution of bond shear, steel and concrete stresses, and steel strains between cracks, considering average crack spacing (λ=0.67); (b) pull-out assumption for non-stabilized cracking with the distribution of bond shear and steel stresses and strains around the crack; (c) resulting tension chord behavior in terms of reinforcement stresses at the cracks and average strains for European B500B steel; (d) detail of the initial branches of the tension chord response.

Stabilized cracking

In fully developed crack patterns, tension stiffening is introduced using the Tension Chord Model (TCM) (Marti et al. 1998; Alvarez 1998) – Fig. 3.2a – which has been shown to yield excellent

response predictions in spite of its simplicity (Burns 2012). The TCM assumes a stepped, rigid-perfectly plastic bond shear stress-slip relationship with $\tau_b = \tau_{b0} = 2f_{ctm}$ for $\sigma_s \leq f_y$ and $\tau_b = \tau_{b1} = f_{ctm}$ for $\sigma_s > f_y$. Treating every reinforcing bar as a tension chord – Fig. 3.1b and Fig. 3.2a – the distribution of bond shear, steel and concrete stresses and hence the strain distribution between two cracks can be determined for any given value of the maximum steel stresses (or strains) at the cracks by equilibrium. Limiting σ_{c1} to a maximum value of f_{ct} at the center between two cracks, the theoretical maximum value of the crack spacing of the chord, s_{r0}, can be calculated as follows:

$$s_{r0} = \frac{\varnothing f_{ct}\left(1-\rho_{eff}\right)}{2\tau_{b0}\rho_{eff}} \tag{3.2}$$

where $\varnothing$ is the bar diameter and ρ_{eff} is the effective amount of reinforcement of the tension chord, calculated based on the procedure described in Fig. 3.3.

For $s_r = s_{r0}$, a new crack may or may not form because at the center between two cracks $\sigma_{c1} = f_{ct}$. Consequently, the crack spacing may vary by a factor of two, i.e., $s_r = \lambda s_{r0}$, with $\lambda = 0.5 \ldots 1.0$. Assuming a certain value for λ, the average strain of the chord (ε_m) can be expressed as a function of the maximum reinforcement stresses (i.e., stresses at the cracks, σ_{sr}). For the idealized bilinear stress-strain diagram for the reinforcing bare bars considered by default in the CSFM, the following closed form analytical expressions are obtained (Marti et al. 1998):

$$\begin{aligned}
\varepsilon_m &= \frac{\sigma_{sr}}{E_s} - \frac{\tau_{b0}s_r}{E_s\varnothing} && \text{for } \sigma_{sr} \leq f_y \\
\varepsilon_m &= \frac{\left(\sigma_{sr}-f_y\right)^2\varnothing}{4E_{sh}\tau_{b1}s_r}\left(1-\frac{E_{sh}\tau_{b0}}{E_s\tau_{b1}}\right) + \frac{\left(\sigma_{sr}-f_y\right)}{E_s}\frac{\tau_{b0}}{\tau_{b1}} + \left(\varepsilon_y - \frac{\tau_{b0}s_r}{E_s\varnothing}\right) \\
& && \text{for } f_y \leq \sigma_{sr} \leq \left(f_y + \frac{2\tau_{b1}s_r}{\varnothing}\right) \\
\varepsilon_m &= \frac{f_s}{E_s} + \frac{\left(\sigma_{sr}-f_y\right)}{E_{sh}} - \frac{\tau_{b1}s_r}{E_{sh}\varnothing} && \text{for } \left(f_y + \frac{2\tau_{b1}s_r}{\varnothing}\right) \leq \sigma_{sr} \leq f_t
\end{aligned} \tag{3.3}$$

where $E_{sh} = (f_t - f_y)/(\varepsilon_u - f_y/E_s)$ is the steel hardening modulus.

The *IDEA StatiCa Detail* implementation of the CSFM considers average crack spacing by default when performing computer-aided stress field analysis. The average crack spacing is considered to be 2/3 of the maximum crack spacing ($\lambda = 0.67$), which follows recommendations made on the basis of bending and tension tests (Broms 1965; Beeby 1979; Meier 1983). It should be noted that calculations of crack widths consider a maximum crack spacing ($\lambda = 1.0$) in order to obtain conservative values, as will be discussed in Section 3.5.

The application of the TCM depends on the reinforcement ratio and hence, the assignment of an appropriate concrete area acting in tension between the cracks to each reinforcing bar is crucial. It is not straightforward to determine the proper concrete area manually, and such an approach is also somewhat arbitrary in elements with complex geometries. To this end, an automatic

numerical procedure has been developed to define the corresponding effective reinforcement ratio (ρ_{eff}) for any configuration, including skewed reinforcement. A detailed description of this procedure is beyond the scope of this document, but the basic method is illustrated in Fig. 3.3. It consists of the following steps: (i) definition of the maximum area of concrete that each reinforcing bar can activate in tension when activated to f_{ct} (Fig. 3.3a); (ii) verification of the symmetry condition of the tensile concrete stresses caused by each reinforcing bar considering the interaction with adjacent bars (as described in Fig. 3.3b); (iii) preliminary assignment of an effective concrete area to each reinforcing bar based on steps (i) and (ii), combined with simple geometric conditions (Fig. 3.3c); and (iv) redistribution of the concrete area among proximate, parallel reinforcing bars in order to ensure the same crack spacing for these bars. Assuming a uniform stress f_{ct} throughout the activated concrete area, the diameter of the maximum area of concrete in tension ($\varnothing_{c,eff}$) required in the first step follows from equilibrium:

$$\varnothing_{c,eff} = \varnothing \sqrt{\frac{f_t}{f_{ct}}} \tag{3.4}$$

where $\varnothing$ = bar diameter.

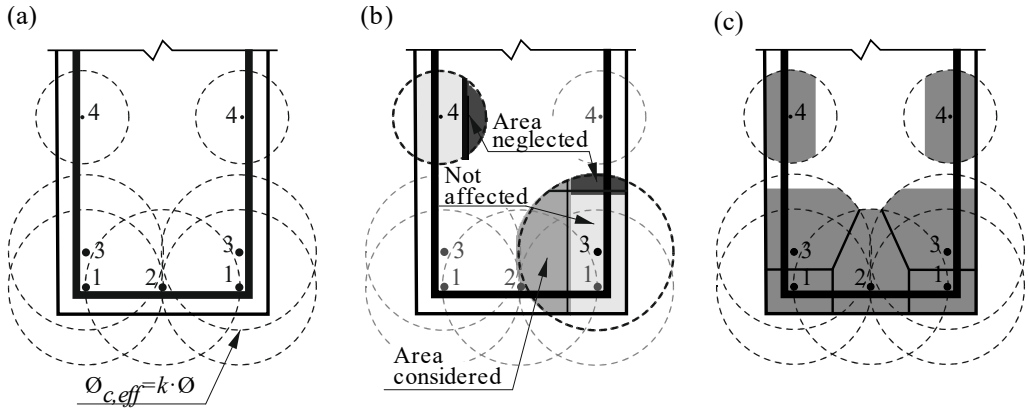

Fig. 3.3 Effective area of concrete in tension for stabilized cracking: (a) Maximum concrete area that can be activated; (b) cover and global symmetry condition; (c) resultant effective area.

Note that the condition of identical crack spacing for proximate bars (100 mm of distance being considered the threshold value by default), which approximately corresponds to the assignment of a constant ratio $\varnothing/\rho_{eff}$ to proximate parallel bars (see Eq. (3.2)), allows the introduction of a clear, mechanically based criterion to the calculation of ρ_{eff}. While this condition is currently imposed separately on the different reinforcing directions, there is considerable potential for generalizing it to ensure the compatibility of the crack spacing between all the reinforcing bars in the model for each point of the structure. This problem has already been solved (Kaufmann 1998; Kaufmann and Marti 1998; Seelhofer 2010) for the particular case of homogenously reinforced membrane elements. However, these available mechanical models are not directly applicable to the general problems addressed by the CSFM.

Non-stabilized cracking

Cracks in regions with geometric reinforcement ratios lower than ρ_{cr}, i.e., below the minimum reinforcement amount for which the reinforcement is locally able to carry the cracking load without yielding, lead to brittle failures at cracking unless their opening (i.e., the strains in the corresponding region) is controlled by reinforcement in adjoining parts of the structure. The value of this minimum reinforcement is:

$$\rho_{cr} = \frac{f_{ct}}{f_y - (n-1) f_{ct}} \tag{3.5}$$

where f_y = reinforcement yield strength; f_{ct} = concrete tensile strength; and $n = E_s / E_c$ = modular ratio. For conventional concrete and reinforcing steel, ρ_{cr} amounts to approximately 0.6%.

For stirrups with reinforcement ratios below ρ_{cr} – which is frequently the case – cracking is considered to be non-stabilized and tension stiffening is implemented by means of the Pull-Out Model (POM) described in Fig. 3.2b. This model analyzes the behavior of a single crack by (i) considering no mechanical interaction between separate cracks; (ii) neglecting the deformability of concrete in tension; and (iii) assuming the same stepped, rigid-perfectly plastic bond shear stress-slip relationship used by the TCM. This allows the reinforcement strain distribution (ε_s) in the vicinity of the crack to be obtained for any maximum steel stress at the crack (σ_{sr}) directly from equilibrium. Given the fact that the crack spacing is unknown for a non-fully developed crack pattern, the average strain (ε_m) is computed for any load level over the distance between points with zero slip when the reinforcing bar reaches its tensile strength (f_t) at the crack ($l_{\varepsilon,avg}$ in Fig. 3.2b), leading to the following relationships:

$$\varepsilon_m = \frac{\sigma_{sr}^2 \cdot \frac{\tau_{b1}}{\tau_{b0}}}{2 \cdot E_s \left[f_t + f_y \left(\frac{\tau_{b1}}{\tau_{b0}} - 1 \right) \right]} \qquad \text{for } \sigma_{sr} \le f_y$$

$$\varepsilon_m = \frac{\frac{f_y}{E_s} \left[\sigma_{sr} + f_y \left(\frac{\tau_{b1}}{2\tau_{b0}} - 1 \right) \right] + \frac{\left(\sigma_{sr} - f_y \right)^2}{2E_{sh}}}{f_t + f_y \left(\frac{\tau_{b1}}{\tau_{b0}} - 1 \right)} \qquad \text{for } \sigma_{sr} > f_y \tag{3.6}$$

where $E_{sh} = (f_t - f_y)/(\varepsilon_u - f_y/E_s)$ is the steel hardening modulus.

The proposed models allow the computation of the behavior of bonded reinforcement, which is finally considered in the analysis. This behavior (including tension stiffening) for the most common European reinforcing steel (B500B, with $f_t/f_y = 1.08$ and $\varepsilon_u = 5\%$) is illustrated in Fig. 3.2c-d. It can be observed that the consideration of tension stiffening does not affect the strength of the reinforcement, but increases its stiffness and significantly reduces its ductility. Still, tension stiffening might indirectly affect ultimate loads in certain cases, either negatively or positively:

(i) The reduction of the ductility of the reinforcement may limit the strength of members with low amounts of transverse reinforcement, as will be discussed in Chapter 6; and (ii) the higher stiffness due to tension stiffening results in lower transverse tensile strains imposed on the concrete in compression and hence, a less pronounced reduction in the concrete compressive strength, along with correspondingly higher ultimate loads in members where concrete crushing is governing.

3.4 Reinforcement design

3.4.1 Workflow and goals

The goal of reinforcement design tools in the CSFM is to help designers determine the location and required amount of reinforcing bars efficiently. The following tools are available to help/guide the user in this process: linear calculation, topology optimization, and area optimization.

As will be described below, these reinforcement design tools consider more simplified constitutive models than the models described in Section 3.3, which are used for the final verification of the structure. Therefore, the definition of the reinforcement in this step should be considered a pre-design to be confirmed and/or refined during the final verification step (see Section 3.5). The use of the different reinforcement design tools will be illustrated using the model shown in Fig. 3.4, which consists of one end of a simply supported beam with variable depth, subjected to a uniformly distributed load.

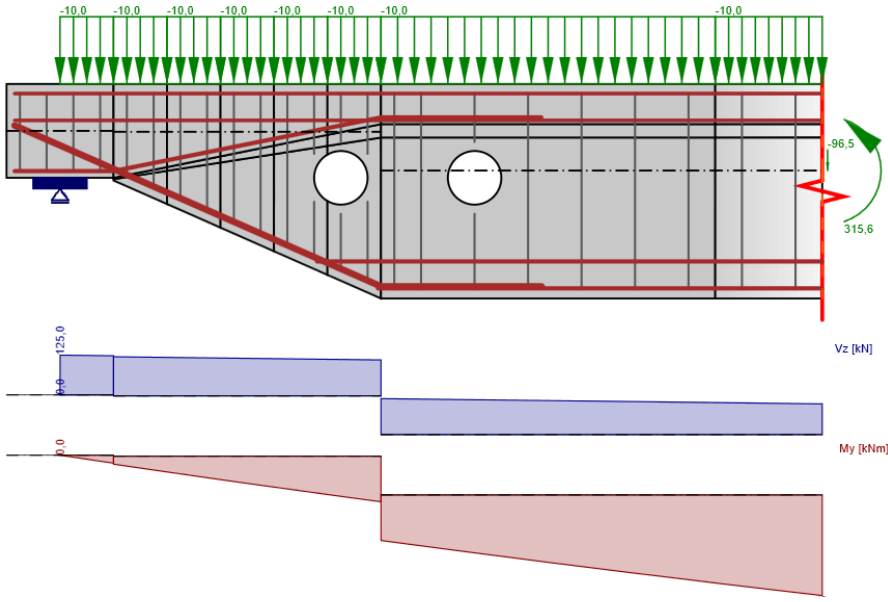

Fig. 3.4 Model used to illustrate the use of reinforcement design tools.

3.4.2 Reinforcement locations

For regions where the reinforcement layout is not known beforehand, there are two methods available in the CSFM to help the user determine the optimum location of reinforcing bars: linear analysis and topology optimization. Both tools provide an overview of the location of tensile forces in the uncracked region for a certain load case. While it is considered good practice to place reinforcement close to the location of tensile forces to reduce the amount of reinforcement and required plastic redistributions (as previously proposed by Schlaich et al. (1987)), designers must interpret the results of these design tools and provide reinforcement layouts that also take into account other constraints (e.g. construction requirements). For instance, these tools typically provide diagonal tensile forces (e.g. to carry shear forces) but this inclined force might be typically resisted by a truss mechanism with orthogonal reinforcement.

Linear analysis

Linear analysis considers linear elastic material properties and neglects reinforcement as well as differences between concrete behavior in compression and tension. It is, therefore, a very fast calculation that provides a first insight into the locations of tension and compression areas. An example of such a calculation is shown in Fig. 3.5.

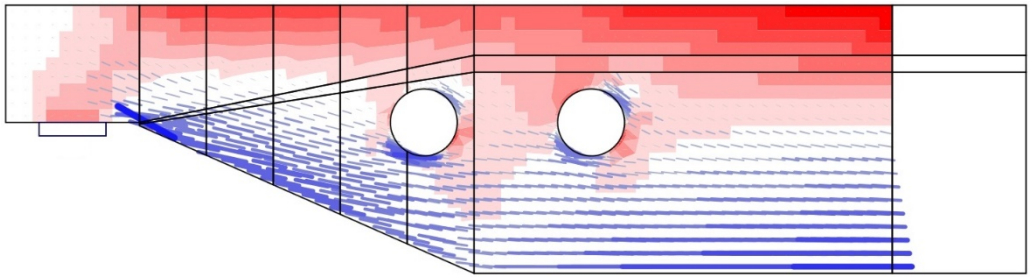

Fig. 3.5 Results from the linear analysis tool for defining reinforcement layout (red: areas in compression, blue: areas in tension).

Topology optimization

Topology optimization is a method that aims to find the optimal distribution of material in a given volume for a certain load configuration. With this method, a given percentage of the volume is filled with material and the rest stays empty. This is achieved by iteratively redistributing the material inside the given volume until the optimal distribution (a shape inside the original volume) is found.

The topology optimization implemented in *IDEA StatiCa Detail* uses a linear finite element model. Each finite element may have a relative density from 0 to 100 %, representing the relative amount of material used. These element densities are the optimization parameters in the optimization problem.

The resulting material distribution is considered optimal for the given set of loads if it minimizes the total strain energy of the system that, since linear elastic behavior is considered, is equal to the complementary energy. By definition, the optimal distribution is thus also the geometry that has the largest possible stiffness for the given loads.

The iterative optimization process starts with a homogeneous density distribution. In every iteration, the material is then redistributed slightly inside the given volume by changing the densities of individual elements in order for the total strain energy to be decreased. This is done until the change in strain energy between iterations is small enough. The calculation is performed for multiple total volume fractions (20%, 40%, 60% and 80%), which allows the user to select the most practical result, as proposed by Konečný et al. (2017).

The resulting shape consists of trusses with struts and ties and represents the optimum shape for the given load cases (Fig. 3.6). Of course, it is often not practical or economical to place reinforcing bars exactly within the proposed ties via topology optimization, so the designer must also take into account practical considerations when positioning reinforcement.

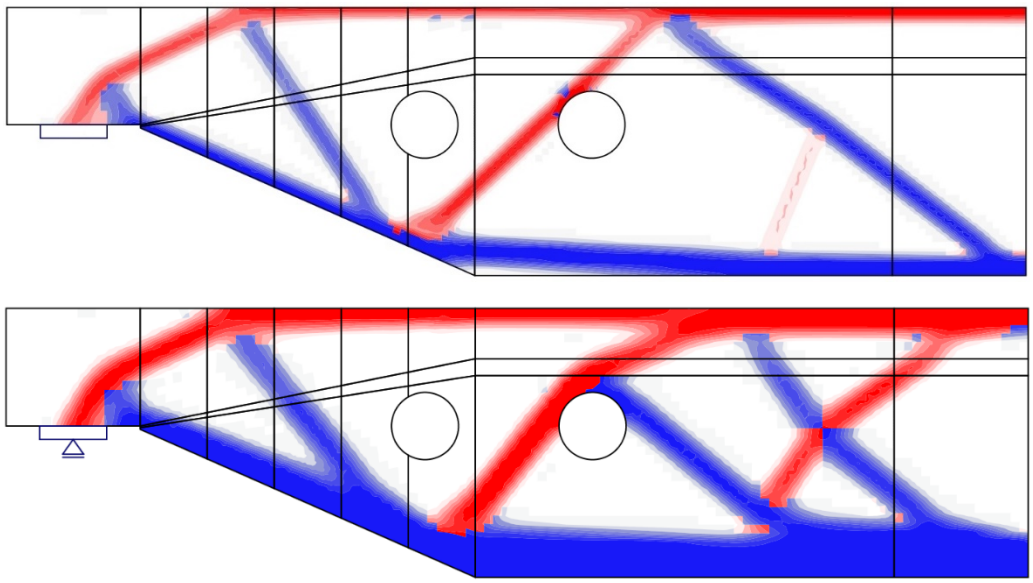

Fig. 3.6 Results from the topology optimization design tool with 20% and 40% effective volume (red: areas in compression, blue: areas in tension).

3.4.3 Amount of reinforcement

Overview

Once the layout of the reinforcing bars has been defined, the required areas must be determined. While topology optimization (Section 3.4.2) provides an insight into the relative amounts of reinforcement required in the different regions of the member (i.e., the thickness of ties is proportional to tension force and therefore to the required area), this information is only qualitative and

does not take into account the reinforcement location chosen by the designer. Hence, the CSFM has been extended to include a tool called 'rebar optimization' (first released in *IDEA StatiCa Detail 10.0*) that helps the user with the dimensioning of the reinforcement, i.e., the determination of reinforcement areas in terms of the number of bars and their diameters.

In the area optimization tool, the user first defines the bars for which the required area should be designed (in the case that not all the bars are to be optimized). Selected bars can be grouped for the optimization, meaning that the resulting area will be constant for each bar in that group. A simplified version of the compatible stress field analysis presented in Sections 3.2 and 3.3 is then used to iteratively load the structure, find the stresses in the reinforcements and adjust their areas to minimize the overall volume of reinforcement. The required reinforcement areas given by the optimization are presented to the user (Fig. 3.7), who can then adjust the number and diameters of bars in order to ensure that the available reinforcement area is higher than the required area. In many cases, using the area optimization tool can reduce the amount of reinforcement used in the structure significantly without affecting its loading capacity.

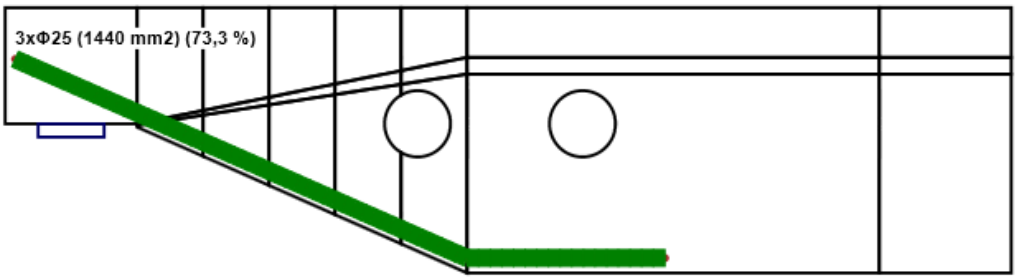

Fig. 3.7 Results from the area optimization design tool for longitudinal reinforcement: total required area, the required number of bars for the selected diameter, and the ratio between the required area and current area for the selected diameter.

Definition of the optimization problem

The aim of good reinforcement design is to minimize the overall volume of reinforcement (using a practical layout defined by the user, as described in Section 3.4.2) whilst keeping the structure in a state that is likely to satisfy all verification requirements (as will be defined in Section 3.5). However, it is necessary to prevent the optimization problem from being over-constrained, so it is convenient to only choose reinforcing bar stresses as constraints. This results in a relatively simple optimization problem which is easy to solve if a suitable algorithm is used.

This described optimization problem can be expressed as follows:

$$\mathbf{min}\left(\sum_{i=1}^{n} l_{s,i} A_{s,i}\right) \tag{3.7}$$

subject to:

$$\sigma_{s,j} \leq f_t \tag{3.8}$$

where $l_{s,i}$ is the length of the i-th reinforcing bar, $A_{s,i}$ is the area of the i-th reinforcing bar, $\sigma_{s,j}$ is the stress on the j-th reinforcing bar and f_t is the tensile strength of the reinforcement.

Optimization algorithm

In the algorithm used in the 'area optimization' tool (Fig. 3.8), the gradient of the cost function (the total reinforcement volume) with respect to the reinforcing bar section areas is calculated first. The value of this gradient is constant and does not need to be updated further on. Then, an FE analysis is computed for all the given load cases. The results of each load case may be different, and therefore the constraint function values (steel stresses) are evaluated for all the load cases, and their gradients with respect to section areas are calculated. The values from all the load cases are then combined and serve as an input for the linear programming problem.

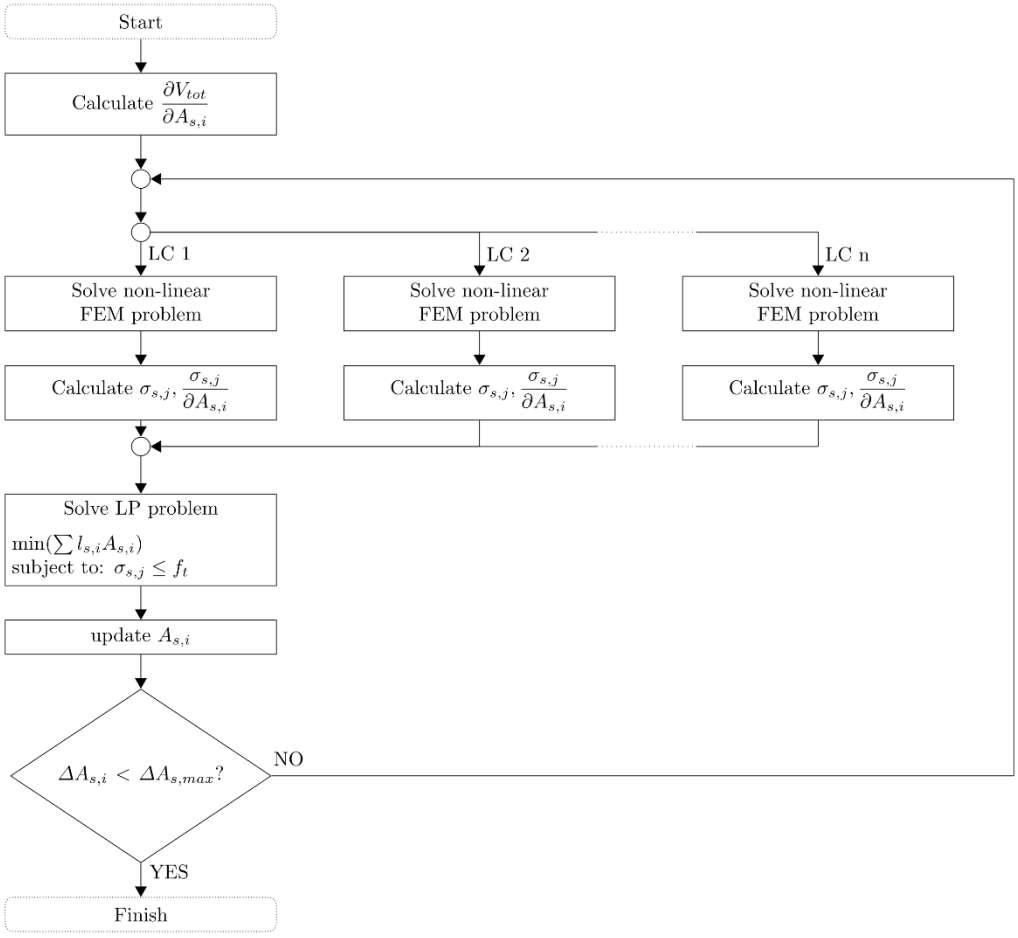

Fig. 3.8 Simplified flowchart depicting reinforcement area optimization.

The problem is solved using the simplex method, which yields new section areas that are subsequently updated in the FE-analysis. This whole process is then repeated with the updated values until convergence is reached (i.e., the overall volume of reinforcement has been minimized).

A higher-order optimization subproblem could possibly be used instead of the linear programming problem described above. However, using appropriate settings, approximation via a linear problem has been shown to behave sufficiently well while offering the important advantages of simpler implementation and the robustness and speed of the simplex algorithm.

Note that the above description of the optimization is simplified. Additional logic had to be included in the algorithm in order to deal with cycling, non-convergence, etc. in particular. However, a more detailed description is beyond the scope of this document.

Constitutive model

As already stated, the FE analysis used in the reinforcement optimization tool contains simplifications in comparison to the constitutive model of the CSFM presented in Section 3.3, which is used to perform the final verifications (as discussed in Section 3.5). The simplifications are:

- Tension stiffening in reinforcing bars is neglected, as it can only be computed when the amount of reinforcement and the diameters are defined.
- The anchorage length is not verified; instead, the bars are connected directly to the concrete mesh by multi-point constraint elements.
- The compression softening effect in concrete is neglected.

These simplifications reduce the non-linearity of the FE analysis and smooth the optimization problem. This approach is justified since the design of the required reinforcement areas is often rather insensitive to the considered simplifications and the user will later perform a final verification step (see Section 3.5) without these simplifications.

Interpretation of results

Once the optimized (required) areas have been estimated, the results are presented to the user. The interpretation of the results for longitudinal bars (see Fig. 3.7) includes the required number of bars for the selected diameter and the ratio between the required area and current area.

For the case of stirrups, the required areas are presented in different zones, which are generated automatically from the spacing of the stirrups and limited by a predefined maximum length. The required and current areas of the stirrups in individual zones are displayed as areas per length. The presentation for each zone includes the required number of stirrups (considering the designer's selected diameter and number of branches) as well as the resultant stirrup spacing in order to provide the exact statically required number of stirrups and ratio between the required area and current area.

3.5 Verification of the structural element

After the location and amount of reinforcement has been perfectly defined (either because it was known beforehand or because it has been defined using the aforementioned reinforcement design tools, see Section 3.4), the structural element has to be verified using Compatible Stress Fields, as described in Sections 3.2 and 3.3. It should be noted that two different analyses are performed: one for serviceability, and one for ultimate limit state load combinations. The serviceability analysis assumes that the ultimate behavior of the element is satisfactory and the yield conditions of the material will not be reached at serviceability load levels. This enables the use of simplified constitutive models for serviceability analysis (the simplifications with respect to the general models shown in Section 3.3 are given in Section 3.5.3) to enhance numerical stability and calculation speed, though this requires designers to disregard the serviceability analysis if the ultimate limit state verifications are not fulfilled. Therefore, it is recommended to use the workflow presented below, in which the ultimate limit state analysis is carried out as the first step.

3.5.1 Safety format factor

As outlined in Sections 3.1, 3.2 and 3.3, the CSFM is compliant with modern design codes. As the calculation models only use standard material properties, the partial safety factor format prescribed in the design codes can be applied without any adaptation. In this way, the input loads are factored and the characteristic material properties are reduced using the respective safety coefficients prescribed in design codes, exactly as in conventional concrete analysis and design.

By using appropriate user-defined combinations of partial safety factors, users can also compute with the CSFM using the global resistance factor method (Navrátil et al. 2017), but this approach is hardly ever used in design practice. Some guidelines recommend using the global resistance factor method for non-linear analysis. Indeed, the use of the global resistance factor method might allow the failure mode of the structural element to be predicted more accurately. However, in simplified non-linear analyses (such as the CSFM), which only require those material properties that are used in conventional hand calculations, most designers will prefer to use the partial safety format to ensure consistency with standard verifications.

3.5.2 Ultimate limit state analysis

To ensure a structural element has an efficient design, it is highly recommended that a preliminary analysis be run, which takes into account the following steps:

- Choose a selection of the most critical load combinations.
- Calculate only ultimate limit state load combinations.
- Deactivate the bond model used to verify the anchorage length.
- Use a coarse mesh (by increasing the multiplier of the default mesh size).

Such a model will calculate very quickly, allowing designers to review the detailing of the structural element efficiently and re-run the analysis until all verification requirements are fulfilled for the most critical load combinations. As stated in Section 3.4, the result obtained from the reinforcement design tools should be considered merely a pre-design, and this might need to be adapted in this step. Once all the verification requirements of this preliminary analysis are fulfilled, it is suggested that the full set of ultimate load combinations be included, activating the verification of the anchorage length and using a finer mesh size (the mesh size recommended by the program). As the last step of the ultimate limit state analysis, the mesh size sensitivity of the results should be checked (though the model generally has a reduced mesh size sensitivity, as will be shown in Chapters 4 and 1 for some examples).

3.5.3 Serviceability limit state analysis

The serviceability analysis contains certain simplifications of the constitutive models presented in Section 3.3, which are used for ultimate limit state analysis. Namely, a perfect bond is assumed, i.e., the anchorage length is not verified at serviceability. Furthermore, the plastic branch of the stress-strain curve of concrete in compression is disregarded. These simplifications enhance the numerical stability and calculation speed and do not reduce the generality of the solution as long as the resulting material stress limits at serviceability are clearly below their yielding points (as required by standards). Therefore, the simplified models used for serviceability are only valid if all verification requirements are fulfilled.

Long term effects

In serviceability analysis, the long-term effects of concrete (creep, shrinkage, and aging of concrete) are considered using an effective infinite creep coefficient (φ, using a value of 2.5 by default) which modifies the secant modulus of elasticity of concrete (E_{cm}) as follows:

$$E_{c,eff} = \frac{E_{cm}}{1+\varphi} \tag{3.9}$$

When considering long-term effects, a load step with all permanent loads is first calculated considering the creep coefficient (i.e., using the effective modulus of elasticity of concrete, $E_{c,eff}$) and subsequently, the additional loads are calculated without the creep coefficient (i.e., using E_{cm}). For short-term verifications, an additional separate calculation is performed in which all loads are calculated without the creep coefficient. Both calculations for long and short-term verifications are depicted in Fig. 3.9.

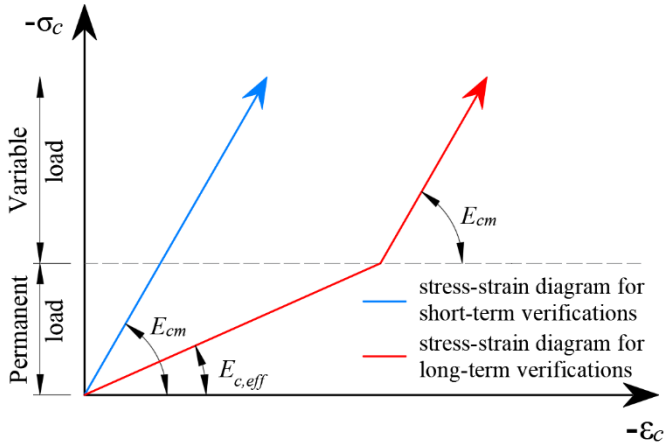

Fig. 3.9 Concrete stress-strain diagrams implemented for serviceability analysis: short- and long-term verifications.

Crack width calculation

The calculation of crack widths is up to now still a controversial topic. Various codes and literature provide a number of different approaches to its modeling, prediction, and design. It should be noted that the behavior of concrete in tension and the cracking behavior itself is imposed to numerous insecurities, such as e.g. environmental conditions, concreting process, curing, shrinkage, creep, deformational restrictions, which are typically not included in the models to calculate crack widths. In spite of these uncertainties, the herein proposed approach, which is based on the Tension Chord Model has proven its soundness in various experimental validations (Burns 2012) in spite of its simplicity.

While the CSFM yields a direct result for most verifications (e.g. member capacity, deflections…), crack width results are calculated from the reinforcement strain results directly provided by FE analysis following the methodology described in Fig. 3.10. A crack kinematic without sliding (pure crack opening) is considered (Fig. 3.10a), which is consistent with the main assumptions of the model (section 3.2). The principal directions of stresses and strains define the inclination of the cracks ($\theta_r = \theta_\sigma = \theta_\varepsilon$). According to Fig. 3.10b, the crack width (w) can be projected in the direction of the reinforcing bar (w_b), leading to:

$$w = \frac{w_b}{\cos\left(\theta_r + \theta_b - \pi/2\right)} \tag{3.10}$$

where θ_b is the bar inclination.

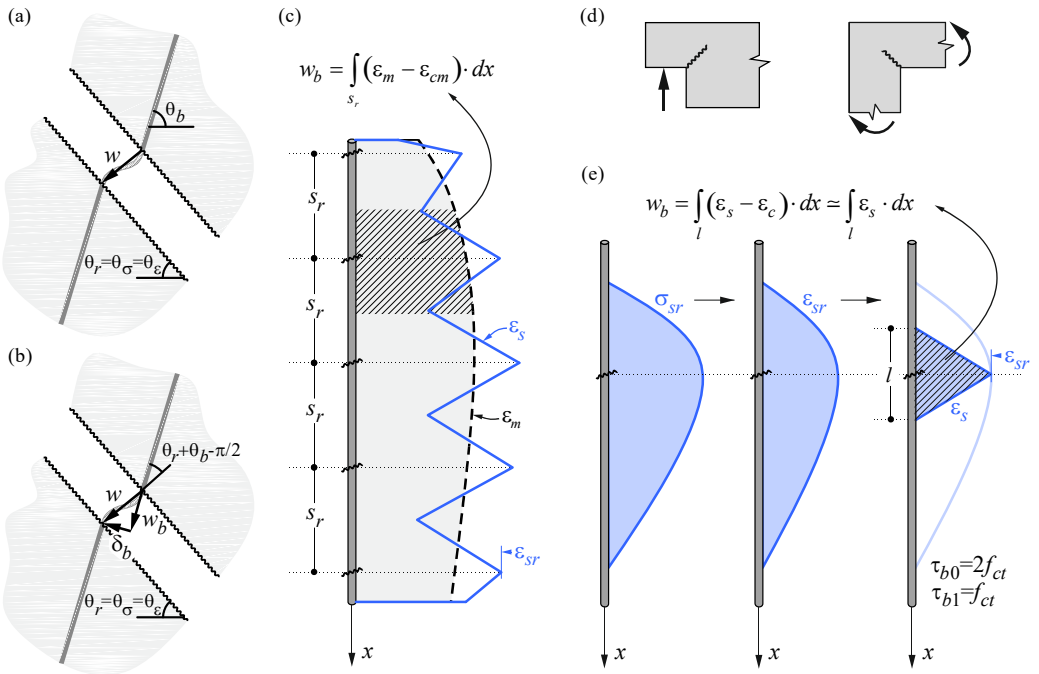

Fig. 3.10 Crack width calculation: (a) Considered crack kinematics; (b) projection of crack kinematics into the principal directions of the reinforcing bar; (c) crack width in the direction of the reinforcing bar for stabilized cracking; (d) cases with local non-stabilized cracking regardless of the reinforcement amount; (e) crack width in the direction of the reinforcing bar for non-stabilized cracking.

The component w_b is consistently calculated based on the tension stiffening models presented in Section 3.3.4 by integrating the reinforcement strains. For those regions with fully developed crack patterns (see Section 3.3.4), the calculated average strains (ε_m) along the reinforcing bars are directly integrated along the crack spacing (s_r) as indicated in Fig. 3.10c, leading to:

$$w_b = \int_{s_r} (\varepsilon_m - \varepsilon_{cm}) \cdot dx = \int_{s_r} \left(\varepsilon_m - \frac{\lambda \cdot f_{ctm}}{2E_s} \right) \cdot dx \tag{3.11}$$

Note that the effect of tension stiffening is included in the average strains (ε_m), which were calculated considering an average crack spacing ($\lambda = 0.67$) as outlined in Section 3.3.4, thereby accounting for the average effect of tension stiffening on all results. On the other hand, in order to obtain safe values for the crack widths, a value of $\lambda = 1.0$ (maximum theoretical crack spacing) is used for the crack width calculations. Hence, in Eq. (3.11) crack spacings s_r are calculated using $\lambda = 1.0$, and the strains obtained from the calculation (using $\lambda = 0.67$) are multiplied by a factor of $1.0/0.67 = 1.5$.

For the case of tension stiffening assuming non-stabilized cracking (currently implemented for stirrups with geometric reinforcement ratios below ρ_{cr}), the crack width w_b is calculated according to the procedure illustrated in Fig. 3.10c based on the results of maximum stresses in the reinforcement (σ_{sr}), which in this case are more reliable than the average strains. This procedure is also applied to the calculation of crack widths in re-entrant corners with opening moments (Fig. 3.10d), regardless of the fact that the tension stiffening model in the adjacent bars assumes stabilized or non-stabilized cracking since the diagonal crack at these corners behaves mainly as a non-stabilized crack for service loads (Mata-Falcón 2015).

3.6 Finite element implementation

3.6.1 Introduction

The CSFM considers continuous stress fields in the concrete (2D finite elements), complemented by discrete tension ties representing the reinforcement (1D finite elements). Therefore, the reinforcement is not diffusely embedded into the concrete 2D finite elements, but explicitly modeled and connected to them. A plane stress state is considered in the calculation model. It should be noted that while *IDEA StatiCa Detail* provides different templates for defining the structure (wall, beam…), the FE model (for the same geometry) will be identical, irrespective of the template.

Several components are used to create the nonlinear finite element analysis model. There are several types of finite elements used to model concrete, reinforcement, and the bond between them, which are described in Section 3.6.5. Moreover, Section 3.6.2 presents existing models for modeling supports and to transfer loads. The geometric properties of the model are generated based on the user-defined structural member. As described in Section 3.6.3, some geometric modifications are done for the case of haunched cross-sections in both transverse and longitudinal directions.

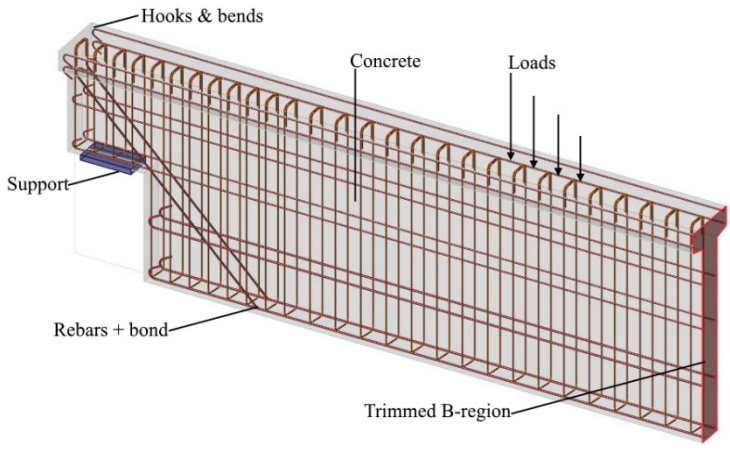

Fig. 3.11 Visualization of the calculation model of a structural element (trimmed beam) in *IDEA Statica Detail*.

Both entire walls and beams, as well as details (parts) of beams (isolated discontinuity region, also called trimmed end), can be modeled. In the case of walls and entire beams, supports must be defined in such a way that they result in an externally isostatic (statically determinate) or hyperstatic (statically indeterminate) structure. The load transfer at the trimmed ends of beams is modelled by means of a special Saint-Venant transfer zone (described in Section 3.6.4), which ensures a realistic stress distribution in the analyzed detail region.

Rules and procedures for meshing concrete, reinforcement, bearing plates, loads and supports are given in Section 3.6.6. The solution procedure for the non-linear FEM problem, including the used load-control algorithm, is revealed in Section 3.6.7. This includes the description of the implementation and "stop criteria" for each structural component (concrete, reinforcement, and bond). The last point of this section (Section 3.6.8) addresses the presentation of results in *IDEA Statica Detail* and the ways of verification for ultimate limit states and serviceability limit states.

3.6.2 Supports and load transmitting components

The types of supports and components used for transferring load available in the CSFM are listed in Fig. 3.12. These components allow the modeling of most situations during the construction process, transportation, and service state.

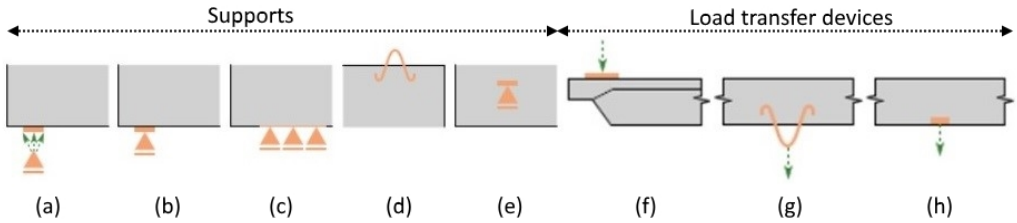

Fig. 3.12 Various types of support and load transfer components: (a)-(e) Supports, i.e., (a) point distributed, (b) bearing plate, (c) line support, (d) hanging, (e) patch support; (f)-(h) load transfer devices, i.e., (f) bearing plate, (g) hanging, (h) patch load.

Point supports can be modeled in several ways in order to ensure that stresses are not localized in one point but rather distributed over a larger area. The first option is a distributed point support (Fig. 3.12a), which can either be placed on an edge with a defined width or inside a volume of concrete with a defined radius. The distributed point support is then connected by rigid elements to the nodes of the concrete mesh within the effective width (or radius). Patch support (Fig. 3.12e), on the other hand, can only be placed inside a volume of concrete with a defined effective radius. It is then connected by rigid elements to the nodes of the reinforcement mesh within this radius. Therefore, it is required that a reinforcing cage be defined around this patch support.

For the more precise modeling of some real scenarios, there are two other options for point supports. Firstly, there is point support with a bearing plate of defined width and thickness (Fig. 3.12b). The material of the bearing plate can be specified, and the whole bearing plate is meshed independently. Secondly, there is hanging support available (Fig. 3.12d), which can be used for

modeling lifting anchors or lifting studs. Currently, there are four types of lifting anchors and one type of lifting stud available.

Line supports (Fig. 3.12c) can be defined on edge (by specifying its length) or inside an element (by a polyline). It is also possible to specify its stiffness and/or nonlinear behavior (support in compression/tension or only in compression).

The introduction of loads into the structure can also be modeled in several ways. For point loads, a bearing plate (Fig. 3.12f) can be used similarly as point support, distributing the concentrated load onto a larger area. Patch loads (Fig. 3.12h) are placed inside the concrete with a certain effective radius and are connected by rigid elements to the nodes of nearby reinforcing bars. Also, lifting anchors or lifting studs can be modeled by a hanging load (Fig. 3.12g). The structure can also be loaded with line loads or by surface loads, representing, e.g., self-weight (which is not automatically considered in the analysis).

3.6.3 Geometric modification of cross-sections

In the case of beam cross sections that include haunches, the width of the finite elements used to model the haunch might be automatically reduced in comparison to the original width so that it is not larger than twice its depth plus the thickness of the adjacent wall. This is based on the assumption that a compression stress field would expand from the wall under an angle of 45° (see Fig. 3.13), so the aforementioned reduced width would be the maximum width capable of transferring loads. For those cases in which the geometry is not defined in the CSFM by means of a beam template (i.e., definition via a wall or general shape templates), the input width is not automatically corrected to account for the shear lag effect when generating the finite element model. Therefore, designers should input the desired effective width in such cases.

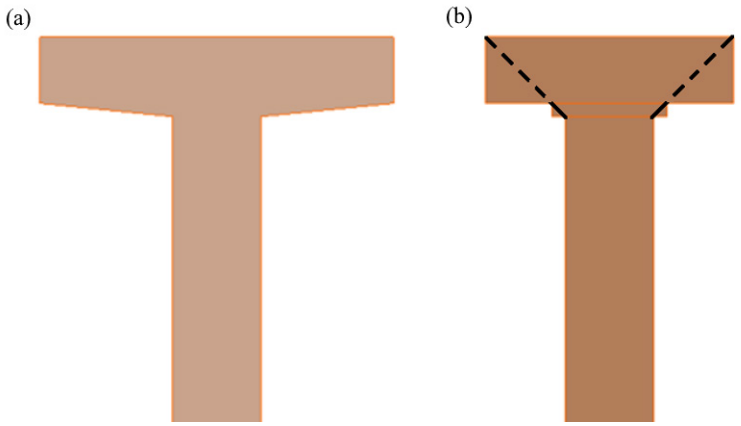

Fig. 3.13 Width reduction of a cross-section: (a) User input; (b) FE model – automatically determined reduced width of a flange.

Note that the method of determining the effective flange width for beams implemented in CSFM is different from the one stated in 5.3.2.1 EN 1992-1-1 (European Committee for Standardization, 2004). Besides geometry, Eurocode based effective flange width is explicitly affected by the span lengths and boundary conditions of a structure. Users can refine the default value of the flange width set in CSFM by inputting the geometry via a wall or general shape templates.

In the case of haunches lying in the horizontal plane (Fig. 3.14), each haunch is divided into five sections along its length. Each of these sections is then modeled as a wall with a constant thickness, which is equal to the real thickness in the middle of the respective section.

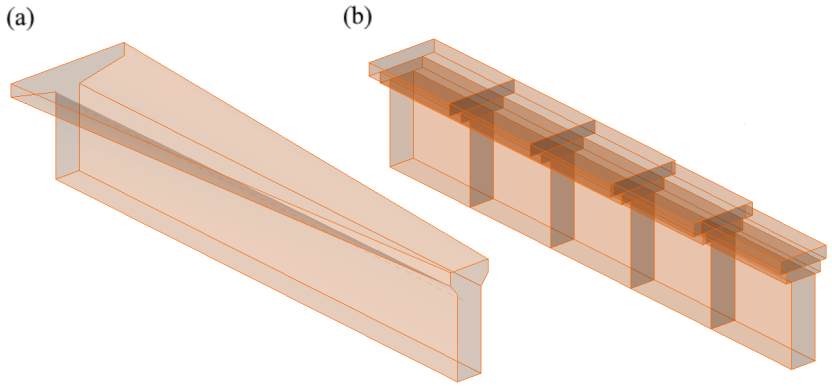

Fig. 3.14 Horizontal haunch: (a) User input; (b) FE model – a haunch automatically divided into five sections.

3.6.4 Load transfer at trimmed ends of beams

In the case of details (parts) of members, support configurations that are unstable are admissible in *IDEA StatiCa Detail* (including the case of no supports). In such cases, it is also necessary to model the section representing the connection to the adjoining B-region, including internal forces at this section that satisfy equilibrium with the applied loads. In certain cases (e.g. when modeling beam support), these internal forces can be determined automatically by the program.

Between this section and the analyzed discontinuity region, a Saint-Venant transfer zone is automatically generated in order to ensure a realistic stress distribution in the analyzed region. Half of the section's depth is used as the width of this zone. As the only purpose of the Saint-Venant zone is to achieve a proper stress distribution in the rest of the model, no results from this area are displayed in verification and no stop criteria are considered here.

The edge of the Saint-Venant zone that represents the trimmed end of the beam is modeled as rigid, i.e., it may rotate, but must remain plane. This is accomplished by connecting all the FEM nodes of the edge to a separate node at the center of inertia of the section, using a rigid body element (RBE2). The internal forces of the element may then be applied at this node, as shown in Fig. 3.15.

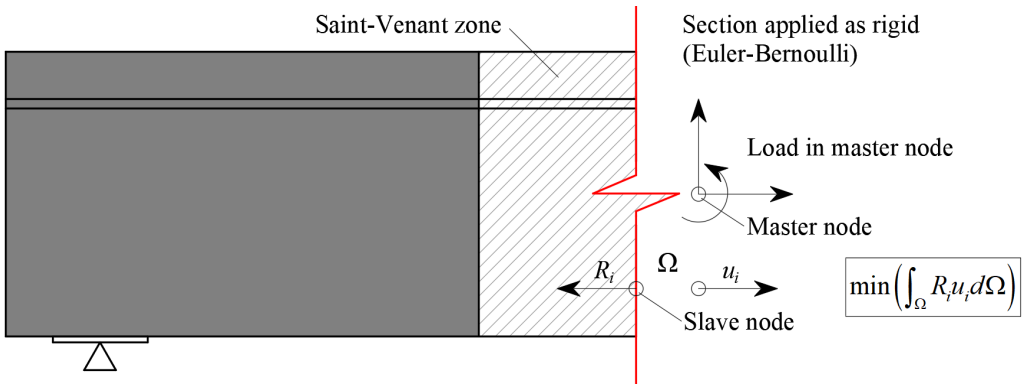

Fig. 3.15 Transfer of internal forces at a trimmed end

3.6.5 Finite element types

There are several finite element types used to model concrete, reinforcement and the bond between them, which are described in the following sections. Concrete and reinforcement finite elements are first meshed independently and then connected using multi-point constraints (MPC elements). This allows the reinforcement to occupy an arbitrary, relative position in relation to the concrete.

If anchorage length verification is to be calculated, bond and anchorage end spring elements are inserted between the reinforcement and the MPC elements. Their shape follows that of already meshed reinforcement elements, so no additional meshing needs to be done.

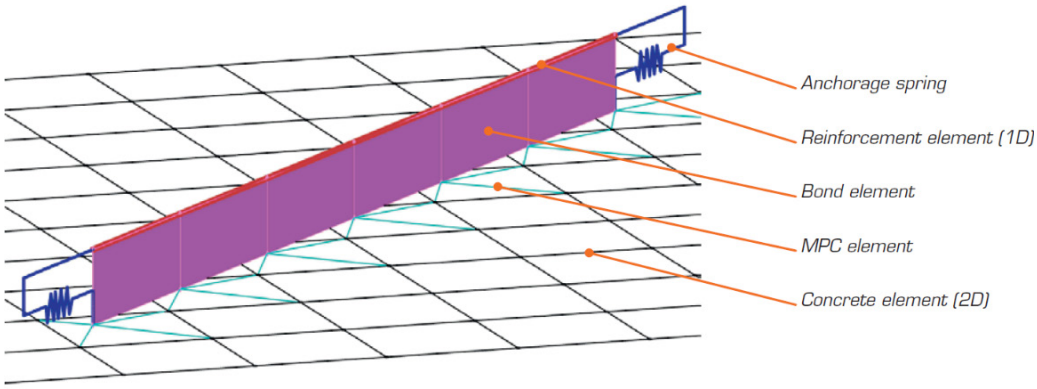

Fig. 3.16 Finite element model: reinforcement elements mapped to concrete mesh using MPC elements and bond elements.

Concrete

Concrete is modeled using quadrilateral and trilateral shell elements, CQUAD4 and CTRIA3. Four or three nodes respectively can define these. Only plane stress is assumed to exist in these elements, i.e., stresses or strains in the z-direction are not considered.

Each element has four or three integration points, which are placed approximately at its quarter points. At each integration point in every element, the directions of principal strains α_1, α_3 are calculated. In both of these directions, the principal stresses σ_{c1}, σ_{c3} and stiffnesses E_1, E_2 are evaluated according to the specified concrete stress-strain diagram, as per Fig. 3.1. The stiffness matrix for each integration point can be assembled as follows:

$$\begin{pmatrix} \sigma_{c1} \\ \sigma_{c3} \end{pmatrix} = \begin{bmatrix} E_1(\varepsilon_1, \varepsilon_3) & 0 \\ 0 & E_3(\varepsilon_1, \varepsilon_3) \end{bmatrix} \begin{pmatrix} \varepsilon_1 \\ \varepsilon_3 \end{pmatrix} \tag{3.12}$$

It should be noted that the impact of the compression softening effect couples the behavior of the main compressive direction to the actual state of the other principal direction. The stiffness matrix is transformed to the global coordinate system and used to assemble the stiffness matrix of a given finite element. The stress components σ_x, σ_y, and τ_{xy} are then calculated for every integration point by rotating the principal stresses to the global coordinate system. Further use is then made of these values in the presentation of results, as is described in more detail in Section 3.6.8.

Reinforcement

Reinforcing bars are modeled by two-node 1D "rod" elements (CROD), which only have axial stiffness. These elements are connected to special "bond" elements that were developed in order to model the slip behavior between a reinforcing bar and the surrounding concrete. These bond elements are subsequently connected by MPC (multi-point constraint) elements to the mesh representing the concrete. This approach allows the independent meshing of reinforcement and concrete, while their interconnection is ensured later.

Anchorage length verification: bond elements

As presented in Section 3.3.3, the anchorage length is verified by implementing the bond shear stresses between concrete elements (2D) and reinforcing bar elements (1D) in the finite element model. To this end a "bond" finite element type was developed.

The definition of the bond element is similar to that of a shell element (CQUAD4). It is also defined by 4 nodes, but in contrast to a shell, it only has a non-zero stiffness in shear between the two upper and two lower nodes. In the model, the upper nodes are connected to the elements representing reinforcement and the lower nodes to those representing concrete. The behavior of this element is described by the bond stress, τ_b, as a bilinear function of the slip between the upper and lower nodes, δ_u, see Fig. 3.17.

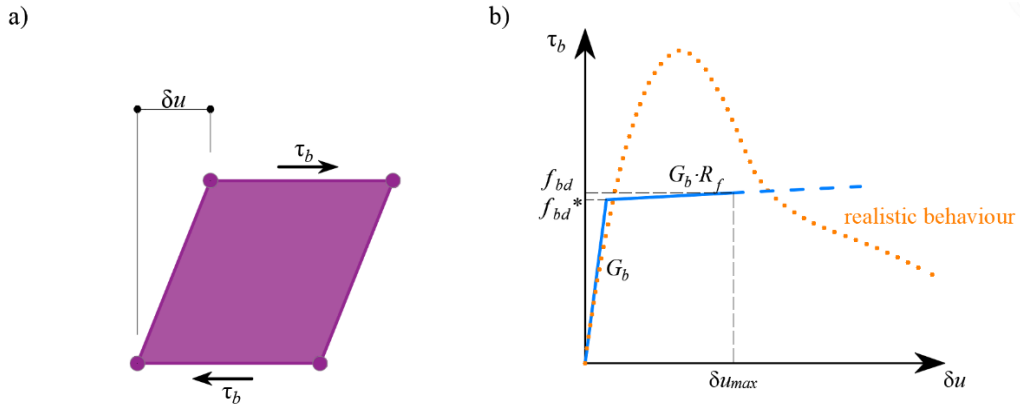

Fig. 3.17 (a) Conceptual illustration of the deformation of a bond element; (b) stress-deformation (bond slip) function. Note that as described in Section 3.3.3, the initial stiffness (G_b) is much higher than the hardening ($G_b R_f \rightarrow 0$), see Fig. 3.1f.

The elastic stiffness modulus of the bond slip relationship, G_b, is defined as follows:

$$G_b = k_g \frac{E_c}{Ø} \tag{3.13}$$

where k_G is coefficient depending on the reinforcing bar surface (by default k_G = 0.2), E_c is modulus of elasticity of concrete, taken as E_{cm} and Ø is the diameter of reinforcing bar.

As stated in Section 3.3.3, the design values of the ultimate bond shear stress, f_{bd}, provided in the respective selected design codes EN 1992-1-1 or ACI 318-14 are used to verify the anchorage length. The hardening of the plastic branch is calculated by default as $G_b/10^5$ (i.e., the default value of R_f is $1 \cdot 10^{-5}$).

Anchorage length verification: spring elements

The provision of anchorage ends to the reinforcing bars (i.e., bends, hooks, loops…), which fulfills the prescriptions of design codes, allows the reduction of the basic anchorage length of the bars ($l_{b,net}$) by a certain factor β (referred to as the 'anchorage coefficient' below). The design value of the anchorage length (l_b) is then calculated as follows:

$$l_b = (1-\beta) l_{b,net} \tag{3.14}$$

The available anchorage types in the CSFM include: straight bar (i.e., no anchorage end reduction), bend, hook, loop, welded transverse bar, perfect bond and continuous bar. All these types, along with the respective anchorage coefficients β, are shown in Fig. 3.18 for longitudinal reinforcement and in Fig. 3.19 for stirrups. The values of the adopted anchorage coefficients are in accordance with EN 1992-1-1. It should be noted that in spite of the different available options, the CSFM just distinguishes three types of anchorage ends: (i) no reduction in the anchorage length, (ii) a reduction of 30 % of the anchorage length in the case of a normalized anchorage and (iii) perfect bond.

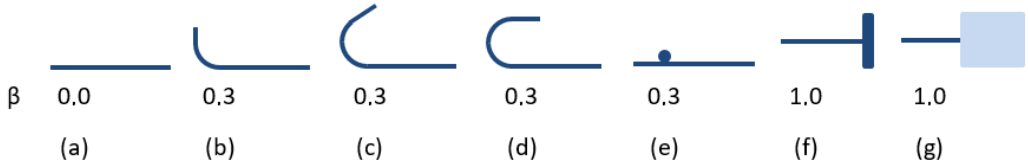

Fig. 3.18 Available anchorage types and respective anchorage coefficients for longitudinal reinforcing bars in the CSFM: (a) Straight bar; (b) bend; (c) hook; (d) loop; (e) welded transverse bar; (f) perfect bond; (g) continuous bar.

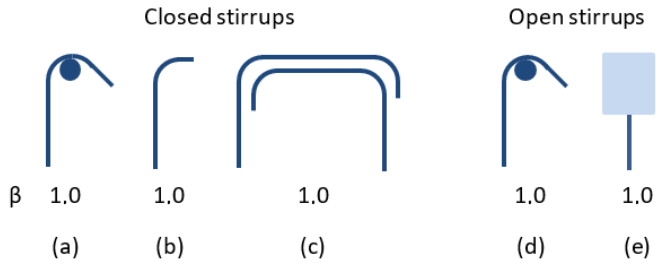

Fig. 3.19 Available anchorage types and respective anchorage coefficients for stirrups. Closed stirrups: (a) Hook, (b) bend, (c) overlap; open stirrups: (d) hook, (e) continuous bar.

The intended reduction in $l_{b,net}$ is equivalent to the activation of the reinforcing bar at its end at a percentage of its maximum capacity given by the anchorage reduction coefficient, as shown in Fig. 3.20a.

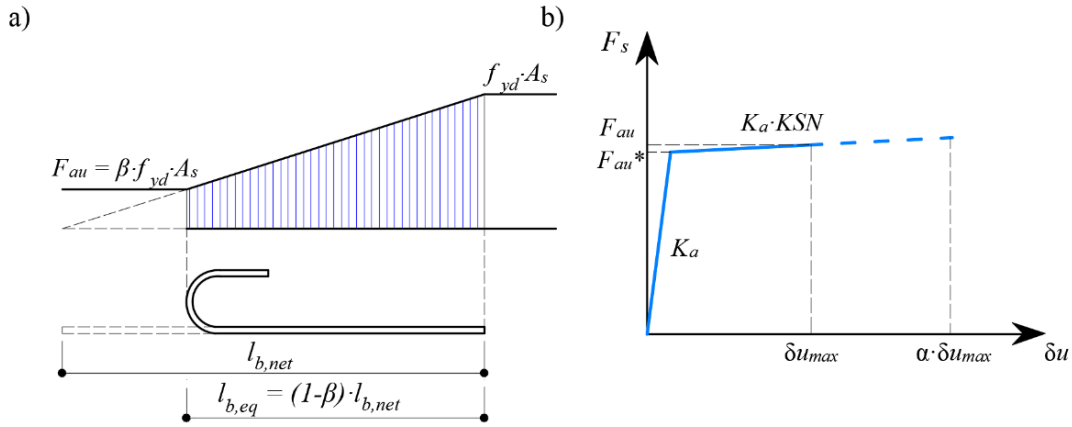

Fig. 3.20 Model for the reduction of the anchorage length: (a) Force in reinforcing bar along the anchorage length; (b) slip-anchorage force constitutive relationship.

The reduction of the anchorage length is included in the finite element model by means of a spring element at the end of the bar (see Fig. 3.16), which is defined by the constitutive model shown in Fig. 3.20b. The maximum force transmitted by this spring (F_{au}) is:

$$F_{au} = \beta A_s f_{yd} \tag{3.15}$$

where β is the anchorage coefficient based on anchorage type, A_s is the cross-section of the reinforcing bar and f_{yd} is the design value of the yield strength of the reinforcement.

The elastic stiffness of the spring depends on the reduction of the anchorage length as well as on the stiffness of the bond finite element (G_b) of the adjacent reinforcing bar, and is defined by the following equation:

$$K_u = \beta l_{b,net} \text{Ø} G_b = \beta l_{b,net} k_g E_c \tag{3.16}$$

where β is the anchorage coefficient based on anchorage type, $l_{b,net}$ is basic required anchorage length according to the considered standard, Ø is the diameter of reinforcing bar and G_b is the bond stiffness modulus of reinforcing bar.

The hardening of the plastic branch is calculated from the elastic stiffness and the hardening coefficient *KSN* (which by default in *IDEA StatiCa Detail* takes a value of $1.0 \cdot 10^{-2}$, as defined in Fig. 3.20b.

The models for verifying the anchorage length are used only for ultimate limit state verifications. For serviceability limit states, the anchorage length is not verified (neither the bond nor the anchor end finite elements are used) and the reinforcement is connected directly to the concrete mesh using MPC elements.

As a final remark, to avoid confusion, the bond and anchorage models described above are neither used for modeling tension stiffening (which is performed using a modified stress-strain characteristic of the reinforcement, see Section 3.3.4), nor for calculating crack spacings or crack widths (which is carried out as outlined in Section 3.5.3).

3.6.6 Meshing

All of the finite elements described in the previous chapter are implemented internally, and the analysis model is generated automatically without any need for proficient user interaction. An important part of this process is meshing. The mesh is generated in such a way that the calculation provides reliable results even for complex shapes. There are several rules for creating the mesh, which are stated below for the different elements.

Concrete

All concrete members are meshed together. A recommended element size is automatically computed by the application based on the size and shape of the structure and taking into account the diameter of the largest reinforcing bar. Moreover, the recommended element size guarantees that a minimum of 4 elements are generated in thin parts of the structure, such as slim columns or thin slabs, to ensure reliable results in these areas. The maximum number of concrete elements is

limited to 5000, but this value is sufficient to provide the recommended element size for most structures. In the case that the maximum number of concrete elements is reached (i.e., the final element size is larger than the recommended one), a warning is provided to the user accompanied by the actual and recommended element size. Designers can always select a user-defined concrete element size by modifying the multiplier of the default mesh size.

Reinforcement

The reinforcement is divided into elements with approximately the same length as the concrete element size. Once the reinforcement and concrete meshes are generated, they are interconnected with bond elements (ULS) or directly by MPC elements (SLS), as shown in Fig. 3.16.

Bearing plates

Auxiliary structural parts, such as bearing plates, are meshed independently. The size of these elements is calculated as 2/3 of the size of concrete elements in the connection area. The nodes of the bearing plate mesh are then connected to the edge nodes of the concrete mesh using interpolation constraint elements (RBE3).

Loads and supports

Patch loads and patch supports are connected only to the reinforcement, as shown in Fig. 3.21. Therefore, it is necessary to define the reinforcement around them. Connection to all nodes of the reinforcement within the effective radius is ensured by RBE3 elements with equal weight.

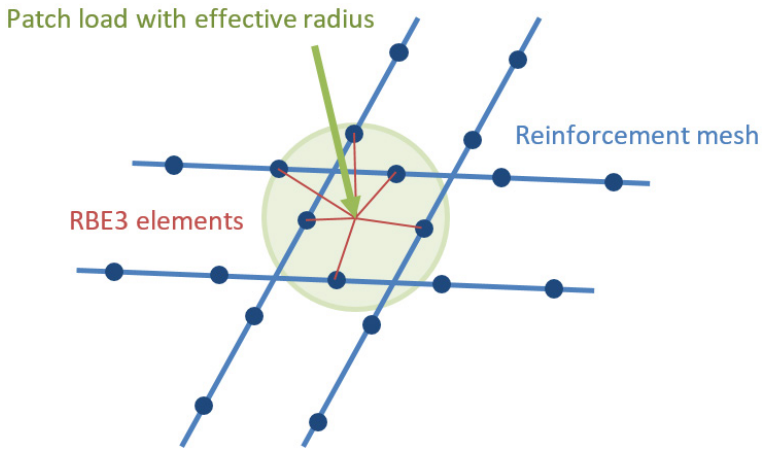

Fig. 3.21 Patch load mapping to reinforcement mesh.

Line supports and line loads are connected to the nodes of the concrete mesh using RBE3 elements based on the specified width or effective radius. The weight of the connections is inversely proportional to the distance from the support or load impulse.

3.6.7 Solution method and load-control algorithm

A standard full Newton-Raphson (NR) algorithm is used to find the solution to the non-linear FEM problem. The implementation is almost identical to the one presented in Crisfield (1997).

Generally, the NR algorithm often does not converge when the full load is applied in a single step. A usual approach, which is also used here, is to apply the load sequentially in multiple increments and use the result from the previous load increment to start the Newton solution of a subsequent one. For this purpose, a load control algorithm was implemented on top of the Newton-Raphson. In the case that the NR iterations do not converge, the current load increment is reduced to half its value, and the NR iterations are retried. This process is repeated until either (i) a minimum load increment size is reached – in this case, the solution is aborted, and the last converged result is exported; or (ii) the NR iterations converge – in this case, another load increment is added unless the full load is reached.

A second purpose of the load-control algorithm is to find the critical load, which corresponds to certain "stop criteria" – specifically the maximum strain in concrete, the maximum slip in bond elements, the maximum displacement in anchorage elements and the maximum strain in reinforcing bars. The critical load is found using the bisection method. In the case that the stop criterion is exceeded anywhere in the model, the results of the last load increment are discarded and a new increment of half the size of the previous one is calculated. This process is repeated until the critical load is found with a certain error tolerance.

For concrete, the stop criterion was set by default to a 5% strain in compression (i.e., around an order of magnitude larger than the actual failure strain of concrete) and 7% in tension at the integration points of shell elements. In tension, the value was set to allow for the limit strain in reinforcement, which is usually around 5% without accounting for tension stiffening, to be reached first. In compression, the value was chosen to ensure numerical but does not allow for an explicit verification of concrete crushing (see Section 3.3.1).

For reinforcement, the stop criterion is defined in terms of stresses. Since stresses at the crack are modeled, the criterion in tension corresponds to the reinforcement tensile strength f_t (see Fig. 3.2c), accounting for the safety coefficient (as per Section 3.5.1). The same value is used for the criterion in compression.

The stop criterion in bond and anchorage elements is $\alpha \cdot \delta u_{max}$, where δu_{max} is the maximum slip used in code checks and $\alpha = 10$. The multiplicator α can be changed in the advanced version. The large α value was chosen to ensure that the stop criteria in concrete and reinforcement are almost always applied first, and the criterion in the bond or anchorage is only reached in very rare cases. This way, if the reinforcement is being torn out of the concrete, this is clearly visible in the results. However, because of the almost horizontal nature of the hardening branch, even if the criterion is reached, this results in only a very small increase in the calculated critical load in comparison to the load at δu_{max}.

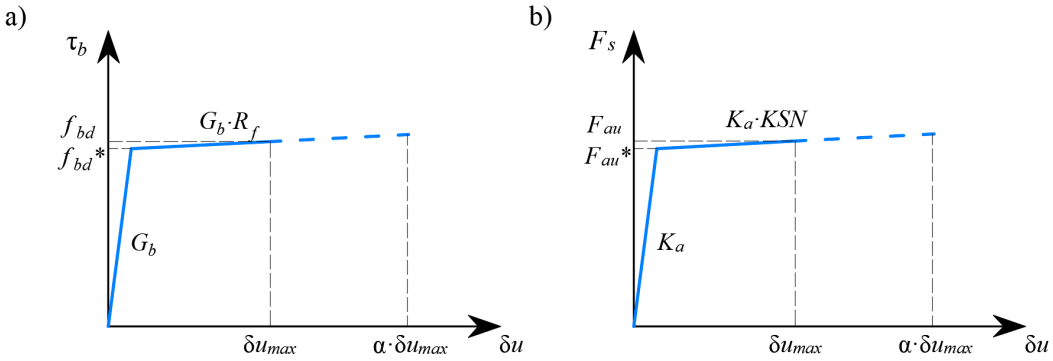

Fig. 3.22 Constitutive relationship of bond and anchorage elements used for anchorage length verification: (a) Bond shear stress slip response of a bond element; (b) force-displacement response of an anchorage element.

It should be noted that often the solution diverges before any of the stop criteria are reached, typically as a result of high compression softening within a concrete element. In such a case, a message warning about the divergence of the model is shown, and the results from the last converged load level are displayed to the user.

3.6.8 Results and verifications

Presentation of results

Results are presented independently for concrete and for reinforcement elements. The stress and strain values in the concrete are calculated at the integration points of shell elements. However, as it is not practical to output the data in such a manner, the results are presented by default in nodes (see Fig. 3.23). It should be noted that this representation might locally underestimate the results at compressed edges of members in cases where the finite-element size is similar to the depth of the compression zone. The results presented in the mesh nodes are minimum, maximum, or average values from adjacent gauss integration points in connected elements (see Fig. 3.23). The same applies to element presentations, but only gauss integration points from the respective element are considered here. In spite of the several possibilities of displaying the results provided by the solver, the *IDEA StatiCa Detail* user can only see the output of results in nodes. By default, the program presents the most restrictive results in nodes (minimum for compressive magnitudes and results of the compression softening value k_c, and maximum for tensile values).

The results for the reinforcement finite elements are either constant for each element (one value – e.g., for steel stresses) or linear (two values – for bond results). For auxiliary elements, such as elements of bearing plates, only deformations are presented.

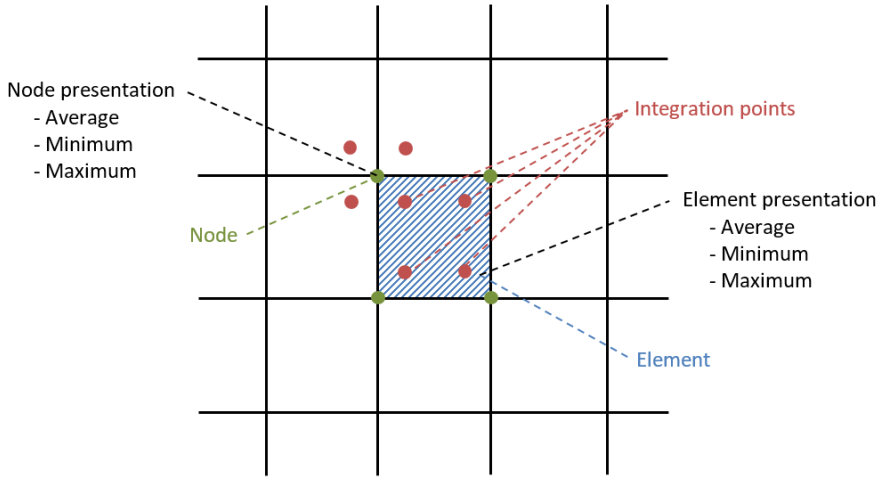

Fig. 3.23 Concrete finite element with integration points and nodes: presentation of the results for concrete in nodes and in finite elements.

Ultimate limit state verifications

The different verifications required by specific design codes are assessed based on the direct results provided by the model. ULS verifications are carried out for concrete strength, reinforcement strength, and anchorage (bond shear stresses).

The concrete strength is evaluated in compression as the ratio between the maximum principal compressive stress σ_{c3} and the limit value $\sigma_{c3,\mathrm{lim}}$, where the latter depends on the concrete grade, the design code and the transverse strain.

$$\sigma_{c3} / \sigma_{c3,\mathrm{lim}} \tag{3.17}$$

The strength of the reinforcement is evaluated in both tension and compression as the ratio between the stress in the reinforcement at the cracks σ_{sr} and the specified limit value $\sigma_{sr,\mathrm{lim}}$:

$$\sigma_{sr} / \sigma_{sr,\mathrm{lim}} \tag{3.18}$$

The anchorage length is evaluated independently as the ratio between the bond stress τ_b and the limit bond stress f_{bd} according to the specified design code:

$$\tau_b / f_{bd} \tag{3.19}$$

These verifications are carried out with respect to the appropriate limit values for the respective parts of the structure (i.e., in spite of having a single grade both for concrete and reinforcement material, their actually used stress-strain diagrams differ in each part of the structure due to tension stiffening and compression softening effects).

The basic results and verifications (stress, strain and utilization = ratio calculated value / limit value, as well as the direction of principal stresses in the case of concrete elements) are displayed by means of different plots. Compression is generally presented in red and tension in blue. Global minimum and maximum values for the entire structure can be highlighted as well as minimum and maximum values for every user-defined part. In a separate tab of the program, advanced results such as tensor values, deformations of the structure and reinforcement ratios (effective and geometric) used for computing the tension stiffening of reinforcing bars can be shown. Furthermore, loads and reactions for selected combinations or load cases can be presented.

Serviceability limit state verifications

SLS assessments are carried out for stress limitation, crack width and deflection limits. Stresses are checked in concrete and reinforcement elements according to the applicable code in a similar manner to that specified for the ULS in Eqs. (3.17) and (3.18).

Deflections can only be assessed for walls or beams (isostatic or hyperstatic). In these cases, the absolute value of deflections is considered (compared to the initial state before loading) and the maximum admissible value of deflections must be set by the user. Deflections at trimmed ends cannot be checked since these are essentially unstable structures where equilibrium is satisfied by adding end forces and hence, the resulting deflections are unrealistic.

Short-term $u_{z,st}$ or long-term $u_{z,lt}$ deflection can be calculated and checked against user-defined limit values:

$$u_z \Big/ u_{z,\mathrm{lim}} \tag{3.20}$$

Crack widths and crack orientations are calculated only for permanent loads, either short-term w_{st} or long-term w_{lt}. The verifications with respect to limit values specified by the user according to the respective design code are presented as follows:

$$w \Big/ w_{\mathrm{lim}} \tag{3.21}$$

As outlined in Section 3.5.3, there are two ways of computing crack widths. In the general case (stabilized cracking), the crack width is calculated by integrating the strains on 1D elements of reinforcing bars. The crack direction is then calculated from the three closest (from the center of the given 1D finite element of reinforcement) integration points of 2D concrete elements. While this approach to calculating the crack directions does not necessarily correspond to the real position of the cracks, it still provides representative values, and the resulting crack widths can directly be compared to the specified crack width requirements at the position of the reinforcing bar.

4 Basic validations

4.1 Introduction

This chapter validates the proper functionality of the material models presented in the previous chapter in the numerical methods used in the *IDEA StatiCa Detail* implementation of the Compatible Stress Field Method (CSFM). Basic cases of pure tension, pure compression, and pull-out loading are examined in order to verify the reinforcement, concrete, and bond models, respectively. The results obtained by the CSFM are then compared to the theoretical material models upon which the implementation is based.

4.2 Uniaxial tension including crack widths

4.2.1 Case description

In this section, the theoretical material models for tension stiffening and crack width calculation are compared to the CSFM results for a uniaxial tension chord. The Tension Chord Model (TCM), which was developed at the ETH (Sigrist 1995; Alvarez 1998) serves as the theoretical basis upon which the effects of tension stiffening are accounted for, and crack widths and crack spacing in sufficiently reinforced regions are determined (in regions where stabilized cracking can be developed, see Section 3.3.4). The initial uncracked behavior is considered in the theoretical calculation, while this effect is neglected in the CSFM for design purposes (see Section 3.2). For stirrups with very low reinforcement ratios ($\rho<\rho_{cr}$, where ρ_{cr} is the minimum reinforcement in direct tension according to Eq. (3.5)), the model known as the Pull-Out Model (POM) is implemented in the CSFM. Both models are described in Section 3.3.4.

The virtual experimental setup illustrated in Fig. 4.1 was chosen in order to generate uniaxial tension loading in the area of interest. The reinforcement ratio varies from a value below ρ_{cr} up to 1.9 %. The complete load-deformation behavior is computed to verify the implementation both at the ULS and at the SLS.

4.2.2 Modeling with the CFSM

The CSFM model in Fig. 4.1 has a length of 5 m and a cross-section of 1.6 m x 0.2 m. The longitudinal reinforcement varies according to Table 4.2. The area of load application is provided with additional transverse reinforcement. However, the area of interest of the tension chord, which is marked in Fig. 4.1, is solely reinforced in the direction of loading. The RC member is supported at its top edge, where deformations in the x – and z – direction are restricted, and a line load is applied close to the bottom edge of the member. An SLS calculation is performed with a load that increases from 0 kN/m to the ultimate load q_u. The verification of the anchorage length is deactivated, as anchorage is not of interest in this validation. All comparisons and calculations

are performed without considering safety factors, while default values are used for the remaining parameters. Values are given for the material parameters related to tensile behavior in Table 4.1, while the longitudinal reinforcement configurations for the four different test cases are shown in Table 4.2.

Table 4.1. Model parameters.

Parameters		Theoretical model & CSFM model
E_s	[GPa]	200
f_{yk}	[MPa]	500
f_{uk}	[MPa]	540
ε_{uk}	[‰]	50
E_c	[GPa]	32.8
f_{ctk}	[MPa]	2.9
τ_{b0}	[MPa]	2.9
τ_{b1}	[MPa]	5.8
λ	[-]	0.67

Table 4.2. Varying geometrical test parameters.

Property		Test 1	Test 2	Test 3	Test 4
$\varnothing_s$	[mm]	10	14	18	22
s	[mm]	100	100	100	100
a_s	[mm^2/m]	785	1539	2545	3801
ρ_{geo}	[%]	0.39	0.77	1.27	1.90
ρ_{eff}	[%]	$< \rho_{cr}$	0.88	1.28	1.91

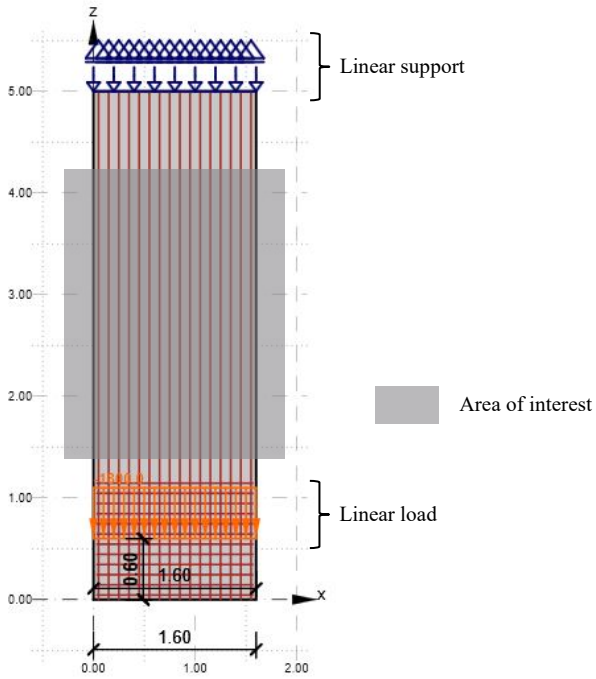

Fig. 4.1. CSFM model: tension chord and area of interest.

4.2.3 Comparison with theoretical constitutive models

In this section, the results from the CSFM model are compared to those provided by the theoretical constitutive models that were taken as a reference for the implementation in the CSFM. Fig. 4.2 shows the stress-strain behavior of the tension chords. The blue lines represent the theoretical constitutive curves, while the black ones are CSFM results. The stress corresponds to the maximum stress at a crack, σ_{sr}, whereas the strain is the mean strain (i.e., the average over a crack element) in the tension chord, ε_{sm}. It can be seen that there is almost perfect agreement between the theoretical and CSFM results for loads above the cracking load considered in the theoretical model. For loads below this cracking load, the curves differ, which is due to the fact that the CSFM neglects the uncracked initial behavior and considers the structural elements to be fully cracked for any load state.

Test 1 is a particular case, as it contains less than the required minimum reinforcement to avoid brittle failures when cracking under direct tension actions. Strictly speaking, the theoretical behavior expected during this test should be a brittle failure of the reinforcement right after cracking. However, Test 1 is analyzed here for the particular case of cracks that are controlled by the main reinforcement and progress into regions with low amounts of reinforcement (e.g., bending cracks progressing into webs with a low amount of stirrups). In this context, the Pull-Out Model (see Section 3.3.4) is used as a theoretical comparison, assuming that the element is fully cracked

before applying the loads. Therefore, both the theoretical and the CSFM results in Test 1 neglect the uncracked initial behavior of the elements and provide very similar results for any stress state.

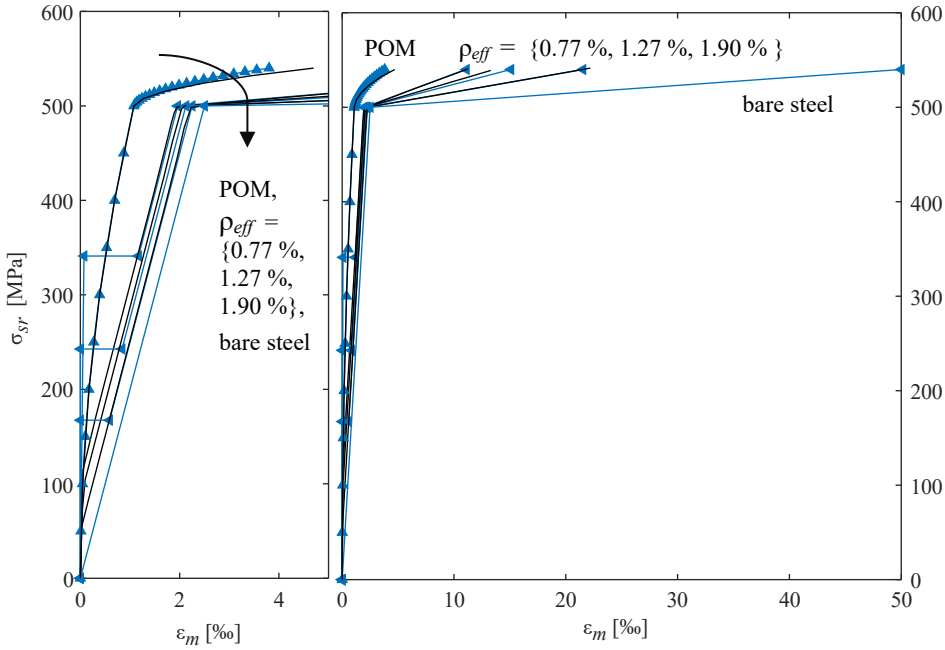

Fig. 4.2. Reference theoretical model (blue markers) and CSFM (black) curves for the reinforcement stresses at the cracks, σ_{sr}, versus the mean reinforcement strains for given reinforcement ratios, ε_m.

A comparison of the crack widths as a function of the applied load is displayed in Fig. 4.3. The same color code as in Fig. 4.2 is used. The agreement between the theoretical constitutive models and the CSFM results is also excellent in this case. The divergence at small loads (at which the theoretical model assumes uncracked behavior) is again explained by the initially cracked state assumed in the CSFM for design purposes (e.g., the element might already be cracked due to shrinkage actions or previous load steps). The prediction of the crack spacing (see Table 4.3) in the CSFM is also consistent with the theoretical constitutive model. It should be noted that in Test 1, the cracking is non-stabilized, and, strictly speaking, a constant representative crack spacing cannot be defined. However, the POM implicitly assumes a constant crack spacing in this situation, $l_{\varepsilon,avg}$, which is equal to the distance between points of zero slip when the reinforcing bar reaches its tensile strength (see further information in Section 3.3.4).

Table 4.3. Mean crack spacing results (CSFM represents the calculation with the CSFM model and *TCM* is the reference theoretical constitutive model).

Property		Test 1	Test 2	Test 3	Test 4
s_{rm}^{CSFM}	[mm]	non-stabilized cracking	262	233	190
s_{rm}^{TCM}	[mm]		260	233	189

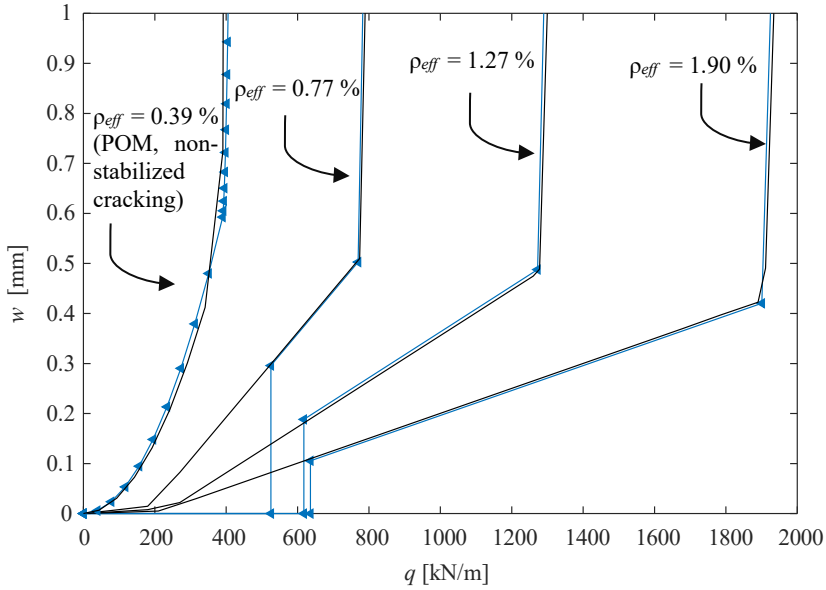

Fig. 4.3. Reference theoretical model (blue markers) and CSFM (black) curves of load against crack width load for different reinforcement ratios
(from left to right: ρ_{eff}[%] = {0.39, 0.77, 1.27, 1.90}).

4.2.4 Mesh size sensitivity

To study the influence of the mesh size on the results of tension elements, an analysis of the mesh size sensitivity was performed for Test 4. To this end, a comparison is made between the resulting curve of the maximum steel stresses (σ_{sr}) and the mean strains of the reinforcement (ε_m). Fig. 4.4 shows the results from the CSFM for the computation with the default finite element mesh size (107 mm in this case), as well as half and double this default finite mesh size. The theoretical results for this test are also displayed in blue. The behavior of the bare reinforcement and Pull-Out Model is included in Fig. 4.4 to serve as a reference. It can be observed that the calculations with different mesh size perfectly overlap with the theoretical reference value. Hence, for this

case of a stress field subjected to uniaxial and uniform tension, the results do not show any mesh size dependency.

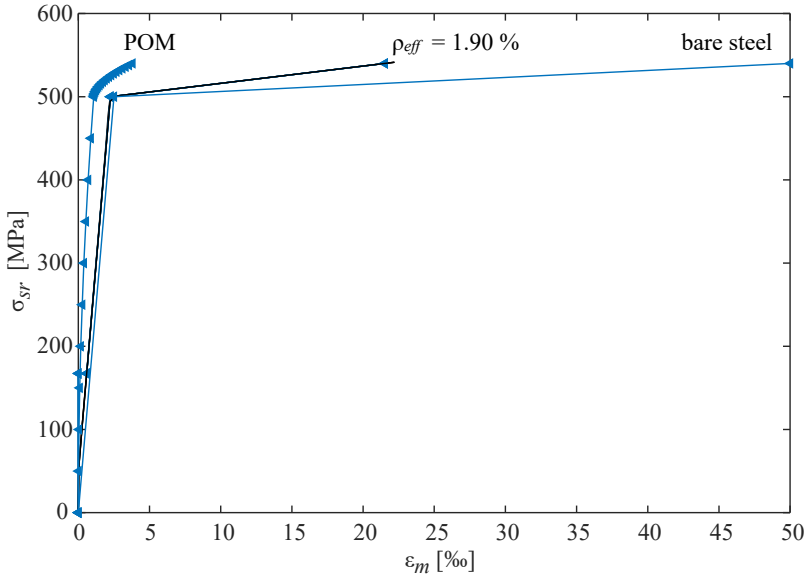

Fig. 4.4. Mesh size sensitivity for Test 4 (ρ_{eff} = 1.90 %) with the default mesh size compared to half and double mesh size.

4.2.5 Conclusions

The results obtained from the CSFM are in excellent agreement with the theoretical constitutive model described in Chapter 2. The following conclusions can be stated for this example:

- The computed crack widths are in good accordance with the theoretical ones. However, the CSFM computes small crack widths even before the onset of cracking, as shown in Fig. 4.3. This is caused by the initially cracked behavior implemented in the CSFM for design purposes. Therefore, crack width predictions on uncracked (in reality) members will err on the side of caution, particularly in the case of small reinforcement ratios.
- The effect of tension stiffening according to the Tension Chord Model and the Pull-Out Model can be reproduced very well. In addition, as predicted by the reference theoretical constitutive models, the deformation capacity markedly decreases with the reduced reinforcement ratios.
- Table 4.3 confirms that the crack spacing is also well captured by the CSFM.
- Furthermore, this loading case consisting of uniaxial and uniform tension does not show any mesh size dependency.

4.3 Uniaxial compression

4.3.1 Case description

This section is dedicated to the validation of a reinforced concrete member subjected to pure compression. The aim of this virtual experiment is to validate the modeled concrete behavior under uniaxial compression.

4.3.2 Modeling with the CSFM

The model consists of a concrete wall with dimensions of 2.0 m x 1.0 m x 0.5 m. As seen in Fig. 4.5, there is only reinforcement transverse to the direction of loading, namely Ø16 mm reinforcing bars with a spacing of 50 mm, with one bar per layer. This reinforcement does not influence the overall behavior in the compression direction but ensures proper load distribution. More specifically, it mitigates local effects due to the spreading of the applied load that tends to generate transversal strains and consequently softens the response of the member.

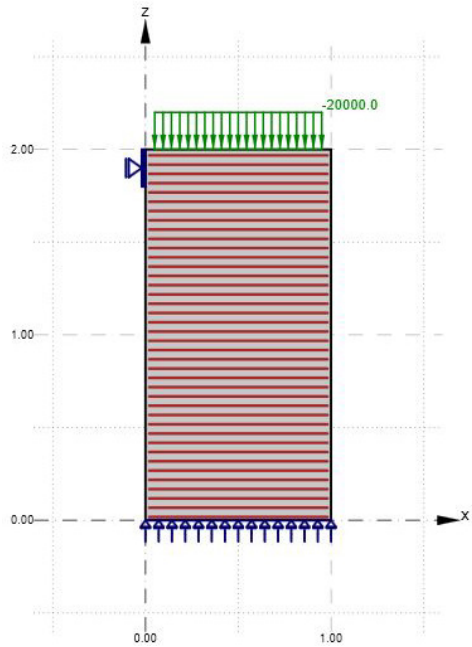

Fig. 4.5. Uniaxial compression model with reinforcement layout, supports, and loading.

Unless stated otherwise, the default parameters of the software are used. C 30/37 concrete and B500B steel reinforcing bars with the properties listed in Table 4.4 were chosen for this validation. The safety factors in this example are set to default, i.e., they are considered according to EN 1992-1-1.

Table 4.4. Model parameters.

Parameters		Theoretical model & CSFM model
E_s	[GPa]	200
f_{yk}	[MPa]	500
f_{uk}	[MPa]	540
ε_{uk}	[‰]	50
E_c	[GPa]	32.8
f_{ck}	[MPa]	30
f_{ctk}	[MPa]	2.9
ε_{cu2}	[‰]	50
ε_{ct}	[‰]	70

4.3.3 Results and comparison to codes

The estimates of strength and cause of failure obtained from the CSFM analyses are compared to the theoretical design values stated in EN 1992-1-1. The results are provided in Table 4.5. It can be observed that there is a very good agreement between the theoretical and CSFM results for the default mesh size.

Table 4.5. Comparison of strength and failure mode for uniaxial compression.

	CSFM – model	EN 1992-1-1
Failure load q_u	9’939 kN/m	10’000 kN/m
Failure mode	Concrete crushing (divergence due to concrete strength being reached)	Concrete crushing

4.3.4 Mesh size sensitivity

The sensitivity of the results to the mesh size is examined in Fig. 4.6. The model is evaluated for half of the default, the default, and twice the default mesh size. The default mesh size in this case is 77 mm. As can be seen, the ultimate capacity of concrete in compression is well predicted for the smaller mesh sizes, while an underestimation of about 10% for the coarsest mesh is observed. This is due to the transverse tensile strains caused by the introduction of load near the edge of the element (i.e., in this local region, there is no longer a uniaxial compressive stress state). Due to these transverse strains, the concrete is softened in the edge element. Hence, the greater the element size, the larger the area affected by this softening, and the more substantial the difference to the theoretical value (which neglects these local effects).

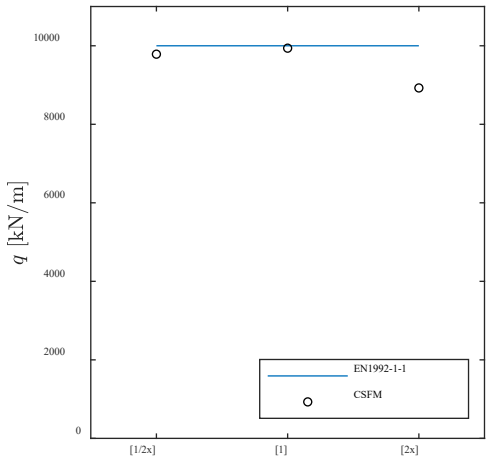

Fig. 4.6. Mesh size sensitivity compression: calculated ultimate load vs. multiplier of the default mesh size.

4.3.5 Conclusions

The following conclusions can be stated regarding the behavior of CSFM models under uniaxial compressive stress states:

- The predicted strength shows reasonable agreement with the reference code value. Furthermore, the failure mode can be captured properly by the CSFM analyses.
- The variation of the mesh size shows that compressive strength predictions are not influenced by the mesh size within a reasonable range. Only at the largest mesh size, a moderately lower load prediction (10%) is obtained due to local softening near the edges, which has a higher influence for large elements.

4.4 Pull-out of reinforcing bars

4.4.1 Case description

The following basic validation model explores the fundamental aspects of the CSFM for the verification of the anchorage length (see description in Section 3.3.3), which reflects the basic constitutive laws implemented for the interface between concrete and reinforcement. To this end, a virtual pull-out test was conducted on a reinforcing bar embedded in concrete.

4.4.2 Modeling with the CSFM

The chosen model is a concrete block of the dimensions 1.0 m x 1.0 m x 0.2 m with a notch running from the bottom edge up to the middle of the specimen. The bottom edge is supported in the x- and z-direction, while the top left corner is supported in the x-direction. The geometry and reinforcement layout are shown in Fig. 4.7.

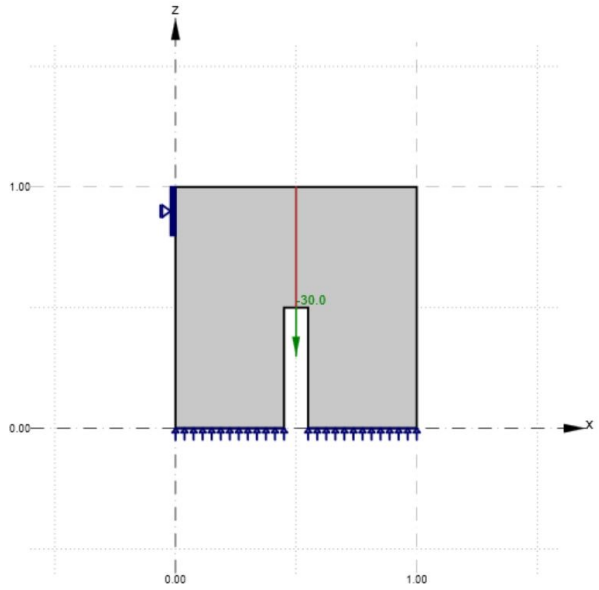

Fig. 4.7. Pull-Out Model in the CSFM with reinforcement layout, supports and loading.

The same material properties as defined for the previous basic validation example are considered, i.e., the material properties are defined in Table 4.4. However, the tension stiffening effect is deactivated in this case in order to isolate the effect of the anchorage models. The safety factors are set to default in the CSFM, i.e., they follow the prescriptions of EN 1992-1-1. Unless stated otherwise, the default parameters are applied.

In the virtual experiments, a reinforcing bar of diameter Ø = 8 mm or Ø = 16 mm embedded in the concrete block over a length of 0.5 m is subjected to a tensile force F. Depending on the reinforcing bar diameter, either bond or reinforcement rupture is decisive.

4.4.3 Comparison with analytical results

The results of failure load (F_u) and failure mode for the two analyzed diameters are summarized in Table 4.6. The predicted failure loads agree very well with the theoretical ones (i.e., within the limits of precision of the numerical methods used) for the two different diameters analyzed.

The Pull-Out Model, with a reinforcement diameter of $Ø_s$ = 8 mm at a tensile force equal to the design yield strength, is examined more closely. In Fig. 4.8 the steel stress and slip distribution over the embedment length are illustrated and compared to the analytical solution of the differential equation of slip (based on the considered rigid-ideally plastic bond stress-slip relationship). The minor differences that can be observed are due to the quasi-rigid (but not rigid-ideally plastic) numerical implementation of the bond stress-slip relationship in the CSFM, which is used to avoid numerical instability.

Table 4.6. Comparison of strength and failure mode for the virtual pull-out experiments.

Bar diameter		CSFM	EN 1992-1-1
$Ø_s$ = 8 mm	Failure load F_u	24.5 kN	23.6 kN
	Failure mode	Steel rupture (reinf. strain limit reached)	Steel rupture
$Ø_s$ = 16 mm	Failure load F_u	78.1 kN	75.4 kN
	Failure mode	Bond failure (divergence due to bond strength reached along all the bar)	Bond failure

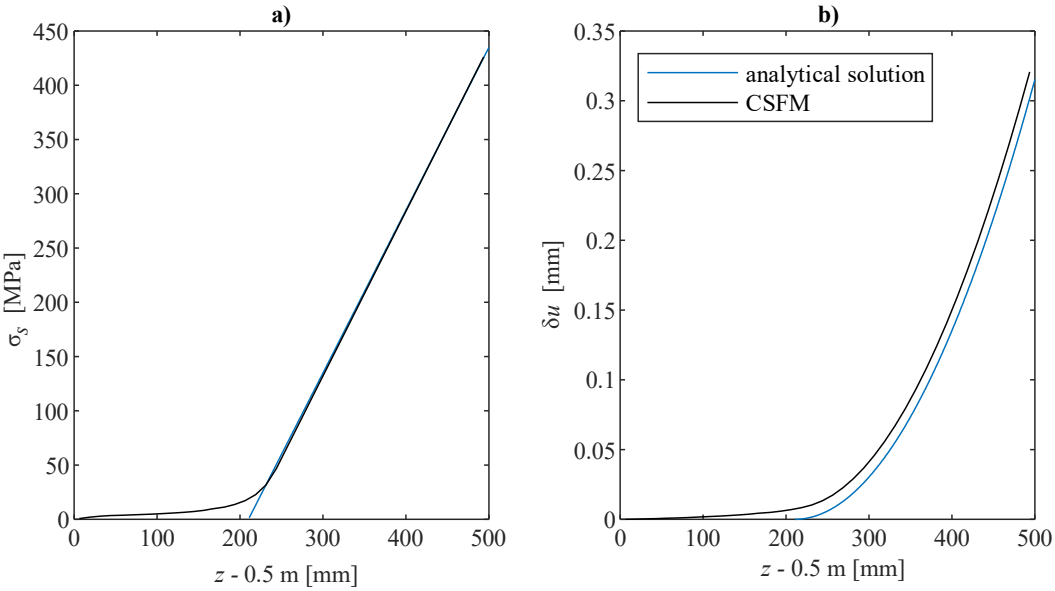

Fig. 4.8. Pull-out situation with $Ø_s$ = 8 mm at F = 21.9 kN: (a) Steel stress; (b) slip distribution over the embedment length.

4.4.4 Mesh size sensitivity

As in the two previous chapters, a mesh size sensitivity analysis was performed for the case of the pull-out test. The models were again evaluated for half of the default, the default, and twice the default mesh size. For both diameters of the reinforcing bars, a default mesh size of 25 mm was obtained. The sensitivity analysis results for the ultimate load are shown in Fig. 4.9. It can be seen that the mesh size has a marginal influence on the ultimate load for this loading case.

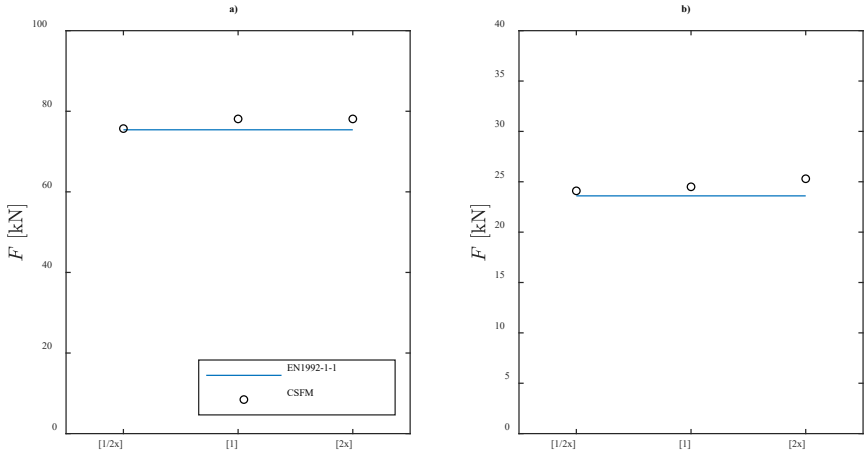

Fig. 4.9. Mesh size sensitivity for the predicted ultimate load for the Pull-Out Model of reinforcing bar with (a) diameter $Ø_s$ = 16 mm and (b) $Ø_s$ = 8 mm.

4.4.5 Conclusions

As in the previous basic validations, the pull-out analysis shows that the anchorage and reinforcement failures predicted via CSFM analyses are very similar to the theoretical, analytical predictions, again showing highly reduced mesh size sensitivity. The slip results are also in good agreement with analytical predictions that consider a rigid-ideally plastic bond stress-slip relationship.

5 Comparison with codes

5.1 Introduction

This chapter contains a detailed comparison of results from the traditional design of details and members based on several national standards with those obtained using the Compatible Stress Field Method (CSFM). In addition to traditional design methods, the CSFM was also compared to the cross-sectional analysis implemented in *IDEA StatiCa RCS/Beam* software for those examples suitable for this analysis (i.e., long members without concentrated loads). *IDEA StatiCa RCS/Beam* software provides a cross-sectional analysis which implements the typical hypotheses considered in structural design codes when analyzing long members (i.e., the internal forces are calculated assuming materials exhibit linear elastic behavior, and that plane sections remain plane, while the dimensioning of the cross-sections considers the non-linear behavior of the materials and neglects the contribution of concrete in tension). A more detailed description of the hypothesis of *IDEA StatiCa RCS/Beam* software is given in Appendix A.

The first example (Section 5.2) compares the results obtained using strut-and-tie models (STM) to the results from the CSFM for the well-known example of a deep beam with a large opening (Schlaich et al., 1987), showing the potential of the CSFM when applied to discontinuity regions. The following topics are discussed in this example:

- The influence of detailing (impact of the anchorage and amount of transverse reinforcement in the concrete strut).
- The influence of the main model parameters with respect to the ultimate load and failure mode.
- The verification of serviceability in the CSFM in order to examine to which extent the ULS verifications from STM are sufficient for this configuration.
- The efficiency of using topology optimization (see Section 3.4) to design the positions and directions of reinforcement.

The second example (Section 5.3) focuses on the ULS and SLS assessment of a simply supported long T-beam defined by Procházka (2006). In this example, the results of the CSFM are compared to analytical verifications by Procházka (2006), as well as to verifications with *IDEA StatiCa Beam* following the prescriptions of EN 1992-1-1. The influence of the different calculations in the following results was investigated:

- Ultimate moment resistance.
- Stresses, crack widths, and deflections in the SLS.

The third example (Section 5.4) is devoted to the verification of the correct implementation in *IDEA StatiCa Detail* of ACI 318-14. A simply supported beam with a rectangular cross-section is analyzed and designed according to ACI 318-14, using *IDEA StatiCa RCS*, and then compared to the results obtained by the CSFM for the following quantities:

- Ultimate design load.
- Ultimate moment resistance.
- Deflection at midspan.

The last verification example (Section 5.5) shows the assessment of a 1D member, namely a simply supported T-beam extracted from the experimental work of Leonhardt and Walther (1963). The verification of the CSFM against the experimental results for this example will be shown in Section 6.2. In this example, the results of the CSFM are compared and verified against results calculated by beam and cross-sectional analysis, according to EN 1992-1-1. These analyses were performed in *IDEA StatiCa Beam/RCS*. The following results are compared for the two procedures:

- Ultimate moment resistance.
- Stresses, crack widths, and deflections at the SLS.

It should be noted that all the examples were analyzed in release version 9.1 of *IDEA StatiCa*, which implements the CSFM. A detailed description of the CSFM can be found in Chapter 3.

5.2 Comparison between the CSFM and the strut-and-tie model

5.2.1 Case description

A deep beam with an opening designed by Schlaich et al. (1987) is analyzed with the CSFM in this section. The results are compared to the original design, which was produced using strut-and-tie models (STM). The dimensions, reinforcement layout, and material properties of the deep beam are shown in Fig. 5.1 and Table 5.1. The member was designed for a factored load (i.e., design load = characteristic load multiplied by load factor) $F_u = F = 3$ MN.

Schlaich et al. (1987) dealt with the problem of ULS design using STM by splitting the beam into a left and right part and then considering two completely different truss models for the left part, designing each of them to carry half of the acting load. Fig. 5.2 shows both strut-and-tie models for the left side of the deep beam: (a) orthogonal and (b) diagonal. The support reactions of 0.535 MN correspond to the share of each model (50%) of the total vertical reaction in the left support, i.e.:

$$R_{left} = F_u \frac{2.5\text{ m}}{7.0\text{ m}} = 1.07\text{ MN} \tag{5.1}$$

The diagonal truss model consists of ties T2 and T9 as well as corresponding struts, while the orthogonal truss model contains ties T1 and T3 to T8. Superposing these models for ULS design, Schlaich et al. (1987) proposed the reinforcement layout shown in Fig. 5.1 (b).

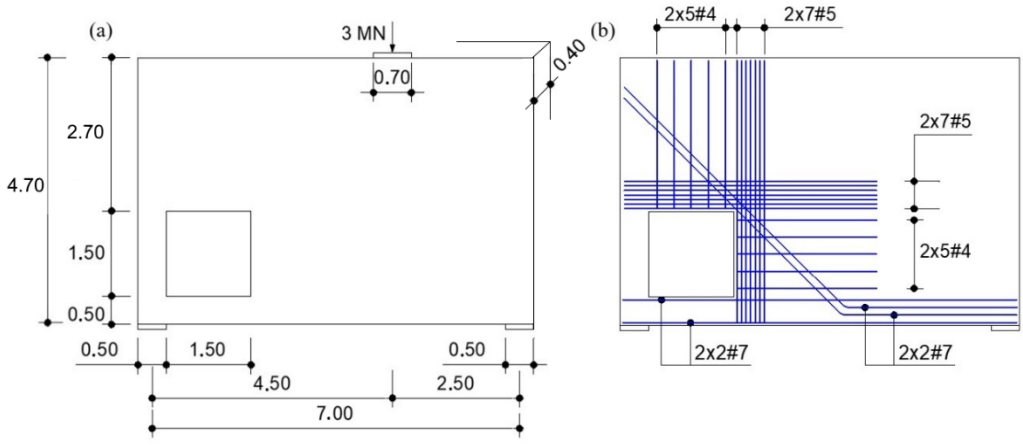

Fig. 5.1 Deep beam: (a) Dimensions in [m]; (b) reinforcement layout.

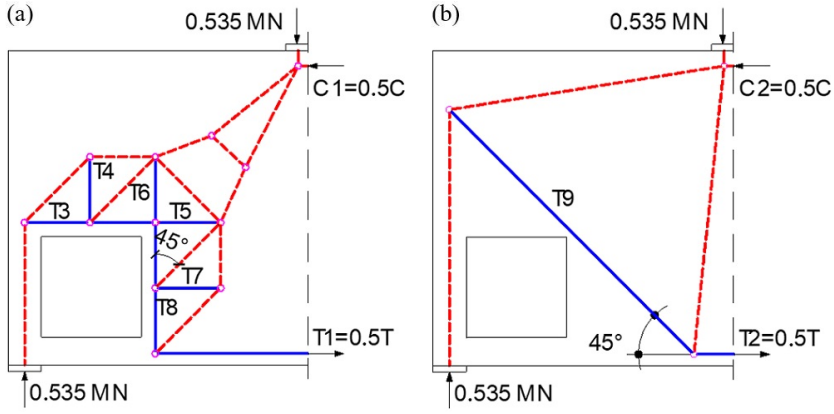

Fig. 5.2 Strut-and-tie models, according to Schlaich et al. (1987): (a) Orthogonal; (b) diagonal.

5.2.2 Modeling with the CSFM

Seven different models of the region were created in *IDEA StatiCa Detail* to analyze the capabilities of the CSFM when modeling discontinuity regions. The model corresponding to the dimensions, materials, and reinforcement layout taken from Schlaich et al. (1987) is referred to as the base model or model No. 1. The topology and reinforcement layout of the base model are shown in Fig. 5.3. A basic anchorage type (straight bar) was used at the ends of all reinforcing bars in the base model. Models No. 2 to 4 simulated different anchorage conditions (see the description

in Table 5.2), while the remaining ones (No. 5 to 7) were used to optimize the location and amount of reinforcement (see Section 5.2.5).

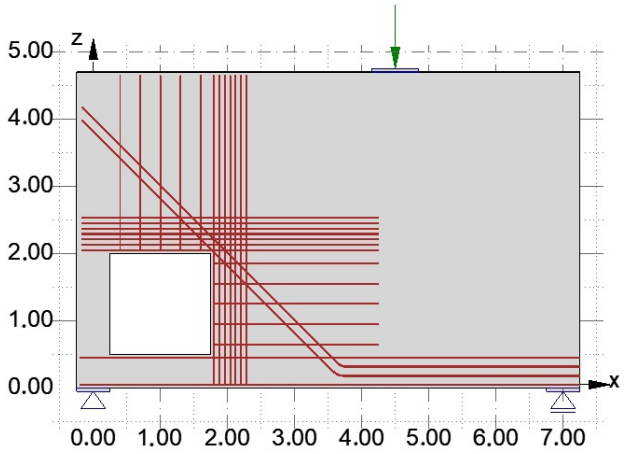

Fig. 5.3 CSFM model topology and the reinforcement layout (dimensions in [m]).

The main material properties considered in the base model are listed in Table 5.1. These properties are either directly extracted from Schlaich et al. (1987) or EN 1992-1-1 in the case of properties not contained in the original study. The thickness of the bearing plate was not defined in Schlaich et al. (1987) – the study just assumed it to be sufficiently stiff – and was considered to be 100 mm for the CSFM models.

Table 5.1 Material properties for the CSFM.

Characteristic tensile strength of reinforcement f_{tk} [MPa]	540[2)]
Characteristic yield strength of reinforcement f_{yk} [MPa]	500[1)]
Partial safety factors for reinforcement γ_s [-]	1.15[1)]
Characteristic strain limit of reinforcement ε_{uk} [‰]	50[1)]
Modulus of elasticity of reinforcement E_s [GPa]	200[2)]
Characteristic concrete compressive strength f_{ck} [MPa]	25.5[1)]
Concrete strain when reaching the maximum strength ε_{c2} [‰]	2.0[2)]
Partial safety factors for concrete γ_c [-]	1.5[1)]

1) Schlaich et al. (1987)
2) Extracted from EN 1992-1-1

5.2.3 Ultimate limit state design

Base model results

The modeling of the deep beam with the CSFM resulted in the compatible stress field model shown in Fig. 5.4a. The load-carrying mechanism and flow of forces can be easily derived by analyzing the compression fields (red) and ties (blue). The stress fields can be seen as generalized struts in which stresses are considered instead of force resultants. The ultimate load calculated by the CSFM for the base model was 2814 kN, which is 94% of the ultimate load (3000 kN) determined by Schlaich et al. (1987) using STM.

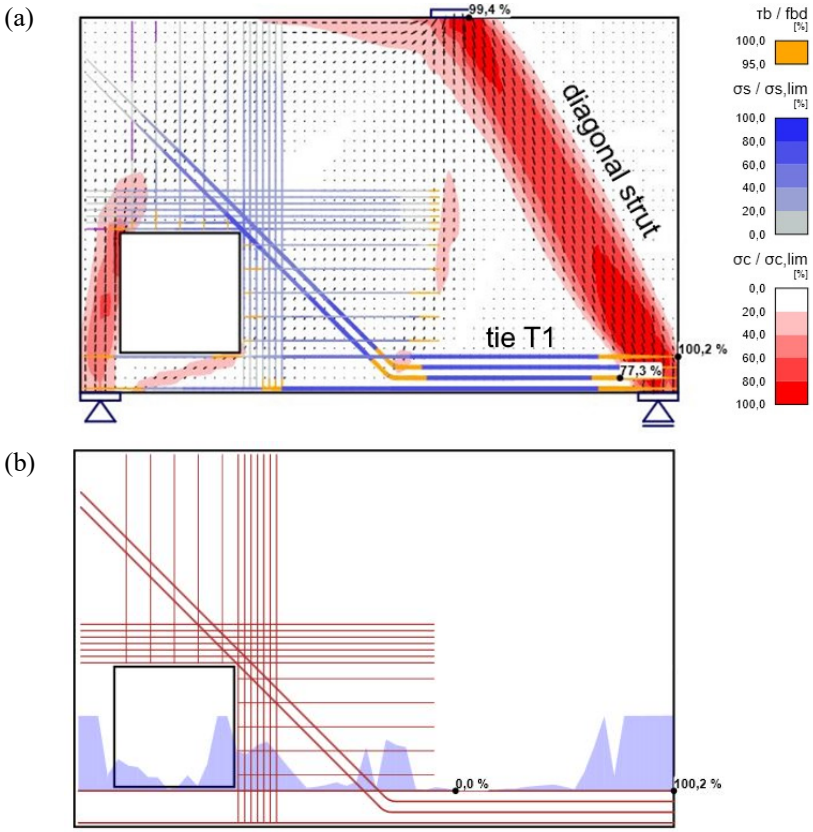

Fig. 5.4 CSFM ultimate limit state verifications for model No.1: (a) Stress-flow at the ULS; (b) ratio between bond stresses and the ultimate bond strength of tie T1.

The anchorage of the top bar of tie T1 (Fig. 5.2a) was identified as critical; see the ratio between the bond stresses and ultimate bond strength in Fig. 5.4b. The stress in this tie reached 77.3% of its strength (83.5% of its yield stress) in the zone close to the anchorage, intersecting the governing (diagonal) strut. Therefore, the presence of high transversal strains in the reinforcement might lead to a high reduction in the compressive strength (low effective concrete strength), as will be discussed below.

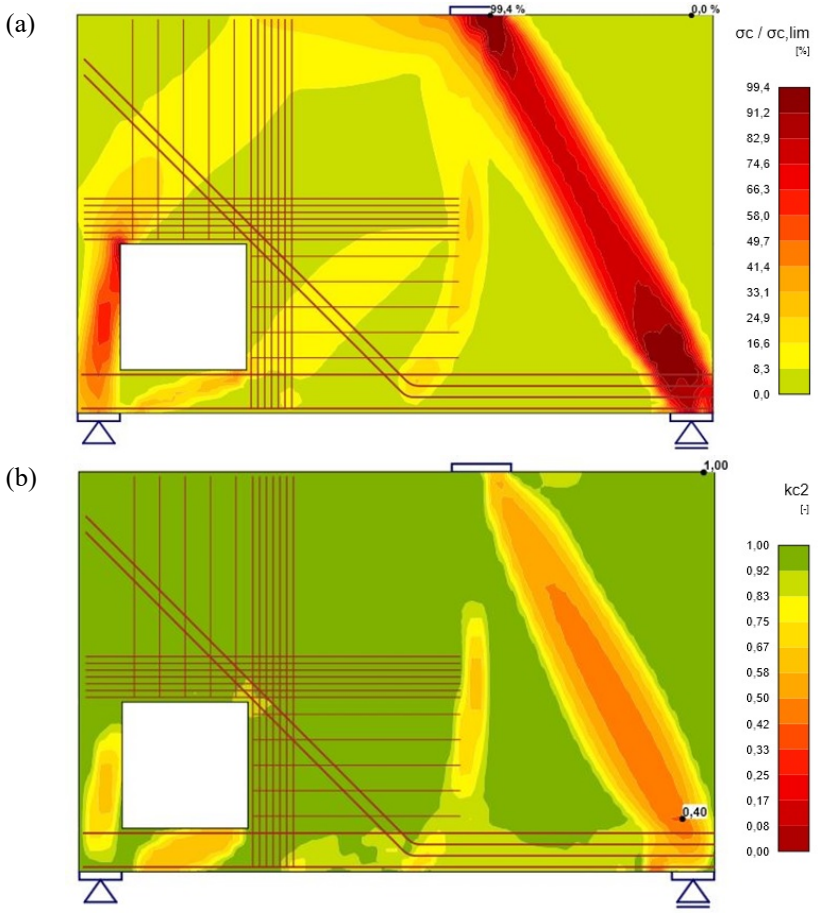

Fig. 5.5 Concrete behavior at ultimate limit state for model No.1: (a) Ratio of stress and strength; (b) concrete compressive strength reduction factor.

In the CSFM the concrete strength reduction due to transversal cracking (compression softening effect) is automatically calculated based on the computed transverse tensile strains (see Chapter 3 for more details). Schlaich et al. (1987) took this phenomenon into account by imposing a stress limit corresponding to a bottle shaped stress field for the diagonal strut at the right side of the deep beam (see Fig. 5.5a and Fig. 5.5b). The concrete stress limit considered by Schlaich et al. (1987) for this condition was $0.62 \cdot f_{cd}$. Schlaich et al. (1987) computed that the stress acting in the strut in the ULS is $0.48 \cdot f_{cd}$, which is lower than the considered stress limit. The reduction factor provided by EN 1992-1-1 for concrete struts in cracked compression zones is $0.54 \cdot f_{cd}$ (for the given value f_{ck}=25.5 N/mm^2), i.e. slightly lower than the value proposed in the original example. Fig. 5.5b shows that the minimum stress limit calculated by the CSFM in the governing strut is $0.40 \cdot f_{cd}$ in the zone close to its anchorage. It should be noted that this local value cannot be directly compared to the values proposed by Schlaich et al. (1987) and EN 1992-1-1, as these correspond to the average strength limits of the strut.

STM and the CSFM show good agreement of their results. Moreover, the results of both models are quite sensitive to the detailing of the reinforcement anchorage, the supports and the imposition of load (nodal zones in general). The specific influence of the anchorage of the reinforcement will be discussed below.

Impact of reinforcement anchorage

In the base model presented above (model No. 1), the bottom reinforcement was extended to the edges of the beam (assuming zero concrete cover) in order to guarantee proper anchorage length. A basic anchorage end was considered (zero reduction of the anchorage length as stated in EN 1992-1-1. The reinforcement is usually made shorter in practice, but there is no specific information in this respect in Schlaich et al. (1987). To investigate the impact of the reinforcement anchorage on the ultimate load predicted by the CSFM, the results of a sensitivity analysis conducted for different anchorage length reductions (simulated by different end types, see Fig. 3.18 and Fig. 3.19) are shown in this section. For this analysis, the reinforcement of ties T1 and T2 was made 5 cm shorter with respect to the base model on the right side of the deep beam in order to fulfill the concrete cover requirement. As described in Table 5.2, model No. 2 considers no reduction in the anchorage length (as in the base model or model No. 1, but 5 cm shorter), while model No. 3 considers a 30% reduction (by applying a standard bend at the end of the bar) and model No. 4 considers fully anchored behavior (by applying a perfect bond at the end of the bar). Note that the different anchorage types are not distinguished in the result figures. They can, however, be viewed using the "real 3D" view option in the software.

Table 5.2 Ultimate load from the CSFM and its ratio to the ultimate load determined by the STM for different anchorage conditions.

Model No.	1	2	3	4
Reduction l_b	0% [1)]	0%	30%	100%
ultimate load CSFM [kN]	2814	2619	3539	3626
ultimate load CSFM/STM [%]	93.8	87.3	118.0	120.9

1) Zero concrete cover

The failure mode of model No. 2 differs clearly from that of models No. 3 and 4. In Model No. 2 the insufficient anchorage length triggers the failure for T1, as can be clearly seen in Fig. 5.6. On the other side, models No. 3 and 4 fail due to concrete crushing below the top bearing plate despite the largest concrete compression softening is produced in the direct diagonal strut (see Fig. 5.7). The ultimate load predicted by the CSFM and its ratio to the ultimate load determined by Schlaich et al. (1987) are displayed in Table 5.2 for models No. 1 to 4. The results show that the proper anchorage of the bottom reinforcement governs the capacity of the deep beam. However, the load-bearing capacity cannot be increased by much above 3500 kN, even if the reinforcement anchorage is considered to be perfect.

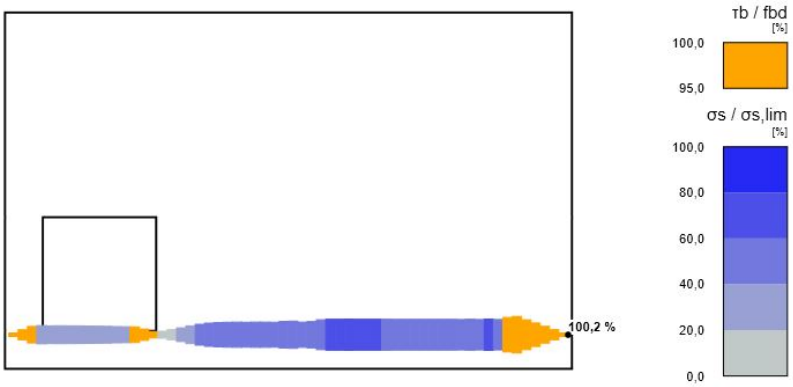

Fig. 5.6 Stress/strength ratio in tie T1 at ULS for model No. 2.

The differences in the anchorage models can be analyzed in more detail. *IDEA StatiCa Detail* software considers the anchorage length according to EN 1992-1-1 but it does not automatically apply a reduction of the anchorage length due to transverse compression, as allowed by EN 1992-1-1 when significant transverse compressive stresses are acting and considered in Schlaich et al. (1987). The consideration of this effect leads to a reduction in the anchorage length of about 30%, as considered in model No. 3, presented above. This reduction ($\beta = 0.3$) can be achieved manually in the CSFM using a standard anchorage end (e.g., bends or hooks), see Fig. 3.18.

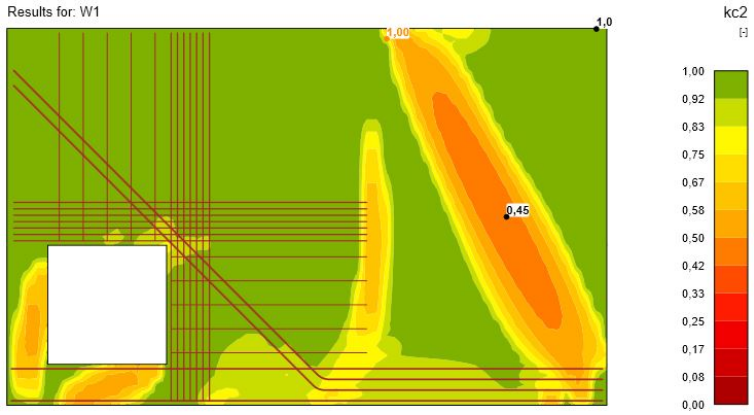

Fig. 5.7 Concrete compression strength reduction factor at ULS for Model No. 3.

5.2.4 Serviceability limit state analysis

Schlaich et al. (1987) did not design this example of a deep beam with an opening for the SLS because STM only considers equilibrium conditions and, therefore, cannot be used for serviceability checks. In this section, different serviceability verifications (stress levels, crack widths and deflections) performed by means of the CSFM are presented and discussed. Model No. 3 (see Table 5.2) was used to compute all serviceability verifications.

The level of service load was estimated based on the known factored design ultimate load ($F_u = F = 3$ MN) and considering EN 1992-1-1 rules for load factors and combinations. The safety load factor was assumed to be $\gamma_G = 1.35$ for permanent actions, and $\gamma_Q = 1.5$ for variable actions. Furthermore, it was assumed that the ratio between permanent and variable service loads could be 1:2 and the combination factor for the variable action of a quasi-permanent combination $\psi_2 = 0.3$. Considering the parameters above, the permanent component of the concentrated load was determined to be $F_G = 0.690$ MN (a force representing the permanent SLS design load), and the variable component $F_Q = 1.379$ MN (a force representing the variable SLS design load). It should be noted that these loads were obtained assuming the ultimate load corresponding to the STM design, but will be applied to a CSFM analysis that has a slightly different ultimate load.

Stress limitation

Fig. 5.8 shows the results of the ratio between concrete stress and the limit concrete stress (-15.3 MPa) for the characteristic combination. According to the results, it seems that the condition for concrete stress limitation at service loads is not satisfied, as the maximum concrete stress below the support (-16.2 MPa) is larger than the limit concrete stress. However, such local peaks of stresses should be carefully interpreted as they might be local artifacts produced by FE-analysis, as will be discussed below.

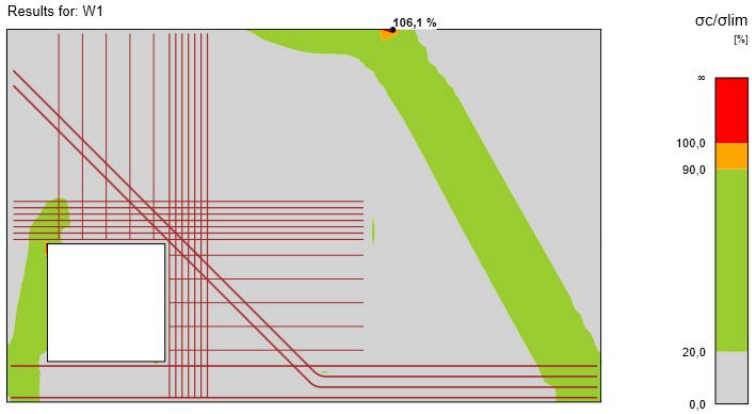

Fig. 5.8 The ratio between the stress and limit stress of concrete at the serviceability limit state.

The results of the ULS analysis have already shown that very high local concrete strains in compression appear below the bearing plate. A similar effect appears in the calculation of the serviceability stresses because unrealistically large strains may result locally in the FE-analysis (known as stress singularity). This effect is particularly important given the fact that the CSFM does not consider a plastic limit for serviceability analysis. Therefore, SLS concrete stress verifications should only be interpreted as having failed if the limit stress is exceeded in a large enough area (i.e., in area as wide as the structure's thickness). When applying this criterion to the analyzed deep beam with an opening, it can be observed that the limit stress is exceeded in an

area significantly smaller than the thickness of the beam (0.4 m). Therefore, the stress-limitation specified in EN 1992-1-1 should be considered verified.

Crack width

The limit value for the crack width generally depends on the exposure class. A limit value of 0.3 mm is usually considered in EN 1992-1-1 for the case of non-prestressed reinforced concrete and quasi-permanent load combinations. Note that the crack width predicted by the CSFM in this example is below the limit value: a maximum crack width of 0.129 mm is obtained (see Fig. 5.9), i.e., 43% of the limit value. It should be noted that the CSFM only computes crack widths at the reinforcing bars and cannot verify them at the diagonal strut in the right part of the deep beam. Also, note that all the plots of cracks represent the calculated cracking direction and the relative magnitude of the cracks. However, the plotted crack spacing is merely schematic, and does not correspond to the actual crack spacing calculated by the CSFM.

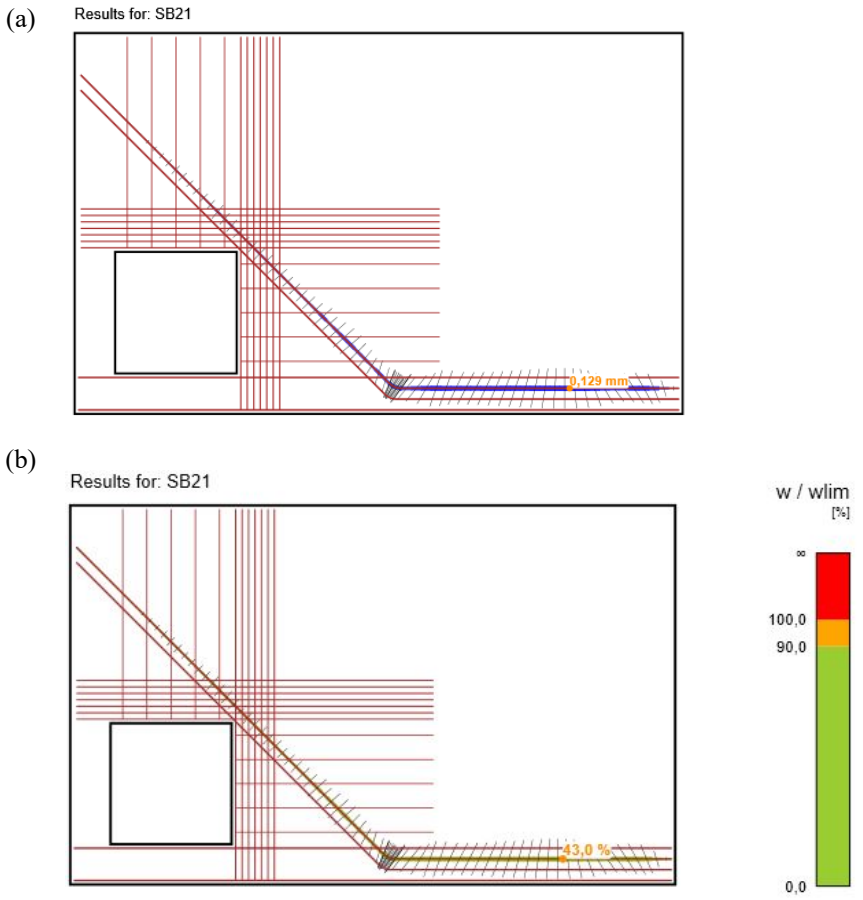

Fig. 5.9 Crack width results: (a) Maximum crack width; (b) ratio between crack width and limit crack width (w_{lim}=0.30 mm).

The inspection of the principal tensile strains ε_1 in the concrete can help to identify the zones in which reinforcement should be provided to avoid excessive crack widths in unreinforced areas. When analyzing these results (see Fig. 5.10), it is clear that inadmissible crack widths could appear in the areas of (i) the diagonal strut, (ii) the vertical strut next to the opening, and (iii) the anchorage of ties T5 and T7. Therefore, it is recommended that at least a minimum amount of reinforcement be provided in these areas.

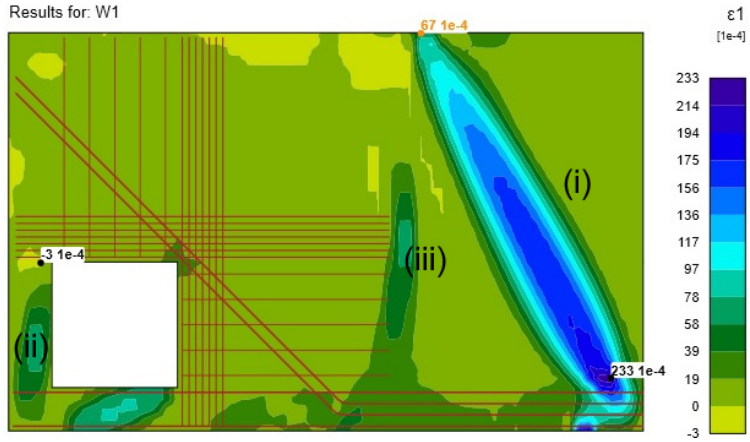

Fig. 5.10 Distribution of principal strain ε_1 in concrete for the applied portion of the load.

Deflection

The limit value of deflection is usually related to the span of the beam. The strictest deflection limit specified in EN 1992-1-1 corresponds to 1/500 of the span for quasi-permanent load combinations. The CSFM calculation for service loads (see Fig. 5.11) leads to a maximum deflection of 3.2 mm, which represents 23% of the span limit value/500.

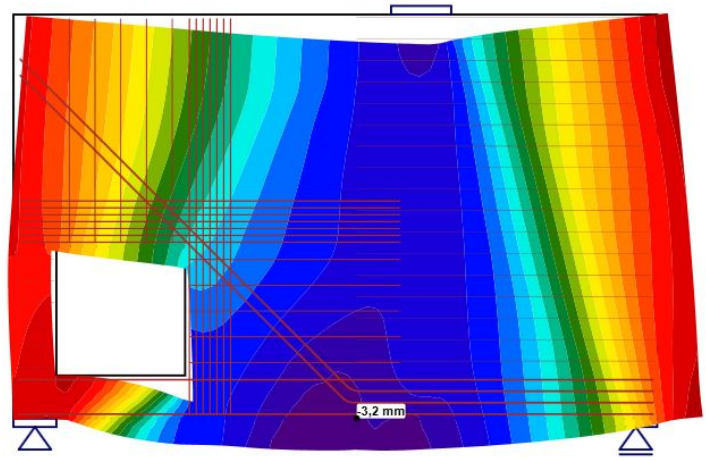

Fig. 5.11 The deflected shape of the deep beam.

5.2.5 Optimization of the locations and directions of reinforcing bars

The design of the reinforcement of discontinuity regions is not a trivial task. The use of the topology optimization method may be of great help in the reinforcement design of such details. A detailed description of the method can be found in Section 3.4 and in Konečný et al. (2017). The effectiveness of topology optimization in finding the most effective shape and the required amount of reinforcement is compared below with manual trial/error approximations. In both approaches, *IDEA StatiCa Detail* software was used. The following models will be discussed:

- Model No. 3: Reinforcement proposed by Schlaich et al. (1987)
- Model No. 5: Orthogonal reinforcement layout proposed by Schlaich et al. (1987) with a reinforcement amount manually optimized for the ULS.
- Model No. 6: Diagonal reinforcement layout proposed by Schlaich et al. (1987) with a reinforcement amount manually optimized for the ULS.
- Model No. 7: Reinforcement fully based on topological optimization.

For the manual reinforcement design, the two strut-and-tie models displayed in Fig. 5.2 (orthogonal and diagonal) were analyzed independently in the ULS. The reinforcement area of each model was "optimized" using the trial and error method. In this process, the area of the least utilized reinforcement was decreased via manual input and the ULS calculation with the CSFM was performed to check the load-bearing capacity of the region; this process was repeated until the load-bearing capacity was equal to the required designed load. The resulting reinforcement amounts calculated with the CSFM (based on ULS verifications only) for the layouts proposed by Schlaich et al. (1987) are displayed in Fig. 5.12.

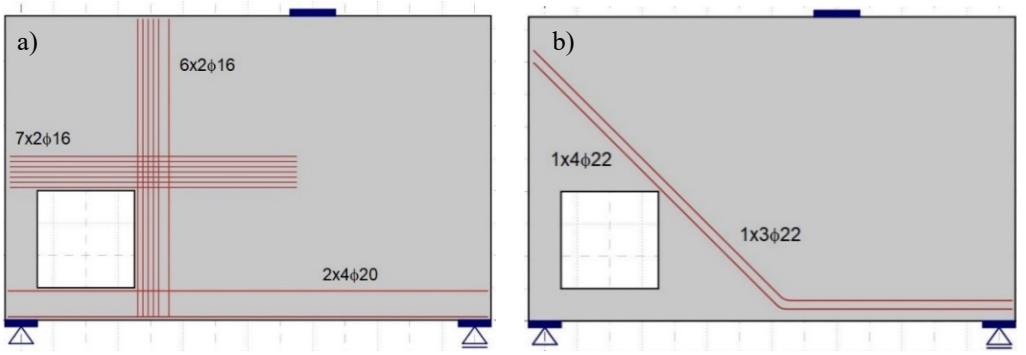

Fig. 5.12 Reinforcement layout proposed by manually optimized using the CSFM: (a) Orthogonal layout (model No. 5); (b) diagonal layout (model No. 6).

It should be noted that the reinforcement positions and directions in Fig. 5.12 were obtained from the STM drawn up intuitively by Schlaich et al. (1987). The reinforcement obtained in this way is compared below with the reinforcement whose locations were determined via topology optimization (see the topology optimization results in Fig. 5.13).

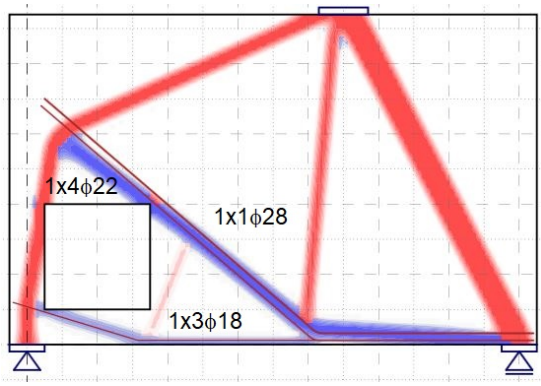

Fig. 5.13 Reinforcement based on topology optimization (model No.7).

Topology optimization produces results that show the areas of tension and compression that can appear in a concrete structure, but it does not enable the design of real reinforcing bars. After the reinforcement layout has been defined based on the topology optimization tool, the amount of reinforcement is optimized using the trial/error method (see Fig. 5.13). A lighter and thinner strip symbolizes the need for a lower amount of reinforcement. It should be emphasized that the designer should account for the detail of the nodal zones when proposing a reinforcement layout based on the results of topology optimization. For example, the reinforcement must be properly anchored; otherwise, any calculation based on this analysis will fail due to improper anchoring. The diagonal tie above the opening (the main tie corresponding to T2-T9 in the original strut-and-tie model, see Fig. 5.2) has to be much longer than the tension zone marked by the topology optimization in order to guide the diagonal strut extending from the loading plate in the vertical direction. In the case that the main tie is shortened by 200 mm – but is still longer than the tension zone marked by topology optimization (see Fig. 5.14) – the concrete will fail in compression at the upper left corner of the opening when a CSFM analysis is performed (see Fig. 5.15). In such a case, the load-bearing capacity is only 74.4% of the design load.

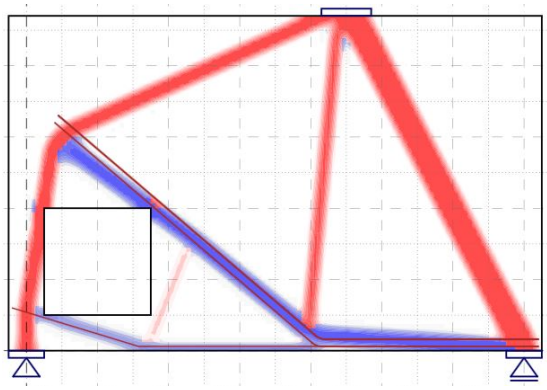

Fig. 5.14 Reinforcement layout based on topology optimization with the main tie shortened by 200 mm.

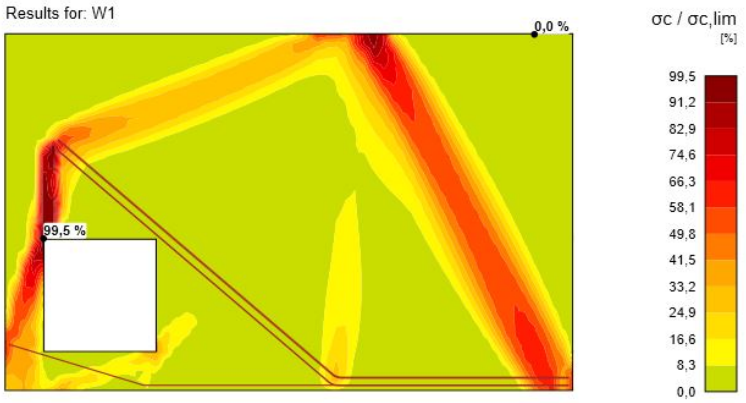

Fig. 5.15 The ratio between the stress and strength of concrete at the ULS for the reinforcement layout defined in Fig. 5.14.

The efficiency of models No. 5 and 6 (manually optimized) can be compared with the results based on topology optimization (model No.7) in terms of total weights of bars (see Table 5.3). Model No. 3 (the model proposed by Schlaich et al. (1987)) is also included in this comparison, but the predicted load-bearing capacity is 18% higher than in the other cases and a direct comparison of the efficiency cannot be drawn. The total weight of the reinforcing bars in model No. 3 was 458 kg, and the deflection of the deep beam calculated using the CSFM at the load level of 3000 kN was 10.6 mm. Very similar values were obtained for models No. 5 and 6 – i.e., the orthogonal and diagonal reinforcement topologies proposed by Schlaich et al. (1987) but with manual optimization of the reinforcement amount using the CSFM, see Fig. 5.12a, b – as well as for the reinforcement fully based on topology optimization (Fig. 5.13).

Table 5.3 Comparison of material consumption for different models

Model	No. 3 (Schlaich)	No. 5 (Schlaich orthogonal + optimized)	No. 6 (Schlaich diagonal + optimized)	No. 7 (Topology optimization)
ULS F_R/F_U[1)] [%]	118.0	99.8	100.7	101.0
Weight of rebars [kg]	458	338	190	190
Deflection[2)] [mm]	10.6	12.6	146.8	13.4

Note: 1) F_R is the load-bearing capacity obtained via the CSFM, F_U is the load taken from Schlaich et al. (1987); 2) Deflection at 3000 kN.

The optimized diagonal truss model, No. 6 (see Fig. 5.2b), is optimal for the ULS, but results in very large deformations (large cracks appear, which results in a significant decrease in stiffness). On the other hand, the model based on topology optimization (model No. 7) not only achieves the same minimal reinforcement weight but also results in a reasonable deflection of the deep beam at a load level of 3000 kN. It shows that the objective of topology optimization is not

to reach maximum load-bearing capacity but to maximize the global stiffness of the structure for a given load set. This is equivalent to minimizing the (complementary) strain energy, which is equal to the work done by external loads.

Although the results yielded by the topology optimization method still require a degree of reflection and interpretation from an engineer, it is a fast and easy-to-use tool that can facilitate and speed up the task of reinforcement design significantly. Especially in cases of non-typical structures and/or multiple load cases, it can lead to results that would not otherwise be obvious if conventional methods were used. This can result in considerable savings not only in engineering time, but also in the amount of reinforcement steel.

5.2.6 Conclusions

Based on the explanations in Sections 5.2.3 and 5.2.5, model No. 3 can be considered the most suitable for ULS and SLS evaluations, as well as for the comparison of results obtained by the CSFM and STM. The latter represents the methodology currently recommended in structural concrete standards for the design of discontinuity regions, while the CSFM provides an innovative approach.

The ULS analysis shows an excellent agreement between the results obtained by STM and the CSFM, meaning that both methods are viable for load-bearing capacity verifications. However, the CSFM appears to provide more economical, yet safe designs. This can be attributed to the ability of the CSFM to exploit all the resistant mechanisms of a structure, which allows CSFM solutions to get closer to the exact solution according to limit analysis. At the same time, the study emphasizes the importance of modeling the details of the model properly (geometry of supports, application of loads, stiffness, anchorage).

The example of a deep beam with an opening shows that a design using STM does not necessarily guarantee that serviceability conditions are also satisfied. Therefore, the STM is of limited use for designing deep beams or other discontinuity regions under serviceability conditions. The example also proves the potential of using the topology optimization method to optimize the positions and directions of reinforcing bars even for complex geometries.

5.3 A Eurocode-based beam analysis

5.3.1 Case description

The goal of this example is to verify the results of the CSFM for a simply supported T-beam subjected to a uniformly distributed load by comparison with the results of beam and cross-sectional analyses carried out according to EN 1992-1-1: (i) An analysis with *IDEA StatiCa Beam* software; and (ii) an analytical solution provided by Procházka (2006). The main hypotheses of *IDEA StatiCa Beam* software can be found in Appendix A, A.1.

The characteristics of the T-beam (see Fig. 5.16 and Fig. 5.17) were extracted from Example No. 1.4 proposed in Procházka (2006). The span of the simply supported beam is 6 m. It is reinforced by 4Ø20 longitudinal reinforcing bars throughout the whole length of the beam. The shear reinforcement consists of 2Ø10/200 vertical stirrups located in the web of the cross-section. An overview of the material properties and safety coefficients is provided in Table 5.4.

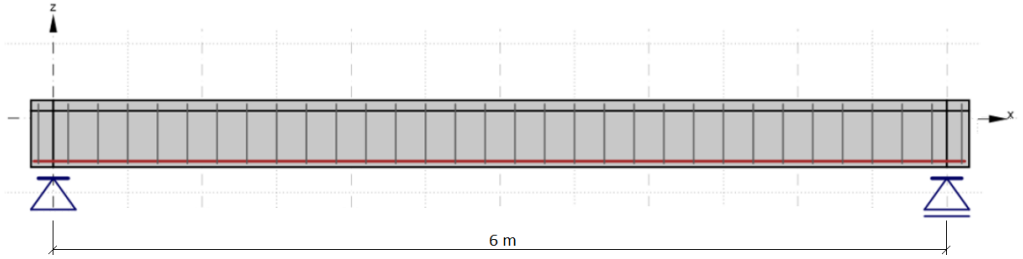

Fig. 5.16 Diagram of the beam geometry in *IDEA StatiCa Detail.*

Table 5.4 Input data for the T-beam.

Characteristic tensile strength of reinforcement f_{tk} [MPa]	540
Characteristic yield strength of reinforcement f_{yk} [MPa]	500
Partial factors for reinforcement γ_s	1.15
Characteristic strain limit of reinforcement ε_{uk} [‰]	50
Modulus of elasticity of reinforcement E_s [GPa]	200
Characteristic concrete compressive strength f_{ck} [MPa]	20
Concrete strain when reaching the maximum strength ε_{c2} [‰]	2.0
Partial factors for concrete γ_c	1.5

The dimensions of a cross-section with a wide flange were modified into those of an effective cross-section, following the default procedure for beams defined in Section 3.6.3. For the purposes of this example, the results from both the effective (Fig. 5.17b) and full (Fig. 5.17a) cross-sections were compared. Note that while models input via a beam template automatically account for the effective width with a default value that cannot be modified, users still can model such beam with a different effective width by defining the structural member with a wall or general templates (see Section 3.6.3).

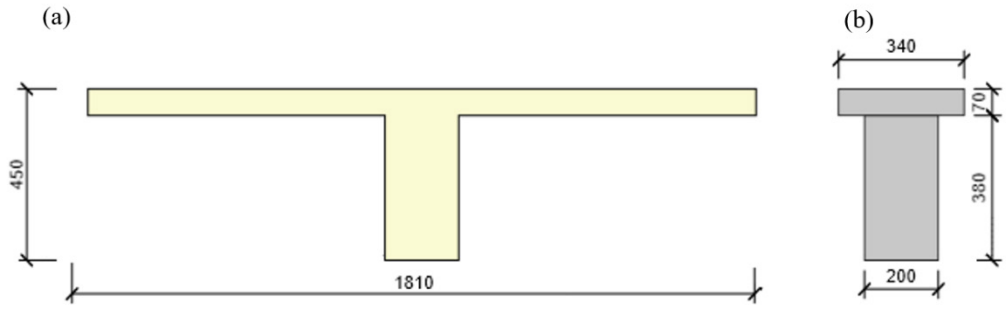

Fig. 5.17 T-shaped cross-section dimensions: (a) Full cross-section; (b) effective cross-section considered for CSFM calculations by default (dimensions in [mm]).

This example considers a uniform line load with a permanent part, g = 8.2 kN/m, and a variable part, q = 23.5 kN/m. These values of the loads are used in ULS fundamental, SLS characteristic and SLS quasi-permanent combinations.

5.3.2 Modeling with the CSFM

The calculation model was created in *IDEA StatiCa Detail* (CSFM). The geometry was defined using three beam members in the Geometry tab, with segment lengths of 0.15 m, 6.0 m and 0.15 m (see Fig. 5.16). The beam material is concrete with strength class C20/25, as stipulated in EN 1992-1-1. The beam is supported by distributed point supports at positions that are 0.15 m and 6.15 m from the left-hand side of the beam. B500B material is used for the longitudinal reinforcement and stirrups, see EN 1992-1-14.

There are two load cases and three combinations defined in the example, with all load cases consisting of a line load as shown in Table 5.5. The combinations are defined according to EN 1992-1-1. The combination rule is controlled by partial factors shown in the rightmost column of Table 5.5.

Table 5.5 Defined load cases and combinations.

Check	Name/Type	Description
No	LC1/Permanent	g = 8.2 kN/m
No	LC2/ Variable	q = 23.5 kN/m
Yes	C1/ULS	1.35 LC1 + 1.5 LC2
Yes	C2/SLS Characteristic	1.0 LC1 + 1.0 LC2
Yes	C3/SLS Quasi-permanent	1.0 LC1 + 0.8 LC2

Basically, the user could use linear analysis (Fig. 5.16a) and/or topology optimization (Fig. 5.16a) as well for this example. However, the results in this case of a simply supported beam are obvious (flexural and shear reinforcement are required).

(a)

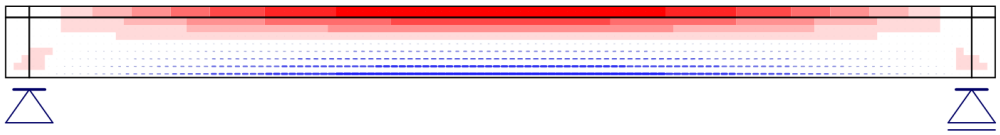

(b)

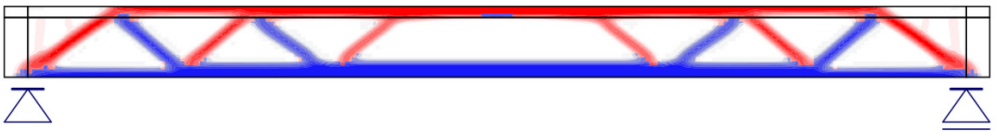

Fig. 5.18 Results of reinforcement design tools: (a) Linear analysis with mesh size multiplier = 0.5; (b) topology optimization with mesh size multiplier = 0.5 and effective volume = 0.4 (see the details of the calculation in Section 3.4.2).

5.3.3 Ultimate limit state

The ULS response of the structure and the checking of individual model components (concrete, reinforcement, anchorage) were carried out using design values for the material parameters (see Table 5.4). In the following, calculations of the ultimate moment resistance according to the two sectional analyses and the CSFM are presented and compared. Further verifications, such as the shear resistance or anchorage, are not discussed in this example.

Ultimate moment resistance according to Procházka (2006)

The analytical calculation of the ultimate moment resistance presented below was taken from Example No. 1.4 contained in Procházka (2006), which follows the main provisions of EN 1992-1-1.

The following geometric and material properties are used:

d	distance of the flexural reinforcement to the upper edge,
$A_s = 1257 \cdot 10^{-6}$ m^2	area of longitudinal reinforcement,
$b_{eff} = 1.81$ m	effective width of the cross-section upper flange,
$f_{yd} = 435$ MPa	design yield strength of the reinforcement and
$f_{cd} = 13.3$ MPa	design concrete compressive strength.

The depth of the compression zone, *x,* is:

$$x = \frac{A_s \cdot f_{yd}}{b_{eff} \cdot \lambda \cdot \eta \cdot f_{cd}} = \frac{1257 \cdot 10^{-6} \cdot 435 \cdot 10^3}{1.81 \cdot 0.8 \cdot 1.0 \cdot 13.3 \cdot 10^3} = 0.028 \text{ m} \tag{5.2}$$

where λ and η are stress block factors defined in Fig. 5.19.

The inner level arm, z, results in:

$$z = d - 0.5 \cdot \lambda \cdot x = 0.41 - 0.5 \cdot 0.8 \cdot 0.028 = 0.399 \text{ m} \tag{5.3}$$

The ultimate moment resistance of the cross-section can then be calculated as follows:

$$M_{Rd} = A_s \cdot f_{yd} \cdot z = 1257 \cdot 10^{-6} \cdot 435 \cdot 10^3 \cdot 0.399 = 218.2 \text{ kN·m} \tag{5.4}$$

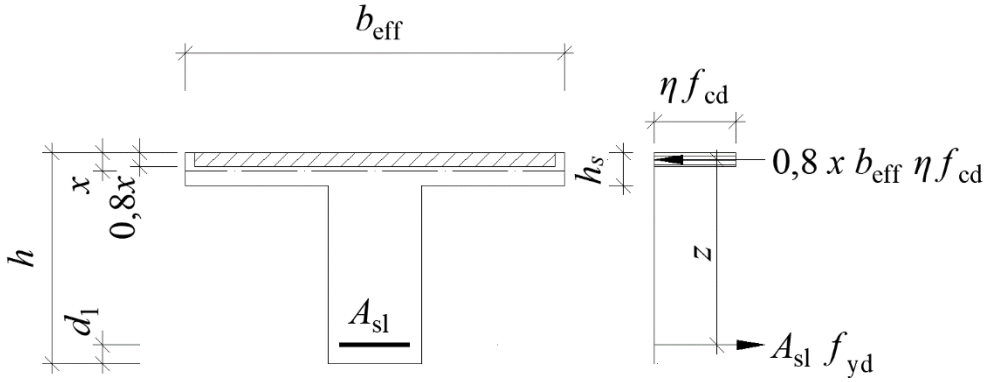

Fig. 5.19 Bending verification extracted from Procházka (2006).

Ultimate moment resistance according to *IDEA StatiCa RCS*

This section presents an additional method to calculate the ultimate moment resistance by means of a cross-sectional analysis according to EN 1992-1-1. In this case, the ultimate moment resistance is calculated in *IDEA StatiCa RCS* by means of the interaction diagram N, M_y, M_z. Detailed descriptions of the assumptions of the cross-sectional analysis carried out in *IDEA StatiCa RCS* are given in Appendix A, A.2.1. It should be noted that in this case a parabolic-rectangular stress block for concrete in compression is considered (see Fig. 5.20a), while the analytical calculation in the previous section considers a simplified rectangular stress block. Furthermore, strain hardening of the reinforcement is considered here (see Fig. 5.20b).

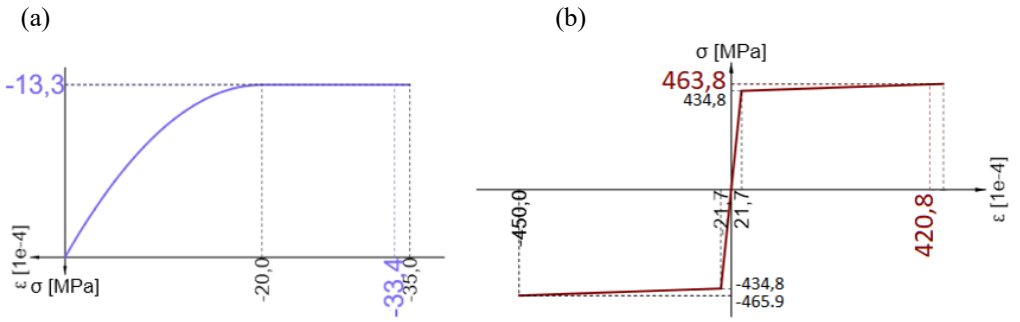

Fig. 5.20 Stress-strain diagrams used in *IDEA StatiCa RCS*: (a) Concrete; (b) reinforcement.

If the full width of the flange is considered in the calculation (similarly as for the analytical calculation presented in the previous section), the interaction diagram shown in Fig. 5.21a is obtained (for $M_z = 0$). The ultimate moment resistance for the case of pure bending with this method is 232.5 kN·m. Note that this result is slightly higher (6%) than the analytical calculation shown in the previous section, due to the fact that this analysis considers the more refined constitutive relationships of the materials. If this analysis is performed considering the effective flange depth assumed by default in the CSFM (Fig. 5.17b), the ultimate moment resistance drops to 186.5 kN.

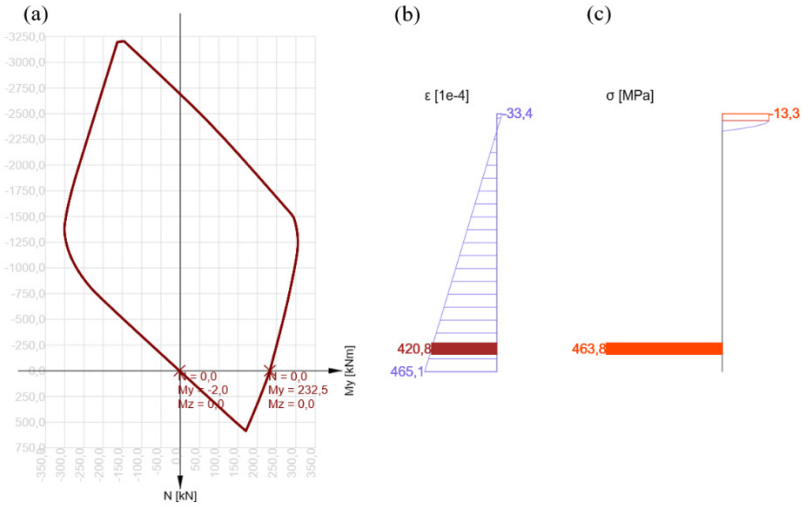

Fig. 5.21 Results from *IDEA StatiCa RCS* considering the full width of the upper flange: (a) Interaction diagram; (b) strain distribution at the ultimate limit state; (c) stress distribution at the ultimate limit state.

Ultimate moment resistance according to the CSFM

Two calculations were performed in the CSFM, one for the effective cross-section dimensions considered by default (reduced flange width – see Fig. 5.17b) and a second one for the full cross-section dimensions (see Fig. 5.17a).

The results considering the default effective flange depth are shown in Fig. 5.22. They reached 100% of permanent load and 93.1% of variable load for combination C1/ULS. The ultimate moment resistance can be obtained as the moment at midspan associated with the resisted loads (198 kN·m). A second way to determine the ultimate moment resistance is to integrate the stress distribution over the cross-section in Fig. 5.23, which leads to approximately 187 kN·m. The difference between the two methods is caused by the approximation used in the stress integration over the cross-section. It should be noted that the reduction of the flange width leads to a very large compression zone depth, which results in a failure of the cross-section due to the failure of concrete in compression.

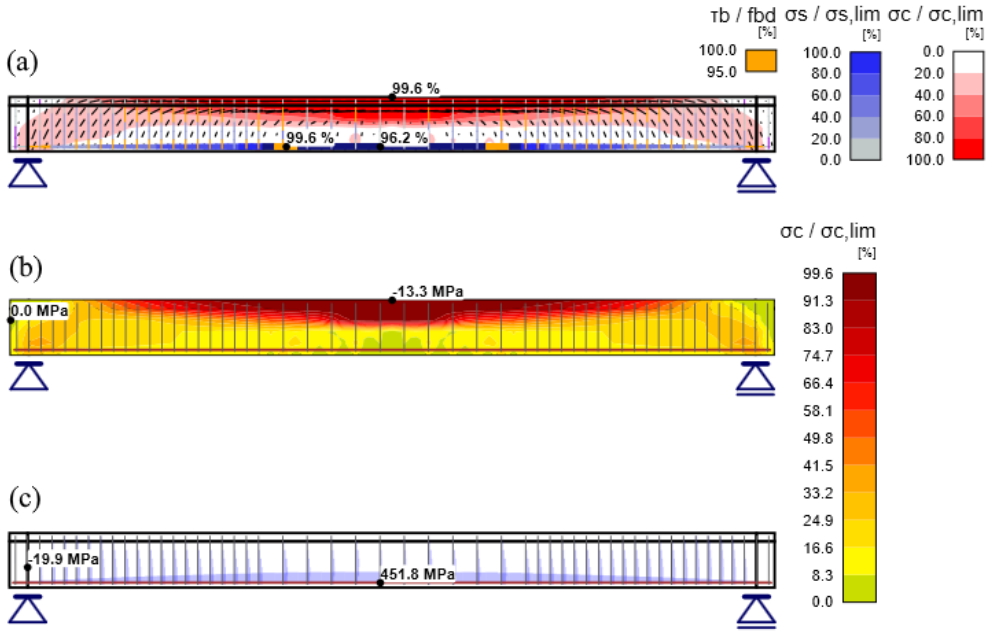

Fig. 5.22 CSFM results at the ULS for the effective cross-section: (a) Stress field; (b) concrete compressive stresses; (c) reinforcement stresses.

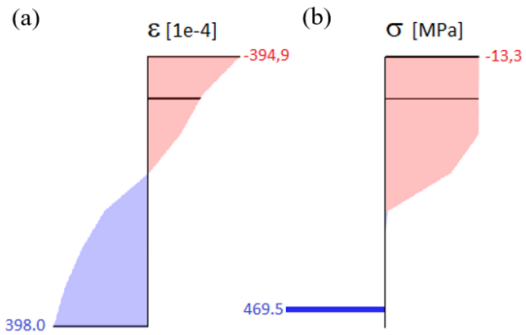

Fig. 5.23 Stress-strain limit state distributions at midspan for the effective cross-section: (a) Concrete strains; (b) stresses in concrete and reinforcement.

Calculations using the full flange depth were carried out at 100% of the design permanent load and 116% of the design variable load (the results are depicted in Fig. 5.24). The moment at midspan for the limit state loads was 233 kN·m, while the approximated integration of the cross-section stresses at midspan led to a similar capacity of around 224 kN·m. It should be noted that, in this case, the compression depth is very small and the concrete is far from crushing. Instead, the beam failed due to the failure of the flexural reinforcement.

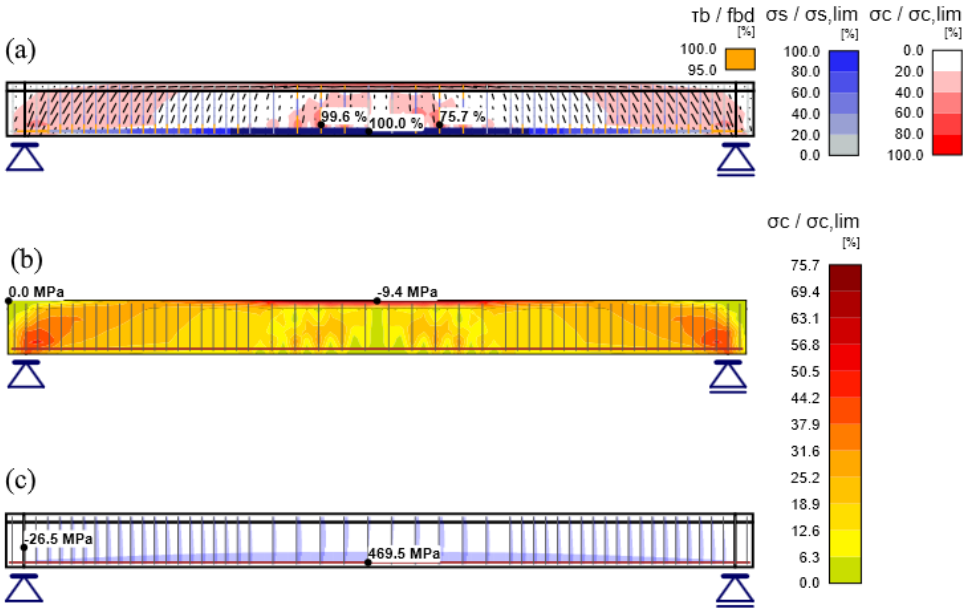

Fig. 5.24 CSFM results at the ULS for the full cross-section: (a) Stress field; (b) concrete compressive stresses; (c) reinforcement stresses.

Table 5.6 provides an overview of the prediction of the ultimate moment resistance with the different methods and assumptions of the effective flange width. This example of a conventional simply supported beam, which can be calculated with the CSFM as well as with simpler methods based on cross-sectional analysis, shows that the CSFM yields very similar results to cross-sectional analysis methods.

Table 5.6 Comparison of moments of resistance.

Type of calculation	Effective cross-section [kN·m]	Full cross-section [kN·m]
Acc. to (Procházka 2006)	-	218.2
IDEA StatiCa RCS	186.5	232.5
CSFM	198.0	233.0

5.3.4 Serviceability limit state

The results obtained from the *IDEA StatiCa Beam/RCS* software were used to compare the correctness of SLS results in *IDEA StatiCa Detail*. In addition, the deflection results were compared with the analytic calculations from Procházka (2006). Only the serviceability results for the full cross-section model (Fig. 5.17a) were analyzed in the CSFM, as the consideration of this model allows comparing the results directly to the results given by the other methods.

Stress limitation

The stress limitation check at serviceability is provided for both, characteristic and quasi-permanent combinations.

The response under the characteristic combination in *IDEA StatiCa RCS* neglects the concrete tensile strength and considers linear stress-strain diagrams for concrete and reinforcement (see the more detailed description in the Appendix A, A.3.1 and A.3.2). The calculation was performed twice – for the short-term response with the modulus of elasticity E_{cm}, and for the long-term response with the effective modulus of elasticity $E_{cm} / (1+\varphi)$, with a default value of $\varphi = 2.5$, see Fig. 5.25.

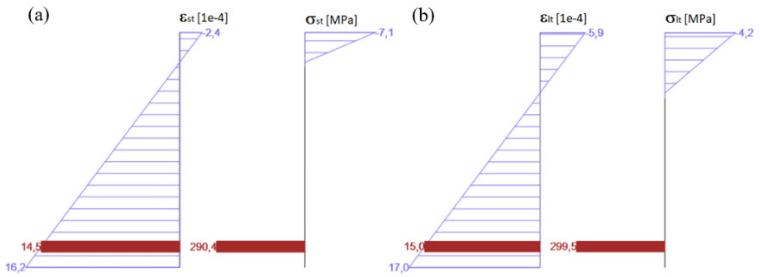

Fig. 5.25 Strain and stress distribution for a characteristic combination calculated in *IDEA StatiCa RCS*: (a) Short-term model; (b) long-term model.

A description of the serviceability verifications in the CSFM can be found in Section 3.6.8. The calculation was also performed twice in this case. The first calculation was performed with permanent and variable loads as defined in Table 5.5, while in the second one, all loads were defined as permanent. The results of the CSFM are shown in Fig. 5.26, and a summary of the maximum results is compiled and compared to the reference method in Table 5.7.

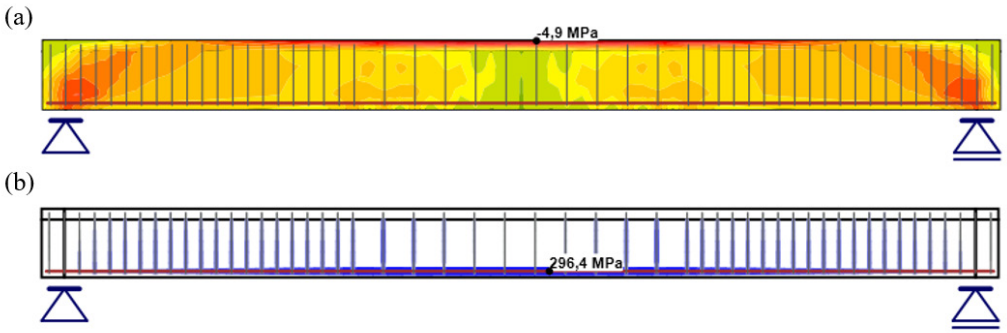

Fig. 5.26 Results from the serviceability stress limitation in the CSFM considering all loads as permanent: (a) Concrete stresses; (b) reinforcement stresses.

Table 5.7 Comparison of the results for maximum stresses at serviceability ($\sigma_{c,st}$ and $\sigma_{s,st}$ are the concrete and reinforcement stresses assuming a short-term application of the total load, which may include long-term loads; $\sigma_{c,lt}$ and $\sigma_{s,lt}$ are the concrete and reinforcement stresses assuming a long-term application of the all loads).

Type of calculation	$\sigma_{c,st}$ [MPa]	$\sigma_{s,st}$ [MPa]	$\sigma_{c,lt}$ [MPa]	$\sigma_{s,lt}$ [MPa]
IDEA StatiCa RCS	-7.1	290.4	-4.2	299.5
CSFM	-4.9	286.8	-4.7	287.6
CSFM – all permanent	-4.9	286.8	-3.4	296.4

Due to the low level of the long-term load (8.2 kN/m) compared to the short-term one (23.5 kN/m), in the default CSFM analysis there is no significant difference between the short- and long-term effects in the first calculation type, see the second line in Table 5.7. The consideration in the CSFM of all loads as permanent (third line in Table 5.7), leads to lower long term concrete stresses, since the long-term concrete diagram is used for the full load. The short-term calculations are identical in both cases.

In this example, we can observe that the stresses obtained via CSFM are always lower than the stresses obtained by *IDEA StatiCa RCS*. These differences cannot be explained by the small differences implemented in both approaches (compare the CSFM approach depicted in Fig. 3.9, and the method integrated in *IDEA StatiCa RCS* in Appendix A, A.3). Rather, the differences are related (i) to the coarse mesh automatically generated in the CSFM for this case; and (ii) to the fact that the CSFM results do not correspond exactly to the edge of the member but to the closest integration point (see also Section 3.6.8). Hence, by refining the finite element mesh, the results of the CSFM will converge to the results given by the *IDEA StatiCa RCS* (which represent the information at the edge of the element).

Crack widths

A crack width check is provided in the CSFM for the quasi-permanent combination in the vicinity of the reinforcement. Fig. 5.27 shows the crack width results obtained from the CSFM, as well as according to *IDEA StatiCa Beam* software (reference calculation of a cross-sectional analysis performed according to EN 1992-1-1. It can be shown that there is excellent agreement in the results from both procedures (below 10%), which can be explained as being due to the small differences between the models considered in both procedures.

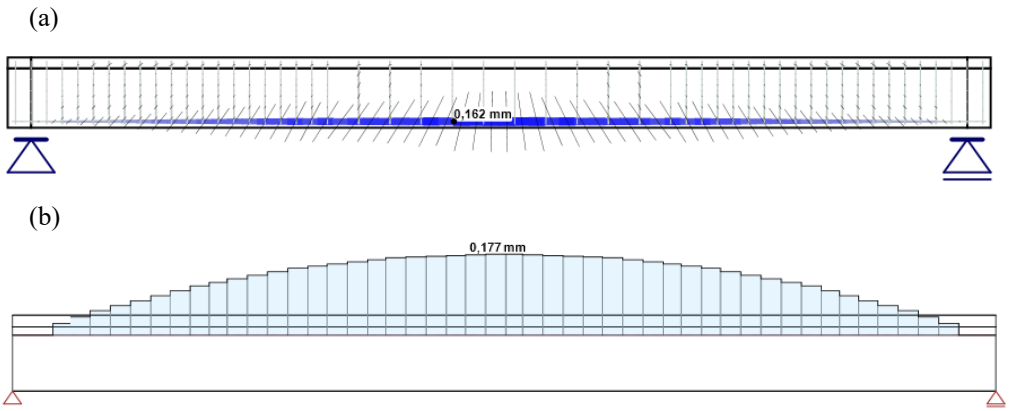

Fig. 5.27 Results of crack width verifications: (a) Crack direction and opening according to the CSFM; (b) calculation according to *IDEA StatiCa Beam*.

Deflections

The deflections resulting from the CSFM were compared with those from *IDEA StatiCa Beam* software as well as those given in Example 6.2 from Procházka (2006). It should be noted that

this example from Procházka (2006) is a continuation of the previously discussed example 1.4, which deals with the calculation of deflections of the same T-beam. The long-term deflection results are shown in Fig. 5.28, and a summary of the results at midspan can be found in Table 5.8, showing a good agreement between all three methods (difference ± 10%). The larger deflection provided by *IDEA StatiCa Beam* software was caused by its different approach to performing deflection analysis (see Appendix A, A.3).

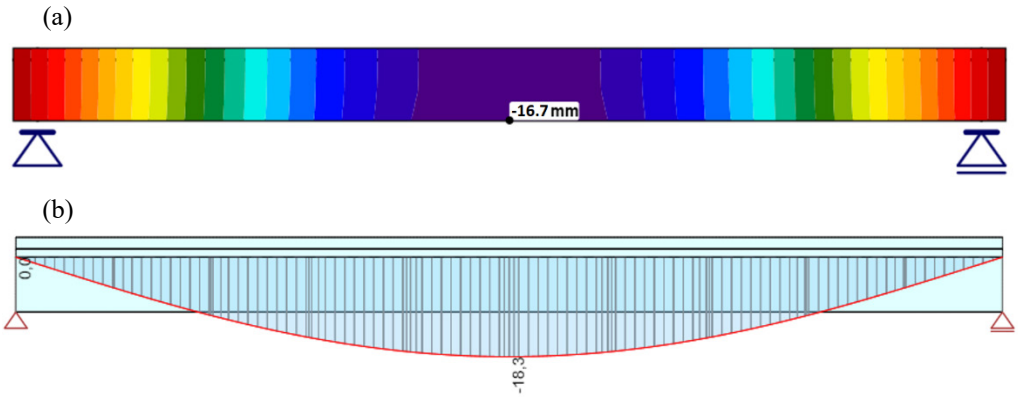

Fig. 5.28 Detailed deflection results according to: (a) CSFM; (b) *IDEA StatiCa Beam*.

Table 5.8 Comparison of long-term deflection results at midspan.

Type of calculation	Δ_{lt} [mm]
Acc. to (Procházka 2006)	15.9
CSFM	16.7
IDEA StatiCa Beam	18.3

5.3.5 Conclusions

This chapter compared the results of the CSFM, a FE-based computer-aided stress field analysis method, with the results of cross-sectional analyses following the prescriptions of EN 1992-1-1. The structure under analysis is a simple supported T-beam that allows using simple cross-sectional analyses as well as refined procedures such as the CSFM, which – other than the simple cross-sectional methods – is also suitable for analyzing regions that are more complex. The cross-sectional analysis results serving as a reference were extracted from analytical calculations reported by Procházka (2006) and results provided by *IDEA StatiCa Beam/RCS* software.

The CSFM predicts higher load-bearing capacity than the analytical cross-sectional analysis reported in Procházka (2006). This difference can be explained by the more conservative perfectly plastic stress-strain diagrams assumed for the concrete and reinforcing steel in Procházka (2006). However, a perfect match between the CSFM and *IDEA StatiCa Beam/RCS* results can

be observed, which is expected since these two approaches consider very similar stress-strain diagrams for the materials used.

With regard to SLS checks, small differences in the results can be observed, too. The differences in the compressive concrete stresses between the different methods are partially caused by slightly different positions of the integration points where the stresses are evaluated. When comparing stresses due to short-term effects at the serviceability limit state, greater differences in the stresses are observed. This is mainly due to the mesh sensitivity of these results in CSFM. A more detailed explanation is given in 3.6.8.

There is good agreement in terms of crack width results between the CSFM and *IDEA StatiCa Beam/RCS* software. This excellent match is presumably caused by the fact that the analysis was performed on a slender beam, where bending cracks prevail. Larger divergence might be expected when analyzing shear cracks. The calculation of deflections also yielded reasonably good agreements between the compared methodologies.

Overall, the comparison of the results is highly satisfactory both at the ULS and at the SLS. The small observed differences correspond to variations in the assumptions of the calculation models, as already discussed above.

5.4 Beam analysis according to ACI 318-14

5.4.1 Case description

The goal of this example is to verify the results obtained from the CSFM for an example of a rectangular simply supported beam proposed by Roberts (2003), following the prescriptions of ACI 318-14. The CSFM results are compared either to analytical calculations provided by Roberts (2003) (SLS) or to the results from a conventional cross-sectional analysis performed with *IDEA StatiCa Beam/RCS* software following the prescriptions of ACI 318-14 (ULS and SLS).

A concrete beam of rectangular cross-section corresponding to the "Full Beam Design Example" included in Roberts (2003) was selected for comparison. The simply supported beam has a clear distance between the faces of the supports of 19 ft (see Fig. 5.29a). It is reinforced by lower longitudinal reinforcement 3 #5s throughout the whole length of the beam, additional 3 #5s in the midspan region of the beam and upper longitudinal 2 #7s throughout the whole length. Shear reinforcement is provided by stirrups #3s. An overview of the material properties and safety coefficients is shown in Table 5.9. Note that the input data are stated in imperial units. The partial factors for concrete and reinforcement are set to 1.0 since these factors are not used according to ACI 318-14.

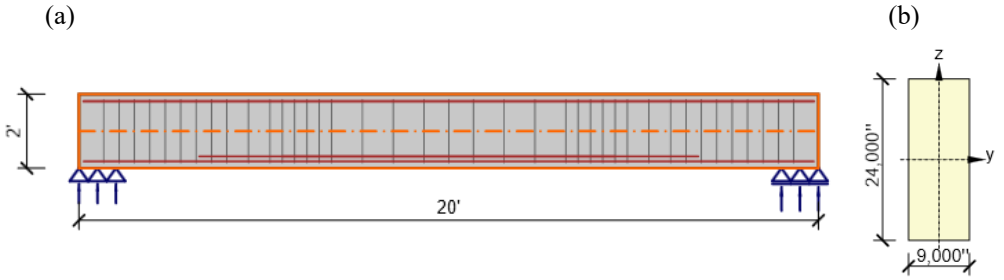

Fig. 5.29 Beam geometry in *IDEA StatiCa Detail*: (a) Longitudinal section (dimensions in [ft]); (b) cross section (dimensions in [in]).

Table 5.9 Input data for the beam.

Specified yield strength of reinforcement f_y [ksi]	60.0
Partial factors for reinforcement γ_s	1.00
Characteristic strain limit of reinforcement ε_{uk} [‰]	50.0
Modulus of elasticity of reinforcement E_s [ksi]	29’000
Specified compressive strength of concrete f'_c [ksi]	4.0
Concrete strain when reaching the maximum strength ε_{cu2} [‰]	2.0
Modulus of elasticity of concrete E_c [ksi]	3’607
Partial factors for concrete γ_c	1.0

In the example, a uniform line load with a permanent part, self-weight (SW) and superimposed dead load (SDL), g = 2.375 kip/ft, and a variable part (live load LL), q = 2.65 kip/ft, is considered. These values of the loads are used in ULS fundamental and SLS combinations.

5.4.2 Modeling with the CSFM

The calculation model was created in *IDEA StatiCa Detail* (CSFM). The geometry was defined as a beam member with a length of 20 ft. The beam material was C4000, and the reinforcement material was Grade 60, as stated in ACI 318-14 and Table 5.9. The model included line supports placed at positions 0 ft and 19 ft from the beginning of the beam.

Two load cases and three combinations were defined. The combinations were defined using the combination rules shown in Table 5.10.

Table 5.10 Defined load cases and combinations.

Check	Name/Type	Description
No	DL/Permanent	g = 2.375 kip/ft
No	LL/Variable	q = 2.65 kip/ft
Yes	C1/ULS	1.2 DL + 1.6 LL
Yes	C2/SLS-Deflection	1.0 DL + 1.0 LL
Yes	C3/SLS-Deflection	1.0 DL + 0.5 LL

5.4.3 Ultimate limit state

In this section, calculations of the ultimate moment resistance according to a sectional analysis and the CSFM are presented and compared. Further verifications, such as of the shear resistance or the anchorage, are not discussed as they are not critical in this structural member.

Ultimate moment resistance according to *IDEA StatiCa RCS*

This section presents the results of a method to calculate the ultimate moment resistance by means of a cross-sectional analysis according to ACI 318-14. In this case, the ultimate moment resistance is calculated in *IDEA StatiCa RCS* by means of the interaction diagram N, M_y, M_z (N and M_z are zero in this particular example). Detailed descriptions of the assumptions of the cross sectional analysis carried out in *IDEA StatiCa RCS* are provided in Appendix A, A.2. The considered stress-strain diagrams for concrete and reinforcement are shown in Fig. 5.30.

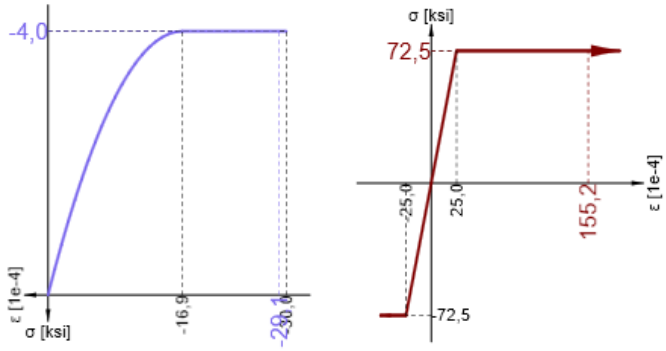

Fig. 5.30 Stress-strain diagrams used in *IDEA StatiCa RCS*: (a) Concrete; (b) reinforcement.

The calculated ultimate moment resistance with this method is 215.4 kip-ft (see Fig. 5.31a). Fig. 5.31b and c show the strain and stress distributions over the depth of the cross-section at the ultimate limit state.

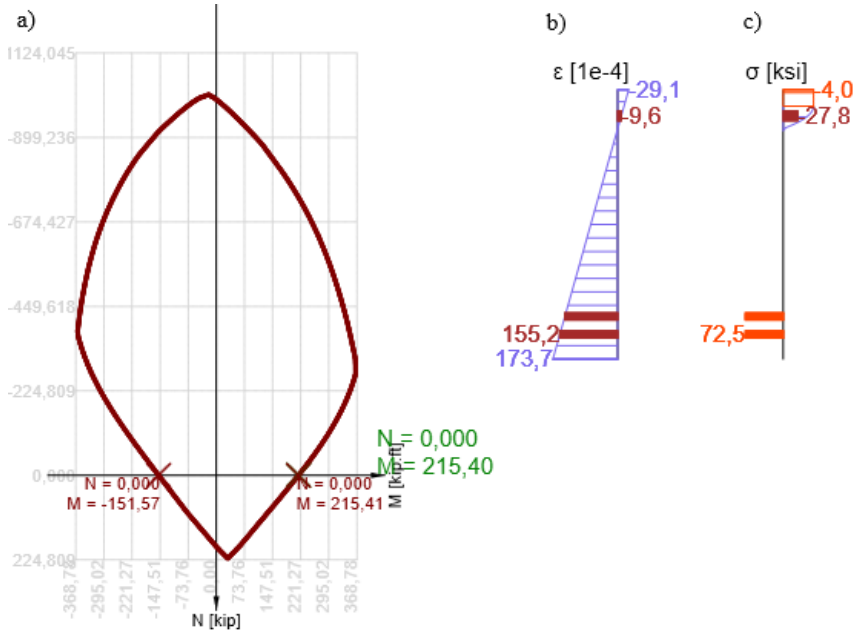

Fig. 5.31 Results from *IDEA StatiCa RCS*: (a) Interaction diagram; (b) strain distribution at the limit state of the reinforced cross-section; (c) stress distribution at the limit state of the reinforced cross-section.

Ultimate moment resistance according to the CSFM

The load-bearing capacity results determined with the CSFM are shown in Fig. 5.32. The calculation of combination C1 reached 100% of permanent load and 53.1% of variable load, which corresponds to a bending moment at midspan equal to 228.8 kip-ft. The concrete stresses are presented in Fig. 5.32b, which shows that the maximum stress in the compression zone at midspan is equal to the stress given by the cross-sectional analysis in *IDEA StatiCa RCS* (see Fig. 5.31c). Similarly, identical maximum stresses in the reinforcement are obtained in the CSFM (Fig. 5.32c) and *IDEA StatiCa RCS* (Fig. 5.31c) analyses.

Table 5.11 provides an overview of the prediction of the ultimate moment resistance with a cross-sectional analysis and with the CSFM. This simple beam example, which can be calculated with the CSFM as well as with simpler methods based on cross-sectional analysis, shows that the CSFM yields very similar results to cross-sectional analysis methods (the CSFM provides a 6% higher prediction of the bending capacity), similarly as already shown for the previous example (Section 5.3).

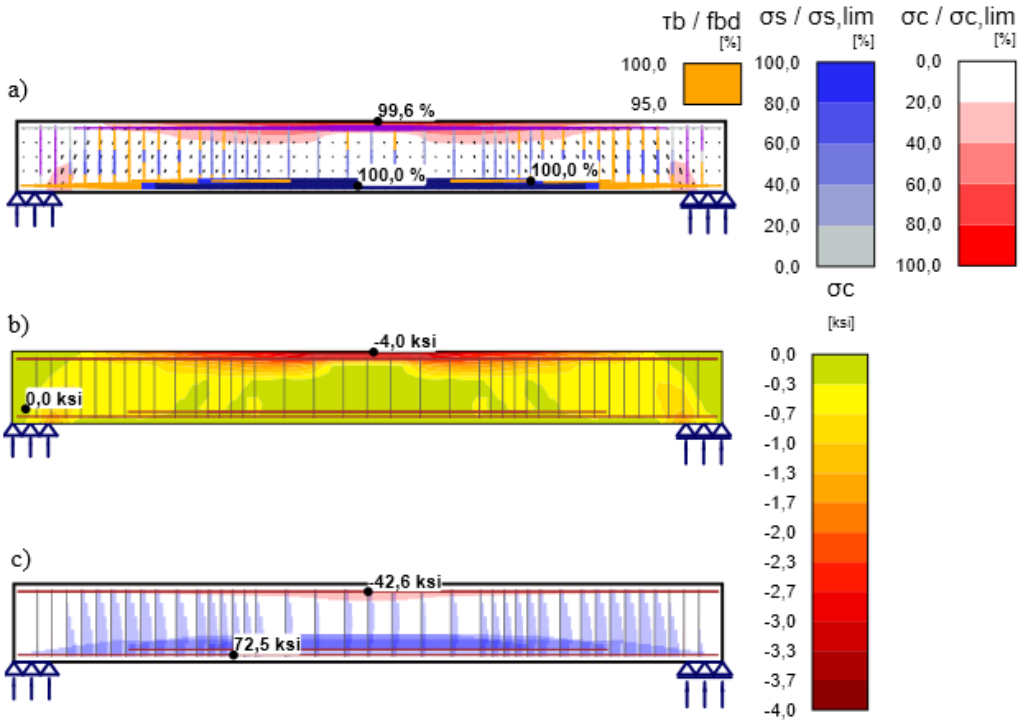

Fig. 5.32 CSFM results at the ultimate limit state: (a) Stress field; (b) concrete compressive stresses; (c) reinforcement stresses.

Table 5.11 Comparison of moments of resistance.

Type of calculation	Ultimate moment resistance [kip-ft]
IDEA StatiCa RCS	215.4
CSFM	228.8

5.4.4 Serviceability limit state

In this chapter, analytical calculations of deflections provided by Roberts (2003) following the main provisions of ACI 318-14 are compared to deflections obtained by the CSFM (see Fig. 5.33a, b, c). A creep coefficient φ = 2.5 is considered in long-term deflection in order to account for creep effects. The calculation of crack widths is not discussed in this example due to the fact that no direct crack width calculation is provided by ACI 318-14.

Deflection according to analytical calculations

ACI 318-14 proposes that deflections be estimated following the method stated in (Branson and Metz 1965), which considers the procedure of the effective moment of inertia (I_e). The effective moment of inertia, I_e, provides a transition between the upper and lower bounds of I_g (the moment of inertia of a gross concrete section) and I_{cr} (the fully cracked moment of inertia). The transition depends on the ratio between the cracking moment (M_{cr}) and the acting moment (M), as follows:

$$I_e = I_{cr} + \left(I_g - I_{cr}\right)\left(\frac{M_{cr}}{M}\right)^3 \tag{5.5}$$

The moment of inertia of the rectangular gross concrete section, neglecting reinforcement, is:

$$I_g = \frac{b \cdot h^3}{12} = \frac{9 \cdot 24^3}{12} = 10368 \text{ in}^4 \tag{5.6}$$

where b is the width of the section and h is its depth.

The fully cracked moment of inertia is calculated as follows:

$$M_{cr} = \frac{f_r \cdot b \cdot h^2}{6} = \frac{7.5 \cdot \sqrt{4000} \cdot 9 \cdot 24^2}{6} = 34.2 \text{ kip-ft} \tag{5.7}$$

where f_r is the modulus of rupture (effective tensile strength) of concrete.

To calculate the fully cracked moment of inertia, the distance from the top edge to the neutral axis, c, is calculated at midspan by solving the following quadratic formula:

$$\frac{b \cdot c^2}{2} + \left[n \cdot A_s + \left(n-1\right) A'_s\right] c - n \cdot A_s \cdot d - \left(n-1\right) \cdot A'_s \cdot d' = 0 \tag{5.8}$$

where $n = E_s/E_c = 8.04$ is the modular ratio, $A_s = 1.86$ in^2 and $A'_s = 1.20$ in^2 are the cross-section of the tensile and the compressive reinforcement, respectively, while $d = 21$ in and $d' = 2.3$ in are the respective distances of the tensile and compressive reinforcement to the upper edge of the beam. Eq. (5.8) yields a solution of c = 6.39 in. The fully cracked moment of inertia can be calculated as follows:

$$I_{cr} = \frac{b \cdot c^3}{3} + \left(n-1\right) A'_s \left(c - d'\right)^2 + n \cdot A_s \left(d - c\right)^2 = 4120 \text{ in}^4 \tag{5.9}$$

For the serviceability load combination C2, which considers dead as well as live loads (see Table 5.10), a bending moment $M = 227$ kip·ft is obtained at midspan. The effective moment of inertia for this combination can be calculated according to Eq. (5.5), leading to $I_e = 4140$ in^2, i.e., a value very close to that of the fully cracked section. The short-term deflection for the load combination C2 can be calculated as follows:

$$\Delta_{st,C2} = \frac{5 \cdot q \cdot l_n^{\,4}}{384 \cdot E_c \cdot I_e} = 0.987 \text{ in} \tag{5.10}$$

where $q = 5.025$ kip/ft is the uniformly distributed load and $l_n = 19$ ft is the beam span.

The same procedure can be followed to calculate the deflection under sustained loads (load combination C3, see Table 5.10). In this load combination, it is assumed that 50% of the live load is permanent, which yields a bending moment at midspan $M = 167$ kip·ft and an effective moment of inertia $I_e = 4170$ in^2 (similarly as for load combination C2, this is very close to the fully cracked inertia). The short-term deflection is also calculated in this case with Eq. (5.10), leading to $\Delta_{st,C3} = 0.721$ in. The long-term deflections, which include creep and shrinkage, Δ_{lt}, are estimated in ACI 318-14 based on the short-term deflections as follows:

$$\Delta_{lt} = \frac{\xi}{1 + 50\rho'} \Delta_{st} \tag{5.11}$$

where ξ is a time-dependent factor that takes a value of 2.0 for a 5-year duration of loading and ρ' is the geometric amount of the compression reinforcement at midspan, which takes a value of 0.63% in this case. This yields a short-term load amplification factor of slightly above 1.5, and a long-term deflection of $\Delta_{lt,C3} = 1.091$ in.

Deflection according to the CSFM

The results of deflections provided by the CSFM are shown in Fig. 5.33. Table 5.12 provides a comparison between the results of simplified analytical calculations and the results provided by the CSFM. The agreement between both approaches for this example is very good.

Table 5.12 Comparison of deflections between hand calculations and the CSFM.

Deflection	$\Delta_{st,C2}$ [in]	$\Delta_{st,C3}$ [in]	$\Delta_{lt,C3}$ [in]
Acc. to Roberts (2003)	0.987	0.724	1.095
CSFM	0.920	0.657	1.184
Differences	-7%	-9%	+9%

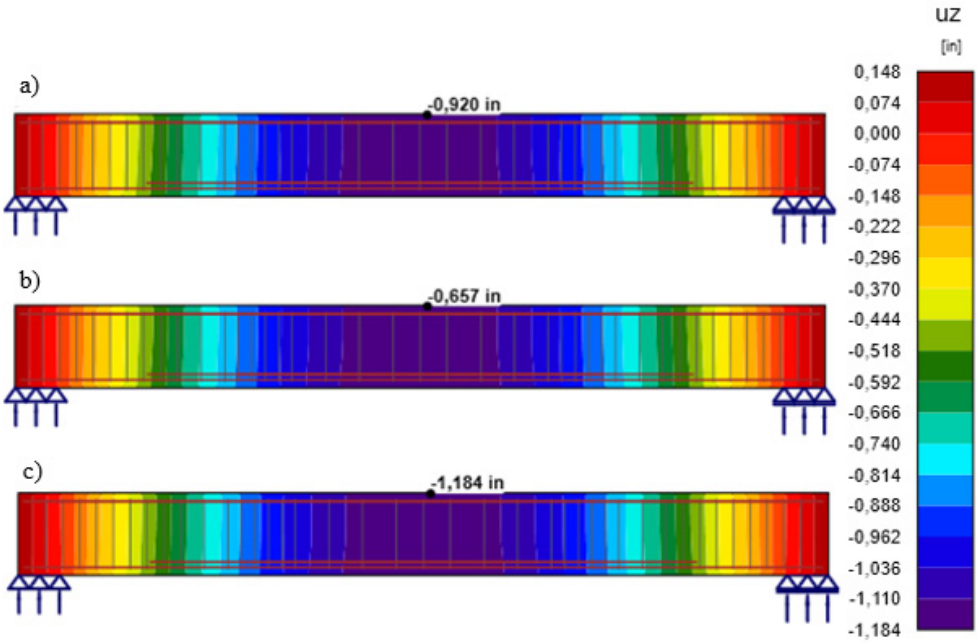

Fig. 5.33 CSFM deflection results: (a) Short-term deflection under dead and live loads (combination C2); (b) short-term deflection under sustained loads (combination C3); (c) long-term deflection under sustained loads (combination C3).

5.4.5 Conclusions

This chapter considered a conventional beam of rectangular cross-section, comparing results obtained from the CSFM (2D model) with those of analytical calculations performed according to ACI 318-14, as well as with cross-sectional analyses (1D models). Similarly as in the previous example, a slightly higher load-bearing capacity was obtained via the CSFM calculation. This can be explained by the fact that some more refined considerations are used in the CSFM (e.g., 2D-problem, consideration of the actual reinforcement layout within the whole beam rather than just a section).

The results in terms of the estimation of deflections differ by a maximum of 9%, which is again a very good match. Slightly smaller deflections were obtained by the CSFM calculation for short-term deflections, while for long-term deflections the CSFM estimates are slightly larger than the analytical calculations according to ACI 318-14. The slightly higher stiffness shown by the CSFM for short-term loads might be caused by the consideration in the CSFM of non-stabilized cracking for the stirrups, which provides a higher stiffness than the consideration of stabilized cracking. The lower stiffness of the CSFM in comparison with the analytical calculations according to ACI 318-14 might be explained by the consideration in Branson's formulae (see Eq. (5.10)) of the effect of compression reinforcement on long-term behavior, a factor that is not explicitly considered in the CSFM.

The results from this code validation example are highly satisfactory, showing very good agreement between the CSFM and the more simplified cross-sectional analysis. The differences can be explained as being due to the differences in the assumptions of the different calculation models.

5.5 Analysis of a T-beam in a four-point bending configuration

5.5.1 Case description

Beam TA9 is one of a seminal series of 18 experiments on simply supported T-beams published by Leonhardt and Walther (1963). All tested beams had the same cross-section and flexural reinforcement but differed in their web reinforcement (stirrups, bent-up bars and horizontal web reinforcement). The main purpose of the experiments was to investigate the load-bearing capacity in relation to web reinforcement. The objective of this section is to compare the results of the CSFM with a cross-sectional analysis based on current design code prescriptions (EN 1992-1-1) for one of these beams (TA9, with a bending failure). The reference cross-sectional analysis is carried out using *IDEA StatiCa Beam* software, whose main assumptions are described in Appendix A, A.1. For the purposes of this comparison to design codes, the model was adapted from the experimental results (e.g., safety coefficients were applied to the model). Therefore, it is not possible to directly compare the results of the CSFM to the experimental results. This comparison will be addressed in Section 6.2 for Specimens TA9, TA10, TA11 and TA12, covering a range of areas from bending to shear failures.

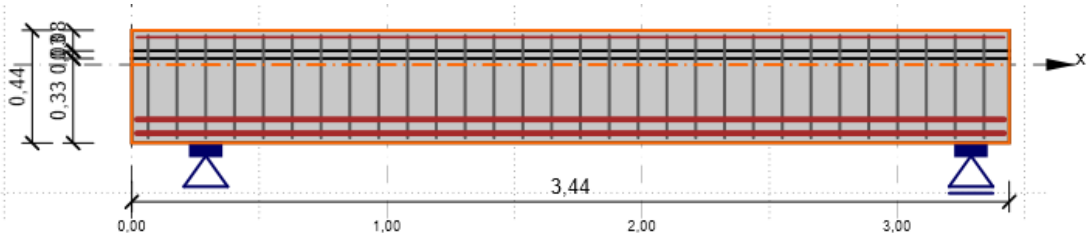

Fig. 5.34 Diagram of beam geometry in the CSFM (dimensions in [m]).

The geometry of Beam TA9 was extracted from Leonhardt and Walther (1963): A simply supported beam with a total length of 3.44 m and a clear distance between supports of 3.00 m (see Fig. 5.34). The beam was reinforced with longitudinal reinforcement, which was 6Ø24 in 2 layers at the bottom of the beam and 4Ø10 at the top. Shear reinforcement was provided by vertical stirrups 2Ø12 with 113 mm spacing, placed in the web of the cross-section.

In the CSFM, if a cross-section has flanges that are too wide, an effective cross-section with reduced flange width is considered by default in the calculation (see 3.6.3). While an effective cross-section would normally be considered by default in this case in the CSFM, in this section the cross-section dimensions were left unchanged compared to the TA9 geometry defined by Leonhardt and Walther (1963), see Fig. 5.35. A comparison of the influence of different effective widths of the upper flange can be found in Section 6.2. It should be noted that while in models input via a beam template the default value of the effective flange depth that cannot be modified, users can freely choose its value when defining the structural member with a wall or general templates (see Section 3.6.3).

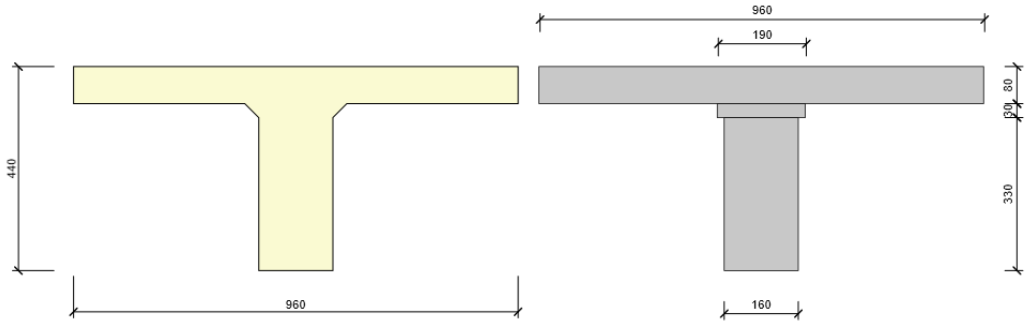

Fig. 5.35 T-shaped cross-section dimensions: (a) Cross-section of the specimen; (b) simplified cross-section used in the calculation model in the CSFM (dimensions in [mm]).

The beam was loaded by a uniform line load, which represented the permanent part of the load g = 3 kN/m, and by two point loads representing the variable part q = 328 kN (see Fig. 5.36). These values of the loads were used in ULS fundamental, SLS characteristic and SLS quasi-permanent combinations (see Table 5.12).

5.5.2 Modeling with the CSFM

The calculation model created in the CSFM contained a beam member (defined by the T-cross-section specified in Fig. 5.35) of length 3.44 m. Two bearing plates with point supports were defined as well at both ends of the beam.

Two load cases and three combinations were defined in *IDEA StatiCa Detail*. Permanent and variable loads were defined in separate load cases. The combinations were defined using the combination rules stated in Table 5.13.

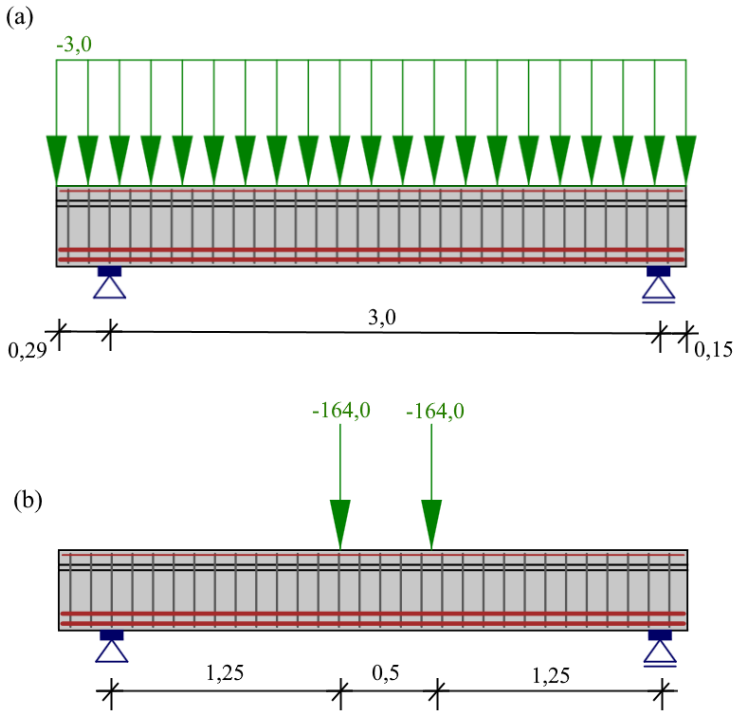

Fig. 5.36 Beam TA9 loaded by: (a) Permanent load; (b) variable loads.

Table 5.13 Defined load cases and combinations.

Name/Type	Description
LC1/Permanent	g = 3 kN/m
LC2Variable	Q = 2 x 164 kN
C1/ULS	1.35 LC1 + 1.5 LC2
C2/SLS Characteristic	1.0 LC1 + 1.0 LC2
C3/SLS Quasi-permanent	1.0 LC1 + 0.3 LC2

The basic material properties were extracted from Leonhardt and Walther (1963). Table 5.14 provides an overview of the most relevant data used in this example.

Table 5.14 Input data for Beam TA9.

Characteristic tensile strength of reinforcement f_{tk} [MPa]	548[2)]
Characteristic yield strength of reinforcement f_{yk} [MPa]	435[1)]
Partial factors for reinforcement γ_s	1.15[2)]
Characteristic strain limit of reinforcement ε_{uk} [‰]	30[2)]
Modulus of elasticity of reinforcement E_s [GPa]	200[2)]
Characteristic concrete compressive strength f_{ck} [MPa]	18.3[1)]
Concrete strain when reaching the maximum strength ε_{c2} [‰]	2.0[2)]
Partial factors for concrete γ_c	1.5[2)]

1) Extracted from Leonhardt and Walther (1963)
2) Extracted from EN 1992-1-1

5.5.3 Ultimate limit state

The design characteristics of the materials were used for the ULS check. The CSFM model and the *IDEA StatiCa RCS/Beam* model were created to be consistent with EN 1992-1-1 specifications for the ULS. The structural response predictions were evaluated and each component (concrete, reinforcement, anchorage) was checked for both models. The main results are outlined and compared below.

Ultimate moment resistance according to *IDEA StatiCa RCS/Beam*

The ultimate moment resistance calculated in *IDEA StatiCa Beam* was 311.8 kN·m. The limited deformation method (see the detailed description in Appendix A, A.2.2) was chosen to check the section in *IDEA StatiCa RCS*. The cross-sectional response for the design moment (M_{Rd} = 311.8 kN·m) is depicted in Fig. 5.37.

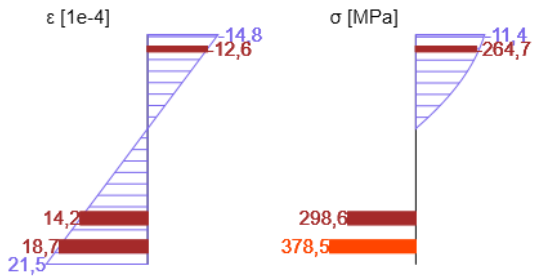

Fig. 5.37 Response of the reinforced cross-section, strain and stress distribution at the limit state according to *IDEA StatiCa RCS* for M_{Rd} = 311.8 kN·m.

Ultimate moment resistance in IDEA StatiCa Detail

The calculation of the C1 ULS combination attained 100% of permanent load and 99.7% of variable load (see the summary results from the CSFM in Fig. 5.38), which corresponds to an ultimate moment resistance for the governing midspan section of M_{Rd} = 311 kN·m. The approximate integration of the stress diagram presented in Fig. 5.39 for the cross-section at midspan leads to an estimation of the ultimate moment resistance of about 326 kN·m, slightly higher than the exact value.

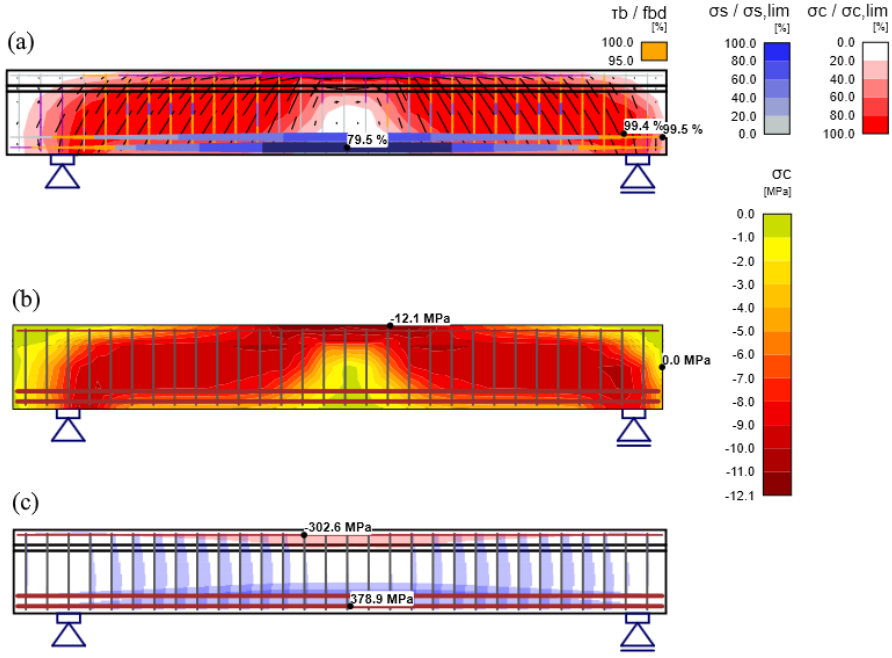

Fig. 5.38 Results from *IDEA StatiCa Detail*: (a) Summary of CSFM results; (b) stresses in concrete; (c) stresses in reinforcement.

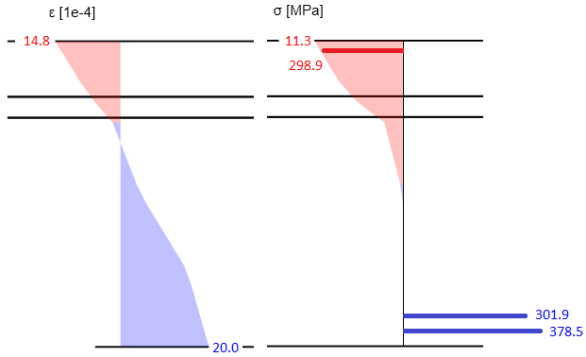

Fig. 5.39 Stress-strain distribution at the ultimate limit state.

Table 5.15 compares the main results from the CSFM and the cross-sectional analysis performed by *IDEA StatiCa RCS*. The results show excellent agreement between both methods, with an almost identical prediction of the ultimate moment resistance.

Table 5.15 Comparison of strains and stresses at the ultimate limit state.

Approach	$\varepsilon_{c,upper}$ [1e-4]	$\varepsilon_{c,lower}$ [1e-4]	σ_c [MPa]	$\sigma_{s,upper}$ [MPa]	$\sigma_{s,lower}$ [MPa]	M_{Rd} [kN·m]
IDEA StatiCa RCS	-14.8	21.5	-11.4	-264.7	378.5	312
CSFM	-14.8	20.0	-11.3	-298.9	378.5	311

5.5.4 Serviceability limit state

Stress limitation

Stress limitation checks are provided in the CSFM for characteristic and quasi-permanent combinations and for both short and long-term effects. The creep coefficient considered was $\varphi = 2.5$ (default value in the CSFM, Section 3.6.8). The main results for a characteristic combination are illustrated in Fig. 5.40.

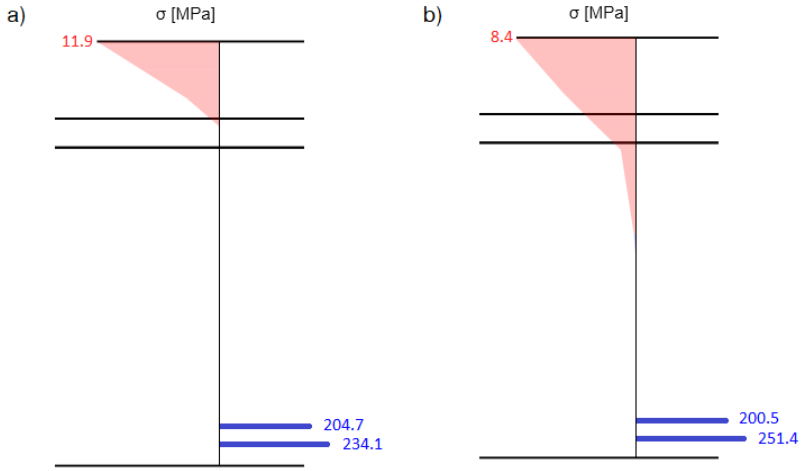

Fig. 5.40 Results of serviceability stress calculations in the CSFM for a characteristic combination: (a) Short-term model; (b) long-term model.

The response under the characteristic combination was also calculated in *IDEA StatiCa RCS* (see the main hypothesis in Appendix A, A.1), and the results are shown in Fig. 5.41. The results of both approaches are compared in Table 5.16, showing excellent agreement for both concrete and reinforcement stresses.

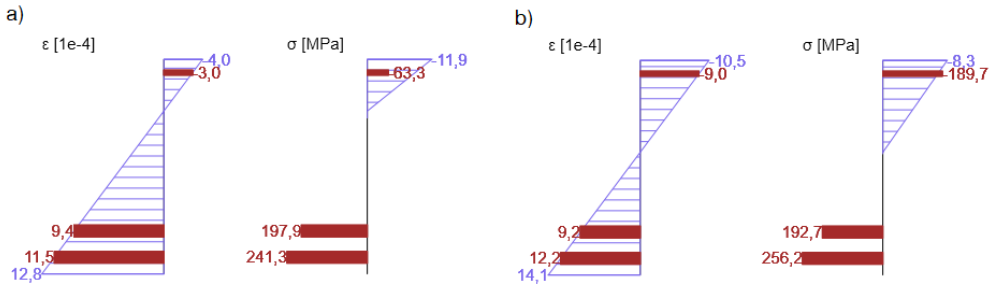

Fig. 5.41 Strain and stress distributions for a characteristic combination calculated in *IDEA StatiCa RCS*: (a) Short-term model; (b) long-term model.

Table 5.16 Comparison of serviceability stress limits.

Approach	$\sigma_{c,st}$ [MPa]	$\sigma_{s,st}$ [MPa]	$\sigma_{c,lt}$ [MPa]	$\sigma_{s,lt}$ [MPa]
IDEA StatiCa RCS	11.9	241.3	8.3	256.2
CSFM	11.9	234.1	8.4	251.4

Crack widths

A crack width check is provided in the CSFM for the quasi-permanent combination (as prescribed in EN 1992-1-1) in the vicinity of the reinforcement. Fig. 5.27 shows the crack width results from the CSFM as well as those obtained from *IDEA StatiCa Beam* software (reference calculation of a cross-sectional analysis performed according to EN 1992-1-1). The agreement is excellent. It should be noted that the presentation of crack spacings in the CSFM is just schematic and does not represent the crack spacing computed internally in the software.

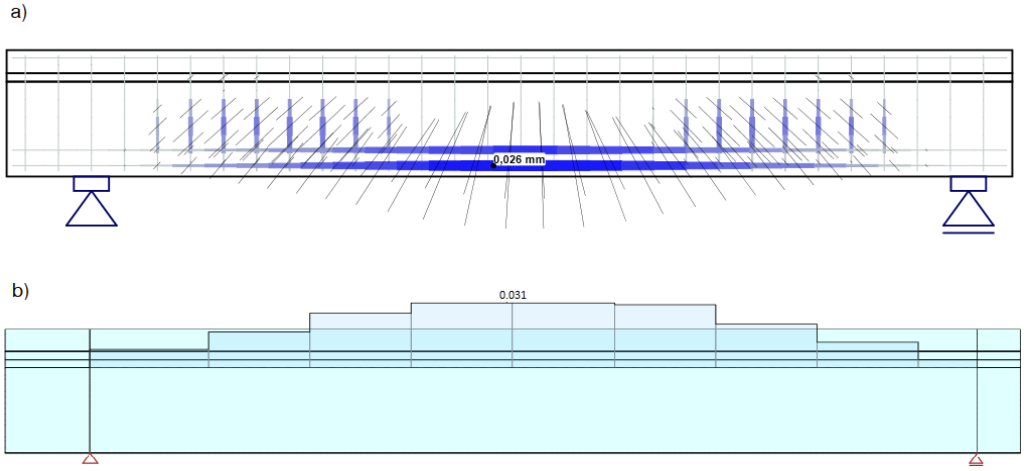

Fig. 5.42 Crack width verification results: (a) Crack direction and opening according to the CSFM; (b) calculation according to *IDEA StatiCa Beam*.

Table 5.17 Comparison of crack width results

Approach	w [mm]
IDEA StatiCa Beam	0.031
CSFM	0.026

Deflections

Short-term and long-term deflection results provided by the CSFM and by *IDEA StatiCa Beam* are presented in Fig. 5.43. The results at midspan are compared in Table 5.18, showing that the CSFM model exhibits significantly lower stiffness in comparison with the conventional cross-sectional analysis performed with *IDEA StatiCa Beam* software.

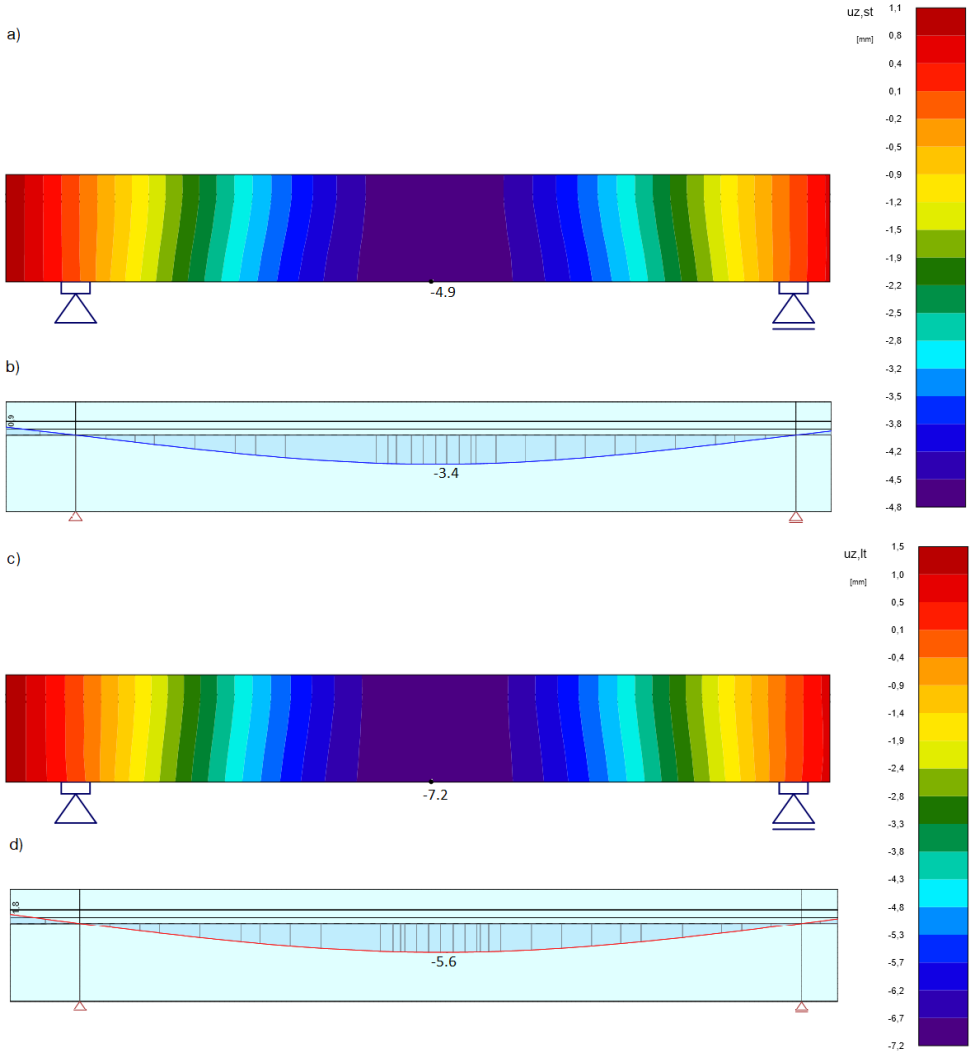

Fig. 5.43 Detailed deflection results: Short-term deflections in (a) CSFM and (b) *IDEA StatiCa Beam;* long-term deflection in (c) CSFM and (d) *IDEA StatiCa Beam.*

Table 5.18 Comparison of deflection results.

Approach	Δ_{st} [mm]	Δ_{lt} [mm]
IDEA StatiCa Beam	3.4	5.6
CSFM	4.9	7.2

It should be noted that the CSFM provides an excellent estimation of the experimental deflections for service loads (see Section 6.2); therefore, the deflections provided by the CSFM should be considered more accurate in this particular case. This might be explained by the better approximation of the shear deformations in the CSFM. In this example of a relatively short beam (shear-to-span to depth ratio in the order of 3.0), the contribution of the shear deformations to the total deflections is high. Hence, the CSFM predicts the deflections well, whereas a cross-sectional analysis in which the shear deformations are neglected tends to underestimate the deformations. However, for other examples of longer beams, where the contribution of shear deformations is very limited (see Sections 5.3.4 and 5.4.4), both approaches provide accurate results.

5.5.5 Conclusions

This chapter considered a simply supported T-beam, comparing the results obtained using the CSFM (2D model of the structure) with those of a cross-sectional analysis performed with *IDEA StatiCa Beam/RCS* software (1D model of the structure). The matching between ultimate limit state results is excellent, both for the prediction of the ultimate moment resistance as well as for the stress and strain results at midspan.

The strain and stress distributions at the midspan section for the serviceability limit state are almost the same, as is the case with the ultimate limit state. The difference in crack width results is satisfactory. However, only stabilized cracks in the main bending reinforcement could be compared. Unlike the previous two examples (both simply supported slender beams with a large shear span-to-depth ratio, which allows shear deformations to be neglected, assuming that plane sections remain plane and normal to the axis of the beam), this beam shows the influence of shear deformations in the deflections of the beam. In order to approximate the deformations properly in this example using a 1D model, it would be necessary to consider Timoshenko's beam theory during the cross-sectional analysis. In the CSFM, the shear deformations are automatically taken into account (if the cross-section is meshed with an appropriate number of elements). Therefore, the CSFM is a general model that provides good results both for slender members as well as for deep members and discontinuity regions that cannot be modeled with conventional cross-sectional analysis.

6 Experimental validation

6.1 Introduction

This chapter describes the validation of the Compatible Stress Field Method (CSFM) via the analysis of its ability to reproduce the real behavior observed in selected experimental campaigns from the literature. The analyzed experiments cover a wide range of structural typologies and failure modes. The validation comprises not only predictions of ultimate load, but also of load-deformation response and, in some cases, crack widths. This strategy of conducting in-depth validations for selected key experiments provides proofing that the CSFM works well for most of the cases to which it is applicable.

The following groups of tests, comprising 29 experiments in total, have been studied for the validation of the CSFM:

- Section 6.2 analyzes four-point bending tests conducted on T-Beams by Leonhardt and Walther (1963). The four selected experiments from this campaign differed in the amount of shear reinforcement employed. The result was a range of different observed failure modes ranging from bending to shear (information about the classification used for failure modes is given in Section 6.1.1).
- Section 6.3 discusses tests performed on cantilever wall-type bridge piers by Bimschas (2010) and Hannewald et al. (2013). Three experiments are analyzed in this case. Each features different amounts of flexural reinforcement and shear slenderness (varying wall height). All of the selected experiments resulted in flexural failure (yielding of the reinforcement and local concrete crushing in the connection with the pier foundation), but the specimens showed different levels of deformation capacity.
- Section 6.4 analyzes 17 shear tests carried out on beams during campaigns performed by Piyamahant (2002), Vecchio and Shim (2004) and Huber (2016). The tests covered a wide number of parameters, including different sizes, varying shear slenderness and differing amounts of shear and longitudinal reinforcement. The observed failure modes in these tests range from shear failures with and without rupture and the stirrups to bending failures and mixed shear-bending failures.
- Section 6.5 describes the analysis of a series of tests on *discontinuity regions*, namely those conducted on concrete pier caps by Geevar and Menon (2018). The test parameters in this experimental campaign were the amount of reinforcement and the size of the load-bearing plates. The failure mode in all cases was concrete crushing of the diagonal strut from the support to the column.

The mean material properties from the experiments were used in the CSFM without any safety coefficient in order to enable it to predict the mean experimental behavior. For all of the numerical

analyses, the modulus of elasticity (E_s) of the reinforcement and the ultimate concrete compressive strain (ε_{cu}) were set to 200 GPa and 3.5‰, respectively. An analysis using the default numerical parameters described in Chapter 3 (implemented in *IDEA StatiCa Detail* software) was conducted for all tests. This default model is referred to as Model 0 (M0). While in *IDEA StatiCa Detail* an infinitely plastic branch of concrete in compression is considered by default, in all of the presented analyses concrete crushing was explicitly verified as described in Table 6.1. This allowed the deformation capacity of the members to be estimated for all possible failure modes. Analyses with parameters which are different from the default ones were also performed. This allowed the sensitivity of the results to the input numerical parameters and the suitability of the default values to be studied. The parameters in question (e.g., the type of tension stiffening modeling) differ from case to case, depending on their relevance. The influence of finite element mesh size was studied in all cases.

6.1.1 Definition of failure modes

In order to compare the observed failure modes in the experiments with those predicted by the CSFM, the failure modes are classified as follows: flexural (F), shear (S) and anchorage (A). It should be noted that none of the experiments covered in this chapter exhibited an anchorage failure. Table 6.1 defines different failure subtypes depending on whether flexural and shear failures are triggered by failure of the concrete or of the reinforcement. While yielding of the reinforcement does not represent a material failure, this is included as a failure subtype in combination with concrete crushing due to the importance of distinguishing concrete crushing failures without reinforcement yielding (very brittle) from those happening after the yielding of the reinforcement (which can exhibit a certain deformation capacity).

Table 6.1. Definition of failure modes.

F: Flexural failure	→	CC	or	CC+FY	or	FR
S: Shear failure	→	CC	or	CC+SY	or	SR
A: Anchorage failure						

FY, SY: Yielding of the flexural or shear reinforcement, respectively (in the CSFM when $f_y \leq \sigma_{sr} < f_t$)
FR, SR: Rupture of the flexural or shear reinforcement, respectively (in the CSFM when $\sigma_{sr} = f_t$)
CC: Concrete crushing (in the CSFM when $|\varepsilon_{c3}| \geq |\varepsilon_{cu2}| = 3.5‰$ over a length equal to the thickness of the region, or if the calculation diverges due to strain softening)

6.2 Four-point bending tests on T-beams

This section analyzes an experimental investigation involving four-point bending tests performed on T-beams by Leonhardt and Walther (1963). This experimental campaign comprised 18 tests conducted on reinforced concrete beams with constant geometry and varying reinforcement layouts for the stirrups. Specimens TA9, TA10, TA11 and TA12 (with vertical stirrups and varying

reinforcement amounts) were chosen for comparison with results gained from the CSFM, since they cover a wide range of failure modes from shear to flexural.

6.2.1 Experimental setup

All of the investigated beams had the same geometry and reinforcement arrangements, as shown in Fig. 6.1. The beam span (spacing between the supports) was 3000 mm. The flanges had a width of 960 mm and a depth of 80 mm. The webs had a width of 160 mm, and the total depth of the beams was 440 mm. Each of the two applied loads ($P/2$) was applied at a distance of 1250 mm from the supports, which resulted in a spacing between loads of 500 mm. The flexural reinforcement consisted of six reinforcing bars of 24 mm in diameter. Four longitudinal reinforcing bars with a diameter of 10 mm were placed in the flange. Open stirrups with hooked ends at the top (see Fig. 6.1a) were used as shear reinforcement; these were always placed at a spacing of $s_t = 113$ mm. The only parameter that varied between specimens TA9, TA10, TA11 and TA12 was the diameter ($Ø_t$) of the stirrups, which led to different geometric reinforcement ratios ($\rho_{t,geo}$) (see Table 6.2).

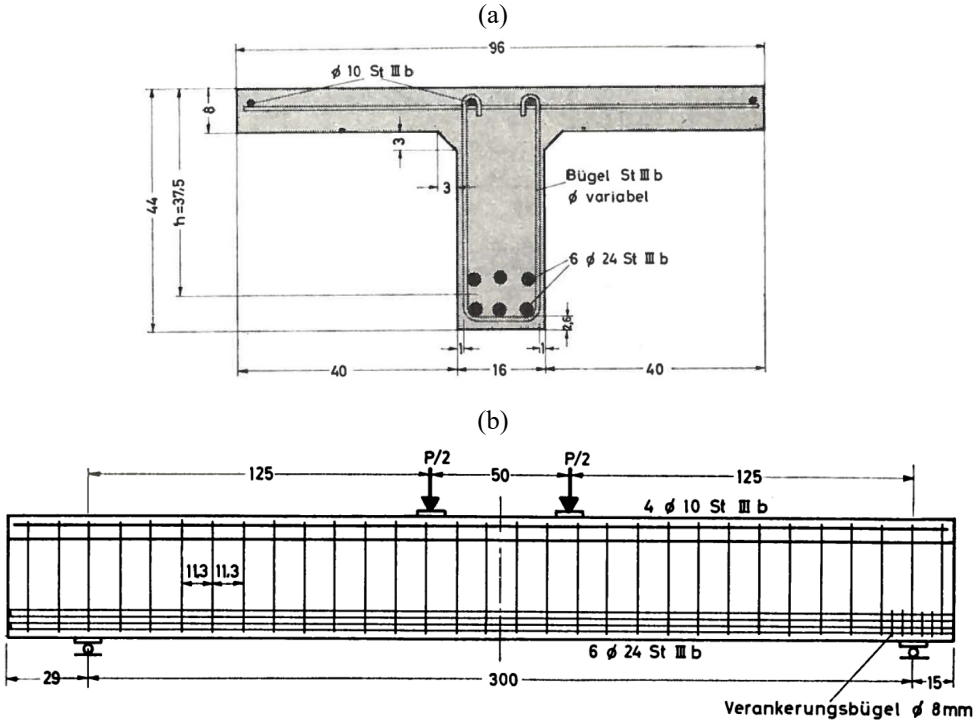

Fig. 6.1. Test setup, geometry and reinforcement of specimens TA9 – TA12: (a) Cross-section; (b) longitudinal view; (dimensions in [cm]; extracted from Leonhardt and Walther (1963)).

Table 6.2. Relevant parameters of the analyzed specimens.

Specimen	$Ø_t$ [mm]	s_t [mm]	$\rho_{t,geo}$ [%]
TA9	12	113	1.25 (>ρ_{cr}=0.7[1)])
TA10	10	113	0.87 (>ρ_{cr}=0.7[1)])
TA11	8	113	0.55 (<ρ_{cr}=0.7[1)])
TA12	6	113	0.31 (<ρ_{cr}=0.7[1)])

1) ρ_{cr} calculated with Eq. (3.5) considering f_{ct}=1.9 MPa.

6.2.2 Material properties

The material properties of the concrete and reinforcement used in the CSFM analysis are summarized in Table 6.3. The modulus of elasticity (E_s), the yield stress (f_y) and the ultimate stress (f_t) of the reinforcement as well as the compressive strength (f_c) of the concrete are directly extracted from the experimental report (Leonhardt and Walther 1963). This report only provides the experimental stress-strain relationships of the reinforcing bars up to a strain of 12 ‰. The ultimate strain of the bare reinforcement (ε_u) is estimated based on the known experimental values (f_y, f_t and incomplete stress-strain relationships) and assuming a bilinear response. Fig. 6.2a illustrates this estimate for the case of $Ø_t$=12 mm. The values obtained for the failure strain ε_u for all used diameters are given in Table 6.3. The compressive strain of concrete at peak stress (ε_{c0}, see Fig. 3.1c) is directly extracted from the experimental concrete stress-strain relationship (see Fig. 6.2b).

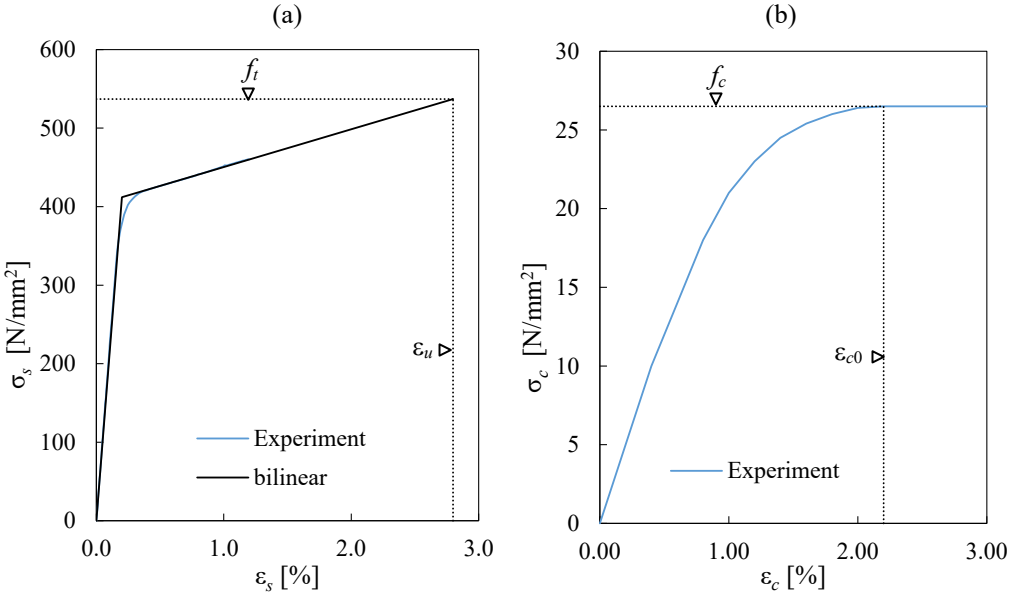

Fig. 6.2. Calculations based on the stress-strain relationships in Leonhardt and Walther (1963): (a) Ultimate strain ε_u of reinforcement (e.g. for $Ø_t$=12 mm); (b) concrete strain ε_{c0}.

Table 6.3. Material properties used in the CSFM analyses.

Specimen	Shear reinforcement			Flexural reinforcement			Concrete	
	f_y [1]	f_t [1]	ε_u [2]	f_y [1]	f_t [1]	ε_u [2]	f_c [1]	ε_{c0} [3]
	[MPa]	[MPa]	[‰]	[MPa]	[MPa]	[‰]	[MPa]	[‰]
TA9	412	537	28	400	536	22.2	26.5	2.2
TA10	420	538	36	400	536	22.2	26.5	2.2
TA11	405	526	27	400	536	22.2	26.5	2.2
TA12	435	570	29	400	536	22.2	26.5	2.2

1) Directly extracted from Leonhardt and Walther (1963)
2) Calculated as shown in Fig. 6.2a
3) Calculated as shown in Fig. 6.2b

6.2.3 Modeling with the CSFM

The geometry, reinforcement, supports and loading conditions were modeled in the CSFM according to the experimental setup (see Fig. 6.3a). Several numerical calculations were carried out using different values for the following parameters:

- The multiplier of the flange depth (MFD), which is the inverse of the slope considered for the expansion of the compression field into the flange (see Figure 6.3) to account for the shear lag effect (see Section 3.6.3). The MFD coefficient was set to 1.0 (default value in *IDEA StatiCa Detail*) and 3.0 (slightly above the recommendation of the *fib* Model Code 2010 for this specific configuration). These settings define the effective flange width (b_{eff}), which yield to b_{eff} = 350 mm and b_{eff} = 670 mm, respectively (Figure 6.3b-c).
- The consideration or not of potentially non-stabilized cracking in stirrups. When considered (by default), the Pull-Out Model (POM) defines tension stiffening in stirrups with geometric reinforcement ratios below (ρ_{cr}) (Eq. (3.5)), while the Tension Chord Model (TCM) is used for other bars and stirrups above (ρ_{cr}). When deactivated, the models account for tension stiffening by means of the TCM in all cases.
- The mesh size, which was 5 (the default value in *IDEA StatiCa Detail* for this particular example), 10 or 15 finite elements over the beam's depth. The default mesh is very coarse in this geometry (i.e., designers should avoid using fewer than four finite elements in a cross section); therefore, only finer meshes than the default one are analyzed in this study.
- The crack spacing coefficient (λ) was varied to consider minimum (λ = 0.5), average (λ = 0.67, default value) and maximum crack spacing (λ = 1.0). This parameter affects the tension stiffening behavior of reinforcing bars with stabilized crack patterns (see Section 3.3.4).

Table 6.4 shows the parameters used in each numerical calculation (model M0 to M6). M0 corresponds to the model with the default settings in the CSFM. As will be discussed in Section 6.2.4, the default value of the multiplier of the flange depth was too conservative in this case and led to an excessively soft response. Therefore, the default value (MFD = 1; b_{eff} = 350 mm) was only used in M0. In the other models, the MFD was set to 3 (b_{eff} = 670 mm).

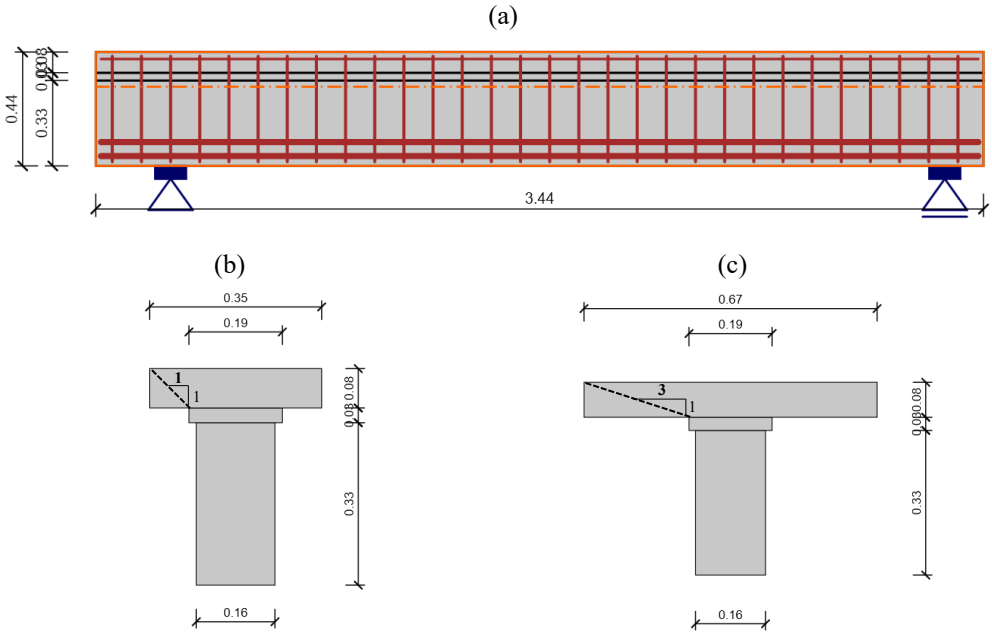

Fig. 6.3. Example of modeling with the CSFM, Specimen TA9: (a) Input geometry; (b)-(c) effective cross section considered in the calculation for a flange depth multiplier of MFD = 1.0 (b_{eff} = 350 mm) and MFD = 3.0 (b_{eff} = 670 mm); (dimensions in [m]).

Table 6.4. Investigated numerical parameters (variations to M1 shaded).

Model	MFD[1] (b_{eff})	Mesh size[2]	λ[3]	POM[4]
M0 (def.)	1 (350 mm)	5	0.67	Yes
M1	3 (670 mm)	5	0.67	Yes
M2	3 (670 mm)	10	0.67	Yes
M3	3 (670 mm)	15	0.67	Yes
M4	3 (670 mm)	5	0.67	No
M5	3 (670 mm)	5	0.50	Yes
M6	3 (670 mm)	5	1.00	Yes

1) Multiplier of Flange Depth
2) Number of elements over the beam's height
3) Crack spacing coefficient
4) Pull-Out Model

6.2.4 Comparison with experimental results

This section provides comparisons between the experimental results and the ultimate loads and failure modes provided by the CSFM. In order to also verify the use of the CSFM for serviceability behavior, the load-deformation response and crack patterns predicted by the numerical analyses are compared with those from the tests. Furthermore, the measured and calculated crack widths are compared for specimens TA9 and TA12, which exhibited flexural and shear failures, respectively.

Failure modes and ultimate loads

Table 6.5 summarizes the ultimate loads measured in the tests ($P_{u,exp}$), the ultimate loads predicted by the CSFM ($P_{u,calc}$), and the respective failure modes. P denotes the total applied force. This table also provides the mean and the coefficient of variation (CoV) of the ratios between the measured and the calculated ultimate loads for each numerical model. Ratios above one denote conservative predictions of the ultimate load. As seen in Table 6.5, the basic failure modes in all CSFM analyses agree with the experimental results, but differences in the failure subtypes are observed in some cases for Specimen TA11, and in one case for TA12. The predictions of the ultimate loads given by the default model (M0) are very satisfactory, yielding slightly conservative results (12% on average) with a very small scatter among the analyzed beams.

Table 6.5. Experimental and predicted ultimate loads (in kN) and failure mechanisms[1)].

Specimen	Test	M0	M1	M2	M3	M4	M5	M6
TA9	700 **F**(CC+FY)	651 **F**(CC+FY)	762 **F**(CC+FY)	735 **F**(CC+FY)	728 **F**(CC+FY)	762 **F**(CC+FY)	761 **F**(CC+FY)	764 **F**(CC+FY)
TA10	714 **F**(CC+FY)	620 **F**(CC+FY)	719 **F**(CC+FY)	705 **F**(CC+FY)	691 **F**(CC+FY)	719 **F**(CC+FY)	717 **F**(CC+FY)	722 **F**(CC+FY)
TA11	684 **S**(CC+SY)	610 **S**(SR)	642 **S**(SR)	618 **S**(SR)	619 **S**(SR)	636 **S**(CC+SY)	641 **S**(SR)	644 **S**(SR)
TA12	540 **S**(SR)	476 **S**(SR)	487 **S**(SR)	463 **S**(SR)	462 **S**(SR)	531 **S**(CC+SY)	486 **S**(SR)	489 **S**(SR)
$\frac{P_{u,exp}}{P_{u,calc}}$	mean	1.12	1.01	1.05	1.06	1.00	1.01	1.01
	CoV	0.03	0.08	0.09	0.08	0.06	0.08	0.08

1) Abbreviations for failure modes according to Table 6.1

The differences among the CSFM analyses can be easily analyzed in Fig. 6.4, where the ratios of experimental and calculated ultimate loads ($P_{u,exp}/P_{u,calc}$) are shown. Increasing the effective flange width from the default value (MFD = 1; b_{eff} = 350 mm) in model M0 to the value specified by the *fib* (International Federation for Structural Concrete 2013) (MFD = 3; b_{eff} = 670 mm) in model M1 led to an increase in the ultimate loads (Fig. 6.4a). The influence of the flange width was very small in those tests where failure in shear occurred (TA11 and TA12), but significant (up to 14%) in the case of bending failures (TA9 and TA10). The consideration of an increased effective flange width (model M1) led on average to better results than with the default model,

but at the cost of a larger scatter. Hence, M1 is used in Fig. 6.4 as the reference model for the following comparative analyses.

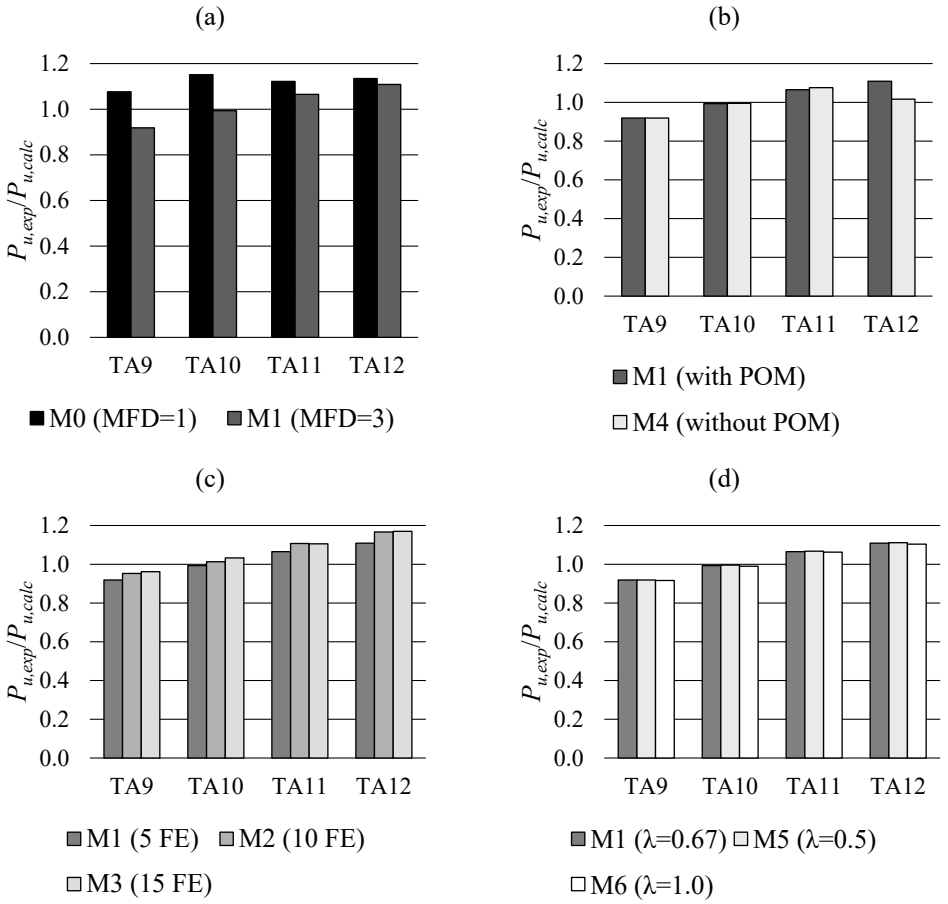

Fig. 6.4. Influence of numerical parameters on the ratio of measured to calculated ultimate loads: (a) Sensitivity to different multipliers of the flange depth (MFD); (b) consideration or not of the Pull-Out Model (POM) in the stirrups for low amounts of reinforcement; (c) mesh size sensitivity; (d) influence of different crack spacing coefficients (λ).

The results of the consideration or not of potentially non-stabilized cracking in stirrups are shown in Fig. 6.4b. This parameter only affected the results for Specimens TA11 and TA12 (TA9 and TA10 have a large amount of stirrups – $\rho_{t,geo} > \rho_{cr}$, see Table 6.2 – and therefore tension stiffening was accounted for by using the Tension Chord Model (TCM) regardless of this setting). In numerical model M1, the tension stiffening of TA11 and TA12 was modeled with the Pull Out Model (POM), but the TCM was used in M4. Using the POM or the TCM had a small impact on the strength predictions in this particular case (a maximum of 10% for TA12), since the amount

of stirrups is quite high in all cases. The consideration of the POM is more relevant when modeling structural elements with a lower amount of stirrups, as will be discussed in Section 6.4. The influence of the mesh size and the crack spacing parameters on the ultimate load was very small in this case (the differences are below 5%, see Fig. 6.4c-d).

Figures 6.5 to 6.8 show the resulting stress fields and the identification of failure modes. In Figures 6.5a to 6.8a, the observed failure modes are marked on top of the photos of the tested specimens (for TA10 the reported concrete crushing in bending is not marked since it is not evident in the photo). The failure modes predicted by the numerical model M1 are highlighted in Figures 6.5c to 6.8c, which show the stress fields at ultimate limit state, including the principal compressive stresses (σ_{cr3}) and the steel stresses (σ_{sr}) at the cracks. M1 corresponds to the default parameters, except for the effective flange width, which is based on the *fib* Model Code 2010 (International Federation for Structural Concrete 2013). The predicted failure modes agree fairly well with the experimental observations, including their location. The model of Beam TA11 is slightly conservative since it predicts a failure of the stirrups, while only their yielding is reported in the experiments. The calculation of cracked regions and the magnitudes of the crack widths (represented by the length of the lines) at the onset of yielding are plotted in Figures 6.5b to 6.8b. The numerical parameters from M1 are also used in this case. The predicted cracked regions and crack orientations agree well with the experimental observations at failure in Figures 6.5a, 6.6a, 6.7 and 6.8a.

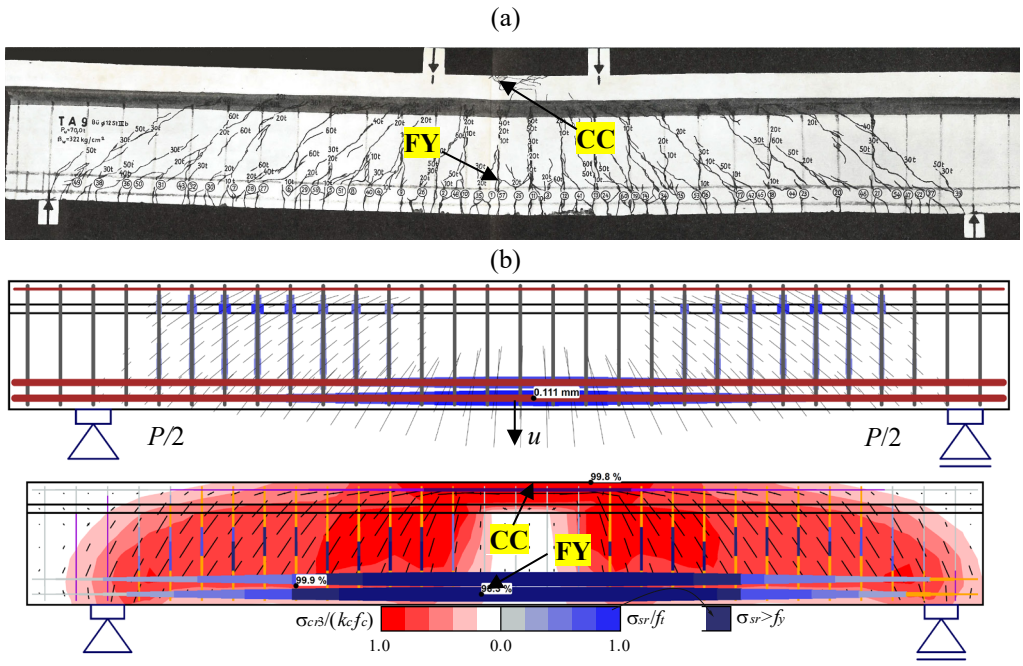

Fig. 6.5. Results for TA9: (a) Observed crack pattern at ultimate extracted from Leonhardt and Walther (1963); (b) calculated crack pattern at yielding and stress fields at ultimate for M1.

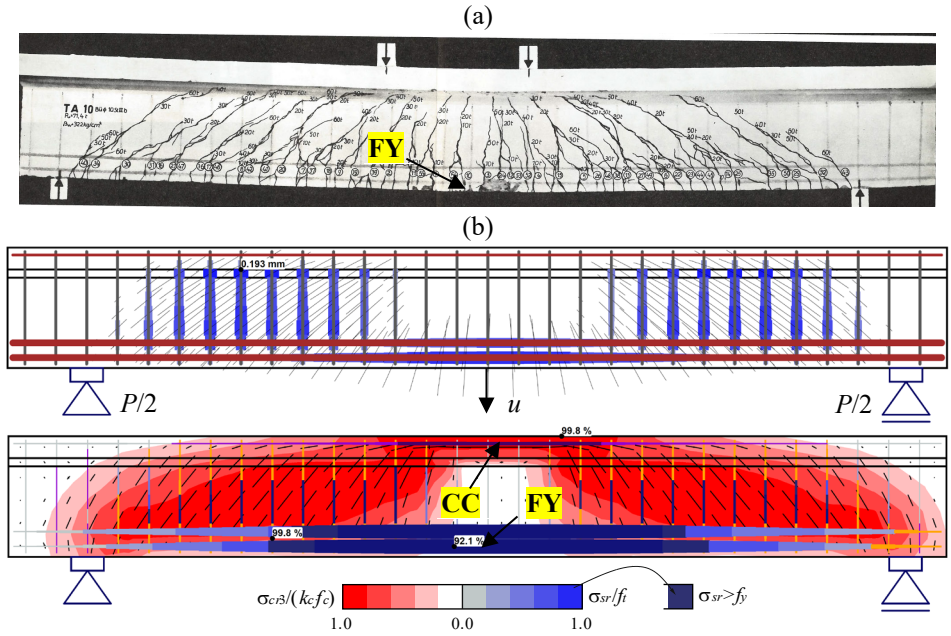

Fig. 6.6. Results for TA10: (a) Observed crack pattern at ultimate extracted from Leonhardt and Walther (1963); (b) calculated crack pattern at yielding and stress fields at ultimate for M1.

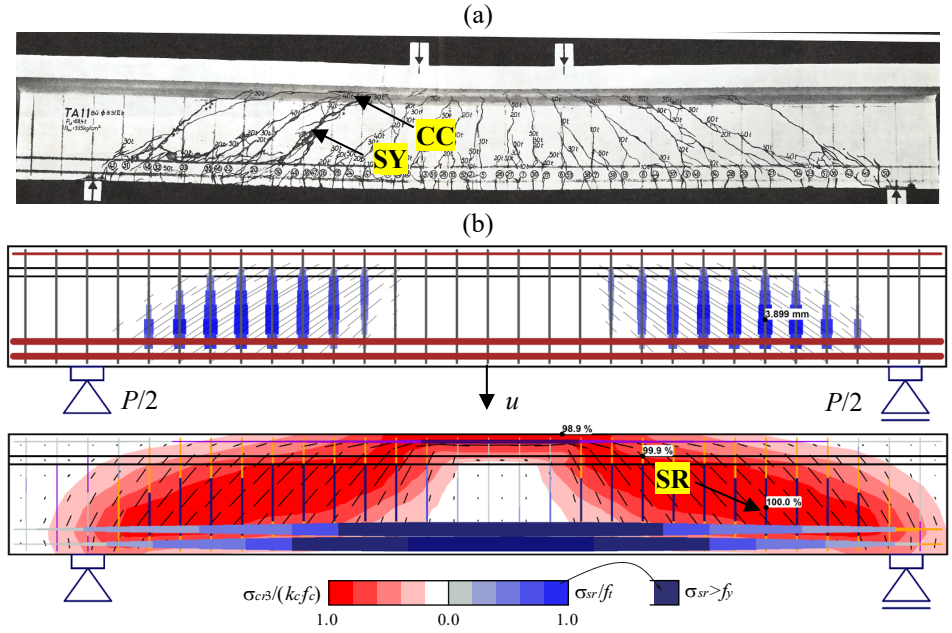

Fig. 6.7. Results for TA11: (a) Observed crack pattern at ultimate extracted from Leonhardt and Walther (1963); (b) calculated crack pattern at yielding and stress fields at ultimate for M1.

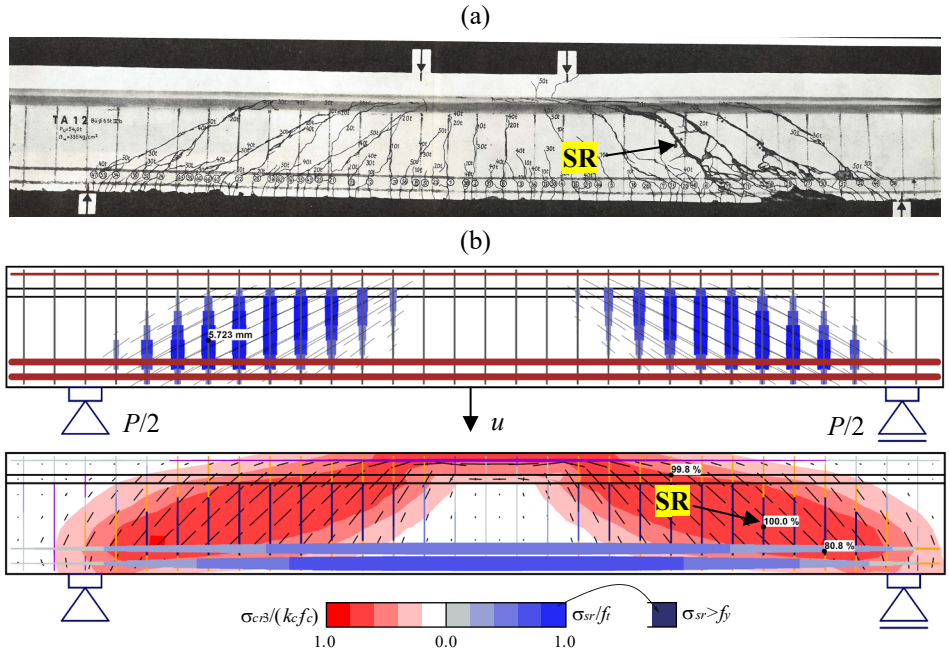

Fig. 6.8. Results for TA12: (a) Observed crack pattern at ultimate extracted from Leonhardt and Walther (1963); (b) calculated crack pattern at yielding and stress fields at ultimate for M1.

Load-deformation response

Fig. 6.9 shows the measured load-deformation response as well as the calculated responses using the default numerical parameters (Model M0 with MFD = 1 and b_{eff} = 350 mm) and the increased flange width according to the *fib* Model Code 2010 (Model M1 with MFD = 3 and b_{eff} = 670 mm). The load-deformation responses predicted by the other analyzed models (M2 to M6) are very similar to those from model M1 and not shown here. The value of the load P corresponds to the total applied force and u corresponds to the deflection at midspan (see e.g., Fig. 6.5b). Leonhardt and Walther (1963) did not report complete load-deformation responses. Hence, the graphs contain two grey horizontal lines: (i) a dashed line indicating the maximum load for which deflections were reported and (ii) a continuous line indicating the ultimate experimental load.

A good agreement was found between the calculated load-deformation response and the experimental results in all tests within the range of the available measurement data. While the calculation using default parameters (M0) is slightly too soft, the use of an increased flange depth (M1) provides an excellent agreement. The comparison of the predictions of the load-deformation response shows that it is possible to realistically capture very different deformation capacities, as obtained in the tests depending on the amount of shear reinforcement.

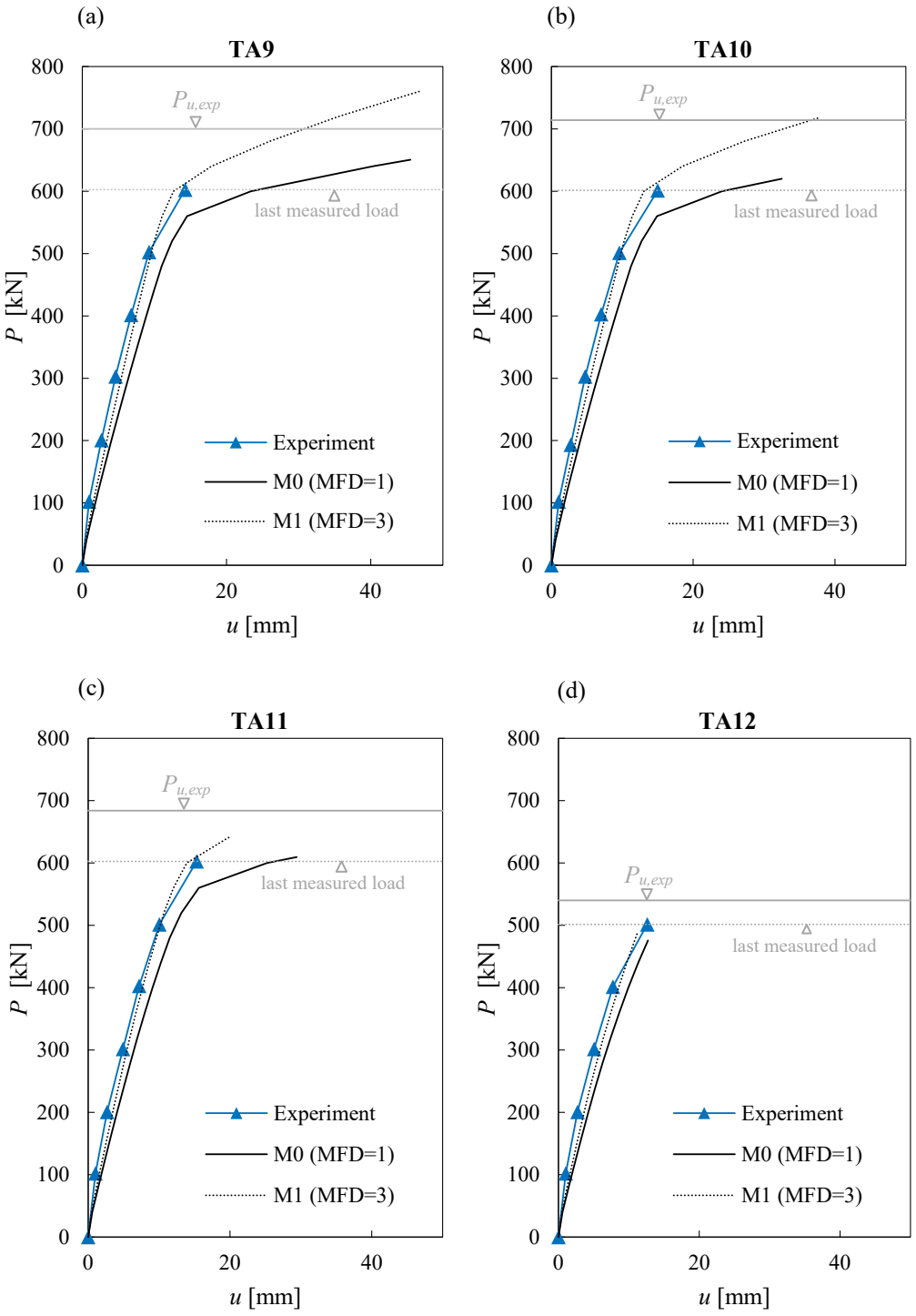

Fig. 6.9. Measured and calculated load-deformation response using the numerical models M0 and M1 for: (a) TA9; (b) TA10; (c) TA11; (d) TA12 (dotted grey lines indicate the loads until which deflections are reported; continuous grey lines indicate the ultimate experimental loads).

Crack widths at service loads

Fig. 6.10a-b compares the crack widths (w) predicted by the CSFM with the maximum values reported by Leonhardt and Walther (1963). Two tests with different failure modes are studied in this comparison: Test TA9 (flexural failure) and TA12 (shear failure). The crack widths were measured for the flexural reinforcement in TA9 and in the middle of the web in TA12 (see Fig. 6.10c). As stated in Section 3.5.4, the models used to calculate crack widths are only valid if the reinforcement remains elastic. Hence, the crack width results in Fig. 6.10 are given only up to the yielding load. It should be noted that the first crack width measurement for specimen TA12 was performed after yielding. Hence, Fig. 6.10b does not show any measuring point, just the linear interpolation up to the first measurement. The predictions were carried out using the numerical models M1, M5 and M6, which only differ in the crack spacing coefficients used for the crack width calculation: $\lambda = 0.67$ (mean), $\lambda = 0.5$ (minimum) and $\lambda = 1.0$ (maximum).

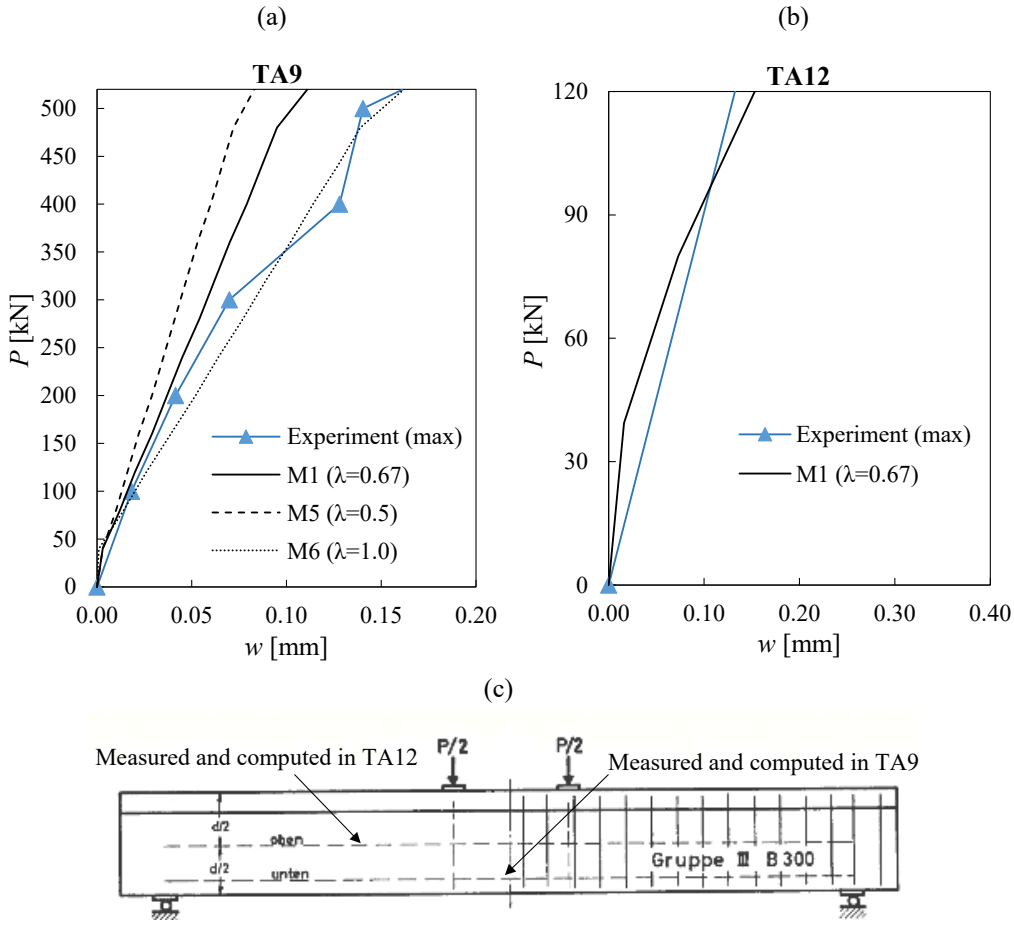

Fig. 6.10. Measured and calculated crack widths (w): (a) TA9; (b) TA12; (c) locations in which the crack widths are measured and computed.

The numerical results for TA9 predict the measured bending crack widths very well (see Fig. 6.10a). The CSFM results for the maximum crack widths (M6 with crack spacing coefficient $\lambda = 1$) agree excellently in this case with the observed maximum crack widths. As expected, a decreasing crack spacing coefficient (λ) leads to smaller crack widths. However, the crack widths calculated in regions with non-stabilized cracking (as in the web of TA12, see Fig. 6.10b) are independent of the crack spacing coefficient, since the calculation does not rely in this case on crack spacing (see Fig. 3.10e). The calculated crack widths in regions with non-stabilized cracking should be interpreted as good estimates of the maximum expected crack widths. Fig. 6.10b shows the predicted crack widths in the web of TA12, which match the measured maximum crack widths fairly well. As already mentioned, only the range in which all reinforcement remains elastic is shown, since only in this range the CSFM provides appropriate crack width results.

6.2.5 Conclusions

A good correspondence is found between the results from the CSFM and the experimental observations. The following conclusions can be stated:

- The use of the default parameters in *IDEA StatiCa Detail* leads to slightly conservative estimates of ultimate loads, load-deformation response and failure modes.
- The analysis of the sensitivity of the model to parameters different from the default ones shows that the most relevant parameter in this case is the considered value of the effective flange width. Designers can change the default width by inputting the geometry via a wall or general shape templates. The larger effective flange width provided by the *fib* Model Code 2010 leads to very accurate estimates of the experimental ultimate loads, deflections and crack widths.
- The consideration of tension stiffening by means of the Pull Out Model in the beam with the lowest amount of stirrups predicts an ultimate load that errs on the safe side by around 10%. When using the Tension Chord Model, the experimental failure mode cannot be properly captured. This mismatch can impact the accuracy of the ultimate load predictions particularly for low amounts of stirrups (as will be discussed in Section 6.4).
- The crack spacing coefficient and the mesh size do not significantly affect ultimate loads and failure modes. The crack spacing coefficient only has a significant influence on the crack width results of those reinforcing bars in which the Tension Chord Model is used for tension stiffening.

6.3 Cantilever wall-type bridge piers

This section is dedicated to the simulation via the CSFM of the load-deformation response of three out of seven cantilever wall-type bridge pier experiments performed by Bimschas (2010) and Hannewald et al. (2013). These experiments were conducted under a vertical constant load,

combined with a cyclic (but quasi-static) horizontal force. The design and detailing of the specimens was similar to that of existing bridge piers with seismic deficiencies. Specimens VK1, VK3 and VK6 were selected for analysis with the CSFM. These specimens had different amounts of flexural reinforcement and shear slenderness (achieved by varying the height of the walls). It should be noted that the CSFM just aims at describing the envelope of the cyclic response (so-called "backbone") using a monotonic model.

6.3.1 Experimental setup

All piers were 1500 mm deep and 350 mm wide. The total height (H) of specimens VK1 and VK3 was 3700 mm, and that of VK6 was 4850 mm, see Fig. 6.11. The specimens stood on a stiff foundation block, which will not be modeled in the CSFM.

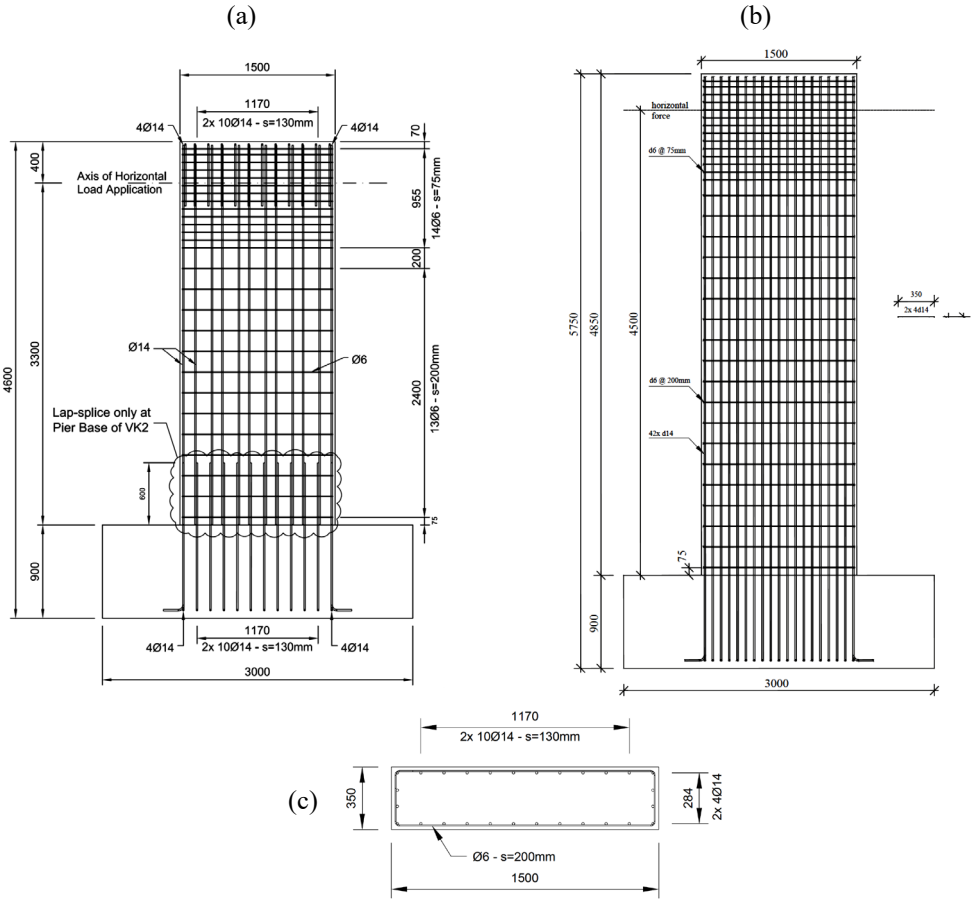

Fig. 6.11. Geometry and reinforcement of the specimens: (a) Longitudinal view of VK1 (VK3 was analogous to VK1 but had twice the flexural reinforcement); (b) longitudinal view of VK6; (c) cross-section of VK1, VK3 and VK6; (extracted from Bimschas (2010) and Hannewald et al. (2013); dimensions in [mm]).

In all tests, a constant vertical load of 1370 kN was applied to the top of the piers. After the vertical force was applied, the specimens were subjected to a horizontal cyclic load (V) applied quasi-statically at an effective height above the foundation block of H_{eff} = 3300 mm in the case of VK1 and VK3 and H_{eff} = 4500 mm for VK6. The application of the horizontal load was displacement-controlled. The flexural reinforcement (vertical direction) consisted of continuous reinforcing bars with a diameter of $Ø_l$ = 14 mm distributed along the cross-section with a spacing s_l of 130 mm for VK1 and 90 mm for VK3 and VK6. The resulting geometric reinforcement ratios $\rho_{l,geo}$ are summarized in Table 6.6. The flexural reinforcement was anchored at the foundation (anchorage length of 200 mm plus end hooks). All specimens had the same shear reinforcement (horizontal direction) consisting of hoops of diameter $Ø_t$ = 6 mm at a spacing of s_t = 200 mm. This resulted in a very low shear reinforcement ratio of $\rho_{t,geo}$ = 0.08 % (which is below the critical reinforcement ratio according to Eq. (3.5)). The stirrup spacing was reduced to 75 mm at the region where load was applied (top of the pier). Relevant parameters are stated in Table 6.6.

Table 6.6. Relevant parameters of the analyzed specimens.

Specimen	$Ø_l$ [mm]	s_l [mm]	$\rho_{l,geo}$ [%]	H [mm]	H_{eff} [mm]
VK1	14	130	0.82	3700	3300
VK3	14	90	1.23	3700	3300
VK6	14	90	1.23	4850	4500

6.3.2 Material properties

Table 6.7 summarizes the material properties used in the CSFM analysis, which are based on the material tests carried out by Bimschas (2010) and Hannewald et al. (2013). The properties not provided in these reports (the ultimate strain of the flexural reinforcement ε_u and the concrete strength f_c for VK6, as well as the concrete strain at peak load ε_{c0} for all tests) were assumed to be as indicated in Table 6.7 (expected mean values for materials used).

Table 6.7. Material properties used in the CSFM analyses.

Specimen	Shear reinforcement			Flexural reinforcement			Concrete	
	f_y [MPa]	f_t [MPa]	ε_u [‰]	f_y [MPa]	f_t [MPa]	ε_u [‰]	f_c [MPa]	ε_{c0} [‰]
VK1	518	681	84	515	630	126[1)]	35[1)]	2
VK3	518	681	84	515	630	126[1)]	34[1)]	2
VK6	528	680	84	521	609	126[2)]	34[2)]	2

1) Directly extracted from Bimschas (2010); Hannewald et al. (2013)
2) Assumed value

6.3.3 Modeling with the CSFM

The geometry, reinforcement, supports and loading conditions were modeled in the CSFM according to the experimental setup (see Fig. 6.12).

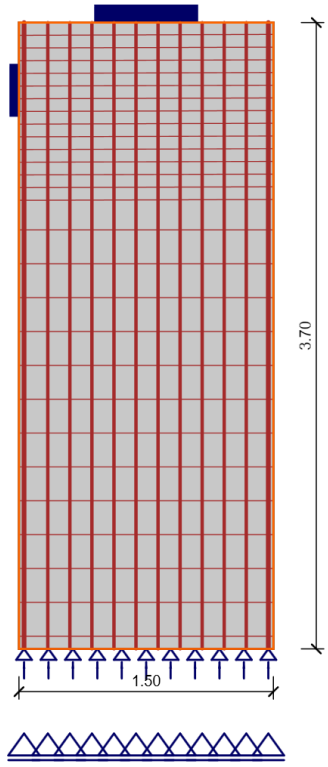

Fig. 6.12. Example of modeling with the CSFM: VK1 (dimensions in [m]).

The foundation was not included in the model. To simulate the fixed-end support properly, the flexural bars were anchored outside of the concrete region and the anchorage length was not verified in the calculation. Several numerical calculations were carried out using different values for the following parameters:

- The mesh size, which was 5, 15 (the default value in *IDEA StatiCa Detail* for this particular example) and 25 finite elements along the wall's width.
- The consideration or not of the tension stiffening effect. By default tension stiffening (TS) is considered in the CSFM.
- The stress-strain relationship for the reinforcement. By default, a bilinear stress-strain relationship is used in the CSFM. A refined analysis was also performed considering the actual stress-strain relationship of the reinforcement (cold-worked for the flexural and hot-rolled for the shear reinforcement) and accounting for the initial

uncracked stiffness. This refined behavior was simulated via a user-defined reinforcement stress-strain relationship.

The parameters used in each numerical calculation (model M0 to M4) are summarized in Table 6.8. Model M0 corresponds to the default settings in the CSFM.

Table 6.8. Investigated numerical parameters (variations to M0 shaded).

Model	Mesh size[1)]	Tension stiffening	Steel law
M0 (def.)	15	Yes	Bilinear
M1	25	Yes	Bilinear
M2	5	Yes	Bilinear
M3	15	Yes	Refined[2)]
M4	15	No	Bilinear

1) Elements over the pier's width
2) The actual reinforcement stress-strain relationship and uncracked stiffness are accounted for.

An example of the influence of the used parameters on the response of the reinforcement (including the tension stiffening effect) is illustrated in Fig. 6.13 for the flexural reinforcement. The consideration of the uncracked stiffness is reflected in the elastic part of these diagrams.

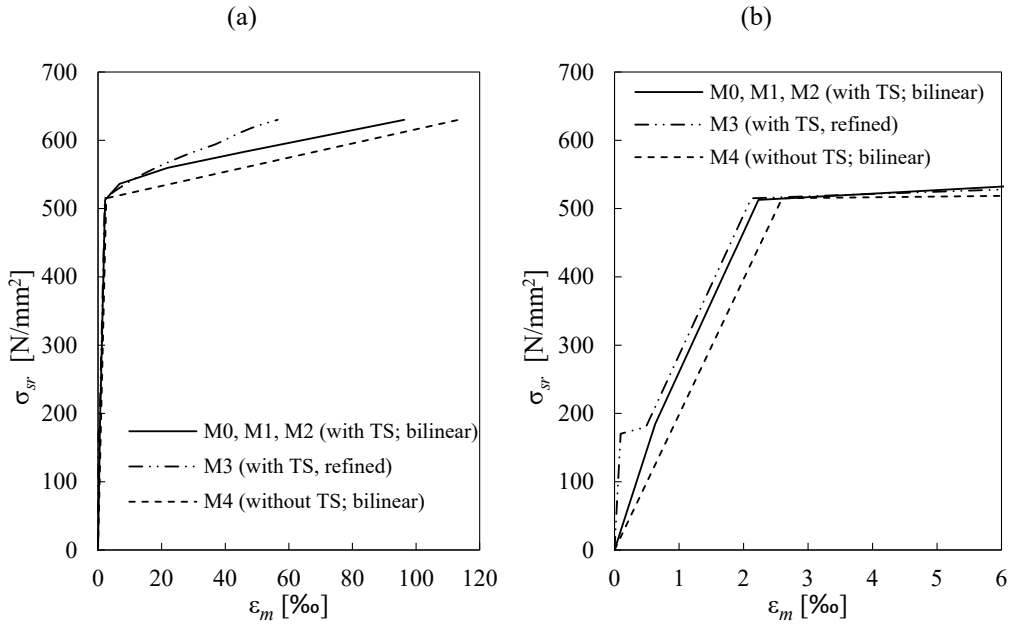

Fig. 6.13. Stress-strain relationships of the flexural reinforcement in terms of average strains (i.e., considering the stiffening effect of concrete between cracks) for different parameters.

6.3.4 Comparison with experimental results

The ultimate shear force (i.e., the horizontal applied load), the failure modes and the load-deformation response determined by the CSFM are compared with the corresponding experimental results below.

Failure modes and ultimate loads

The ultimate shear forces predicted by the CSFM ($V_{u,calc}$) and measured in the experiments ($V_{u,exp}$), and the respective failure modes, are summarized in Table 6.9. This table also provides the mean and the coefficient of variation (CoV) of the ratios between measured and calculated ultimate loads for each numerical model. Ratios above one denote conservative predictions of the ultimate load. As seen from Table 6.9, the failure mechanisms of all tests were predicted well by the CSFM, independently of the used parameters. The default model M0 leads to slightly unsafe strength predictions (on average 5%): A minor issue, which can be solved by using a finer mesh.

Table 6.9. Experimental and predicted ultimate shear forces (in kN) and failure mechanisms[1)].

Specimen	Test[2)]	M0	M1	M2	M3	M4
VK1	725 **F**(CC+FY)	744 **F**(CC+FY)	685 **F**(CC+FY)	778 **F**(CC+FY)	751 **F**(CC+FY)	720 **F**(CC+FY)
VK3	876 **F**(CC+FY)	963 **F**(CC+FY)	882 **F**(CC+FY)	1003 **F**(CC+FY)	913 **F**(CC+FY)	945 **F**(CC+FY)
VK6	658 **F**(CC+FY)	684 **F**(CC+FY)	642 **F**(CC+FY)	695 **F**(CC+FY)	681 **F**(CC+FY)	667 **F**(CC+FY)
$\frac{V_{u,exp}}{V_{u,calc}}$	mean	0.95	1.03	0.91	0.96	0.97
	CoV	0.03	0.03	0.04	<0.01	0.04

1) Abbreviations for failure modes according to Table 6.1
2) Calculated as average values of the push and pull direction of the first cycle of each load level (Bimschas 2010)

The sensitivity of the strength predictions of the CSFM to the different analyzed numerical parameters is shown in Fig. 6.14 by means of the ratio of experimental to calculated ultimate shear forces ($V_{u,exp}/V_{u,calc}$). The strength predictions show a moderate mesh size sensitivity in these tests (see Fig. 6.14a). A decrease in mesh size leads to a decrease in the computed ultimate loads. However, the predicted failure modes remain insensitive to the considered mesh size (see Table 6.9). The difference in the ultimate loads when using 5 (Model M2) or 25 (Model M1) elements over the width of the wall is up to 12%. Moreover, the ultimate load is nearly independent of the consideration or not of tension stiffening (see Fig. 6.14b), or the use of a refined stress-strain relationship for the reinforcement (see Fig. 6.14c). In the analyzed experiments, these effects only have a relevant influence on the stiffness of the members, as will be shown below.

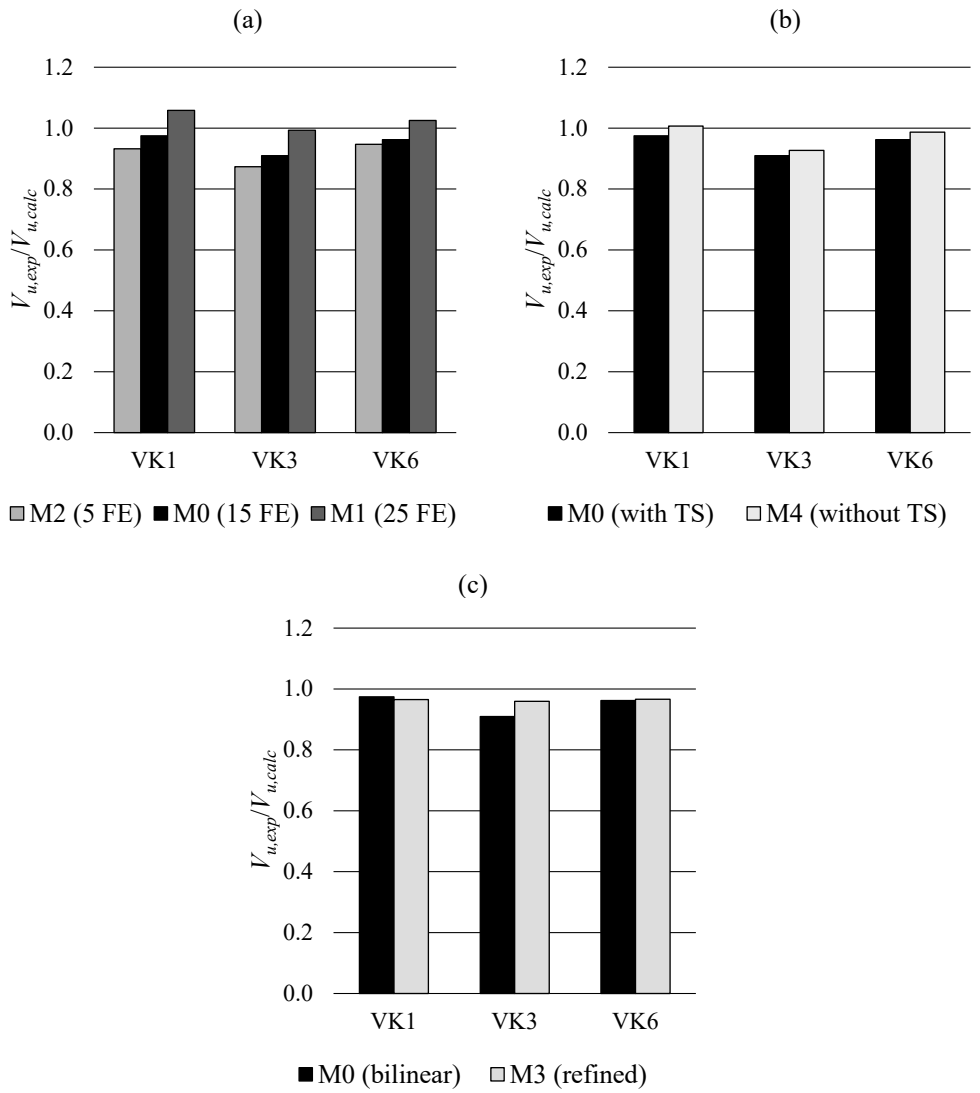

Fig. 6.14. Influence of numerical parameters on the ratio of measured to calculated ultimate loads: (a) Mesh size sensitivity; (b) consideration or not of tension stiffening (TS); (c) default (bilinear) and refined reinforcement stress strain relationships.

Fig. 6.15a-b shows the continuous stress field results in Specimen VK1 provided by the CSFM for two load steps ($0.5V_{u,calc}$ and $V_{u,calc}$). These results were calculated using default numerical parameters (M0). It can be seen that due to plastic redistributions, the compression field was significantly steeper (more inclined with respect to the vertical wall axis) at ultimate. The predicted failure mode (concrete crushing with yielding of the flexural reinforcement) is highlighted in Fig. 6.15b. The location agrees with the experimental observations (highlighted in Fig. 6.15c, where it can be seen that the cyclic loading produced concrete crushing in both sides).

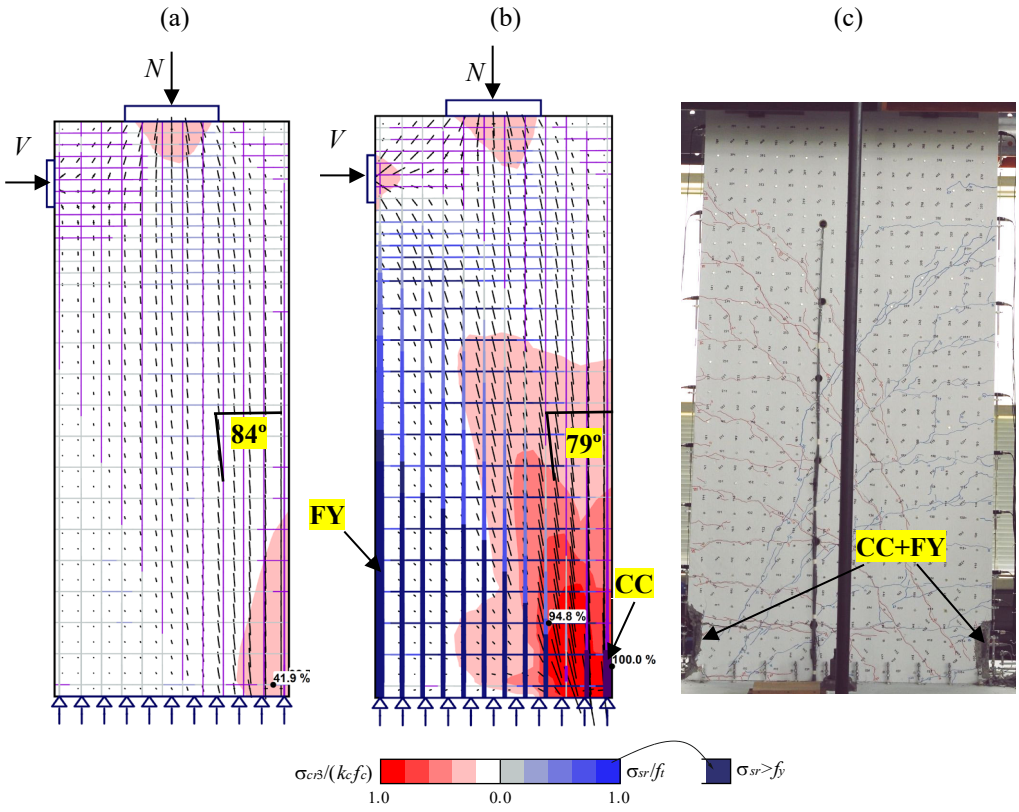

Fig. 6.15. Results for VK1: (a)-(b) Calculated stress fields for M0 (default parameters) at $0.5V_{u,calc}$ and $V_{u,calc}$ respectively; (c) experimental crack pattern at ultimate load extracted from Bimschas (2010).

Load-deformation response

Fig. 6.16 shows a comparison of the calculated load-deformation response provided by the CSFM with the envelope (backbone) of the cyclic response of the experiments. The experimental response was calculated as average values of the push and pull direction of the first cycle of each load level (Bimschas 2010). The numerical predictions were calculated using the following numerical parameters: Default parameters (M0), refined stress-strain relationship of the reinforcement (M3), and neglecting tension stiffening (M4). The reference experimental displacement u was obtained by subtracting the part due to anchorage slip from the total measured displacement at the height at which load was applied. This allows a direct comparison with the numerical results since the foundation is not modeled in the CSFM analysis. The contribution of anchorage slip was evaluated following the assumptions given in Bimschas (2010).

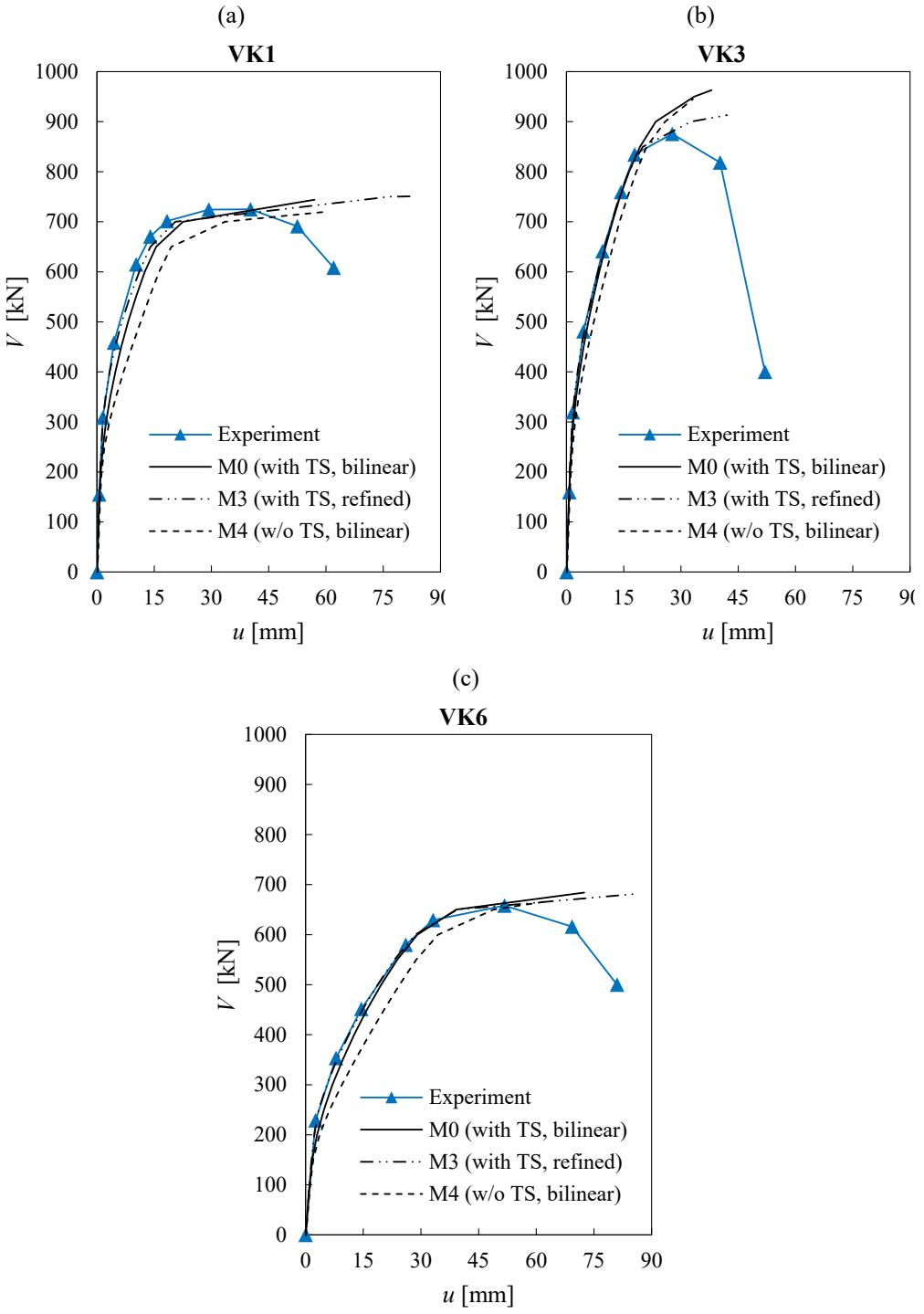

Fig. 6.16. Measured and calculated load-deformation response using different numerical parameters for: (a) VK1; (b)VK3; (c) VK6.

The results in Fig. 6.16 show that it is essential to account for tension stiffening if one needs to have a good estimate of a member's stiffness. Both numerical calculations considering tension stiffening (M0 and M3) fit the experimental results very well. However, the behavior was too soft when this effect was neglected (M4), particularly for VK1 and VK6. The consideration of the actual stress-strain relationship of the reinforcement (hot-rolled and cold-worked) and the uncracked stiffness of the reinforcement (model M3) improved the already accurate load-deformation prediction obtained with the default parameters, leading to excellent agreement with the experimental data up to the peak load. The load-deformation response shows very small sensitivity to the analyzed range of finite element mesh sizes (the results for M1 and M2 are very similar to the results with a default mesh size and are not plotted in Fig. 6.16). Hence, it can be concluded that the mesh size only affects the load bearing capacity but not the deformations in this particular case.

It should be noted that the CSFM does not account for the concrete softening after reaching peak load (instead, a code compliant plastic plateau is implemented). Clearly, the intention of the CSFM is not to capture the softening branch of the experiments. Still, it provides a good estimate of the deflection in the post-peak phase, during which a significant amount of load-bearing capacity is lost (i.e., to give a good estimate of the deformation capacity of the structural members). The results with default parameters (model M0) in Fig. 6.16 show that the numerical analyses detected the failure for a displacement at which the specimens had lost around 15% of their maximum strength. This is a good estimate of the deformation capacity and highlights the capabilities of the CSFM besides the implementation of simple and code-compliant constitutive relationships.

6.3.5 Conclusions

As in the tests analyzed in Section 6.2, a good agreement can be found between the predictions given by the CSFM and the experiments, showing that the model exhibits only a small sensitivity to changes in the parameters. The following conclusions can be stated:

- Using the default parameters implemented in *IDEA StatiCa Detail* results in the CSFM slightly overestimating the ultimate load (by 5% on average), which might be attributed to the cyclic loading in the experiments causing progressive damage. Hence, the CSFM provides appropriate predictions of ultimate loads but also failure modes.
- The CSFM predictions exhibit moderate changes when the size of the finite element mesh varies significantly. In this case, refining the default mesh leads to better estimation of the ultimate loads. Therefore, it is highly recommended that the sensitivity of the model to changes in the mesh size should always be investigated.
- The tension stiffening effect has no influence on ultimate load, but is essential for the proper estimation of deflections and deformation capacity.
- Using a refined stress-strain relationship for the reinforcement and considering the uncracked stiffness of the walls leads to excellent deflection predictions. For design purposes, it is recommended that the default simplified bilinear relationship be used, as it also provides good estimates of deflections, slightly on the safe side.

6.4 Shear tests in beams with low amounts of stirrups

This section discusses the use of the CSFM to analyze shear failures in beams with low amounts of stirrups. To this end, a selection of tests performed on simply supported reinforced concrete beams by Huber (2016), Piyamahant (2002) and Vecchio and Shim (2004) are analyzed. These tests comprised a wide number of parameters, including different sizes, shear slenderness and amounts of shear and longitudinal reinforcement. This section describes the analysis of 17 experiments from these campaigns using the CSFM, exploring the ability of the CSFM to properly model very different failure modes ranging from shear failures with and without rupture of the stirrups to bending failures and mixed shear-bending failures.

Experimental setupFig. 6.17 shows the geometry, test setups and reinforcement layouts of the analyzed experiments. Information on the shear reinforcement (diameter ($Ø_t$), spacing (s_t) and geometric reinforcement ratio ($\rho_{t,geo}$)), the flexural reinforcement (number (n_l) and diameter ($Ø_l$)) and geometry (effective depth (d), shear slenderness (a/d) and width of the beams (b)) is presented in Table 6.10. Tests R1000m60 and R500m351 conducted by Huber (2016) had one-leg hooks, while in all other tests used two-leg closed stirrups. In the analyzed tests from Piyamahant (2002) the geometry and the flexural reinforcement were kept constant, while in the other two studies they were varied.

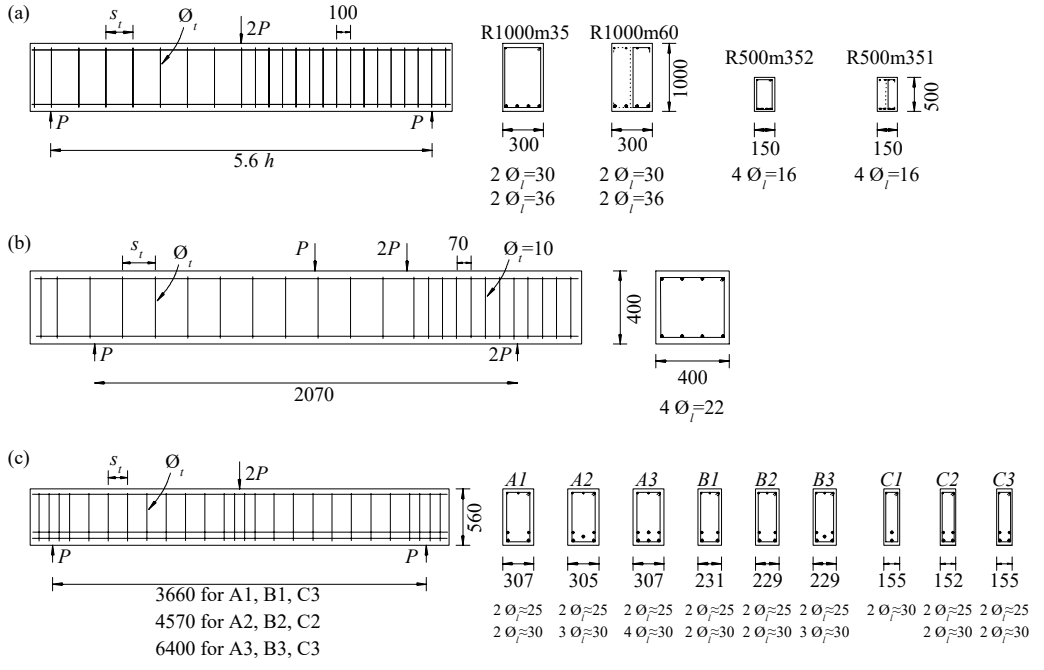

Fig. 6.17. Test setup, geometry and reinforcement of specimens: (a) Huber (2016); (b) Vecchio and Shim (2004); (c) Piyamahant (2002); (dimensions in [mm]).

Table 6.10. Relevant parameters of the analyzed specimens.

Specimen	$Ø_t$ [mm]	s_t [mm]	$\rho_{t,geo}$ [%]	n_l-$Ø_l$ [mm]	l [mm]	d [mm]	a/d [-]	b [mm]
Huber (2016)								
R500m351	6	200	0.09	4-16	2800	460	3.0	150
R500m352	4	200	0.08	4-16	2800	460	3.0	150
R1000m60	12	400	0.09	2-30 2-36	5600	920	3.0	300
R1000m35	6	200	0.09	2-30 2-36	5600	920	3.0	300
Piyamahant (2002)								
T1	4	80	0.08	4-22	2070	359	3.0	400
T2	4	100	0.06	4-22	2070	359	3.0	400
T3	4	130	0.05	4-22	2070	359	3.0	400
T4	4	180	0.03	4-22	2070	359	3.0	400
Vecchio and Shim (2004)								
A1	6.4	210	0.10	2-25 2-30	3660	457	4.0	305
A2	6.4	210	0.10	2-25 3-30	4570	457	5.0	305
A3	3.7	168	0.04	2-25 4-30	6400	457	1.4	305
B1	6.4	190	0.15	2-25 2-30	3660	457	4.0	229
B2	6.4	190	0.15	2-25 2-30	4570	457	5.0	229
B3	3.7	152	0.06	2-25 3-30	6400	457	1.4	229
C1	6.4	210	0.20	2-30	3660	457	4.0	152
C2	6.4	210	0.20	2-25 2-30	4570	457	5.0	152
C3	3.7	168	0.08	2-25 2-30	6400	457	1.4	152

6.4.1 Material properties

The material properties of the shear reinforcement, the flexural reinforcement and the concrete used in the CSFM analysis are summarized in Table 6.11. Most of the material properties required for the CSFM analysis were available in the corresponding test reports. The values that had to be assumed are indicated in Table 6.11.

Table 6.11. Material properties used in the CSFM analyses.

Specimen	Shear reinforcement				Flexural reinforcement				Concrete	
	$Ø_t$[1)]	f_y[1)]	f_t[1)]	ε_u[1)]	$Ø_l$[1)]	f_y	f_t	ε_u	f_c[1)]	ε_{c0}
	[mm]	[MPa]	[MPa]	[‰]	[mm]	[MPa]	[MPa]	[‰]	[MPa]	[‰]
Huber (2016)										
R500m351	6	569	638	31	16	550[2)]	594[1)]	50[2)]	38	2.0[2)]
R500m352	4	653	712	49	16	550[2)]	594[1)]	50[2)]	36	2.0[2)]
R1000m60	6	569	657	31	30 36	550[2)]	594[1)]	50[2)]	61	2.0[2)]
R1000m35	12	552	638	31	30 36	550[2)]	594[1)]	50[2)]	29	2.0[2)]
Piyamahant (2002)										
T1	4 10	350 391	457 586	50	22	718[1)]	985[1)]	50[2)]	42	2.0[2)]
T2	4 10	350 391	457 586	50	22	718[1)]	985[1)]	50[2)]	42	2.0[2)]
T3	4 10	350 391	457 586	50	22	718[1)]	985[1)]	50[2)]	42	2.0[2)]
T4	4 10	350 391	457 586	50	22	718[1)]	985[1)]	50[2)]	42	2.0[2)]
Vecchio and Shim (2004)										
A1	6.4	600	649	35	25 30	445[1)] 436[1)]	680[1)] 700[1)]	50[2)]	22.6	1.6
A2	6.4	600	649	35	25 30	440[1)] 436[1)]	615[1)] 700[1)]	50[2)]	25.9	2.1
A3	5.7	600	651	37	25 30	445[1)] 436[1)]	680[1)] 700[1)]	50[2)]	43.5	1.9
B1	6.4	600	649	35	25 30	445[1)] 436[1)]	680[1)] 700[1)]	50[2)]	22.6	1.6
B2	6.4	600	649	35	25 30	440[1)] 436[1)]	615[1)] 700[1)]	50[2)]	25.9	2.1
B3	5.7	600	651	37	25 30	445[1)] 436[1)]	680[1)] 700[1)]	50[2)]	43.5	1.9
C1	6.4	600	649	35	25	445[1)]	680[1)]	50[2)]	22.6	1.6
C2	6.4	600	649	35	25 30	440[1)] 436[1)]	615[1)] 700[1)]	50[2)]	25.9	2.1
C3	5.7	600	651	37	25 30	445[1)] 436[1)]	680[1)] 700[1)]	50[2)]	43.5	1.9

1) Directly extracted from test reports for all tests
2) Assumed value

6.4.2 Modeling with the CSFM

The geometry, reinforcement, support and loading conditions were modeled in the CSFM according to the experimental setups. Fig. 6.18 shows the modeling of Test A3 from Vecchio and Shim (2004) as an example.

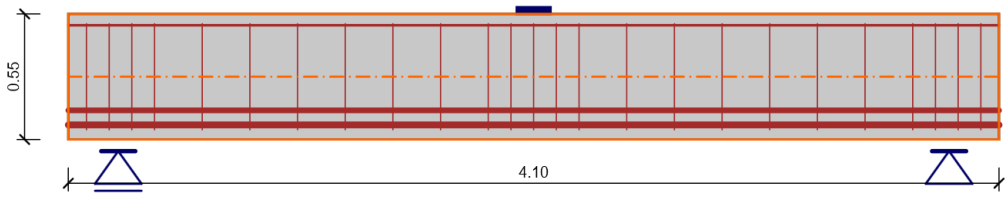

Fig. 6.18. Example of modeling with the CSFM: Test A3 from Vecchio and Shim (2004) (dimensions in [m]).

For each test, four numerical calculations were carried out using the following parameters:

- The mesh size, which varied from 5 (default value for these particular examples), through 10 up to 20 finite elements over the beam depth. Since the default mesh is already very coarse, only finer meshes are analyzed in this study, and the mesh with 10 elements was used except in M0.
- The consideration or not of the tension stiffening effect. By default tension stiffening is considered in the CSFM.
- The consideration or not of potentially non-stabilized cracking in stirrups. When considered (by default), the Pull-Out Model (POM) defines tension stiffening in stirrups (the geometric reinforcement ratios of all beams is below (ρ_{cr}) (Eq. (3.5), so the Tension Chord Model is never used). When deactivated, the models account for tension stiffening by means of the TCM.

Table 6.12 shows the parameters used in each numerical calculation. M0 corresponds to the model with the default settings in the CSFM.

Table 6.12. Investigated numerical parameters (variations to M1 shaded).

Model	Mesh size[1)]	Tension stiffening for flexural reinforcement	Tension stiffening for shear reinforcement
M0 (def.)	5	TCM[2)]	POM[3)]
M1	10	TCM[2)]	POM[3)]
M2	20	TCM[2)]	POM[3)]
M3	10	deactivated	deactivated
M4	10	TCM[2)]	TCM[2)]

1) Elements over the beam's depth
2) Tension Chord Model
3) Pull-Out Model

6.4.3 Comparison with experimental results

This section contains comparisons between the ultimate loads and failure modes provided by the CSFM and the experimental results. In order to also verify the CSFM for serviceability behavior and deformation capacity, the load-deformation responses furnished by the model are compared with those from the tests for selected beams.

Failure modes and ultimate loads

Table 6.13 summarizes the ultimate shear forces measured in the tests ($V_{u,exp}$), the ultimate shear forces predicted by the CSFM ($V_{u,calc}$), and the respective failure modes. This table also provides the mean and coefficient of variation (CoV) of the ratios between the measured and the calculated ultimate loads for each numerical model. In all analyses (except M3, in which tension stiffening was neglected) a shear failure in the stirrups was predicted by the CSFM. This corresponds well with the failure mechanisms observed in the tests from Huber (2016) and Piyamahant (2002), but mismatches those observed in Vecchio and Shim (2004). The failure to capture the failure modes well led in this case to slightly conservative estimates of the ultimate load. Overall, the default parameters provide good strength estimates but slightly on the unsafe side (by 6% on average).

The sensitivity of the strength predictions of the CSFM to the different analyzed numerical parameters is shown in Fig. 6.19 by means of the ratio of experimental to calculated ultimate shear forces ($V_{u,exp}/V_{u,calc}$). The ultimate load is markedly sensitive to the selected size of the finite elements (see Fig. 6.19 a). The maximum difference between the coarsest and finest mesh (M0 and M2) amounts to 36% (Test 4 from Piyamahant (2002)), with an average difference around 15%. The predictions using default parameters (5 finite elements over the beam's height in model M0) slightly overestimate the experimental strength (around 5%). When refining the mesh to 10 or 20 finite elements over the beam's height (models M1 and M2, respectively), excellent strength predictions which are slightly on the safe side of the ultimate loads can be achieved. No changes in the failure modes were observed when varying the finite element mesh size. Even the results with the default mesh size are very satisfactory, considering that several experiments exhibited brittle shear failures, which are challenging to predict using design approaches.

The way tension stiffening is considered has a highly relevant impact on the strength predictions, as can be seen in Fig. 6.19 b-c. The consideration of tension stiffening in the stirrups by means of the POM (the default setting in the CSFM) leads on average to excellent agreement with the experimental results (see Fig. 6.19 b). However, neglecting tension stiffening leads to an average overestimation of the ultimate load of around 22% (see Table 6.12). When neglecting tension stiffening, the failure mode changes to flexural failure (see Table 6.12) and the observed shear failure modes are mismatched. The results are also very sensitive to the considered compression softening relationship. As can be seen in Fig. 6.19 c, the use of the Tension Chord Model in the stirrups (model M4) instead of the Pull-out Model (model M1) provides slightly better results than when neglecting tension stiffening (model M3), but still strongly overestimates the ultimate loads by about 15% (see Table 6.12). Therefore, it can be concluded that the use of the Pull-Out-Model is crucial in these examples for the proper modeling of load-bearing behavior.

Table 6.13. Experimental and predicted ultimate shear forces (in kN) and failure mechanisms[1].

	Specimen	Test	M0	M1	M2	M3	M4
Huber (2016)	R500m351	106 **S**(SR)	109 **S**(SR)	98 **S**(SR)	97 **S**(SR)	146 **F**(CC+FY)	118 **S**(SR)
	R500m352	109 **S**(SR)	116 **S**(SR)	103 **S**(SR)	101 **S**(SR)	137 **F**(CC+FY)	122 **S**(SR)
	R1000m35	348 **S**(SR)	424 **S**(SR)	384 **S**(SR)	381 **S**(SR)	600 **F**(CC+FY)	457 **S**(SR)
	R1000m60	402 **S**(SR)	548 **S**(SR)	484 **S**(SR)	476 **S**(SR)	639 **F**(CC+FY)	618 **S**(SR)
Piyamahant (2002)	T1	227 **S**(CC+SR)	267 **S**(SR)	223 **S**(SR)	209 **S**(SR)	334 **F**(CC+FY)	300 **S**(SR)
	T2	188 **S**(CC+SR)	250 **S**(SR)	209 **S**(SR)	191 **S**(SR)	319 **F**(CC+FY)	281 **S**(SR)
	T3	191 **S**(SR)	235 **S**(SR)	189 **S**(SR)	176 **S**(SR)	305 **F**(CC)	264 **S**(SR)
	T4	188 **S**(SR)	219 **S**(SR)	173 **S**(SR)	161 **S**(SR)	294 **F**(CC)	249 **S**(SR)
Vecchio and Shim (2004)	A1	230 **S**[2]+**F** (CC)	209 **S**(SR)	199 **S**(SR)	185 **S**(SR)	260 **F**(CC+FY)	234 **S**(SR)
	A2	220 **S**[2]+**F** (CC)	195 **S**(SR)	189 **S**(SR)	179 **S**(SR)	253 **F**(CC+FY)	218 **S**(SR)
	A3	210 **F**(CC)	190 **S**(SR)	186 **S**(SR)	173 **S**(SR)	237 **F**(CC+FY)	214 **S**(SR)
	B1	217 **S**[2]+**F** (CC)	205 **S**(SR)	197 **S**(SR)	185 **S**(SR)	242 **F**(CC+FY)	227 **S**(SR)
	B2	183 **S**[2]+**F** (CC)	185 **S**(SR)	179 **S**(SR)	168 **S**(SR)	203 **F**(CC+FY)	201 **S**(SR)
	B3	171 **F**(CC)	176 **S**(SR)	172 **S**(SR)	164 **S**(SR)	192 **F**(CC+FY)	191 **S**(SR)
	C1	141 **S**[2]+**F** (CC)	139 **S**(SR)	133 **S**(SR)	124 **S**(SR)	143 **F**(CC+FY)	153 **S**(SR)
	C2	145 **S**[2]+**F** (CC)	158 **S**(SR)	155 **S**(SR)	146 **S**(SR)	179 **F**(CC+FY)	173 **S**(SR)
	C3	133 **F**(CC)	143 **S**(SR)	139 **S**(SR)	131 **S**(SR)	144 **F**(CC+FY)	146 **S**(SR)
	$\frac{V_{u,exp}}{V_{u,calc}}$	mean	0.94	1.03	1.08	0.78	0.85
		CoV	0.13	0.09	0.10	0.17	0.13

1) Failure modes according to Table 6.1
2) Mixed failure due to diagonal tension (without stirrup rupture) and concrete crushing in the compression zone

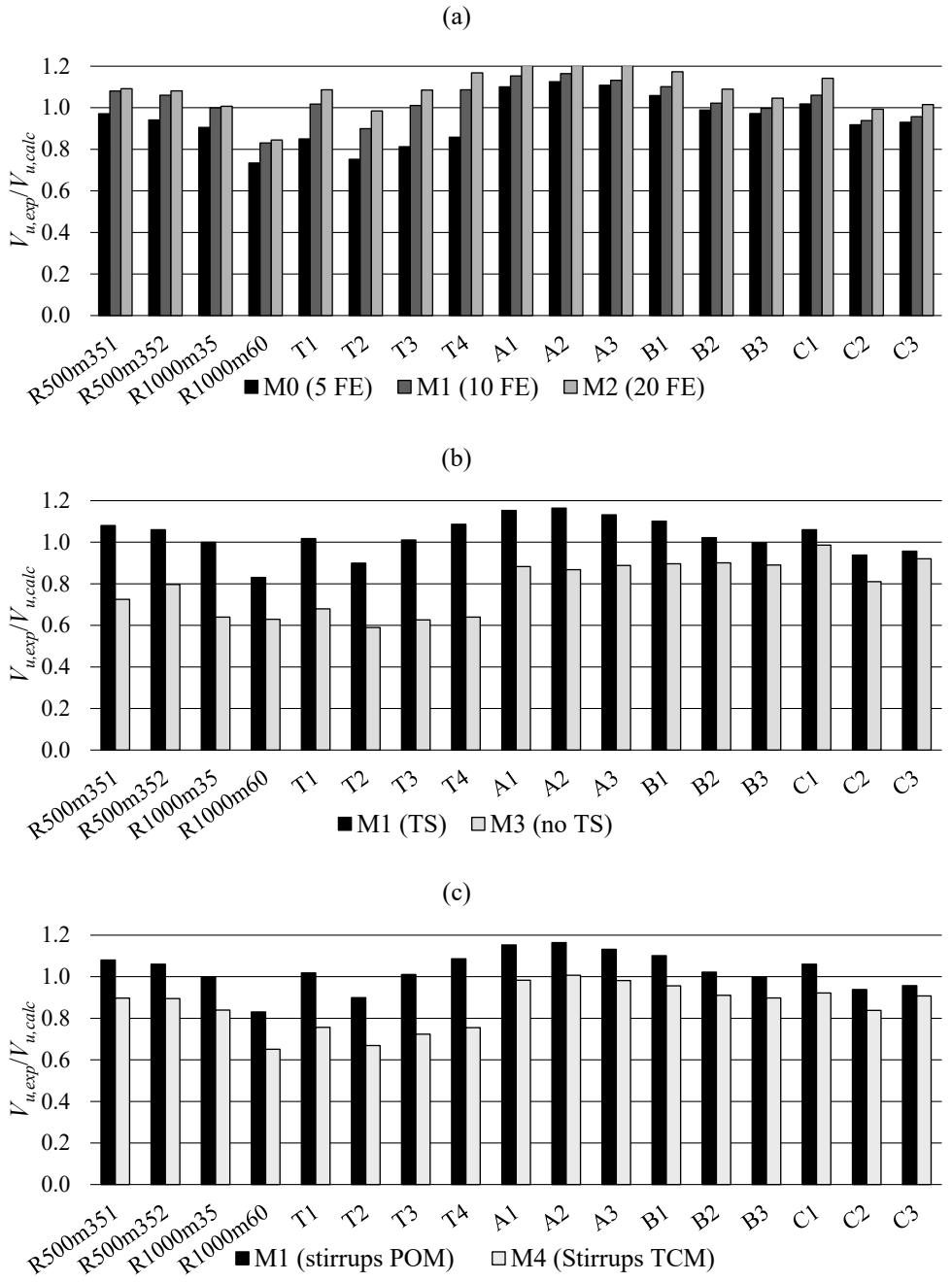

Fig. 6.19. Influence of numerical parameters on the ratio of measured to calculated ultimate loads: (a) Mesh size sensitivity; (b) consideration or not of tension stiffening (TS); (c) consideration of tension stiffening in the stirrups with the Pull Out Model (POM) or with the Tension Chord Model (TCM).

Fig. 6.20 shows the continuous stress field results (principal compressive stresses (σ_c) and steel stresses (σ_{sr}) at the cracks) for specimens A1 and A3 from Vecchio and Shim (2004), in which the predicted shear failures are highlighted. These results were calculated using the numerical parameters M1 (default parameters, except for the mesh size, which is half of the default value). As can be seen from the stress fields, the compressive stress in the compression zone due to bending is in the plastic branch (99.5 %). However, due to the considered criteria for concrete crushing, the rupture of the stirrups occurs before concrete crushing happens.

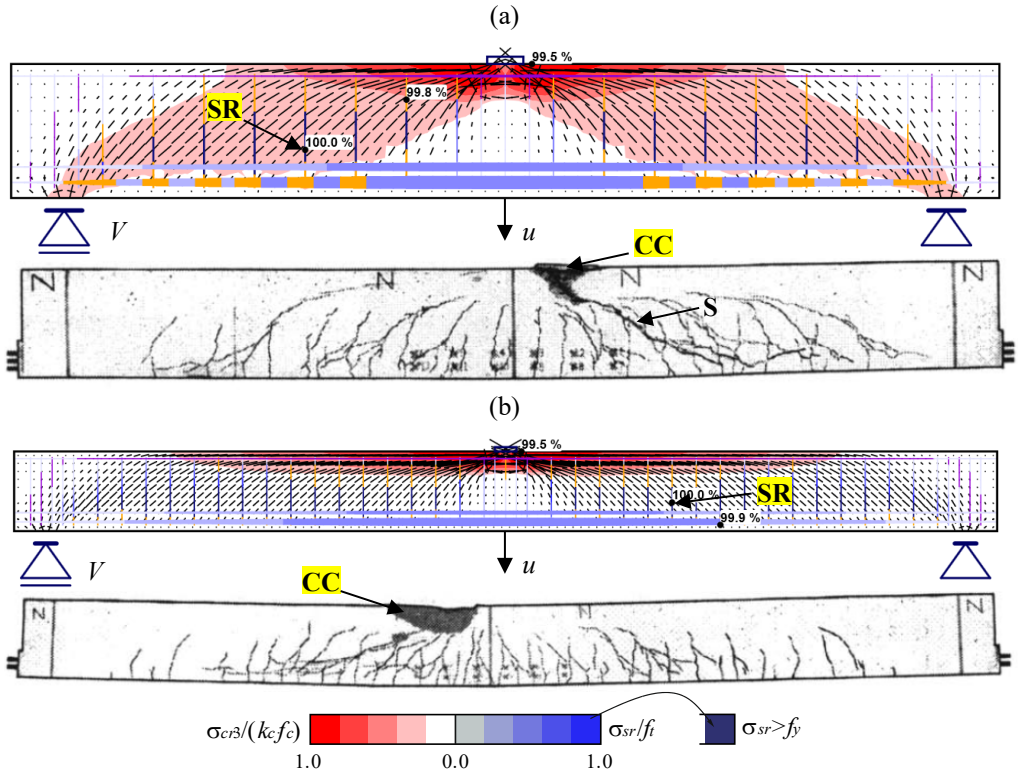

Fig. 6.20. Results for stress fields at ultimate for selected tests using M1 numerical parameters: (a) A1 (Vecchio and Shim 2004), including experimental crack patterns extracted from the test report; (b) A3 (Vecchio and Shim 2004), including experimental crack patterns extracted from the test report; (the figures are not to scale).

Load-deformation response

The calculated load-deformation responses obtained using the numerical parameters from M1 (considering the TCM for the flexural reinforcement and the POM for the stirrups) and M3 (neglecting any tension stiffening effects) are compared with the measured load-deformation responses in Fig. 6.21 for the Tests R500m352, T1, A1 and A3. The load V corresponds to the applied shear force and u corresponds to the deflection at midspan (see Fig. 6.20a).

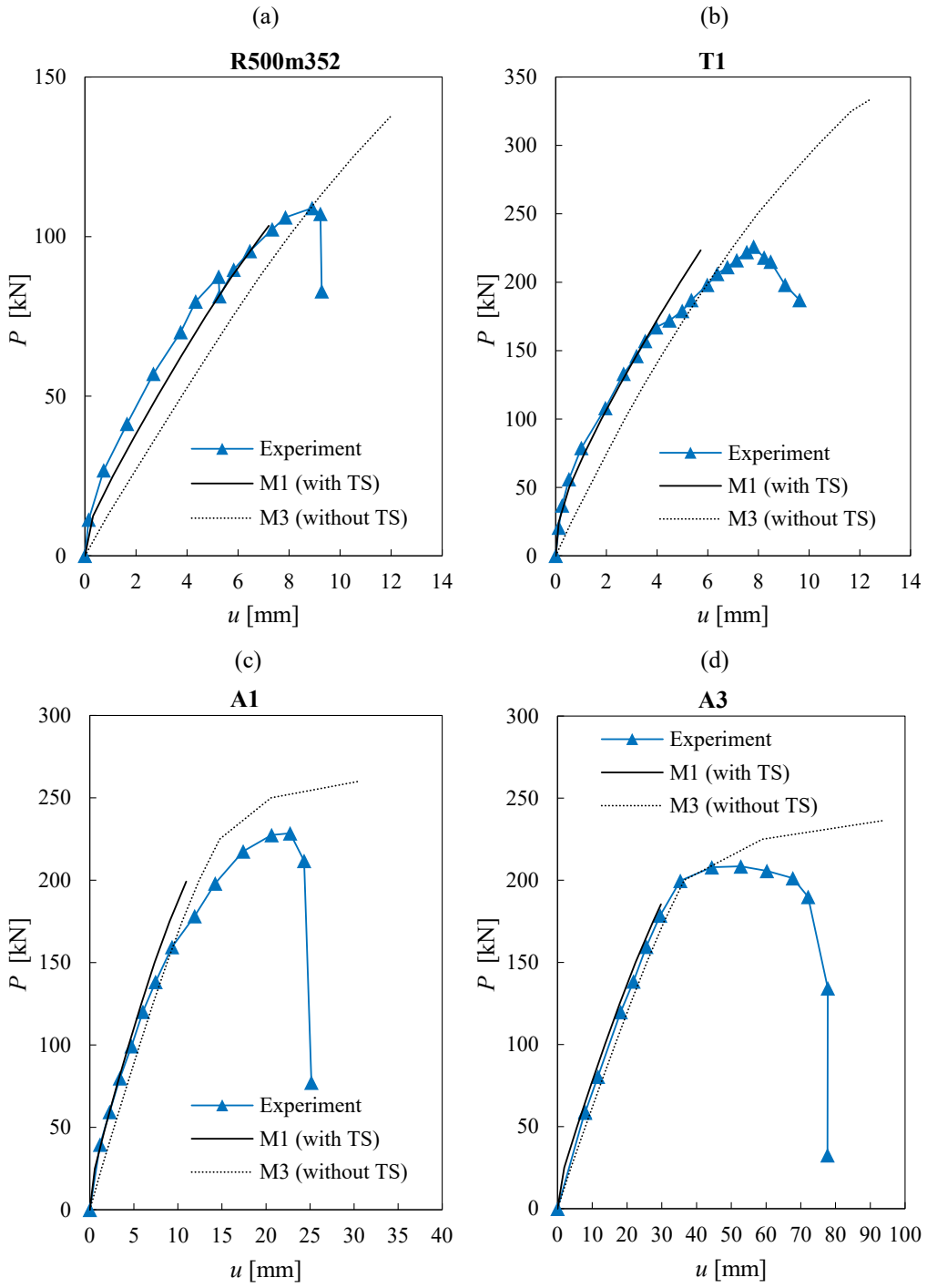

Fig. 6.21. Measured and calculated load-deformation responses using different numerical parameters for: (a) R500m352 (Huber 2016); (b) T1 (Piyamahant 2002); (c) A1 (Vecchio and Shim 2004); (d) A3 (Vecchio and Shim 2004).

By taking into account tension stiffening effects, the experimental deflections can be predicted fairly well for the whole loading history, though the deflections at peak load are slightly underestimated. In particular, in Test A3 from Vecchio and Shim (2004), the observed plateau in the experiments due to yielding of the flexural reinforcement cannot be properly captured in the numerical analysis since the rupture of the stirrups is predicted first. Neglecting tension stiffening effects leads to the overestimation of the ultimate loads and deformations. These statements for the analyses without tension stiffening are also valid when using M4 parameters (the TCM used both in the stirrups and the flexural reinforcement).

6.4.4 Conclusions

The following conclusions can be stated regarding the comparison of the CSFM results and the observed behavior in the analyzed tests performed on simply supported beams with low amounts of stirrups:

- The CSFM yields good estimates of the ultimate load, which is slightly overestimated (on average by 5%) when using the default numerical parameters. It is difficult to capture combined failure modes due to shear and concrete crushing in bending; the CSFM predicts failures due to rupture of the stirrups, which leads to strength predictions that err on the conservative side.
- The ultimate load predictions are somewhat sensitive to variations in the finite element mesh size. The best predictions are obtained when the default finite element mesh is refined. Therefore, it is always recommended that the influence of the finite element size on the results be investigated when performing final verifications.
- Neglecting tension stiffening leads to a very pronounced overestimation of the ultimate load and deformation capacity. Even when modeling tension stiffening in the stirrups by means of the Tension Chord Model, the predicted ultimate load is clearly on the unsafe side. The best results are obtained when considering the effect of non-stabilized cracking in the stirrups for low amounts of reinforcement by means of the Pull Out Model. This is the tension stiffening model implemented by default in the CSFM.

6.5 Concrete pier caps

This section addresses the analysis of *discontinuity regions*. The modeling of pier caps, which contain both static and geometric discontinuities, will be studied with the aid of an experimental study performed by Geevar and Menon (2018). Their study consisted of experiments on pier caps with four concentrated loads. The specimens were reinforced following standard rules used in design practice. Eight specimens were tested to investigate the influence of various parameters, such as the size of the bearing plates, the reinforcement layout, the geometry and the eccentricity of the applied loads. Given that the eccentricity of loading did not have a significant influence on

the behavior of the specimens in the experiments, only the specimens with constant geometry and no load eccentricity (S1, S2, S3, S4 and S5) were analyzed with the CSFM.

6.5.1 Experimental setup

Fig. 6.22a shows the geometry of the specimens. The dimensions and reinforcement were designed at a scale of around 1:3.5 compared to typical pier caps used in bridge construction. To ensure stability while testing, the test setup was inverted with respect to the normal configuration of a pile cap. The specimens stood on four vertical supports (consisting of load cells, steel plates and thin neoprene pads) and were subjected to a vertical force at the top (see Fig. 6.22b). The vertical load was applied with zero eccentricity to Specimens S1, S2, S3, S4 and S5. The size of the loading plate (l_b) varied in the tests, as indicated in Table 6.14. The reinforcement layout of the specimens is shown in Fig. 6.22c and the number and amount of reinforcing bars is detailed in Table 6.14. The layout was composed of primary reinforcement (A_{s1}), which was supplemented by additional reinforcement (A_{s2}) in Tests S3, S4 and S5. This reinforcement was fully anchored outside the zone of applied loads. The reinforcement also comprised distributed horizontal reinforcement (A_h with spacing s_h) and distributed vertical reinforcement (A_v). The distributed vertical reinforcement was observed to work mainly in compression and to not be effective. Therefore, this reinforcement was not modeled in the CSFM, as will be discussed in Section 6.5.3.

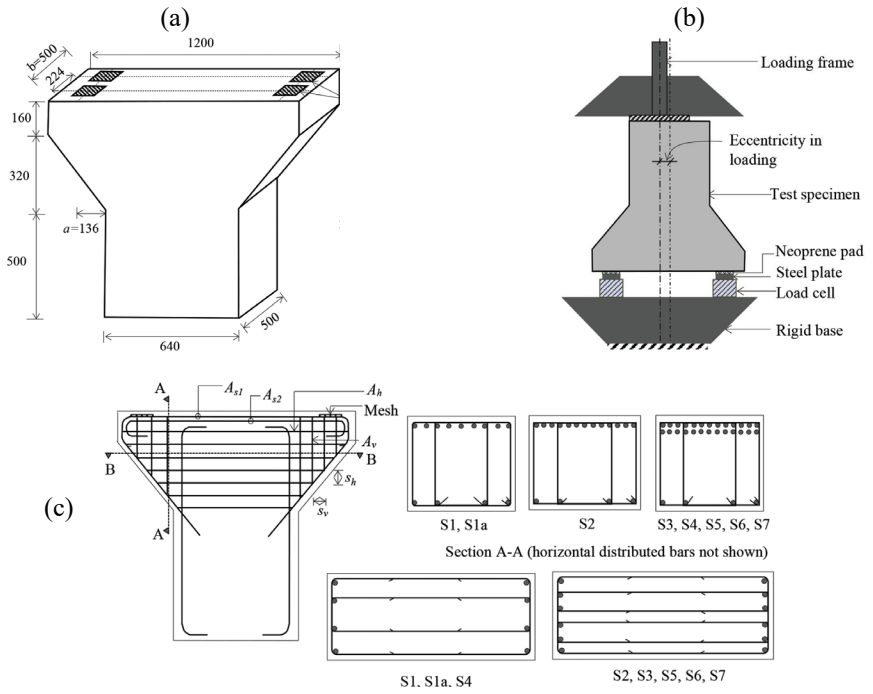

Fig. 6.22. Experimental setup of the pier caps: (a) Geometry; (b) test setup; (c) reinforcement detail; (dimensions in [cm]).

Table 6.14. Relevant parameters of the analyzed pier caps.

Specimen	A_{s1} [-]	A_{s2} [-]	$\rho_{s,geo}$	A_h [-]	s_h [mm]	$\rho_{h,geo}$	l_b [mm]
S1	9Ø10	-	0.32	4Ø4	75	0.13	130
S2	13Ø8	-	0.29	6Ø4	58	0.26	145
S3	13Ø8	13Ø8	0.58	6Ø4	58	0.26	145
S4	13Ø8	13Ø8	0.58	4Ø4	58	0.17	145
S5	13Ø8	13Ø8	0.58	6Ø4	58	0.26	170

6.5.2 Material properties

The material properties used in the numerical CSFM analyses are listed in Table 6.15. The strength f_t and the ultimate strain ε_u of the reinforcement as well as the concrete strain ε_{c0} were not given in the test report; plausible values were thus assumed for these parameters.

Table 6.15. Material properties used in the CSFM analyses.

Specimen	main reinf. (A_{s1}, A_{s2})			distributed reinf.(A_h)			Concrete	
	f_y[1)] [MPa]	f_t[2)] [MPa]	ε_u[2)] [‰]	f_y[1)] [MPa]	f_t[2)] [MPa]	ε_u[2)] [‰]	f_c[1)] [MPa]	ε_{c0}[2)] [‰]
S1	620	670	50	605	653	50	31.2	2.0
S2	631	681	50	605	653	50	35.7	2.0
S3	631	681	50	605	653	50	30.1	2.0
S4	631	681	50	605	653	50	34.9	2.0
S5	631	681	50	605	653	50	34.1	2.0

1) Geevar and Menon (2018)
2) Assumed value

6.5.3 Modeling with the CSFM

The geometry, reinforcement, supports and loading conditions were modeled in the CSFM according to the experimental setup. Fig. 6.18 shows the modeling of the S1 pier cap. It is assumed that the very thin (10 mm) neoprene plates do not allow significant horizontal deformation and therefore a fixed support is used in the horizontal and vertical directions. The load bearing plates are not arranged over the entire thickness of the pier caps (see Fig. 6.22a). Hence, the thickness in the CSFM analyses was set to be equal to the sum of the thickness of the load bearing plates (i.e., twice l_b). By considering this, any positive triaxial confining effect due to the simultaneous spreading of the load in-plane and out-of-plane is implicitly neglected. As already indicated, the

distributed vertical reinforcement (A_v) was not modeled since it works mainly in compression and does not have a significant influence on specimen behavior. The Tension Chord Model was used in all cases to capture the tension stiffening effects (no reinforcement modeled as stirrups).

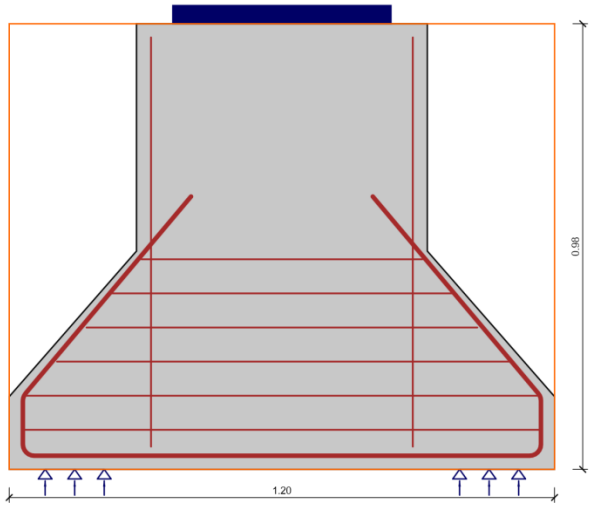

Fig. 6.23. CSFM model of S1 (dimensions in [m]).

For each test, four numerical calculations were carried out using the following parameters:

- The mesh size, which was 10 (the default value for this particular example) and 20 finite elements along section A-A, as defined in Fig. 6.22c.
- The consideration or not of the tension stiffening effect. By default, tension stiffening (TS) is considered in the CSFM (the Tension Chord Model is used for all bars in this particular case).
- The strain limit for concrete crushing (ε_{cu2}), which was set to 2‰ and 3.5‰ (the default value used in other analyses in this chapter).

The parameters used in each numerical calculation are summarized in Table 6.16. Model M0 corresponds to the default settings in the CSFM.

Table 6.16. Investigated numerical parameters (variations to M0 shaded).

Model	Mesh size[1)]	ε_{cu} [‰]	Tension stiffening
M0 (def.)	10	3.5	Yes
M1	20	3.5	Yes
M2	10	3.5	No
M3	10	2.0	Yes

1) Number of finite elements along section A-A, as defined in Fig. 6.22c

6.5.4 Comparison with experimental results

This section provides comparisons between the ultimate loads and failure modes provided by the CSFM and the studied experimental results.

Failure modes and ultimate loads

Table 6.17 summarizes the ultimate loads measured in the tests ($P_{u,exp}$) and predicted by the CSFM ($P_{u,calc}$), as well as the respective failure modes. The ultimate load P_u corresponds to the mean of the four reaction forces (i.e., a quarter of the total applied load). Table 6.17 also provides the mean and the coefficient of variation (CoV) of the ratios between the measured and the calculated ultimate loads for each numerical model. Ratios above one denote conservative predictions, while those below one indicate unsafe estimates of the ultimate load.

In all of the numerical analyses, failure was triggered by concrete crushing (see Table 6.17). In the experiments, the failure was also due to concrete crushing, but it was preceded by a slight yielding of the main reinforcement (A_{s1}), which does not limit the ultimate load. While the yielding of the reinforcement is not captured by the CSFM, this does not have a significant impact on the quality of the results. The default model M0 leads to slightly unsafe strength predictions (by 4% on average). It should be noted that the predictions are clearly unsafe for specimen S5 regardless of the considered numerical parameters. These unsatisfactory results from the CSFM might be partially explained by the fact that the strength result from the experiment was abnormally low. In spite of S5 being similar to S4 but containing a 50% higher amount of transversal reinforcement and 20% larger loading plates, its strength is significantly lower than that of S4. This could either be an abnormal experimental result or just a consequence of the large scatter, which is expected in compressive failures of a strut.

Table 6.17. Experimental and predicted ultimate loads (in kN) and failure mechanisms[1)].

Specimen	Test[2)]	M0	M1	M2	M3
S1	556 CC+FY	629 CC	610 CC	609 CC	568 CC
S2	767 CC+FY	840 CC	846 CC	811 CC	765 CC
S3	859 CC+FY	763 CC	770 CC	738 CC	689 CC
S4	902 CC+FY	828 CC	831 CC	803 CC	758 CC
S5	866 CC+FY	1085 CC	1086 CC	1044 CC	1003 CC
$\frac{P_{u,exp}}{P_{u,calc}}$	mean	0.96	0.96	1.06	0.99
	CoV	0.13	0.12	0.13	0.13

1) Failure modes according to Table 6.1
2) Mean of the measured loads at the four supports

The disparities among the different CSFM analyses can be easily analyzed by means of the ratio of the experimental to the calculated ultimate load ($P_{u,exp}/P_{u,calc}$). The variation in the mesh

size and the consideration or not of tension stiffening do not significantly influence the ultimate loads (variations below 5%; see Fig. 6.24a-b). While the consideration of tension stiffening might impact the results in concrete crushing failures with transverse reinforcement (as it lowers the reinforcement strains and consequently increases the effective compressive strength), this is not the case here since the transverse strains remain very small and the compressive strength is hardly affected by the compression softening factor. The results are sensitive though to the considered ultimate compressive strain in the concrete (ε_{cu2}). Considering an ultimate strain of 2‰ (model M3) instead of the 3.5 ‰ in the default model, reductions of up to 10% of the predicted ultimate loads are obtained (see Fig. 6.24c).

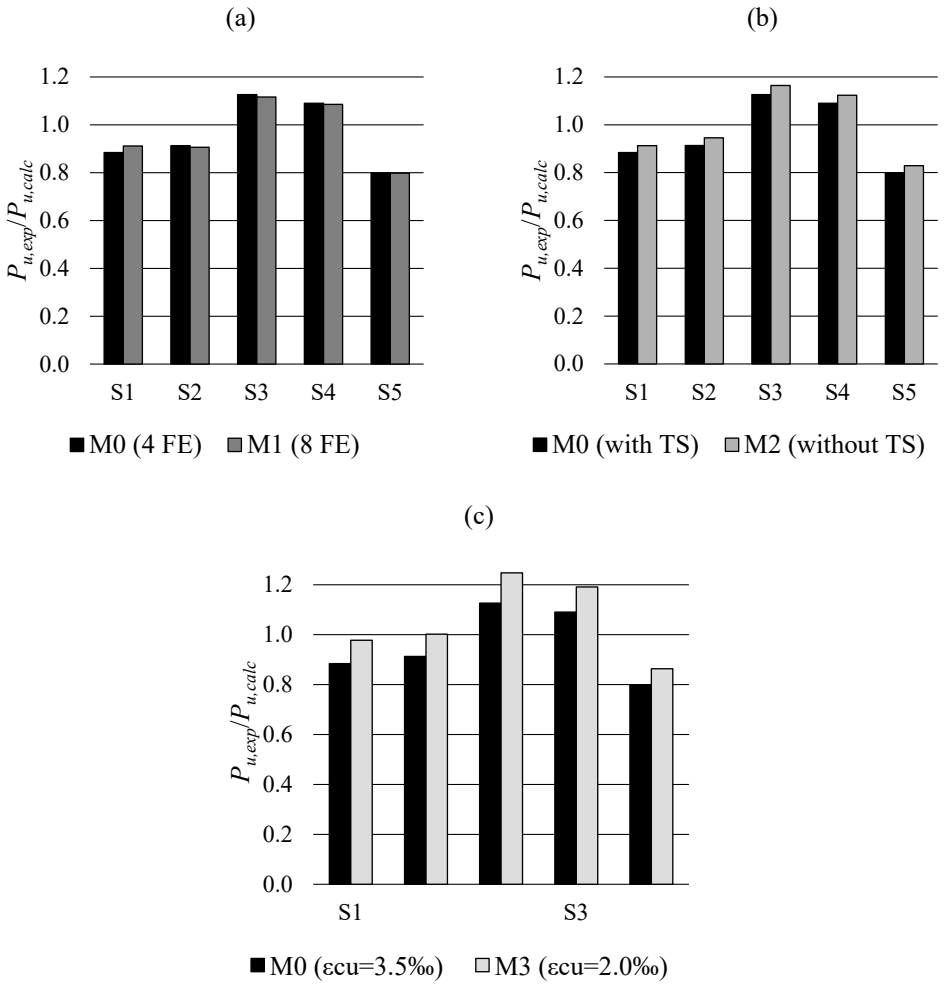

Fig. 6.24. Influence of numerical parameters on the ratio of measured to calculated ultimate loads: (a) Mesh size sensitivity; (b) consideration or not of tension stiffening (TS); (c) default (bilinear) and refined reinforcement stress-strain relationships.

Fig. 6.25a shows the continuous stress field results (principal compressive stresses (σ_c) and steel stresses (σ_{sr}) at the cracks) for specimen S1; the predicted failure mode and location are marked. These results were calculated using the default numerical parameters M0. The observed crack patterns at ultimate are shown in Fig. 6.25b. The predicted locations where concrete is expected to be crushed agree with the experimental observations.

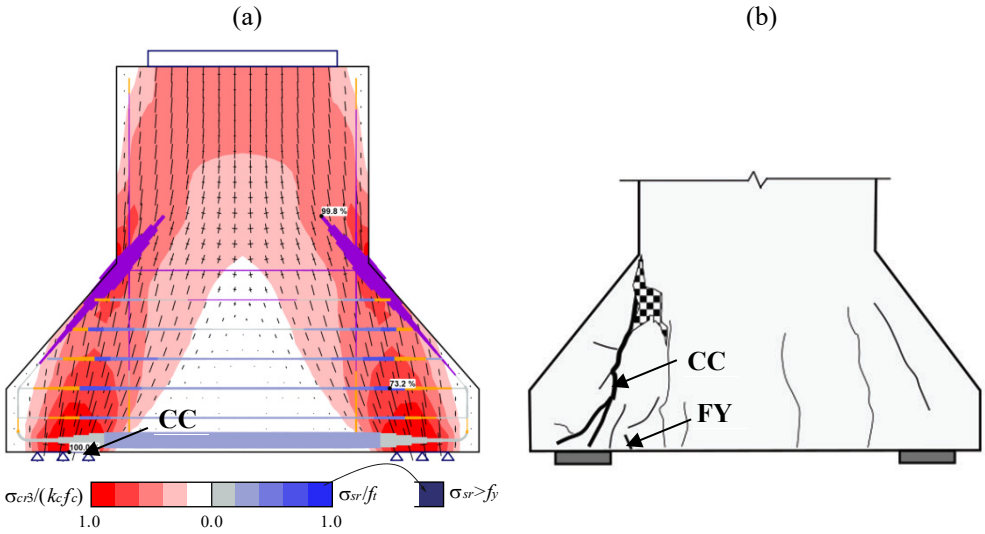

Fig. 6.25. Results for S1: (a) Calculated stress fiels for M0 at ultimate; (b) observed crack pattern at ultimate (extracted from Geevar and Menon, 2018).

6.5.5 Conclusions

A good correspondence between the results from the CSFM and experimental observations can be found for the case of the *discontinuity regions* analyzed in this section. The following conclusions can be stated:

- CSFM analyses using default numerical parameters provide appropriate estimates of ultimate loads and failure modes. However, the results show that local compressive failures in a strut cannot be predicted with the same accuracy as failures in which the strength is limited by yielding of the reinforcement. This was an expectable result, which is compensated for in design codes by the higher safety coefficient for concrete in compression than for reinforcement.
- The variation in the mesh size and the consideration or not of tension stiffening do not significantly influence the ultimate loads in this case.

7 Conclusions

This book presents the principles and validation of the Compatible Stress Field Method (CSFM), a new method for the computer-aided structural design of concrete structures. The CSFM targets the automated design and assessment of structural concrete members subjected to in-plane loading. The method is applicable for conventional beams and walls, but is particularly suitable for *discontinuity regions* (e.g., corbels, deep beams, walls with openings, dapped beam-ends and frame corners), where abrupt changes in geometry and/or concentrated loads render Bernoulli's hypothesis of plane sections remaining plane – and hence, sectional design methods and the corresponding, established tools for automated design – inappropriate.

Since sectional analysis cannot be applied to *discontinuity regions*, designers today typically design them by using strut-and-tie models and stress fields. These models are powerful tools that yield direct insight into load-carrying behavior and give the engineer control over the design. However, stress fields and strut-and-tie models are essentially still being used as hand calculations. This is a bottleneck for the ongoing digitalization process of structural engineering: *Discontinuity regions* are present in every structural concrete member and, in most cases, decisive for a safe design. The CSFM aims at overcoming this unsatisfactory situation by introducing an easy to use software tool implementing the basic design concepts of strut-and-tie models and stress fields.

The CSFM consists of a continuous, FE-based stress field analysis, which is used to assess the entire load-deformation behavior of concrete members. The basic concepts of classic strut-and-tie models and stress fields are complemented with kinematic considerations, i.e., the state of strain is evaluated throughout the structure. Hence, the effective compressive strength of concrete, as a function of transverse strains, can be automatically computed. By considering equilibrium at stress-free cracks, simple uniaxial constitutive laws as provided in concrete standards for concrete and reinforcement are used, without the need for the additional material properties required to perform nonlinear FE analyses. This makes the CSFM suitable for design and assessment in engineering practice and allows the partial safety factor method to be used for code-compliant design. While the concrete tensile strength is not considered in terms of strength (just as in standard structural concrete design), the CSFM accounts for its influence on member stiffness (i.e., tension stiffening) in order to cover all design code prescriptions, including serviceability (deflections, crack widths, …), load-deformation and deformation capacity aspects, which are not consistently addressed by previously formulated approaches. The CSFM has been implemented in *IDEA StatiCa Detail*, a new user-friendly commercial software tool that includes design aids for reinforcement design (location and amount).

The results of a thorough validation of the CSFM were summarized in Chapters 4, 5 and 6. As expected, the results of the CSFM are in perfect agreement with the theoretical models it is based on for simple load cases (pure tension, pure compression and pull-out loading). These basic

comparisons (Chapter 4) include crack widths, concrete stresses, bond shear stresses and reinforcement stresses and strains. The mesh size sensitivity is very small for cases where reinforcement failure or bond (anchorage length) are decisive. Failures due to concrete in compression show a certain mesh size dependency. This dependency is mainly caused by variations of the transverse strains for different finite element mesh sizes, which affects the compressive strength via the compression softening factor.

A thorough comparison of results calculated by the CSFM with those obtained using conventional design procedures, based on several national standards, was given in Chapter 5. For the classic example of a deep beam with an opening, the CSFM is in good agreement with strut-and-tie models for ultimate limit state verifications. However, since the CSFM is able to exploit all the resistant mechanisms, it allows for a more refined estimation of the ultimate load and yields correspondingly higher predicted ultimate loads. This example also shows that the use of the CSFM in *discontinuity regions* allows verifying serviceability criteria, which cannot be evaluated consistently with stress fields or strut-and-tie models. Further examples examined in Chapter 5 correspond to beams with rectangular and T cross-sections. These beams were analyzed with the CSFM and with simple cross-sectional analyses, following EN 1992-1-1 and ACI 318-14 design codes. The results provided by both approaches are very similar, in ultimate as well as in serviceability limit states. The observed differences can be explained by slightly different assumptions of the constitutive models in the two approaches. These verifications for beams confirm that the CSFM is compliant with the design provisions given in building codes for members and regions where all static and geometric quantities vary only slightly (i.e., Bernoulli's hypothesis of plane sections remaining plane applies).

Chapter 6 studied the capability of the CSFM to reproduce the observed behavior (ultimate load, load-deformation response, crack widths, …) of selected experimental campaigns from the literature. The analyzed experiments were chosen to cover a wide range of failure modes. In all analyses with the CSFM, the sensitivity of the results to different values of the most relevant parameters of the model was investigated. This allowed checking the suitability of the default parameters defined in Chapter 3. The analysis of T-beams showed that the results are significantly sensitive only to the value of the effective flange width. The default value of this parameter in the CSFM provided slightly conservative estimations of the experimental ultimate loads and deflections. Designers might thus refine the default value of the effective flange (see Section 3.6.3) based on alternative recommendations to consider the shear lag effect in cases where the compression zone depth is significant. The value provided by *fib* Model Code 2010 leads to very accurate estimations of the experimental ultimate loads, deflections and crack widths for the experiments compared in this book.

The analysis of cantilever wall-type bridge piers (shear walls) and pier caps in Chapter 6 aims at validating failures due to concrete crushing, which is a failure mode generally difficult to be captured precisely; this is the main reason why the safety coefficient for concrete compressive strength is higher than the one considered for the reinforcement. Despite this difficulty, the CSFM yields good estimations of the experimental ultimate loads and deflections. The estimations are

more accurate in cases where the main reinforcement reaches yielding (i.e., for the cantilever shear walls). Good estimations of the deformation capacity are obtained if the ultimate strain of concrete is verified, which is not activated by default in the software *IDEA StatiCa Detail* (an infinite plastic branch is considered for concrete in compression). The results show a moderate mesh size sensitivity for this failure mode: The ultimate loads obtained with the default finite element mesh size proposed by the CSFM varied up to 10% when the mesh size was doubled or halved. Similar results were obtained for the case of shear failures with low amounts of stirrups: The smaller the finite element mesh, the lower and more conservative the strength predictions by the CSFM. Hence, it is recommended to use initially a finite element mesh size equal to the default one or even coarser for quick analyses, but include in the final verifications an analysis with a finer mesh, in order to confirm that the mesh size sensitivity is within a reasonable range (as observed in the herein presented examples).

The comparison with experimental results confirmed that the automatic, mechanically consistent consideration of tension stiffening in the CSFM is perfectly suitable for realistically predicting the behavior. On one hand, it ensures reliable predictions of serviceability criteria: (i) Deflections were overestimated when neglecting the stiffening effect of concrete tensile stresses between cracks; and (ii) the tension stiffening model implemented in the CSFM – yielding direct information on reinforcement stresses at cracks, crack spacings and average strains between cracks – was essential to obtain realistic predictions of crack widths. On the other hand, the validations proved that the consistent implementation of tension stiffening is also crucial for ultimate limit state verifications: (i) Other than models considering average stresses between cracks, the tension stiffening implemented in the CSFM does not modify the strength of the bare reinforcement, but (ii) it stiffens its response, and (iii) reduces its deformation capacity. These combined features resulted in excellent predictions of the experimental results: The analyses of 17 tests of beams with low amounts of stirrup reinforcement (failing mostly in shear and including failures with rupture of the stirrups, see Section 6.4) showed that the CSFM provides excellent predictions when considering at least 10 finite elements over the depth of the beams.

In particular, the CSFM analyses consistently captured failures by reinforcement ruptures caused by insufficient ductility observed in experiments, while significantly higher loads would have been predicted in these cases if tension stiffening was neglected (around 20% on average in the experiments evaluated in Section 6.4). In models neglecting tension stiffening, failures by diagonal concrete crushing would be predicted instead, which is however highly dependent on the specific compression softening relationships considered. Here, the approach implemented in the CSFM is more accurate and provides consistent results for a wide range of constitutive relationships.

In the ultimate limit state, the stress fields obtained from the CSFM can be interpreted as solutions according to the lower-bound theorem of plasticity theory: They satisfy equilibrium and static boundary conditions, and do not infringe the “yield conditions”. Note that the yield conditions are set in quotation marks since rather than using ideally plastic material laws, realistic

stress-strain relationships accounting for the limited ductility of reinforcement and concrete compression softening are considered in the CSFM. However, using the peak stresses obtained in the final step of the CSFM analysis as material strengths, the stress fields would result in identical ultimate loads for ideally plastic behavior.

In conclusion, the verifications carried out in this book, including (i) the validation of basic load cases; (ii) a comparison with codes and established design methods; and (iii) an extensive validation on experimental data demonstrate that the Compatible Stress Field Method is well suited for the reliable and transparent analysis of two-dimensional concrete structures of any geometry, subjected to arbitrary in-plane loads.

In particular, the CSFM:

- yields realistic predictions of the load-deformation behavior
- maintains the advantages of classic stress fields and strut-and-tie models, such as control over the design and transparency
- merely requires standard material parameters known in the design stage
- is compatible with the design concepts of modern codes (e.g., neglecting the contribution of the tensile strength of concrete to the strength)
- provides all typically required validations in design, both in ULS as well as SLS
- enables the designer to optimize the structure regarding reinforcement layout and quantities
- is implemented in a user-friendly software application: IDEA StatiCa Detail.

Based on these features, the CSFM enables designers to design or assess any concrete structure that can be modelled as two-dimensional elements subjected to on-plane loads more reliably and efficiently than using other design methods.

Moreover, since optimization of the reinforcement is possible at little extra effort in design, the authors hope that the CSFM will foster the design of more economical and sustainable concrete structures in the future, reducing material use and greenhouse gas emissions.

Appendix A: Hypotheses of IDEA StatiCa RCS/Beam software

A.1 Main hypotheses

IDEA StatiCa Beam is a 1D FEM-based application enabling the modeling, design and checking of concrete beams according to the provisions for cross-sectional design included in structural concrete design codes. The geometry of the model is formed by a 1D bar element defined by a cross-section and its length. The assumptions of static analysis in *IDEA StatiCa Beam* are:

- The cross-sections of the beam remain plane and perpendicular to the centerline after deforming (i.e., the Euler-Bernoulli hypothesis is used).
- Materials exhibit linear elastic behavior (i.e., stiffness is constant).

Besides internal forces, *IDEA StatiCa Beam* calculates deflections as well. The deflection calculation consists of a linear FE analysis with modified stiffness of the finite elements, in which second-order effects are neglected. The main assumptions of the deflection analysis are:

- The stiffness of cracked sections is reduced.
- The tension stiffening effect is considered according to EN 1992-1-1.
- Creep effects are considered by means of an effective modulus of elasticity.
- Shrinkage effects are neglected.

The stiffness of the cross-sections is calculated by *RCS*, a separate application in *IDEA StatiCa*, which assumes strain compatibility between concrete and reinforcement.

A.2 Calculation assumptions for ULS checks

The main assumptions for ULS verifications are:

- The tensile strength of concrete is neglected (all tensile stresses are transmitted by the reinforcement).
- Concrete compressive stresses in a compression zone are calculated determined from the strains using stress-strain diagrams.
- Reinforcement stresses are calculated from the strains using stress-strain diagrams.
- For compressive concrete strains, an ultimate strain limit ε_{cu2} (parabola-rectangle diagram for concrete under compression) or ε_{cu3} (bi-linear stress-strain relation) is considered, see EN 1992-1-1.

- Strains of reinforcement are not limited in the case of ideally plastic idealization (no strain hardening). If strain hardening is considered, the strain is limited by ε_{ud}, see EN 1992-1-1.
- The state when at least one of the materials exceeds the ultimate limit strain (if ε_u is not limited, the concrete compressive strength is governing) is considered a limit state.

Two well-known methods defined in the following sections can be used to check the ultimate limit state.

A.2.1 Interaction diagram

This method provides the cross-sectional ultimate strength in the form of an interaction surface or interaction diagram. The points, which define the ultimate limit state of the cross-section under analysis, are located on the interaction surfaces. The cross-sectional capacity can be determined as a ratio between the acting internal forces and the limit state forces.

A.2.2 Response of the cross-section (method of limited deformation)

This method (also known as the method of limited deformation) involves the determination of stress and strain distributions and the equilibrium of the cross-section when applying the acting internal forces. A plane of strain can be determined from equilibrium, and the strain anywhere in the cross-section can be calculated. The stresses in each fiber of the cross-section and in each reinforcing bar are calculated depending on the strain using the stress-strain diagram of the materials.

A.3 Calculation assumptions for SLS checks

Within the calculation of the serviceability limit states (i.e., stress limitations, crack widths and deflections), two states that only differ in the considered tensile strength of the concrete are analyzed:

- The tensile strength of concrete is considered for uncracked cross-sections, but neglected for cracked cross-sections.
- The concrete tensile stress is limited by the tensile strength of the concrete at the time of crack formation, $f_{ct,eff}$, for uncracked cross-sections.
- The concrete and the reinforcement stresses are directly proportional to the distance to the neutral axis (the materials are considered to exhibit a linear stress distribution).

It should be noted that only stabilized crack patterns are considered when checking the crack width (compare to the consideration of non-stabilized cracking patterns in CSFM (Section 3.3.4).

When calculating deflections, it is necessary to determine the varying stiffness of the beams along their length. To this end, *IDEA StatiCa RCS* focuses on analyzing and checking individual

cross-sections, not the whole beam. The stiffnesses of selected cross-sections are calculated in *IDEA StatiCa RCS* and then used to compute deflections in *IDEA StatiCa Beam* (see above).

A.3.1 Stiffness for calculating short-term effects

When calculating stiffnesses to obtain short-term deflections, a reinforced concrete section, 28 days old with a secant modulus of elasticity (E_{cm}, i.e., without creep effects) is considered. The following stiffnesses are considered in the calculation:

- The stiffness of an uncracked section (this stiffness is considered if no cracks occur).
- The stiffness of a fully-cracked section (the compression zone, based on the strain plane calculated in the previous step, is considered when transformed cross-sectional characteristics of a reinforced section are calculated).
- A distribution coefficient, ζ, is calculated according to Eq. (A.1):

$$\zeta = 1 - \beta\left(\frac{\sigma_{sr}}{\sigma_s}\right)^2 \tag{A.1}$$

where β is a coefficient that takes account of the influence of the duration of the loading or of repeated loading on the average strain (β=1.0 for a single instance of short-term loading), σ_s is the stress in the tensile reinforcement calculated on the basis of a cracked section, and σ_{sr} is the stress in the tension reinforcement calculated on the basis of a cracked section under the loading conditions causing the onset of cracking. The resultant stiffness (I) is obtained using the distribution coefficient according to Eq. (A.2):

$$E \cdot I \cdot \zeta = E \cdot I_{cr} \cdot \zeta + E \cdot I_{un} \cdot (1 - \zeta) \tag{A.2}$$

where $E{\cdot}I_{cr}$ is the stiffness of a fully-cracked section and $E{\cdot}I_{un}$ is the stiffness of an uncracked section.

A.3.2 Stiffness for calculating long-term effects, including creep effects

To obtain long-term deflections, a reinforced concrete section loaded at time t_0 = 28 days with the following effective modulus of elasticity is considered:

$$E_{c,eff} = \frac{E_{cm}}{1 + \varphi(t_\infty, t_0)} \tag{A.3}$$

where E_{cm} is the secant modulus of elasticity of concrete and $\varphi(t_\infty, t_0)$ is a creep coefficient calculated for the design working life. Finally, a distribution coefficient, ζ, is calculated according to Eq. (A.1), with the difference that the β coefficient is set to β = 0.5 in this case because of long-term effects. The final stiffness is again obtained according to Eq. (A.2).

References

ACI Committee 318. 2009. *Building Code Requirements for Structural Concrete (ACI 318-08) and Commentary*. Farmington Hills, MI: American Concrete Institute.

Alvarez, M. 1998. *Einfluss des Verbundverhaltens auf das Verformungsvermögen von Stahlbeton*. Vol. 236. IBK Report. Basel, Switzerland: Birkhäuser.

AStrutTie 2017. HanGil IT. n.d. "Http://Astruttie.Aroad.Co.Kr/." Accessed January 31, 2019. http://astruttie.aroad.co.kr/.

Beeby, A. W. 1979. "The Prediction of Crack Widths in Hardened Concrete." *The Structural Engineer* 57A (1): 9–17.

Bimschas, M. 2010. *Displacement Based Seismic Assessment of Existing Bridges in Regions of Moderate Seismicity*. IBK Report 326. Zurich, Switzerland: vdf Hochschulverlag, ETH Zurich.

Branson, D. E, and G. A. Metz. 1965. *Instantaneous and Time-Dependent Deflections of Simple and Continuous Reinforced Concrete Beams*. Auburn, AL: State of Alabama Highway Dept., Bureau of Research and Development.

Broms, B. B. 1965. "Crack Width and Crack Spacing in Reinforced Concrete Members." *ACI Journal Proceedings* 62 (10): 1237–56. https://doi.org/10.14359/7742.

Burns, C. 2012. "Serviceability Analysis of Reinforced Concrete Based on the Tension Chord Model." Working Paper. *IBK Bericht*. Vol. 342. Institute of Structural Engineering, Swiss Federal Institute of Technology Zurich. https://doi.org/10.3929/ethz-a-009753066.

Comisión Permanente del Hormigón. 2008. *EHE-2008. Instrucción de Hormigón Estructural*. Madrid, Spain: Ministerio de Fomento.

Crisfield, M. A. 1997. *Non-Linear Finite Element Analysis of Solids and Structures*. Wiley.

European Committee for Standardization (CEN). 2002. *Eurocode: Basis of Structural Design (EN 1990:2002)*. Brussels, Belgium.

———. 2004. *Eurocode 2: Design of Concrete Structures - Part 1-1: General Rules and Rules for Buildings (EN 1992-1-1:2004)*. Brussels, Belgium.

Fernández Ruiz, M., and A. Muttoni. 2007. "On Development of Suitable Stress Fields for Structural Concrete." *ACI Structural Journal* 104 (4): 495–502.

Geevar, I., and D. Menon. 2018. "Strength of Reinforced Concrete Pier Caps - Experimental Validation of Strut-and-Tie Method." *ACI Structural Journal* 116 (1): 261–73. https://doi.org/10.14359/51711138.

Hannewald, P., M. Bimschas, and Alessandro Dazio. 2013. *Quasi-Static Cyclic Tests on RC Bridge Piers with Detailing Deficiencies*. IBK Report 352. Zurich, Switzerland: vdf Hochschulverlag, ETH Zurich.

Hoang, L. C., and M. P. Nielsen. 1998. "Plasticity Approach to Shear Design." *Cement and Concrete Composites*, Shear in Reinforced Concrete, 20 (6): 437–53. https://doi.org/10.1016/S0958-9465(98)00026-2.

Huber, P. 2016. "Beurteilung der Querkrafttragfähigkeit bestehender Stahlbeton- und Spannbetonbrücken." PhD thesis, Wien: TU Wien, Faculty of Civil Engineering.

Ingerslev, A. 1923. "The Strength of Rectangular Slabs." *Journal of the Institution of Civil Engineers* 1 (1): 3–14.

International Federation for Structural Concrete. 2013. *Fib Model Code for Concrete Structures 2010*. Edited by Paul Beverly. Fib CEB-FIP. Berlin: Ernst & Sohn.

Johansen, K. W. 1962. *Yield-Line Theory*. London: Cement and Concrete Association.

Kaufmann, W. 1998. *Strength and Deformations of Structural Concrete Subjected to In-Plane Shear and Normal Forces*. Basel: Birkhäuser Basel. https://doi.org/10.1007/978-3-0348-7612-4.

Kaufmann, W., and P. Marti. 1998. "Structural Concrete: Cracked Membrane Model." *Journal of Structural Engineering* 124 (12): 1467–75. https://doi.org/10.1061/(ASCE)0733-9445(1998)124:12(1467).

Kaufmann, W., J. Mata-Falcón, and A. Beck. 2018. "Future Directions for Research on Shear in Structural Concrete." In *Fib Bulletin 85: Towards a Rational Understanding of Shear in Beams and Slabs*.

Konečný, M., J. Kabeláč, and J. Navrátil. 2017. *Use of Topology Optimization in Concrete Reinforcement Design*. 24. Czech Concrete Days (2017). ČBS ČSSI. https://resources.ideastatica.com/Content/06_Detail/Verification/Articles/Topology_optimization_US.pdf.

Leonhardt, F., and R. Walther. 1963. *Schubversuche an Plattenbalken mit unterschiedlicher Schubbewehrung*. Heft 156. Berlin: Deutscher Ausschuss für Stahlbeton.

Marcus, H. 1932. *Die Theorie elastischer Gewebe und ihre Anwendung auf die Berechnung biegsamer Platten*. Berlin: Springer.

Marti, P. 1985. "Truss Models in Detailing." *Concrete International* 7 (12): 66–73.

———. 2013. *Theory of Structures: Fundamentals, Framed Structures, Plates and Shells*. First edition. Berlin, Germany: Wiley Ernst & Sohn, A Wiley Company.

Marti, P., M. Alvarez, W. Kaufmann, and V. Sigrist. 1998. "Tension Chord Model for Structural Concrete." *Structural Engineering International* 8 (4): 287–298.

———. 1999. "Tragverhalten von Stahlbeton." ETH Zurich. https://www.research-collection.ethz.ch/handle/20.500.11850/95676.

Marti, P., and P. Stoffel. 1999. "Beurteilung der Tragsicherheit bestehender Betonbauten: Fortbildungskurs für Bauingenieure, ETH Zürich." IBK Special Publication nº 9. Institut für Baustatik und Konstruktion, ETH Zürich.

Mata-Falcón, J. 2015. "Serviceability and Ultimate Behaviour of Dapped-End Beams (In Spanish: Estudio Del Comportamiento En Servicio y Rotura de Los Apoyos a Media Madera)." PhD thesis, Valencia: Universitat Politècnica de València.

Meier, H. 1983. "Berücksichtigung des wirklichkeitsnahen Werkstoffverhaltens beim Standsicherheitsnachweis turmartiger Stahlbetonbauwerke." Institut für Massivbau, Universität Stuttgart.

Melan, E. 1938. "Der Spannungszustand eines Mises-Henckyschen Kontinuums bei veraenderlicher Belastung." *Sitzungsberichte der Kaiserlichen Akademie der Wissenschaften in Wien* 147: 73–78.

Mörsch, E. 1908. *Der Eisenbetonbau - Seine Theorie und Anwendung (Reinforced Concrete Construction – Theory and Application)*. Vol. 3. Auflage, 1908, 376 pp., 5. Auflage, 1. Band, 1. Hälfte, 1920, 471 pp., 2. Hälfte, 1922, 460 pp. Stuttgart: Verlag Konrad Wittwer.

Muttoni, A., M. Fernández Ruiz, and F. Niketic. 2015. "Design versus Assessment of Concrete Structures Using Stress Fields and Strut-and-Tie Models." *ACI Structural Journal* 112 (05): 605–16.

Navrátil, J., P. Ševčík, L. Michalčík, P. Foltyn, and J. Kabeláč. 2017. *A Solution for Walls and Details of Concrete Structures*. 24th Czech Concrete Days.

Nielsen, M.P. 1984. *Limit Analysis and Concrete Plasticity*. Prentice-Hall Series in Civil Engineering. New Yersey: Englewood Cliffs.

Piyamahant, S. 2002. "Shear Behavior of Reinforced Concrete Beams with a Small Amount of Web Reinforcement." PhD thesis, Kochi University of Technology.

Procházka, J. 2006. *Navrhování betonových konstrukcí podle EN 1992-1-1 (Eurokódu 2): sbírka příkladů ke školení.* Praha: ČBS Servis.

Ritter, W. 1899. "Die Bauweise Hennebique." *Schweizerische Bauzeitung* 33 (5): 41–43, 49–52, 59–61.

Roberts, D. M. 2003. "CEE 3150 : Reinforced Concrete Design - University of Wisconsin, Platteville." 2003. https://www.coursehero.com/sitemap/schools/2575-University-of-Wisconsin-Platteville/courses/2128396-CEE3150/.

Rosenblueth, E. 1955. "Shell Reinforcement not Parallel to Principal Stresses." *ACI Journal Proceedings* 52 (9): 61–71. https://doi.org/10.14359/11586.

Schlaich, J., K. Schäfer, and M. Jennewein. 1987. "Toward a Consistent Design of Structural Concrete." *PCI Journal* 32 (3): 74–150.

Seelhofer, H. 2010. *Ebener Spannungszustand im Betonbau: Grundlagen und Anwendungen*. IBK-Bericht 320. Zürich: vdf Hochschulverl. an d. ETH.

SIA (Swiss Society of Engineers and Architects). 2013. *Swisscode SIA 262:2013 Concrete Structures*. Zurich, Switzerland: Swiss Society of Engineers and Architects (SIA).

Sigrist, Viktor. 1995. *Zum Verformungsvermögen von Stahlbetonträgern*. IBK-Bericht 210. Basel: Birkhäuser.

Thürlimann, B., P. Marti, J. Pralong, P. Ritz, and B. Zimmerli. 1983. *Anwendung der Plastizitätstheorie auf Stahlbeton: Vorlesung zum Fortbildungskurs für Bauingenieure*. Institut für Baustatik und Konstruktion, ETH Zürich.

Tjhin, T. N., and D. A. Kuchma. 2002. "Computer-Based Tools for Design by Strut-and-Tie Method: Advances and Challenges." *ACI Structural Journal* 99 (5): 586–94.

Vecchio, F.J., and M.P. Collins. 1986. "The Modified Compression Field Theory for Reinforced Concrete Elements Subjected to Shear." *ACI Journal* 83 (2): 219–31.

Vecchio, F.J., and W. Shim. 2004. "Experimental and Analytical Reexamination of Classic Concrete Beam Tests." *Journal of Structural Engineering* 130 (3): 460–69.

Notation

Latin lower-case letters

a	shear span
a_s	cross-sectional area of reinforcement per meter
b	width of a cross-section; thickness of a member
b_{eff}	effective flange width
d	effective depth of a cross-section
f_{bd}	design bond strength
f_c	cylinder compressive strength of concrete
f_{cd}	design value of concrete compressive strength
f_{ck}	characteristic compressive cylinder strength of concrete (at 28 days)
f_{ct}	axial tensile strength of concrete
$f_{ct,eff}$	axial tensile strength of concrete at time of crack formation
f_{ctm}	mean value of axial tensile strength of concrete
f_t	tensile strength of reinforcement
f_{td}	design value of the tensile strength of reinforcement
f_y	yield strength of reinforcement
f_{yd}	design yield strength of reinforcement
f_{yk}	characteristic yield strength of reinforcement
h	cross-section depth
k_c	concrete strength reduction factor (due to the transversal strain state and increasing brittleness with strength)
k_{c2}	concrete strength reduction factor (due to the transversal strain state)
l	length of a member
l_b	anchorage length; size of the loading plate
$l_{b,net}$	basic anchorage length of the reinforcing bars
$l_{\varepsilon,avg}$	assumed distance between fictitious cracks in the pull-out tension stiffening model (POM)
n_l	number of reinforcing bars of the flexural reinforcement
q_u	Ultimate load at ULS
s_h	spacing of the distributed reinforcement
s_l	spacing of the flexural reinforcement
s_r	crack spacing
s_{r0}	theoretical maximum value of the crack spacing
s_t	spacing of the transverse reinforcement

u	deflection
u_{tot}	total deflection
w	crack width
w_b	projection of the crack width in the direction of a reinforcing bar
x	depth of the compression zone
z	lever arm of internal forces

Latin upper-case letters

A_h	cross-sectional area of transversal horizontal reinforcement
A_s	cross-sectional area of reinforcement
A_{s1}	cross-sectional area of the main reinforcement
A_{s2}	cross-sectional area of the secondary reinforcement
A_{sl}	cross-sectional area of longitudinal reinforcement
A_v	cross-sectional area of transversal vertical reinforcement
E	modulus of elasticity
E_c	modulus of elasticity of concrete
$E_{c,eff}$	effective modulus of elasticity of concrete
E_{cm}	secant modulus of elasticity of concrete
E_s	modulus of elasticity of reinforcement
E_{sh}	hardening modulus of reinforcement
F	action in general; applied load or load effect
F_{au}	maximum force at the end of the reinforcement when using a normalized anchorage end
F_G	permanent design load
F_Q	variable design load
F_{sl}	force in the longitudinal reinforcement
F_u	ultimate design load
G_b	elastic stiffness of the bond-slip model implemented for anchorage length verifications
H	height of a member
I_{cr}	second moment of area of fully cracked section
K_a	elastic stiffness of the force-slip model at the end of the reinforcement to implement reductions in the basic anchorage length
L	span
M	bending moment
M_{cr}	cracking moment
M_{Ed}	design value of the applied bending moment
M_{Rd}	design value of ultimate moment resistance

N	normal (axial) force
N_{Ed}	design value of the applied normal (axial) force
$P_{u,calc}$	ultimate load predicted by the CSFM
$P_{u,exp}$	experimental ultimate load
$V_{u,calc}$	ultimate shear force predicted by the CSFM
$V_{u,exp}$	experimental ultimate shear force

Greek lower-case letters

β	coefficient of reduction of the basic anchorage length of the reinforcing bars when using a normalized anchorage end
δu	bond slip (relative displacement between concrete and reinforcement)
δu_{max}	axial displacement of the bond finite elements connecting the reinforcement and concrete, which represents the slip between both materials
ε_3	principal compressive strain
ε_{c2}	concrete strain at reaching the compressive strength
ε_{cu2}	ultimate compressive strain in the concrete
ε_{lt}	strain due to long-term effects of load
ε_m	average strain of reinforcement
ε_{st}	strain due to short-term effects of load
ε_u	limit strain value; strain of reinforcement at maximum load
ε_{ud}	limit strain value of reinforcement in case of inclined plastic top branch
ε_{uk}	characteristic strain of reinforcement at maximum load
γ_c	partial safety factor for concrete material properties
γ_G	partial safety factor for permanent actions
γ_Q	partial safety factor for variable actions
γ_s	partial safety factor for the material properties of the reinforcing steel
η_{fc}	concrete strength reduction factor (due to the increasing brittleness with strength, acc. to *fib* Model Code 2010)
φ	creep coefficient
λ	crack spacing coefficient ($=s_r/s_{r0}$), stress block factor
θ_b	orientation of the reinforcing bar
θ_r	crack orientation with respect to horizontal / longitudinal axis
θ_ε	orientation of the strain field with respect to horizontal / longitudinal axis
θ_σ	orientation of the compressive stress field with respect to horizontal / longitudinal axis
ρ_{cr}	minimum reinforcement ratio
ρ_{eff}	effective reinforcement ratio
ρ_{geo}	geometric reinforcement ratio

$\rho_{h,geo}$	geometric reinforcement ratio of the horizontal distributed reinforcement
$\rho_{l,geo}$	geometric reinforcement ratio of the flexural reinforcement
$\rho_{s,geo}$	geometric reinforcement ratio of the primary and additional reinforcement
$\rho_{t,geo}$	geometric reinforcement ratio of the transverse reinforcement
σ_c	concrete stress
$\sigma_{c,lt}$	stress in concrete due to long-term effects of load
$\sigma_{c,st}$	stress in concrete due to short-term effects of load
σ_{c3r}	principal concrete compressive stress at the cracks
σ_s	reinforcing steel stress, stress in the tension reinforcement calculated on the basis of a cracked section
$\sigma_{s,lt}$	stress in reinforcement due to long-term effects of load
$\sigma_{s,st}$	stress in reinforcement due to short-term effects of load
σ_{sr}	reinforcing steel stress at the cracks
σ_{st}	stress due to short-term effects of loads
τ_{b0}	bond shear stress before yielding
τ_{b1}	bond shear stress after yielding
ξ	time-dependent factor for sustained load
ψ_2	factor defining representative values of variable actions
ζ	distribution coefficient

Greek upper-case letters

Δ	deflection
Δ_{cs}	deflection under sustained loads including creep
$\Delta_{I,L}$	deflection under service dead + live loads
$\Delta_{I,SU\,ST}$	deflection under sustained loads

Special symbols

#	bar size according to imperial units in 1/8 of inches; e.g. #7 indicates reinforcing bar with diameter of 7/8'' ≈ 22 mm
′	foot (ft) – unit length in the imperial system of measurement
″	inch (in) – unit length in the imperial system of measurement
Ø	diameter of reinforcing bar
$Ø_l$	diameter of flexural reinforcing bar
$Ø_t$	diameter of transverse reinforcing bar

Abbreviations

B-region	regions where plain sections remain plain after deforming
CSFM	Compatible Stress Field Method
DL	dead load
D-region	discontinuity region
EPSF	elastic-plastic stress field method
MFD	multiplier of the flange depth
NLFEA	non-linear finite element analysis
POM	Pull Out Model
RCS	Reinforced Concrete Section (appliaction *IDEA StatiCa RCS*)
SLS	serviceability limit states
STM	strut-and-tie models
SW	load due to self-weight
TCM	Tension Chord Model
ULS	ultimate limit state

COVER PHOTO CREDITS:
Inn Bridge Vulpera, Scuol, Switzerland, 2010

Designer:
Walter Kaufmann and Beat Meier (dsp Ingenieure + Planer AG),
Rudolf Vogt (ACS Partner AG), and Eduard Imhof

Photo:

COMPATIBLE STRESS FIELD DESIGN OF STRUCTURAL CONCRETE

Principles and Validation

Prof. Dr. Walter Kaufmann,
Dr. Jaime Mata-Falcón, Dr. Marius Weber,
Tena Galkovski, Duc Thong Tran,
Dr. Jaromir Kabelac, Michael Konecny,
Ass. Prof. Dr. Jaroslav Navratil,
Michal Cihal, Petra Komarkova

This publication presents the principles and validation of the Compatible Stress Field Method (CSFM).
This new method can be used for the design and assessment of any concrete structure subjected to in-plane loading, and is particularly suited for the dimensioning of "discontinuity regions" such as corbels, deep beams, walls with openings, dapped beam-ends, and frame corners. The CSFM represents a significant step forward for structural engineering practice, as it allows the efficient checking of all design code provisions, including serviceability, load-deformation and deformation capacity aspects even for concrete members with complex geometry. The method is based on Finite Element Analysis and uses only basic material parameters employed in standard structural concrete design.
The results of the CSFM for a set of verification examples are presented and discussed, during which the influence of the main parameters of the method and its underlying models are also covered. The results are compared to a wide range of analytical solutions, design code provisions and experimental results, and show good agreement with all of them.

ISBN 978-3-906916-95-8
9 783906 916958 >

ETH Zurich, Institute of Structural Engineering
IDEA StatiCa s.r.o., Brno, Czech Republic
July 2020
ISBN 978-3-906916-95-8